Rod photoreceptor specific expression and function of *Frmpd1* (FERM and PDZ domain containing 1)

Christie K. Campla



Worcester College
Nuffield Laboratory of Ophthalmology, University of Oxford
Neurobiology Neurodegeneration & Repair Laboratory, National Eye Institute

A thesis submitted to the University of Oxford for the degree of Doctor of Philosophy (DPhil)

October 2017

Acknowledgements

First and foremost I want to thank my thesis supervisors Drs. Anand Swaroop, Stephanie Halford, and Sumathi Sekaran for their tremendous support and guidance both academically and personally throughout my time in their labs. I appreciate all of the time, patience, and wisdom they've dedicated to mentoring me to make my DPhil experience a productive and stimulating one.

I'm thankful to Steph, Sum, Suze, and Eleni for always making me feel like there were people I could turn to while being so far away from home in Oxford. I'd also like to extend my gratitude to all of the members of the NLO, especially Steve, who helped me a ton when adjusting to working in a different lab environment "across the pond". Back in the US, I owe my thanks to everyone in the N-NRL for being great co-workers and providing all kinds of technical assistance and expertise. Many of the experiments in this thesis couldn't have been done without the help of Jerome, Jacob, Thad, Matthew, and VJ.

I'm also not sure what I would have done without the camaraderie of the "Tina's" (Passley, Thad, and Andrew) to constantly troubleshoot, vent, and laugh with both in and out of the lab during these last few years. Finally, I especially want to thank Brittany and my parents for always being there for me regardless of the circumstances and particularly during some of the most stressful weeks when I needed it most. I have been blessed with such a great support system and I can't thank them enough for all of their advice and encouragement.

Table of contents

Acknowledgements ii
Table of contents iii
List of figures vii
List of tables ix
Abbreviations x
Statement of originality xiv
Abstract xv

Chapter 1: Introduction 1

1.1 The mammalian retina 1
1.2 Photoreceptor differentiation 4
1.3 Photoreceptor morphology and development 8
1.4 Phototransduction 12
1.5 Retinal degenerative diseases 18
1.6 Therapeutic approaches 22
1.7 Hypothesis and specific aims 24

Chapter 2: Selection of candidate gene *Frmpd1* 28

2.1 Introduction 28
2.2 Materials and methods 31
2.2.1 Materials 31
2.2.2 RNA-seq differential expression analysis 31
2.2.3 Hierarchical clustering and heat maps 34
2.2.4 Nrl/Crx chromatin immunoprecipitation sequencing (ChIP-Seq) 34
2.2.5 Mouse lines & husbandry 35
2.2.6 RNA isolation 35
2.2.7 Plasmid DNA isolation 36
2.2.8 DNA precipitation 36
2.2.9 *In vivo* electroporation 37
2.2.10 Retina cryosectioning 37
2.2.11 In situ hybridisation (ISH) 39
2.3 Results 40
2.3.1 Differential expression analysis of purified rod photoreceptors 40
2.3.2 Selection of candidate genes for further analysis 43

2.3.3 Validation of RNA expression profiles of candidate genes 48
2.3.4 ShRNA-mediated Frmpd1 knockdown disrupts retinal organisation 50
2.4 Discussion 54

Chapter 3: Alternative promoter of *Frmpd1* is regulated by Nrl and Crx 59

3.1 Introduction 59
3.1.1 The Frmpd family of proteins 59
3.1.2 FERM domain 60
3.1.3 PDZ domain 62
3.1.4 Frmpd family members 2-4 63
3.1.5 Frmpd1 65
3.2 Materials and methods 66
3.2.1 Materials 66
3.2.2 Methods described in other sections 67
3.2.3 Immunohistochemistry 67
3.2.4 *In situ* hybridisation and immunohistochemistry 68
3.2.5 General PCR protocol and primer design 68
3.2.6 Recombinant DNA plasmid cloning 70
3.2.7 Cell lines 72
3.2.8 Cell passaging and seeding 72
3.2.9 Cell transfection 72
3.2.10 Dual luciferase assay 73
3.2.11 Site-directed mutagenesis 74
3.2.12 5'-Rapid Amplification of cDNA Ends (RACE) 75
3.2.13 5'-untranslated region (UTR) analysis 79
3.2.14 cDNA synthesis 80
3.2.15 Nuclear protein extraction 80
3.2.16 Bicinchoninic acid (BCA) assay 81
3.2.17 Electrophoretic mobility shift assay (EMSA) 81
3.3 Results 82
3.3.1 Frmpd1 RNA expression is upregulated primarily in rod photoreceptors during development 82
3.3.2 Frmpd1 is expressed in retinal bipolar cells in the inner nuclear layer ..... **Error! Bookmark not defined.**
3.3.3 Frmpd1 uses an alternative tissue-specific 5'-UTR in the retina 85
3.4 Discussion 97

Chapter 4: Localisation and interacting partners of Frmpd1 in the retina 101

4.1 Introduction 101
4.2 Materials and methods 105
4.2.1 Materials 105
4.2.2 Methods described in other sections 105
4.2.3 Preabsorption assay with blocking peptide for commercial Frmpd1 antibody 106
4.2.4 Antigen prediction 106
4.2.5 Custom polyclonal antibody production 107
4.2.6 Quantitative PCR (qPCR) 108
4.2.7 Immunoprecipitation 109
4.2.8 Immunoblotting 110
4.3 Results 111
4.3.1 Frmpd1 protein localises to photoreceptor inner segments and synapses 111
4.3.2 Generation of custom polyclonal antibodies against Frmpd1 115
4.3.3 Frmpd1 forms a complex with Gpsm2 and T_α 119
4.3.4 Frmpd1 expression, but not localisation, varies during light/dark cycles 125
4.4 Discussion 126

Chapter 5: Loss of *Frmpd1* modulates rod phototransduction 130

5.1 Introduction 130
5.2 Materials and methods 134
5.2.1 Materials 134
5.2.2 Methods described in other sections 134
5.2.3 CRISPR/Cas9 genetic engineering 134
5.2.4 PCR genotyping 136
5.2.5 Electroretinography 136
5.3 Results 138
5.3.1 Disruption of Frmpd1 protein-coding region results in embryonic lethality before E10.75 138
5.3.2 Deletion of retina-specific Frmpd1 promoter and 5'-UTR results in tissue specific knockdown 139
5.3.3 Retinal lamination and individual cell morphologies are unaltered in Frmpd1$^{-/-}$ mice 146
5.3.4 Deletion of Frmpd1 delays T_α return to outer segments following light exposure 146
5.3.5 Frmpd1 deletion delays a-wave recovery after moderate rhodopsin bleach 148
5.4 Discussion 151

Chapter 6: Conclusions and future directions 155

6.1 Overview 155
6.2 Significance and connection to original hypothesis 156
6.3 Future directions 158
6.3.1 Identification of additional Frmpd1 protein interactors 158
6.3.2 Effects of Frmpd1 on activation/inactivation of T_{α} 159
6.3.3 Function of Frmpd1 in bipolar cells 160
6.3.4 Role of Frmpd1 in embryogenesis 161
6.3.5 Patient screening 161

References 163

Appendices 184

6.4 Appendix A: Reagents and buffer compositions 184
6.5 Appendix B: Plasmid maps 188
6.6 Appendix C: Primers used for genotyping, cloning, RACE, and PCR assays. 191
6.7 Appendix D: Antibodies used for immunofluorescence and immunoblot staining. 193
6.8 Appendix E: Differentially expressed genes also containing Nrl and Crx ChIP-seq peaks. 196

List of figures

Chapter 1: Introduction

Figure 1.1: Mammalian retina anatomy.. 2
Figure 1.2: Mouse retinal cell type birth order.. 6
Figure 1.3 Photoreceptor differentiation in humans and mice. 7
Figure 1.4: Photoreceptor morphogenesis. 9
Figure 1.5: Rod phototransduction and recovery. 16
Figure 1.6: Light-dependent translocation of phototransduction components. 17
Figure 1.7: Rod photoreceptor disease.. 21

Chapter 2: Selection of candidate gene *Frmpd1*

Figure 2.1: RNA-Seq of purified rod and "cone-like" photoreceptors. 32
Figure 2.2: *In vivo* electroporation of neonatal mouse retina. 38
Figure 2.3: Hierarchical clustering of differentially expressed genes. 41
Figure 2.4: Hierarchical clustering of Nrl-Crx filtered differentially expressed genes. 42
Figure 2.5: Candidate gene selection overview. 46
Figure 2.6: RNA expression of candidate genes in $Nrl^{+/+}$ and $Nrl^{-/-}$ retina. 49
Figure 2.7: Retina morphology after shRNA knockdown screen 52
Figure 2.8: Retinal architecture is disrupted with *Frmpd1* knockdown. 52

Chapter 3: Alternative promoter of *Frmpd1* is regulated by Nrl and Crx

Figure 3.1: The Frmpd family of proteins.. 61
Figure 3.2: 5'-Rapid amplification of cDNA ends (5'-RACE) 76
Figure 3.3: *Frmpd1* expression is enriched in rod photoreceptors during development 83
Figure 3.4: *Frmpd1* expression can be detected in bipolar cells of the inner nuclear layer 84
Figure 3.5: *Frmpd1* uses a retina-specific 5'UTR in mice and humans. 87
Figure 3.6: Exon 1a is expressed by all *Frmpd1*-expressing retinal cell types. 88
Figure 3.7: Identification of sequence elements upstream of *Frmpd1* required for ONL expression *in vivo*.. 91

Figure 3.8: Putative transcription factor binding sites in *Frmpd1* minimal promoter.. 93

Figure 3.9: Mammalian conservation of Nrl and Crx binding sites within Frmpd1 promoter 96

Figure 3.10: Nrl and Crx directly bind to and upregulate *Frmpd1* minimal promoter. 96

Chapter 4: Localisation and interacting partners of Frmpd1 in the retina

Figure 4.1: Preabsorption assay for commercial Frmpd1 antibody..... 112

Figure 4.2: Tagged Frmpd1 protein localisation in electroporated retina..... 114

Figure 4.3: Custom Frmpd1 immunising peptide design.. 116

Figure 4.4: Immunoreactivity of guinea pig and chicken custom antibody sera.. . 117

Figure 4.5: Frmpd1 and Gpsm2 colocalise in rod inner segments and synapses... 120

Figure 4.6: Immunoprecipitation of Frmpd1 complexes from dark- and light-adapted retinae. 123

Figure 4.7: *Frmpd1* transcript expression and protein localisation in light and dark. 124

Figure 4.8: Proposed mechanism of Frmpd1-Gpsm2- T_{α} protein binding. 127

Chapter 5: Loss of Frmpd1 modulates rod phototransduction

Figure 5.1: Comparison of traditional and CRISPR/Cas9 genetic engineering of mice. 133

Figure 5.2: Electroretinography. 137

Figure 5.3: CRISPR targeting of protein-coding portion of *Frmpd1* results in early embryonic death..... 140

Figure 5.4: Deletion of *Frmpd1* retina 5'-UTR leads to tissue-specific protein knockout. 142

Figure 5.5: Retinal lamination and individual cell morphologies in *Frmpd1*$^{-/-}$ mice.. 144

Figure 5.6: Immunostaining of *Frmpd1*$^{-/-}$ outer plexiform layer synapses. 145

Figure 5.7: Transducin return to outer segments is delayed in *Frmpd1*$^{-/-}$ mice..... 147

Figure 5.8: Photopic and scotopic ERG responses in *Frmpd1*$^{-/-}$ mice are largely unaffected. 149

Figure 5.9: Recovery of rod photoresponse is delayed in *Frmpd1*$^{-/-}$ mice.. 150

List of tables

Table 1.1: Photoreceptor transduction protein isoforms in mouse rods and cones.... 15

Table 2.1: Overrepresented gene ontology categories of differentially expressed genes containing Nrl and Crx ChIP-seq peaks. 44

Abbreviations

BAM	Binary Sequence Alignment Map
BCA	Bicinchoninic Acid Assay
BODIPY	Boron-Dipyrromethene
BP	Base Pair
C-	Carboxyl Terminus
CAS9	CRISPR Associated Protein 9
CDNA	Complementary DNA
CDS/M2	Candela Per Square Metre
CGMP	Cyclic Guanosine Monophosphate
CHIP	Chromatin Immunoprecipitation
CRISPR	Clustered Regularly Interspaced Short Palindromic Repeats
CRX	Cone-Rod Homeobox
CRX	Cone–Rod Homeobox
CT	Cycle Threshold
CT	Circadian Time
DAPI	4',6-Diamidino-2-Phenylindole
DDM	N-Dodecyl-B-D-Maltoside
DEG	Differentially Expressed Gene
DNA	Deoxyribonucleic Acid
E	Embryonic Day
EMSA	Electrophoretic Mobility Shift Assay
ERG	Electroretinogram
ES	Embryonic Stem
ESCS	Embryonic Stem Cells
FACS	Fluorescence Activated Cell Sorting
FERM	4.1/Ezrin/Radixin/Moesin

FLAG	DYKDDDDK Epitope
FPKM	Fragments Per Kilobase Of Transcript Per Million Mapped Reads
FRMPD1	FERM And PDZ Domain Containing 1
FWK	Fetal Week
GALNT7	UDP-N-Acetyl-Alpha-D-Galactosamine:Polypeptide N-Acetyl Galactosaminyl Transferase 7
Gβ5	G Protein Beta 5
GCAP	Guanylate Cyclase-Activating Protein
GCL	Ganglion Cell Layer
GDP	Guanosine Diphosphate
GDPβS	Guanosine 5′-[B-Thio]Diphosphate
GFP	Green Fluorescent Protein
GLB1L2	Galactosidase, Beta 1-Like 2
GMP	Guanosine Monophosphate
GPR	G Protein Regulatory
GPSM1	G-Protein Signaling Modulator 1
GPSM2	G-Protein Signaling Modulator 2
GRNA	Guide RNA
GTP	Guanosine Triphosphate
GTPγS	Guanosine 5'-O-(3-Thiotriphosphate)
HEK293	Human Embryonic Kidney Cells 293
HPRT	Hypoxanthineguanine Phosphoribosyltransferase
HR	Hour
IHC	Immunohistochemistry
INDEL	Insertion/Deletion
INL	Inner Nuclear Layer
IP	Immunoprecipitation
IPL	Inner Plexiform Layer

IS	Inner Segment
ISH	In Situ Hybridisation
KDA	Kilodalton
KIND	Kinase Non-Catalytic C-Lobe Domain
KLH	Keyhole Limpet Hemocyanin
L-	Long Wavelength
M-	Medium Wavelength
μM	Micrometer
MRNA	Messenger RNA
MS	Millisecond
N-	Amino Terminus
NHEJ	Non-Homologous End Joining
NR1D1	Nuclear Receptor Subfamily 1, Group D, Member 1
NR2E3	Nuclear Receptor Subfamily 2, Group E, Member 3
NRL	Neural Retina Leucine Zipper
OCT	Optimal Cutting Temperature
ONL	Outer Nuclear Layer
OPL	Outer Plexiform Layer
OS	Outer Segment
OTX2	Orthodenticle Homeobox 2
P	Postnatal Day
PAX6	Paired Box 6
PBS	Phosphate-Buffered Saline
PCR	Polymerase Chain Reaction
PDE	Phosphodiesterase
PDZ	Psd-95/Dlg1/Zo-1
PFA	Paraformaldehyde

PKCα	Protein Kinase C Alpha
QPCR	Quantitative PCR
RACE	Rapid Amplification of Cdna Ends
RD1	Pde6b$^{-/-}$Retinal Degeneration Model
RGS9	Regulator Of G-Protein Signalling 9
RIPA	Radioimmunoprecipitation Assay Buffer
RNA	Ribonucleic Acid
RORβ	RAR-Related Orphan Receptor Beta
RP	Retinitis Pigmentosa
RPE	Retinal Pigment Epithelium
RPE65	Retinal Pigment Epithelium 65
S	Second
S-	Short Wavelength
SHH	Sonic Hedgehog
SHRNA	Small Hairpin RNA
SYBR	N',N'-Dimethyl-N-[4-[(E)-(3-Methyl-1,3-Benzothiazol-2-Ylidene)Methyl]-1-Phenylquinolin-1-Ium-2-Yl]-N-Propylpropane-1,3-Diamine
TPR	Tetratricopeptide
TRβ2	Thyroid Hormone Receptor Beta 2
TSS	Transcription Start Site
TUNEL	Terminal Deoxynucleotidyl Transferase Dutp Nick-End Labeling
Tα	Transducin Alpha Subunit
Tβγ	Transducin Beta Gamma Subunits
UTR	Untranslated Region
V	Volt
X G	Number of Times The Gravitational Force, G
ZT	Zeitgeber Time

Statement of originality

I declare that the data presented in this thesis is my own original work, with exception of the experiments in the sections listed below, which were done in collaboration with the following scientists:

Chapter 2:

- Flow-sorting of photoreceptors and library preparations (Sections 2.2.2, Figure 2.1) were carried out by Hyun-Jin Yang and Jung-Woong Kim.
- RNA-seq read mapping, FPKM normalisation, and Cuffdiff analysis was performed by Jerome Roger (Sections 2.2.2, Figure 2.1).

Chapter 3:

- RNA-seq analysis in Figure 3.3 was performed by Matthew Brooks.
- Subretinal injections in Figure 3.7 were performed in collaboration with Thad Whitaker.
- DNase-seq, Nrl ChIP-seq, and Crx ChIP-seq reads were aligned by Vijender Chaitankar (Section 3.2.13.1, Figure 3.9).

Chapter 4:

- Peptide conjugation and immunisations for custom antibody production were performed by CoCalico Biologicals (Section 4.2.5, Figure 4.3).
- cDNA samples for circadian qPCR were isolated by Christiana Katti and Sumathi Sekaran (Section 4.2.6, Figure 4.7).

Chapter 5:

- CRISPR gene editing was performed by the National Eye Institute Genetic Engineering Core (Section 5.2.3, Figure 5.1, Figure 5.4).
- E14.75 embryo dissections in Figure 5.3 were performed in collaboration with Thad Whitaker.
- Maximum a-wave values in Figure 5.9 were extracted from R-scripts generated by Matthew Brooks and Thad Whitaker.

Abstract

Vision loss from retinal degeneration is largely associated with the death or dysfunction of photoreceptor cells (rods and cones). Many therapeutic approaches are thus targeted toward protecting against cell death or replacing photoreceptors, as no new rods or cones are formed after maturation. It is not completely understood why rods seem to be more vulnerable to disease than cones, yet a precocious degeneration of rods often leads to a secondary loss of cone function and severe visual defects. A more thorough understanding of the molecular mechanisms contributing to proper rod photoreceptor development and function are therefore necessary for advancing the development of more effective treatments for vision-related diseases.

We hypothesised that genes dramatically increasing in expression during rod photoreceptor development and regulated by key rod transcription factors would play a substantial role in the functional maturation and homeostasis of these cells. Using temporal RNA-seq transcriptome data from purified photoreceptors, we identified *Frmpd1* (FERM and PDZ domain containing 1) as a novel gene associated with rod development. An investigation of the regulatory mechanisms of *Frmpd1* revealed that transcription of this gene is initiated from a unique retina-specific alternative promoter, which is modulated by key rod transcription factors Nrl (neural retina leucine zipper) and Crx (cone-rod homeobox). Interestingly, a CRISPR/Cas9-mediated genomic deletion of this alternative promoter resulted in a retina-specific deletion of *Frmpd1* at both the RNA and protein levels.

Subsequent analyses of Frmpd1 demonstrate that it localises to the inner segments and synapses of rod photoreceptors, where it interacts with the key

phototransduction component transducin and its effector Gpsm2 (G-protein signalling modulator 2). *Frmpd1*$^{-/-}$ mice exhibit a delayed return of transducin to outer segments following light adaptation, and a delay in the recovery of rod photoresponse after a moderate visual pigment bleach. Frmpd1 thus appears to play a role in the maintenance of rod homeostasis through mediating the adaptive response of rods following light exposure, making it an interesting potential therapeutic target for better preserving both natural and stem-cell derived photoreceptors to restore vision. Moreover, these studies demonstrate the novel approach of targeting tissue-specific promoters by CRISPR-Cas9 to generate tissue-specific knockdown mouse lines.

1

Introduction

1.1 The mammalian retina

The retina, a thin layer of tissue lining the inner part of the eye, is responsible for capturing and converting light signals from the environment into electrical signals and passing these on to the brain to be interpreted as visual images (reviewed in Rodieck and Nirenberg 1973). All vertebrate retinae consist of three cell body layers divided by two neuropils where synaptic connections between cells occur (Figure 1.1). Farthest towards the back of the eye is the outer nuclear layer where the cell bodies of photoreceptors are located, followed by the inner nuclear layer containing the cell bodies of bipolar, horizontal, and amacrine cells, and closest to the vitreous body of the eye is the ganglion cell layer where the cell bodies of both ganglion cells and displaced amacrine cells are located (Kolb, 1995b). The axons of the ganglion cells converge to form a bundle known as the optic nerve, transmitting the information captured by the retina to the brain for further processing.

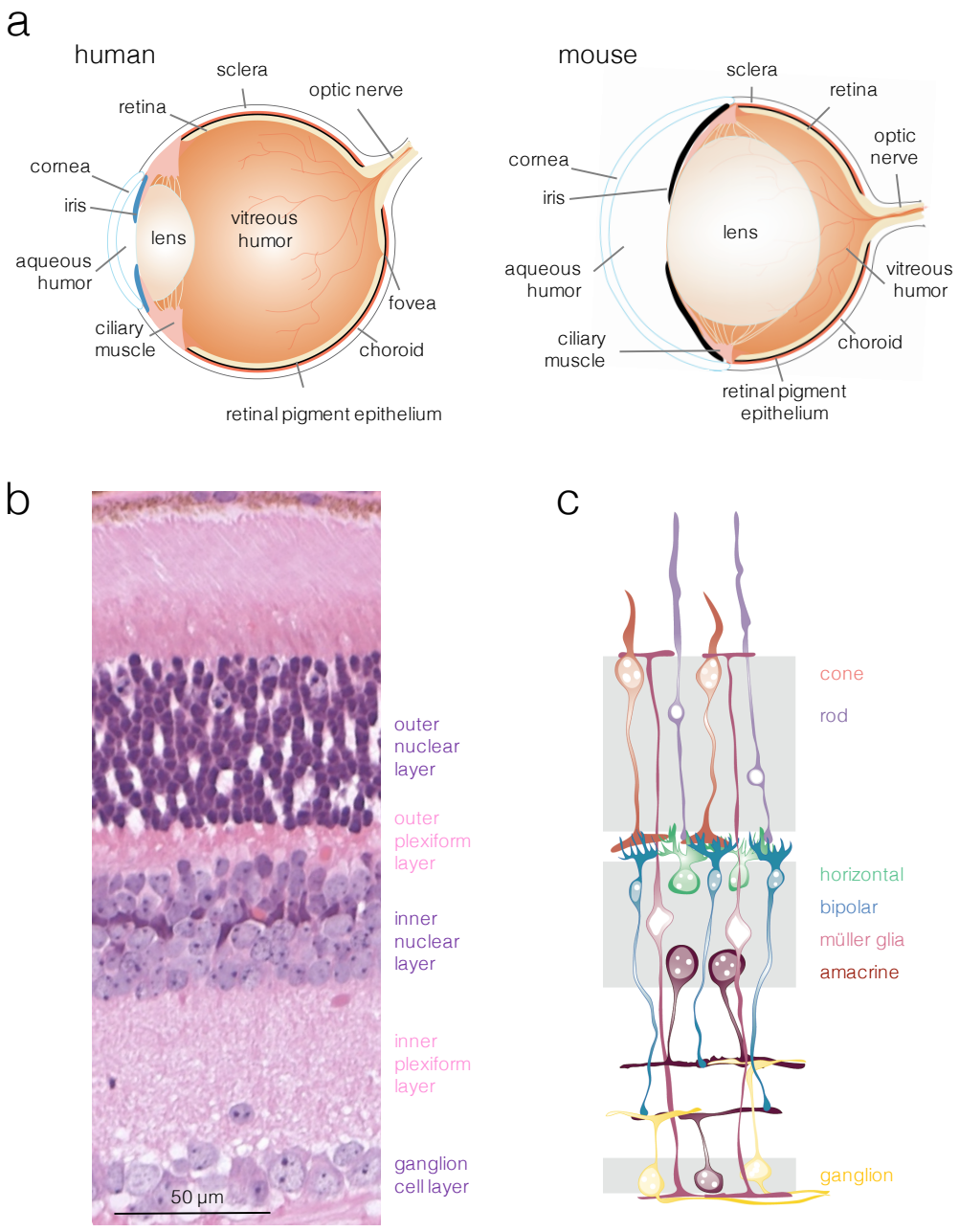

Figure 1.1: Mammalian retina anatomy. (A) Cross-sections of the human and mouse eye. Light travels through the clear cornea and is focused by the lens (adjusted by the ciliary muscle) onto the retina. In humans and primates, most light is focused onto the cone-rich fovea which mice lack. (B) Nuclear layers of the retina. Haematoxylin and eosin staining of P21 mouse retina cross-section showing the three cell layers (outer nuclear layer (ONL), inner nuclear layer (INL), and ganglion cell layer (GCL)) separated by the two neuropils (outer plexiform layer (OPL), inner plexiform layer (IPL)) where synaptic connections between cells occur. (C) Cell types of the retina. Rod and cone photoreceptors form synaptic connections with bipolar and horizontal cells in the OPL. Bipolar cells carry their signals to the amacrine and ganglion cells in the IPL, then ganglion cell axons carry signals to the brain via the optic nerve. Müller glia provide structural support to the other retinal neurons. Figure adapted from (Veleri et al., 2015).

The photoreceptors in the outer nuclear layer consist of rods and cones, which contact the retinal pigment epithelium and serve distinct functions (Swaroop et al., 2010). Rods function only in low light and are extremely sensitive to even a single photon, while cones are responsible for bright light vision and can produce high-resolution images (Swaroop et al., 2010). While there is only one type of rod photoreceptor in the mammalian retina, there are multiple types of cone photoreceptors classified by the visual opsin pigment they possess. Opsins consist of a transmembrane G protein-coupled receptor protein paired with a non-protein chromophore retinal; each photoreceptor type expresses a unique opsin pigment that responds maximally to a specific wavelength of light, thus helping to differentiate between colors (Kolb, 1995a). Rods contain rhodopsin, which in humans is maximally sensitive to light with a wavelength of 500 nm (Wald and Brown, 1958). L-cones, M-cones, and S-cones contain opsins maximally sensitive to 560 nm (L-opsin), 530 nm (M-opsin), and 430 nm (S-opsin) respectively (Schnapf et al., 1987, Solomon and Lennie, 2007). The ratio of rods to cones and the composition of each cone type vary by species, as does their spatial distribution within the retina.

In humans, rods greatly outnumber the cones (~92 million rods vs 4.6 million cones) (Curcio et al., 1990), yet as a diurnal species cone-dominated vision is relied on more heavily. Unlike many other species, the human (and primate) retina contains a small area of densely packed cone photoreceptors known as the fovea, which is located in the macula near the centre of the retina (Figure 1.1) (Kolb, 1995b). It is this region that allows for high resolution central daylight vision. Much of the cone density is concentrated within the macula and fovea in humans, leaving the peripheral retina largely rod-dominated. Non-primate mammals such as mice, however, lack a

fovea and macula and have a more regular distribution of rods and cones across the retina (albeit still highly rod-enriched, with only about 3% of the photoreceptors being cones) (Carter-Dawson and LaVail, 1979a). Mice lack L-opsin, while M- and S-opsin expression exhibits a dorsoventral gradient across the retina with most cones expressing varying amounts of both visual pigments responsive to 359 nm (S-opsin) and 505 nm (M-opsin) (Applebury et al., 2000). Despite the anatomical differences of human and murine retina, many aspects of the differentiation and homeostasis of photoreceptors in both species are highly conserved, and the mouse has proven to be a very useful model system for the study of photoreceptor development and disease (Veleri et al., 2015, Chang, 2013).

1.2 Photoreceptor differentiation

Despite the complexity and diversity of cell types within the retina, all retinal cells arise from common pools of progenitors that differentiate at various time points (Figure 1.2). The differentiation program is dependent on a variety of transcription factors, specific combinations of which can direct a cell towards a particular fate by restricting the competence (multipotent potential) of the cell at a given time point. One of the earliest events in photoreceptor development is the restriction of retinal progenitor cells to a photoreceptor fate through Notch signalling: high Notch levels encourage the cycling of progenitor cells, while inhibition of Notch leads the cells to commit to photoreceptor fates (Yaron et al., 2006, Jadhav et al., 2006). Reinforcing this generic photoreceptor lineage are the transcription factors Otx2 (orthodenticle homeobox 2) and its downstream target Crx (cone-rod homeobox) (Nishida et al., 2003). From this point there is a battle for transcriptional dominance which

determines which type of photoreceptor a precursor will become: a rod, S cone, or L/M cone (Swaroop et al., 2010) (Figure 1.3). It is believed that photoreceptor precursor cells are inclined to become S-cones by default as a result of early Crx and Rorβ (RAR-related orphan receptor beta) induction of S-opsin (Srinivas et al., 2006). However, Rorβ can also upregulate Nrl (neural retina leucine zipper) expression and vice-versa in a feedback activation loop (Kautzmann et al., 2011, Fu et al., 2014, Jia et al., 2009). If enough functional Nrl is produced during this process, the cell may be redirected to a rod cell fate which is then reinforced by an Nrl-Nr2e3 (nuclear receptor subfamily 2, group E, member 3) complex that activates rod while suppressing cone genes (Oh et al., 2008, Cheng et al., 2004). In the event that there is not enough active Nrl produced to cause the cell to differentiate into a rod, then the precursor continues developing as a cone: either an S-cone by default, or as an M-cone by Trβ2 (thyroid hormone receptor beta) induction of M-opsin expression (Roberts et al., 2006). In humans, there is a third type of cone photoreceptor, L-cones, which develop as a result of stochastic selection between the L- and M- opsin gene by an upstream locus control region (the two genes are located next to each other on the same chromosome) (Wang et al., 1999, Smallwood et al., 2002).

Gene regulatory events governing retina development and homeostasis after cell type differentiation involve a variety of mechanisms including transcription factor binding, epigenetic regulation, extrinsic signalling, posttranslational modifications, and alternative splicing and promoter usage. As with other components of the central nervous system, alternative splicing is particularly common in the retina and recent reports have shown that alternative promoter usage and novel transcripts are abundant in this tissue (Popova et al., 2017, Farkas et al., 2013). Even the rod

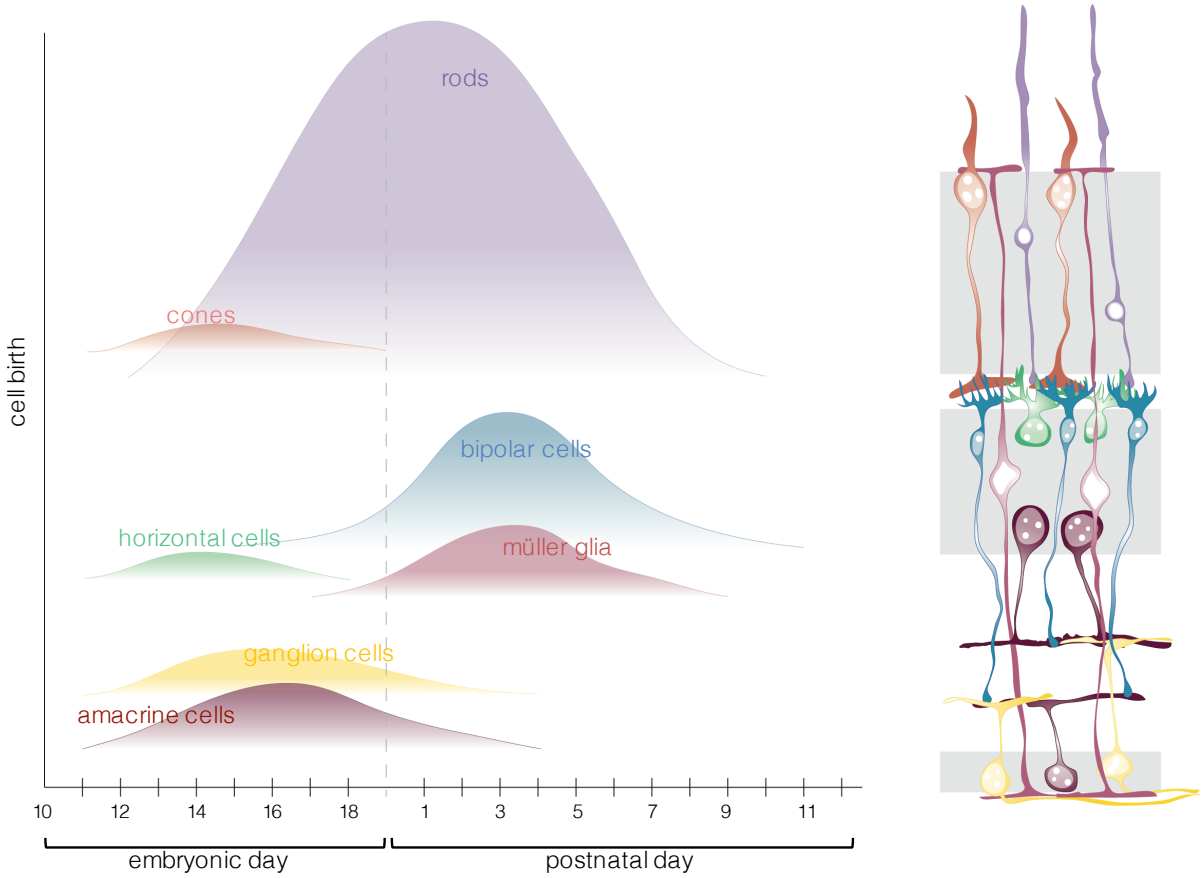

Figure 1.2: Mouse retinal cell type birth order. Murine retinogenesis occurs in a stereotyped order, beginning prenatally as early as embryonic day (E)10 and continuing several postnatal days (P) after birth before eye opening at P14. The relative number of cells born at each age is depicted by each curve. Most cone photoreceptors and inner retinal neurons differentiate prenatally, while the majority of rod photoreceptors, Müller glia, and bipolar cells are formed postnatally. Figure adapted from (Young, 1985).

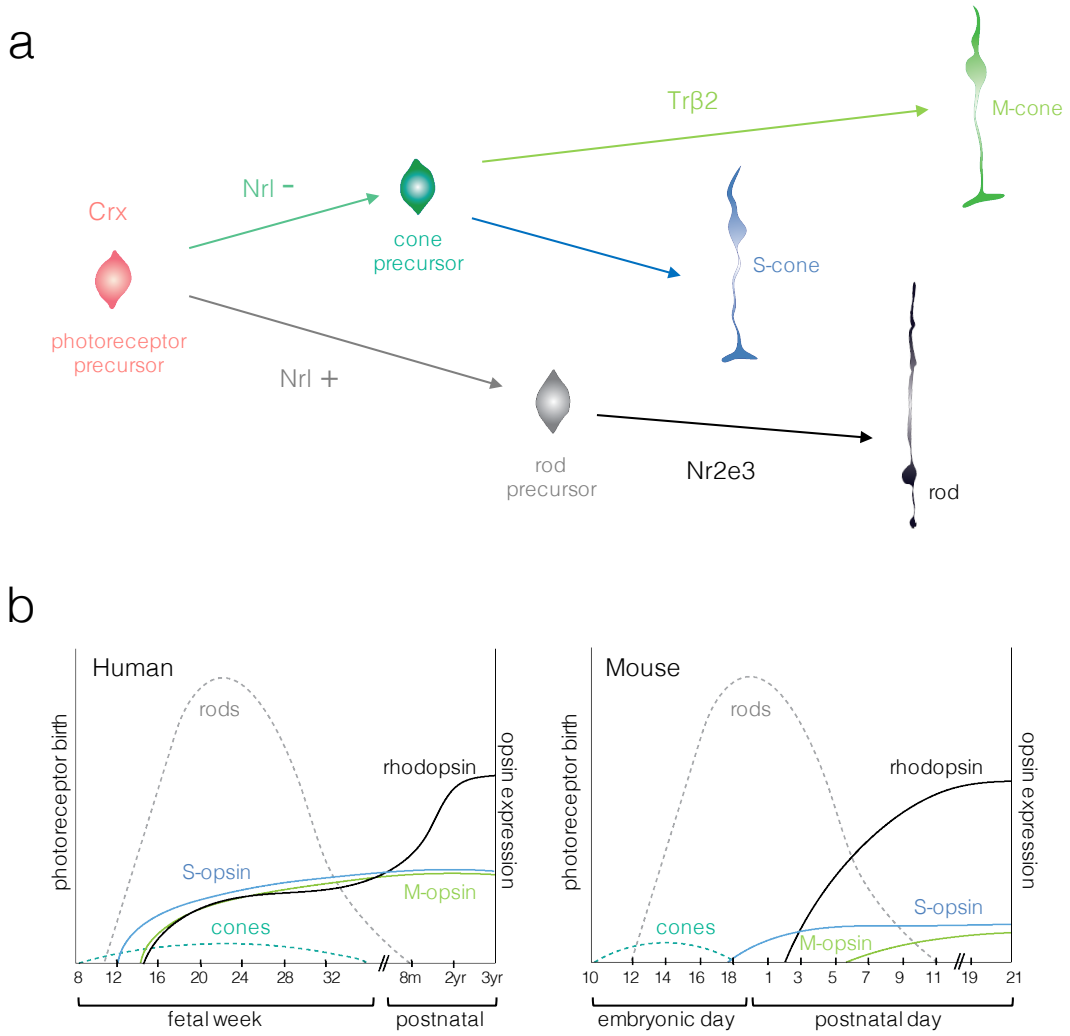

Figure 1.3 Photoreceptor differentiation in humans and mice. (A) Rod and cone photoreceptors both develop from a common postmitotic precursor expressing Crx (cone-rod homeobox). Precursors expressing Nrl (neural retina leucine zipper) develop as rod photoreceptors through induction of rod-specific genes by additional downstream effectors such as Nr2e3 (nuclear receptor subfamily 2, group E, member 3). Precursors not expressing Nrl develop as either S-cones or M-cones through induction of cell-specific gene signatures by downstream transcription factors Rorβ (RAR-related orphan receptor beta) and Trβ2 (thyroid hormone receptor beta 2), respectively. Adapted from Oh et al., 2007 (Oh et al., 2007). (B) Rod and cone precursors (dashed lines) exit the cell cycle, with cone cell birth preceding that of rods. In humans, rod precursors can be identified from fetal week (fwk) 10.5 with rhodopsin expression beginning at fwk 15(Hendrickson et al., 2008), whereas cone precursors can be identified from fwk 8 with S- and M- opsin expression beginning at fwk 12 and 15, respectively (O'Brien et al., 2003). Expression of opsins reach adult levels by 3 years of age. In mice, rods are born around embryonic day (E)12 (peak between postnatal day (P)0-2) with rhodopsin expression beginning at P2 (Carter-Dawson and LaVail, 1979b). Cones are born as early as E11 (peak between E13-14), with S- and M- opsin expression beginning at E18 and P6, respectively (Carter-Dawson and LaVail, 1979b). Expression of opsins reach adult levels by P21. Figure adapted from (Besharse et al., 2010).

photoreceptors have been shown to possess unique cell-specific transcript variants of many genes (Popova et al., 2017). This is likely a result of the highly specialised function and unique demands of these cells.

1.3 Photoreceptor morphology and development

The rod and cone photoreceptors, while similar in many regards, do vary considerably in their morphology (Figure 1.4). Both cell types consist of a basic structure composed of a cell body containing the nucleus, inner and outer segments separated by a connecting cilium, and an axon leading to the synaptic ending. As their names suggest, rod photoreceptors have longer, rod-shaped outer segments whereas cones have shorter, cone-shaped outer segments (Carter-Dawson and LaVail, 1979a). The opsin pigments (rhodopsin in rods and M- and/or S-opsin in mouse cones) are densely packed within disc membranes in the outer segment to allow for efficient light capture as photons pass through the retina before being absorbed by the adjacent retinal pigment epithelium (Dell'Orco, 2013). In cones, these disc membranes are contiguous with the outer plasma membrane and exposed to the extracellular space, while in rods the outer segment discs are stacked together and contained within the plasma membrane much like thylakoids in a chloroplast (Carter-Dawson and LaVail, 1979a, Mustafi et al., 2009).

Outer segment proteins are transported across the connecting cilium to their final destinations after being produced in the inner segments, which are split into two regions: an ellipsoid region containing mitochondria to meet the high energy demands of the cells, and a myoid region for protein synthesis containing ribosomes, endoplasmic reticulum, and the golgi body (Wheway et al., 2014).

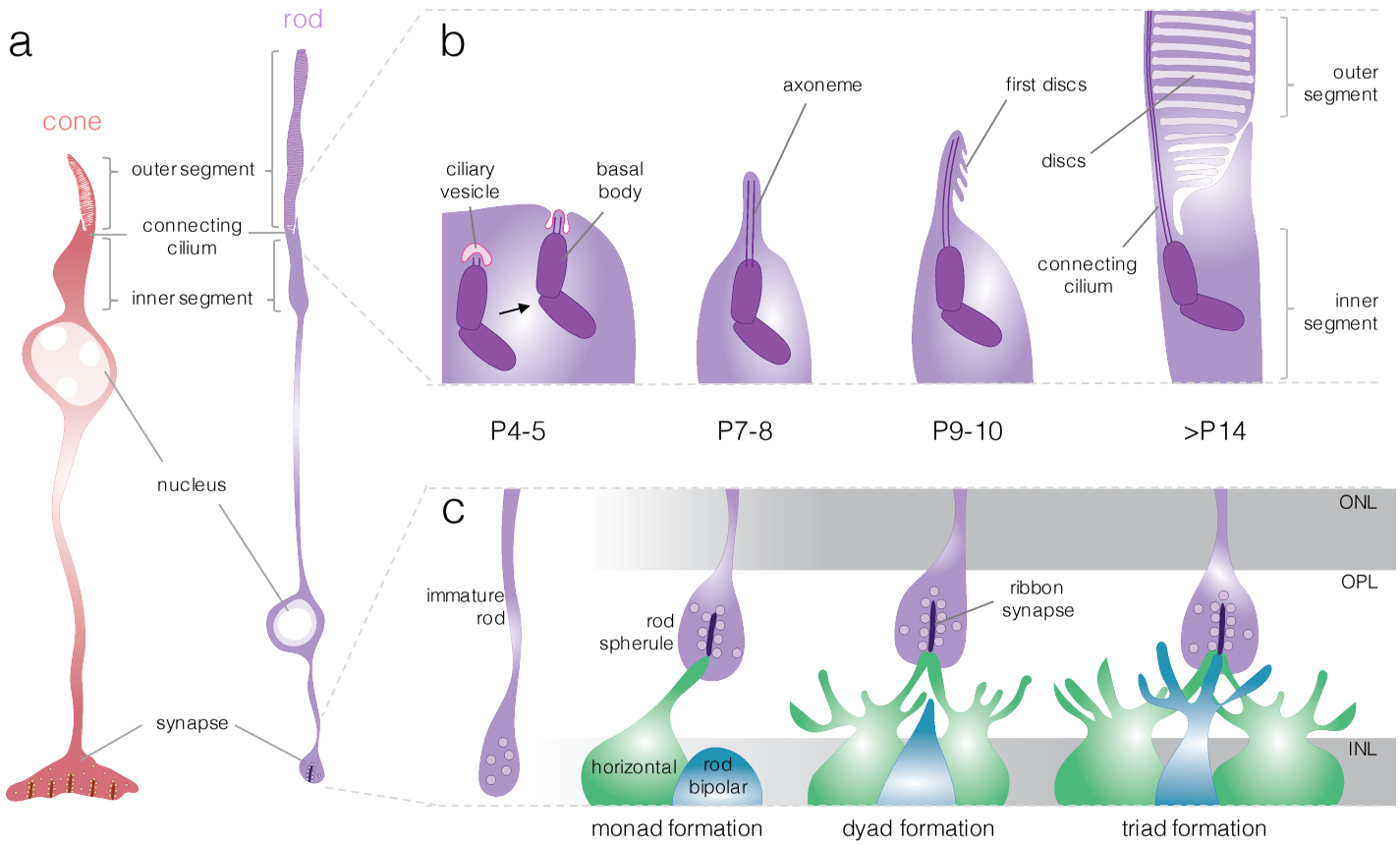

Figure 1.4: Photoreceptor morphogenesis. (A) Schematic representation of rod and cone photoreceptors, which share several features. Both have outer segments where phototransduction takes place, inner segments where mitochondria are localised and protein synthesis occurs, and a connecting cilium for traffic of proteins across the two segments. The synapses of cones (pedicles) contain multiple ribbon synapses, and the synapses of rods (spherules) only have one. (B) Rod ciliogenesis. The primary connecting cilium in rods is formed over the course of several days spanning from postnatal day (P)4-14. The axoneme is derived from paired centrioles and outer segment discs arise from membrane vesicles. Adapted from (Salinas et al., 2017)(C) Rod synaptogenesis. The maturation of the rod spherule and its connections with neurons in the inner nuclear layer (INL) occurs over the course of several days postnatally. As the outer nuclear layer (ONL) is formed, immature spherules become restricted to the outer plexiform layer (OPL) where they first form monad contacts with horizontal cells. After dyad formation with two horizontal cells, a bipolar cell invaginates the rod spherule to form a triad. Adapted from (Sherry et al., 2003).

The positioning and chromatin organisation of nuclei differ considerably between rods and cones. The nuclei cones possess several chromocentres and tend to lie on the scleral side of the outer nuclear layer, while rod cell bodies contain a single dense chromocentre and are spaced throughout the remainder of the outer nuclear layer (Carter-Dawson and LaVail, 1979a, Solovei et al., 2009).

The synapses are distinct as well; rods have a smaller spherule structure that generally contains a single ribbon synapse (a specialised structure which holds vesicles close to the active zone for rapid release), whereas cones have a larger pedicle structure that can contain dozens of ribbon synapses (Mercer and Thoreson, 2011). Rod spherules tend to lie closer to the cell bodies in the outer nuclear layer, while cone pedicles rest below these closer to the inner nuclear layer (Carter-Dawson and LaVail, 1979a).

Synaptogenesis in the murine retina is an orderly process that begins before eye opening and continues for several days postnatally (Figure 1.4). Amacrine and ganglion cell synapses (IPL) occur first post-natal day 1-3 (P1-3), followed by connections between photoreceptors and horizontal cells (OPL) (P4-P9), then by connections of bipolar cells with photoreceptors and ganglion cells (IPL) (P10-11) (Morgan and Wong, 1995, Olney, 1968). Most photoreceptor synaptic connectivity develops after P6. During early stages, ~80% of the rod synapses and some cones project past the OPL and into the IPL (with amacrine cells as the predicted targets) (Johnson et al., 1999). Upon maturation, however, the photoreceptor synapses retract to the OPL (Johnson et al., 2001). Ribbon synapse formation is initiated between P4-5 (cones) or P8 (rods) when the photoreceptor terminals enter the OPL and form monad contacts with horizontal cells. Starting at P6 (cones) or P9 (rods), an

additional horizontal cell invaginates the terminal to form a dyad, followed by recruitment of a bipolar cell to form a triad beginning at P7-8 (cones) or P10 (rods) (Sherry et al., 2003, Olney, 1968, Blanks et al., 1974, Rich et al., 1997). By eye opening (P14), ribbon synapse formation is complete (Olney, 1968, Fisher, 1979).

Photoreceptor biogenesis also involves formation of the inner and outer segments, which occurs in several stages spanning the first postnatal month of development (Figure 1.4). Rod cell birth peaks from P0-P2 (Carter-Dawson and LaVail, 1979b), after which ciliogenesis followed by outer segment formation begins in several stages not necessarily synchronised amongst cells (Tokuyasu and Yamada, 1959, De Robertis, 1956, Sorokin, 1962, Sorokin, 1968, Sedmak and Wolfrum, 2011, Greiner et al., 1981). First, paired centrioles (a mother and daughter centriole) are recruited to the apical surface of postmitotic precursor cells (Sedmak and Wolfrum, 2011, Wheway et al., 2014, Tokuyasu and Yamada, 1959, Sorokin, 1962). The mother centriole of differentiating photoreceptors matures into a basal body with distal (projecting into the membrane of the primary vesicle) and sub-distal (projecting into the cytoplasm) appendages (Sedmak and Wolfrum, 2011, Wheway et al., 2014, Tokuyasu and Yamada, 1959, Sorokin, 1962). Next, a ciliary bud is formed from the distal appendage to form a ciliary shaft projecting into the ciliary vesicle, which has formed from the primary vesicle (Sedmak and Wolfrum, 2011, Wheway et al., 2014, Tokuyasu and Yamada, 1959, Sorokin, 1962). Eventually, the ciliary vesicle fuses with the plasma membrane as the cilium continues to grow (axoneme), leaving a small ciliary pocket at the base of the ciliary shaft (Sedmak and Wolfrum, 2011, Wheway et al., 2014, Tokuyasu and Yamada, 1959, Sorokin, 1962). The distal part of the cilium continues to grow as membrane vesicles form, later fusing to form disc membranes of

the outer segments (Sedmak and Wolfrum, 2011, Wheway et al., 2014, Salinas et al., 2017).

The adult murine photoreceptor outer segments measure approximately 23.6 x 1.4 μm and 13.4 x 1.2 μm for rods and cones, respectively (Carter-Dawson and LaVail, 1979b). Rods continually renew their outer segments, with new discs being formed at the base of the outer segment and old discs being shed and phagocytosed by the RPE (LaVail, 1976). The length of rod outer segments increases most rapidly during development from P11-P17, reaching its final adult length between P19-P25 (LaVail, 1973). Because these outer segment discs are packed with key phototransduction proteins such as rhodopsin (over 90% of the protein in disc membranes (Filipek et al., 2003)) transducin, and others (see Section 1.4, below), it is not surprising that these genes are highly upregulated in rods during the same period of development. Most of these genes are also known to be upregulated by key rod transcription factors Nrl and Crx (Hao et al., 2012), and even further augmented by Nrl's downstream target Nr2e3 whose expression is also dramatically upregulated after P6 (Cheng et al., 2006).

1.4 Phototransduction and the visual cycle

In contrast to other neurons which depolarise and release neurotransmitter in response to a stimulus, rod photoreceptors are constitutively releasing glutamate in the dark and hyperpolarise when presented with a light stimulus (Purves, 2001). It is thus a cessation of glutamate release at the synapse that signals to downstream bipolar and horizontal cells that a stimulus has been detected. The initial light capture and triggering of the phototransduction cascade occurs in the outer segments on disc

membranes (Figure 1.5) (reviewed in Arshavsky et al. 2002 and Burns 2010). In rods, the visual pigment rhodopsin is coupled to 11-cis retinal derived from vitamin A (Wald and Hubbard, 1950, Wald et al., 1950). When stimulated by a photon of light, the 11-cis retinal is isomerised to all-trans retinal, which induces a structural change in rhodopsin allowing it to activate its downstream effectors (Wald et al., 1950). An activated rhodopsin molecule then contacts the alpha subunit of holotransducin (alpha, beta, and gamma subunits of transducin bound together) on the disc membrane to prompt the alpha subunit to release GDP in exchange for cytosolic GTP (T_α^{GDP} to T_α^{GTP}) (Shichida and Morizumi, 2007). T_α^{GTP} then dissociates from the disc membrane and interacts with inhibitory gamma units of phosphodiesterase (PDE_γ), activating $PDE_{\alpha\beta}$ so that it can catalyse the hydrolysis of cyclic GMP to 5'-GMP (Wensel and Stryer, 1990). The reduced levels of cGMP caused by this cascade of events causes sodium channels on the rod plasma membrane to close, hyperpolarising the cell thus causing voltage-gated calcium channels to close as well (Karpen et al., 1988). The calcium level drop prevents glutamate-containing vesicles in the presynaptic terminal from releasing their contents, signalling to downstream bipolar and horizontal cells the detection of a light stimulus (Witkovsky et al., 1997). Interestingly, rods can generate graded changes in membrane potential, resulting in a graded inhibition of glutamate release depending on intensity of light detected (Witkovsky et al., 1997).

Following the activation of this phototransduction cascade, each activated component must be restored to an inactivated state so that it can readily respond to a fresh light stimulus (Figure 1.5). All-trans retinal is released from rhodopsin and shuttled to the retinal pigment epithelium (RPE), where it is isomerised back to 11-cis

retinal in a process referred to as the “visual cycle” (Wald, 1968, Dowling, 1960). First, an ATP binding cassette transporter moves all-trans retinal complexed with phosphatidylethanolamine from the rod disc bilayer and releases it into the sub-retinal cytoplasm (Tsybovsky et al., 2010, Liu et al., 2000). Here, all-trans retinal is converted to all-trans retinol by all-trans retinol dehydrogenase, then transported to the RPE by interphotoreceptor retinoid binding protein (Parker and Crouch, 2010, Gonzalez-Fernandez, 2002). In the smooth endoplasmic reticulum of the RPE, all-trans retinol is converted to 11-cis retinal in a series of enzymatic reactions catalysed by LRAT, RPE65, and 11cRDH, with intermediates shuttled by CRBP and CRALBP (reviewed in (Kiser et al., 2014). Finally, interphotoreceptor retinoid binding protein then transports 11-cis retinal back to the rod outer segments where it can be conjugated again to rhodopsin (Gonzalez-Fernandez, 2002).

Meanwhile, T_{α} hydrolyses its bound GTP molecule to GDP with the help of GTPase accelerating protein, reassociating with $T_{\beta\gamma}$ on the disc membrane to assemble holotransducin ready to be activated again by rhodopsin (Makino et al., 1999, He et al., 1998). Rhodopsin itself is deactivated via phosphorylation by rhodopsin kinase, which reduces its affinity for T_{α} (rhodopsin kinase is released from its inhibitor recoverin during the calcium drop in an activated rod) (Palczewski et al., 1992, Ames et al., 2006, Krupnick et al., 1997). Arrestin then binds to the phosphorylated rhodopsin to fully inactivate it (Kuhn and Wilden, 1987). During all of this, guanylate cyclase activating protein (GCAP) releases its bound calcium ions because of the calcium drop and instead interacts with guanylate cyclase to induce the production of cGMP (Burns et al., 2002). This rise in cGMP re-opens the sodium channels to depolarize the cell and return it to its dark-adapted state (Molday and Molday, 1998).

Rods and cones use similar general pathways for phototransduction, with some protein isoform differences as summarised in Table 1.1.

When exposed to light for extended periods of time, most of the rhodopsin molecules become "bleached" and unresponsive to additional light stimuli (Figure 1.4) (Hubbard, 1958). To avoid becoming saturated under such conditions, several changes occur in the rods, making them less sensitive to the background light levels and allowing them to re-establish (at least partially) a circulating current. Among these changes is the light-driven translocation of several components of the phototransduction cascade such as transducin, arrestin, recoverin, Rgs9-1, and Gβ5 (Artemyev, 2008, Sommer et al., 2014, Strissel et al., 2005, Tian et al., 2013) (Figure 1.6).

Table 1.1: Photoreceptor transduction protein isoforms in mouse rods and cones (Ingram et al., 2016).

Component	Rods	Cones
Photopigment	Rhodopsin	L,M, and S-opsin
G-protein (transducin)	α1, β1, and γ1	α2, β3, and γ8
Phosphodiesterase	Pda6a and Pde6b	Pde6c
	Rod Pde6γ (Pde6g)	Cone Pde6γ (Pde6h)
cGMP-gated channels	Cnga1 and Cngb1	Cnga3 and Cngb3
(Rhod)opsin kinase	Grk1	Grk1
Arrestin	Arrestin-1	Arrestin-1 and Arrestin-4
GAPs	Rgs9-1, Gβ5, and R9ap-1	Rgs9-1, Gβ5, and R9ap-1
Guanylyl cyclase	RetGC1 and RetGC2	RetGC1
GCAPs	Gcap1 and Gcap2	Gcap1
$Na^+/Ca^{2+}–K^+$ exchanger	Nckx1	Nckx2 and Nckx4

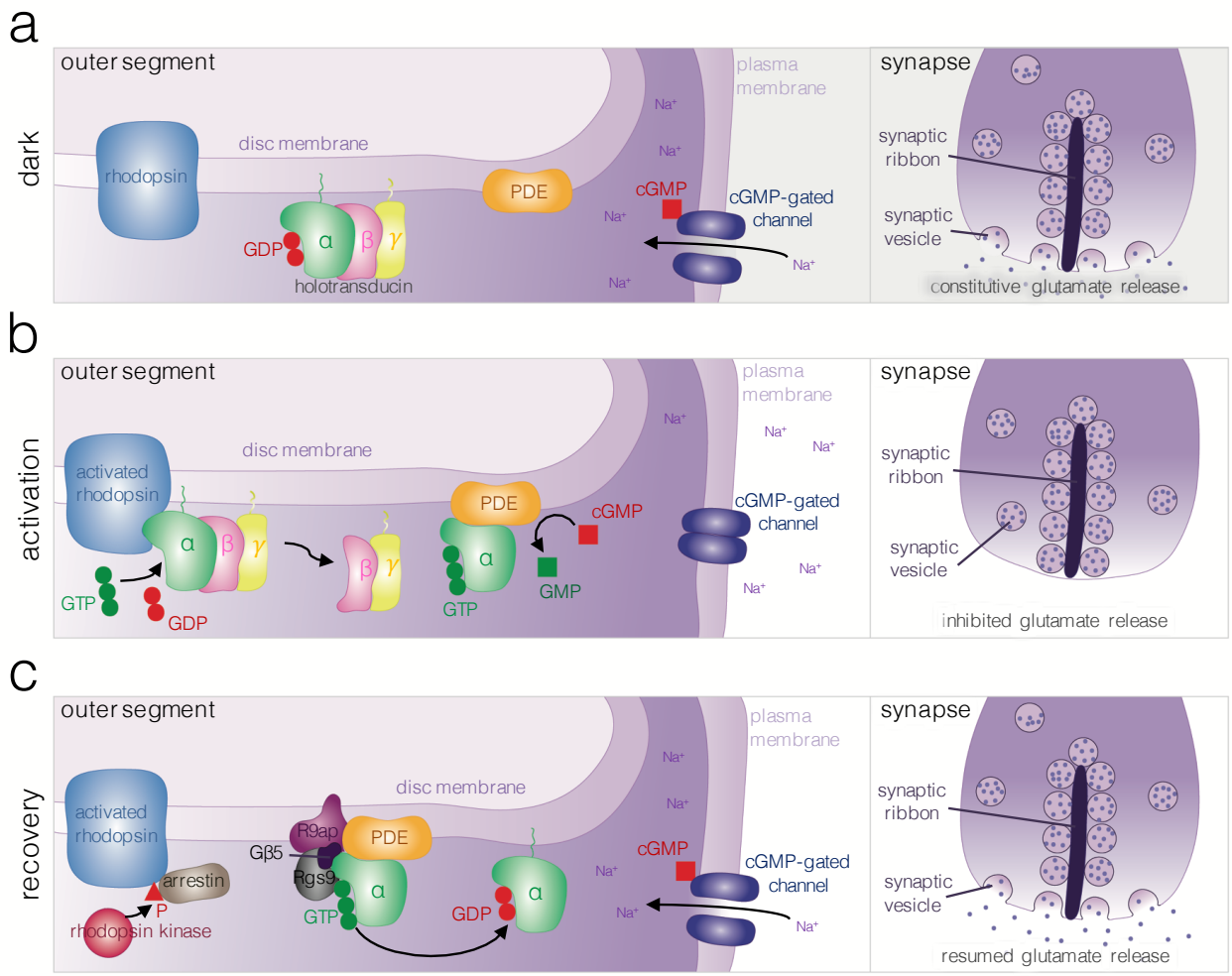

Figure 1.5: Rod phototransduction and recovery. (A) Dark-adapted steady state. In the absence of a light stimulus, an inactive form of holotransducin ($T_{\alpha\beta\gamma}$) is bound to guanosine diphosphate (GDP) on outer segment disc membranes. Cyclic guanosine monophosphate (cGMP) levels are high, which keeps cGMP-gated channels on the outer segment plasma membrane open to allow sodium ions (Na^+) into the cell. The depolarisation from intracellular Na^+ signals the release of glutamate from vesicles at the synapse. (B) Photoactivation. Rhodopsin is activated by a photon of light, causing it to interact with T_α. The release of GDP in exchange for cytosolic guanosine triphosphate (GTP) causes T_α to dissociate from $T_{\alpha\beta\gamma}$ and interact with phosphodiesterase (PDE). PDE activity reduces intracellular cGMP, thereby closing cGMP-gated channels on the plasma membrane. The hyperpolarisation of the cell inhibits the release of glutamate from the synapse, signalling to downstream neurons that a light stimulus has been detected. (C) Phototransduction recovery. Phosphate groups (P) are added to rhodopsin by rhodopsin kinase, promoting its interaction with arrestin to prevent re-association with T_α. The GTP group on T_α is hydrolysed to GDP by intrinsic GTPase activity of T_α, which is accelerated by a protein complex of PDE, Rgs9, Gβ5, and R9ap. Increased levels of cGMP by guanylyl cyclase re-opens cGMP-gated channels on the plasma membrane, and glutamate release from the synapse resumes. Figure adapted from (Burns and Arshavsky, 2005)



Figure 1.6: Light-dependent translocation of phototransduction components. In the dark-adapted state, all three transducin subunits (αβγ) are concentrated in rod outer segments, while Rgs9, Arrestin, and Gβ5 localise to the inner segments and synapses. Under certain light-exposure thresholds, a massive translocation of several proteins occurs. All three transducin subunits (αβγ) relocate to the inner segments and synapses, whereas Rgs9, Arrestin, and Gβ5 move to the outer segments

In a dark-adapted state, transducin and recoverin are most concentrated in the outer segments while arrestin, Rgs9-1, and Gβ5-L are located in other cellular compartments (Artemyev, 2008, Sommer et al., 2014, Strissel et al., 2005, Tian et al., 2013). Under extended exposure to certain thresholds of light, the two groups of proteins switch places so that arrestin, Rgs9-1, and Gβ5-L are more abundant in the outer segments while transducin and recoverin are distributed to the inner segments and synapses (Artemyev, 2008, Sommer et al., 2014, Strissel et al., 2005, Tian et al., 2013). The exact mechanism of the translocation of each molecule is still not completely understood, although one prevailing theory is that it occurs through diffusion with directional and light-dependent properties mediated by binding site "sinks" within the different compartments of the cell (Slepak and Hurley, 2008). It is thought that this movement of molecules serves as a type of "molecular sunglasses" to help tone down the sensitivity of rods to light, preventing them from being constitutively activated by high background illuminances by requiring greater light stimuli to activate them (Sokolov et al., 2002). This is hypothesised to serve a protective role in rod homeostasis by reducing the stress and high metabolic demands that would be induced by continuous and unnecessary activation of phototransduction in the rods under bright conditions where cone mediated-vision dominates (Elias et al., 2004).

1.5 Retinal degenerative diseases

The photoreceptors are critical for proper vision, and any dysfunction of these cells can be detrimental to an organism's sense of sight; this is particularly true for the terminally differentiated photoreceptors, which cannot be regenerated in mammals

(Wright et al., 2010). Unfortunately, retinal degeneration affects thousands of people each year. It is a heterogeneous disease both genetically and clinically, which combined with other complicating factors, makes it difficult to prevent and treat effectively (Sullivan and Daiger, 1996, Berger et al., 2010). Inherited retinal degenerative diseases can be classified broadly as either monogenic (Mendelian) or multifactorial (complex), with nearly 300 genes identified as retinal disease-causing to date. A summary of diseases and identified mutations can be found on RetNet (https://sph.uth.edu/retnet).

The most common type of inherited retinal degeneration is retinitis pigmentosa (RP), a leading cause of blindness affecting 1 in 3000-7000 individuals (an estimated 1.5 million people) worldwide that poses a significant burden on healthcare costs (Ferrari et al., 2011, Koberlein et al., 2013, Rein et al., 2006, Frick et al., 2012). Retinitis pigmentosa is a phenotypic description of several related inherited diseases causing photoreceptor degeneration that are characterised by concentrated spots or large areas of dark pigmentation in the fundus (Figure 1.7) (Hamel, 2006). The age of diagnosis, progression, and severity of the disease varies from patient to patient, as its underlying causes are complex and its genetic basis is widely variable (Figure 1.7). Initial symptoms generally present between the ages of 10-30 (but can occur anywhere from early infancy to late adulthood) and include impaired night vision and slow adjustment between dark/light environments (Alexander and Fishman, 1984, Gouras and MacKay, 1989, Hamel, 2006). More severe symptoms present as total night blindness and/or loss of peripheral vision as rods, which tend to atrophy first in RP, are concentrated in the outer region of the retina and are necessary for night vision (Hamel, 2006, Hartong et al., 2006). As the disease progresses, patients

experience increasing “tunnel vision” as peripheral rods become further compromised. In some cases, a secondary loss of cones leads to decreased visual acuity, loss of central vision as the macula degenerates, and ultimately blindness (Hamel, 2006, Hartong et al., 2006).

The underlying genetic basis of retinitis pigmentosa typically involves genes expressed in the photoreceptors and/or retinal pigment epithelium, and its inheritance can be described as autosomal recessive, autosomal dominant, X-linked, or even mitochondrial depending on the causative mutation(s) (Ferrari et al., 2011). Its causes are diverse, however, with 63 genes implicated as disease-causing to date and more being discovered each year with the advent of next-generation sequencing and improved diagnostic methods (https://sph.uth.edu/retnet; Ratnapriya and Swaroop 2013). Currently, clinical genetic testing is available for 111 of the most common factors including RHO, ABCA4, RPE65, RLBP1, RP1, PRPF8, PRPF3, and CRB1 (a complete list can be found at http://www.ouh.nhs.uk/services/referrals/genetics/genetics- laboratories/molecular-genetics-laboratory/services-by- disorder/documents/InheritedEyeDiseaseNGSServices.pdf). Unfortunately, while some steps can be taken to help manage the rate of progression of the disease, there is no known effective cure for RP and predictive testing serves more to help provide counselling and prepare patients with disease genotypes for the psychological and social consequences of progressive vision loss (Mezer et al., 2007).

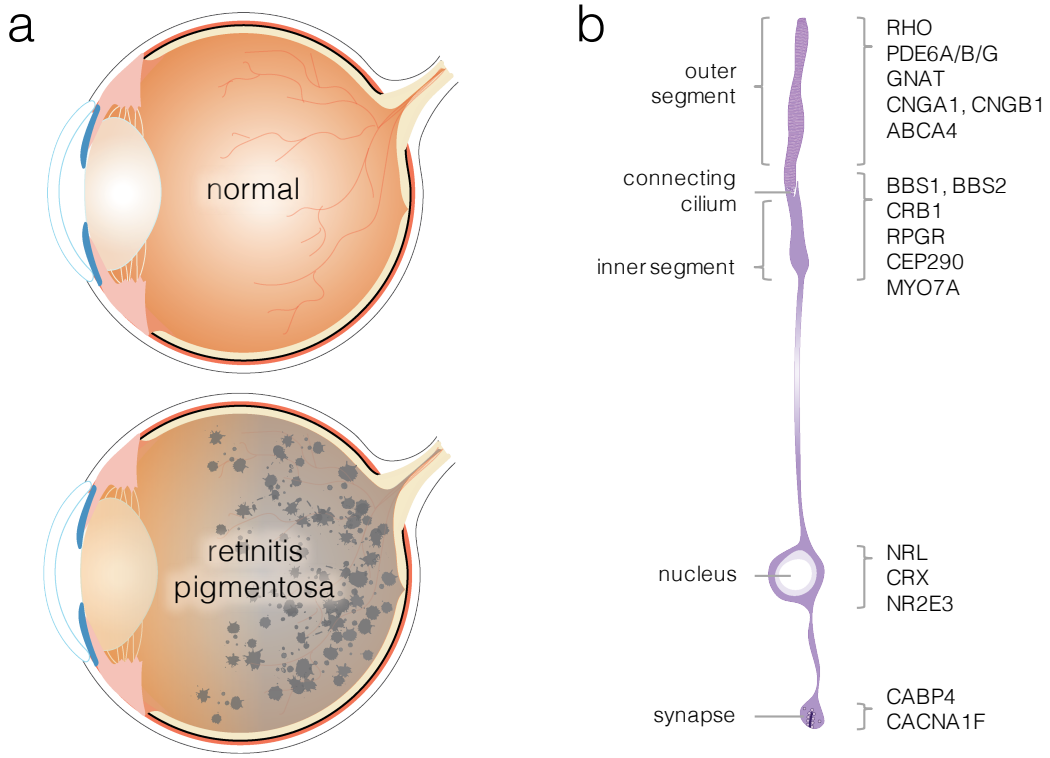

Figure 1.7: Rod photoreceptor disease. (A) Schematic of normal and retinitis pigmentosa-affected eyes. Widespread pigmentation can be observed in the retina of those affected by retinis pigmentosa. Dark "bone spicule" deposits of pigmentation can also be seen. (B) Localisation of several proteins associated with photoreceptor disease. Human mutations have been identified for genes encoding proteins localised in almost every rod cellular compartment, including the outer segment, connecting cilium, nucleus, and synapse. Many other mutations have also been identified and are described on RetNet (https://sph.uth.edu/ retnet/). Adapted from (Veleri et al., 2015).

1.6 Therapeutic approaches

While much of what causes the onset of retinal degeneration is yet to be elucidated, scientists have built upon what is known to develop several prospective treatment options - many of which are currently being evaluated in clinical trials with varying levels of success. Compared to other systems, the retina is particularly amenable to clinical testing by merit of its small size and accessibility, ocular immune privilege (ability to tolerate antigens without an inflammatory response) (Zhou and Caspi, 2010), and relative ease of assessing treatment efficacy by methods such as electroretinography and visual assessment tasks. Moreover, the retinal physiology of model organisms such as mice and dogs is often close enough to humans to provide appropriate disease models for preclinical testing (Veleri et al., 2015, Beltran, 2009). Current advances include the use of neuroprotective factors, antioxidants, drugs, and gene therapies to slow the progression of disease and/or rescue photoreceptor function; in advanced cases with widespread cell death, methods of completely replacing the photoreceptors with prosthetic devices or transplanted stem/progenitor cells are currently being investigated (Wright et al., 2010, Singh and MacLaren, 2011, Boye et al., 2013).

One of the most popular current efforts in developing therapeutics for inherited retinal disorders is that of gene replacement therapy, where viral or other shuttles (such as nanoparticles) are used to deliver normal copies of defective genes directly to the affected cells (Boye et al., 2013). The first successful example of this was in 2008 delivering the RPE65 gene to patients with congenital blindness caused by Leber's Congenital Amaurosis (Cideciyan, 2010, Cideciyan et al., 2008, Hauswirth et al., 2008, Bainbridge et al., 2008, Maguire et al., 2008). Additional clinical trials are

currently underway including those for X-linked Retinitis Pigmentosa, Choroideremia, Stargardt's Macular Degeneration, and Usher Syndrome (clinicaltrials.gov: NCT03116113, NCT01461213, NCT01367444, and NCT01505062, respectively).

Gene editing technologies such as CRISPR/Cas9 may be used to correct DNA mutations in patients' cells so that they can make functional protein "naturally" from their own permanently modified genome rather than having a copy delivered through gene replacement therapy. Much uncertainty surrounds this approach, however, as the method is still being pioneered and the consequences of off-target effects are not yet fully accounted for (Smith et al., 2017). The advent and subsequent popularity of CRISPR technologies have also reignited some longstanding legal and ethical issues with regards to genome editing in humans (Shinwari et al., 2017, Ishii, 2017, Krishan et al., 2016). One of the first human trials involving CRISPR technologies was initiated just last year in lung cancer patients in China (clinicaltrials.gov: NCT02793856). This trial involved *ex vivo* gene editing before the cells were returned to the body, but at least one new trial has been approved within the past few months that will attempt to edit human cells *in vivo* (clinicaltrials.gov: NCT03057912).

This is an exciting era for gene editing and replacement therapies, and while they do show much promise, we are still far from a "cure" for blindness. The heterogeneity of retinal degenerative diseases poses one of the greatest obstacles for designing effective treatments. Not only are there hundreds of individual genes implicated in retinal diseases, but oftentimes it is a combination or "snowball effect" of multiple inherited mutations exacerbated by environmental stressors that spur the onset of disease, in many cases only becoming apparent late in life. In some cases, the photoreceptors may be beyond repair, or even completely dead, before intervention

takes place. In instances such as these, transplanted photoreceptors or prosthetics may be a more viable option for restoring vision, although these remain areas of active research and have not yet been perfected (Singh and MacLaren, 2011).

The better we understand the complex pathways and interplay of risk factors contributing to retinal degeneration, the earlier we will be able to identify patients predisposed to these disorders and the more accurately we will be able to tailor their treatments (through "personalised medicine") to halt disease progression (Chan and Ginsburg, 2011). Likewise, a deeper understanding of photoreceptor development and homeostasis would help to inform the derivation of photoreceptors from patient cells and proper incorporation and survival of these cells following transplantation. Since vision loss from retinal degeneration is largely associated with the death or dysfunction of photoreceptor cells, filling in the mechanistic gaps about how they develop and function is of paramount importance in advancing the development of effective treatments for the thousands of individuals who currently are or who will one day be affected by debilitating retinal diseases.

1.7 Hypothesis and specific aims

Vision loss from retinal degeneration is largely associated with the death or dysfunction of photoreceptor cells (rods and cones). The photoreceptors are highly metabolically active cells, yet rods seem to be more vulnerable to disease than cones, and often the degeneration of rods leads to a secondary loss of cone function and severe visual defects (Jackson et al., 2002, Curcio et al., 2000). The maturation of rod photoreceptors is stringently regulated by a variety of transcription factors such as Crx and Nrl. While Crx plays a role in activating photoreceptor-specific genes (both rod

and cone), Nrl is sufficient to induce rod photoreceptor differentiation by regulating the expression of a cascade of rod-specific maturation and homeostasis genes (Swaroop et al., 2010). A thorough understanding of the genes and proteins involved in rod photoreceptor development and homeostasis would not only help us to understand mechanisms underlying outer retinal degeneration leading to vision loss, but would also aid in the design of cell replacement therapies that require manipulation of these interactions for successful generation, integration and survival of transplanted photoreceptors. **We hypothesised that genes demonstrating both a dramatic increase in expression during rod photoreceptor development, and regulation by key rod transcription factors Nrl and Crx, would play a substantial role in the functional maturation and homeostasis of these cells.** To this end, we pursued the following specific aims:

1.7.1 Aim 1: Select Nrl-regulated candidate gene(s) associated with rod photoreceptor development for further analysis.

Candidate genes associated with rod photoreceptor development will be identified by RNA-seq on developmental mouse retinal samples. Expression of candidate genes in the retina will be validated by *in situ* hybridisation, and gross morphological consequences of their knockdown will be assessed by *in vivo* shRNA electroporation in neonatal mice. We will select one of these three genes whose knockdown results in the most dramatic change in retina morphology to further characterise.

Based on results from Aim 1, *Frmpd1* (which encodes FERM and PDZ domain-containing protein 1) was selected to conduct a detailed molecular and functional characterisation on in Aims 2-4.

1.7.2 Aim 2: Characterise the regulatory elements contributing to Frmpd1 expression in the retina.

To determine the transcriptional start site and potential alternative promoter usage for the *Frmpd1* gene in different tissue types, we will perform 5'-rapid amplification of cDNA ends (5'-RACE) analysis. To delineate conserved regions upstream of the *Frmpd1* transcription start site that are likely promoter regions, we will conduct an *in silico* analysis of the gene sequence using several bioinformatic tools. We will identify the minimal promoter region of *Frmpd1* and test its activity *in vivo* by electroporation of GFP constructs driven by various predicted promoter sequence fragments. Finally, we will assess whether Nrl and/or Crx can directly bind to and activate gene transcription from the minimal *Frmpd1* promoter *in vitro* using electrophoretic mobility shift and luciferase reporter assays.

1.7.3 Aim 3: Determine localisation and protein-protein interactions of Frmpd1 in the retina.

We will evaluate the subcellular localisation of Frmpd1 protein by *in vivo* electroporation of tagged constructs into mouse retina and confirm by immunohistochemistry with custom designed antibodies. Potential interacting partners of Frmpd1 will be tested using immunoprecipitation followed by immunoblotting. *In vivo* colocalisation of Frmpd1 and its putative protein partners in the retina will be assessed by immunohistochemistry.

1.7.4 Aim 4: Examine the role of Frmpd1 in the retina using a loss-of-function mouse model.

Finally, we will generate an *Frmpd1* loss-of-function mouse line using CRISPR/Cas9 technology. We will examine the functional and morphological

consequences of *Frmpd1* knockdown in these mice by immunohistochemistry and electroretinography.

These studies have demonstrated the usefulness of transcriptome profiling and existing data set mining to help identify a previously uncharacterized gene, *Frmpd1*, as having a novel function in the retina (Chapter 2). We have also identified the use of a tissue-specific alternative promoter in both mice and humans that drives expression of this gene in the retina (Chapter 3). Furthermore, we provide evidence that Frmpd1 aids in the homeostasis and functional optimisation of rod photoreceptors by mediating adaptation of these cells following light exposure (Chapters 4 and 5). Finally, we demonstrate the potential use of CRISPR technologies to generate tissue-specific knockdowns by targeting untranslated regulatory, rather than protein-coding, regions of genes- a useful approach that could be used in various tissues of the central nervous system which characteristically express tissue-specific isoforms of genes (Chapter 5).

2

Selection of candidate gene *Frmpd1*

2.1 Introduction

It remains unclear why the death of rod photoreceptors often leads to a secondary loss of cones, although it is known that photoreceptors are functionally coupled by gap junctions and may form surface interactions via adherens junctions and cell-surface glycoproteins (Raviola and Gilula, 1973, Campbell et al., 2006, Pulimeno et al., 2010). As rods comprise >95% of the mammalian photoreceptors (Carter-Dawson and LaVail, 1979a), it is possible that rod death disrupts the structural integrity of the retina, and a loss of proper organization causes subsequent cone death. Adherens junctions are protein complexes occurring at cell-cell junctions; in the retina, they allow for interactions between photoreceptors and other cell types and likely help to stabilize the mosaic architecture of the photoreceptors in the outer nuclear layer (Alves et al., 2014, Mehalow et al., 2003, Gosens et al., 2008). Indeed, aberrant

expression of adherens junction proteins has been observed in the retinae of mice with retinitis pigmentosa (Campbell et al., 2007, Campbell et al., 2006). We were therefore initially interested in identifying novel genes that may be involved in surface interactions between rod photoreceptors and other cells within the retina. To identify genes that may play a role in establishing these cell-cell interactions, we took advantage of previously generated RNA-seq and ChIP-seq data sets to select three likely rod-enriched target genes related to this process on which to conduct a detailed molecular and functional analysis.

The differentiation of rod and cone photoreceptors is dependent on a variety of intrinsic and extrinsic factors, most notably the influence of a small number of key transcription factors that direct a postmitotic photoreceptor precursor cell into one of the three fates in mice: rod, M-, or S-cone (Section 1.2, Figure 1.3). Neural retina leucine zipper (Nrl) is a key regulator of rod photoreceptor differentiation (Oh et al., 2007). When knocked out in mice, all photoreceptors that were originally fated to become rods instead transform into S-cone-like cells (Mears et al., 2001). The photoreceptors of *Nrl*$^{-/-}$ mice, while not considered true S-cones, do exhibit most morphological and functional features of S-cones (Section 1.2, Figure 1.4), such as basal discs open to the extracellular space, heterochromatin clumping in nuclei, extracellular matrix sheaths stained by PNA (peanut agglutinin, which binds to lectins of cone outer sheaths but not rods), expression of key cone phototransduction molecules (S-opsin, cone transducin, and cone arrestin), and maximum sensitivity to 360 nm with a secondary sensitivity of 510 nm (corresponding to S- and M- opsin, respectively) (Daniele et al., 2005, Nikonov et al., 2005). In contrast, ectopic overexpression of Nrl driven by Crx promoter in postmitotic photoreceptor precursors

results in an all-rod outer nuclear layer (Oh et al., 2007). Nrl is thus considered both necessary and sufficient for rod photoreceptor differentiation.

To label rod photoreceptors, transgenic mice were previously generated by the Neurobiology-Neurodegeneration and Repair (N-NRL) lab carrying 3 copies of a 2.5 kb *Nrl*-promoter fragment driving GFP (Akimoto et al., 2006). In this mouse model, GFP expression is directed specifically to rod photoreceptors and the pineal gland (Akimoto et al., 2006). GFP-positive cells in the *Nrl*-GFP retina can first be detected by embryonic day (E)12 and increase in number and GFP intensity over time, correlating with the time course of rod cell birth, which ranges from E13-P10 (Akimoto et al., 2006). *Nrl*-GFP mice were also crossed to $Nrl^{-/-}$ mice to produce a line (*Nrl*-GFP:$Nrl^{-/-}$) expressing GFP in the S-cone-like photoreceptors of the $Nrl^{-/-}$ retina (Akimoto et al., 2006). Since expression of the GFP transgene is controlled by the promoter of the *Nrl* gene rather than Nrl protein itself, the upstream regulatory mechanisms acting on this promoter can drive GFP expression in photoreceptor precursors fated to become rods. However, because functional Nrl protein cannot be made in *Nrl*-GFP:$Nrl^{-/-}$, rods are instead transformed into S-cone-like cells. GFP-positive cells in *Nrl*-GFP:$Nrl^{-/-}$ retina are therefore cone-like photoreceptors (Akimoto et al., 2006).

The retina can be dissociated and individual GFP-expressing cells isolated by fluorescence activated cell sorting (FACS) (Akimoto et al., 2006) allowing for purified cell populations of rod photoreceptors (from *Nrl*-GFP) or S-cone-like photoreceptors (from *Nrl*-GFP:$Nrl^{-/-}$). These 2 mouse lines have thus proven to be incredibly useful for a variety of transcriptomic studies comparing rod and cone gene expression profiles (Kim et al., 2016a, Kim et al., 2016b, Akimoto et al., 2006). This method has been

instrumental in temporal expression profiling during early rod and cone development, as expression of GFP in *Nrl*-GFP and *Nrl*-GFP:*Nrl*$^{-/-}$ is activated much earlier than rod- and cone-specific gene expression signatures can be distinguished (Kim et al., 2016b, Kim et al., 2016a).

To select candidate genes that may be associated with rod photoreceptor development for further analysis, we first identified rod-enriched genes based on RNA-seq data from purified *Nrl*-GFP and *Nrl*-GFP:*Nrl*$^{-/-}$ photoreceptors in conjunction with Nrl and Crx ChIP-seq data. Three novel genes that may play a role in establishing rod photoreceptor cell-cell interactions were then predicted based on gene ontology analysis. Morphological consequences of knockdown of each of these 3 genes was assessed by *in vivo* shRNA electroporation of neonatal mouse retina followed by histological analysis. *Frmpd1* (FERM and PDZ domain containing 1), whose knockdown resulted in the most dramatic change in rod photoreceptor morphology, was chosen based on these results to conduct a detailed molecular and functional characterisation on as described in further chapters.

2.2 Materials and methods

2.2.1 Materials

For reagent details, buffer compositions, and plasmid maps refer to Appendices A-D.

2.2.2 RNA-seq differential expression analysis

Prior to this thesis, the N-NRL lab purified *Nrl*-GFP and *Nrl*-GFP:*Nrl*$^{-/-}$ mouse photoreceptors at various time points during development (P2, P4, P6, P10, P14, P28)

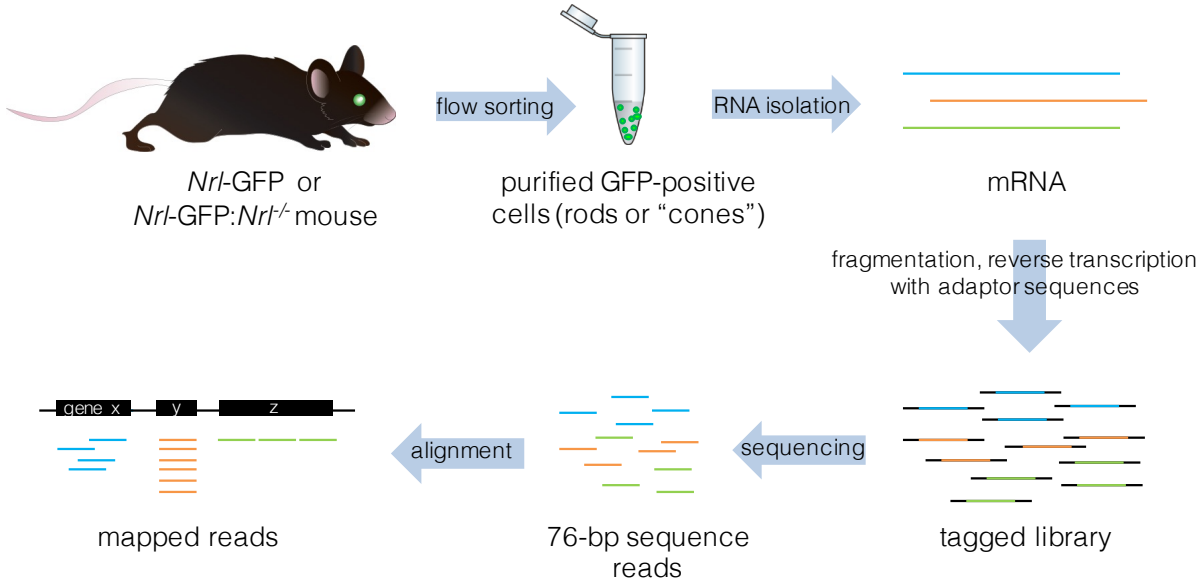

Figure 2.0.1: RNA-Seq of purified rod and "cone-like" photoreceptors. FACS-sorted GFP+ cells were isolated from two mouse lines, *Nrl*-GFP (with a transgene expressing GFP under the Nrl promoter, where GFP+ cells are rods) and *Nrl*-GFP:*Nrl*$^{-/-}$ (Nrl-L-EGFP crossed with *Nrl*$^{-/-}$, where GFP+ cells have been converted into S-cone-like cells in the absence of Nrl) for 2 distinct cell populations at ages P2, P4, P6, P10, P14, and P28. RNA was isolated from these cells and directional cDNA libraries were prepared and deep sequenced using an Illumina GAIIx sequencer to yield a series of 76-nucleotide length reads. RNA-seq was performed in the lab prior to this thesis (Kim et al., 2016a, Kim et al., 2016b).

and RNA was used to construct directional cDNA libraries that were then deep sequenced using Illumina GAIIx producing 76 bp reads (Brooks et al., 2012, Kim et al., 2016a, Kim et al., 2016b). 2-4 biological replicates for each time point were used; each biological replicate was comprised of pooled samples from at least 2 animals, and 20 ng of total RNA derived from 1-5 x 10^5 flow-sorted cells was used for library construction. Sequence reads were available for use in this project and analysed in collaboration with Jerome Roger following a similar protocol as previously described (Campla et al., 2017). Briefly, RNA-seq reads were mapped against a reference transcriptome and annotated via TopHat2 (Kim et al., 2013), then gene level counts were calculated and FPKM (Fragments Per Kilobase of exon model per Million fragments mapped) normalised with Cufflinks (Roberts et al., 2011, Trapnell et al., 2012). Only genes for which FPKM $\geq$ 2 in at least 1 time point (where FPKM = Fragments Per Kilobase of exon per Million fragments mapped) were considered as "expressed". Cuffdiff (Trapnell et al., 2013) was then used to analyse differential transcript expression by calculating the fold change of expression differences between every pairwise combination of time points. Any genes not undergoing a fold change of at least 2 (with $p \leq 0.05$) between at least 2 time points were then filtered out. P-values were calculated by Cufflinks, using a method based on sampling from the beta negative binomial model to estimate the null distribution of fold changes for each transcript.

2.2.3 Hierarchical clustering and heat maps

Hierarchical clustering was performed in JMP (statistical discovery software, SAS Institute) to identify groups of genes undergoing similar changes in expression during rod photoreceptor development. The following script was used:

```
Hierarchical Cluster(
    Y( :Log2_P2, :Log2_P4, :Log2_P6, :Log2_P10, :Log2_P14, :Log2_P28 ),
    Label( :gene ),
    Method( "Ward" ),
    Standardize( 0 ),
    Color Clusters( 1 ),
    Legend( 1 ),
    Dendrogram Scale( "Distance Scale" ),
    Number of Clusters( 15 ),
    Color Map( "Blue to Gray to Red" )
)
```

2.2.4 Nrl/Crx chromatin immunoprecipitation sequencing (ChIP-Seq)

Nrl chromatin immunoprecipitation (ChIP) was performed previously on C57BL/6J retinae in the N-NRL lab as described (Hao et al., 2011). This publicly available dataset (http://datashare.nei.nih.gov/HhaoNrlServlet?docName=NrlGA0350_20120607.bed.gz) was used to identify genes containing Nrl ChIP-Seq peaks. Crx ChIP-seq was performed by another group as previously described (Corbo et al., 2010) using a similar method as above on 6-week-old mice. This publicly available dataset (GEO accession # GSM499736, GSM499737) was used to identify genes containing Crx ChIP-Seq peaks.

2.2.5 Mouse lines & husbandry

C57BL/6J and CD1 mice were purchased from Jackson Laboratory and Charles River Laboratories, respectively. All experiments were conducted according to protocols approved by a local Institutional Animal Care and Use Committee and adhered to the Association for Research in Vision and Ophthalmology Statement for animal use in ophthalmic and vision research. Mice were reared in regular animal housing under ~100 lux 12:12 hour light/dark cycle, and mice of either sex were used in this study.

2.2.6 RNA isolation

Retinae were quickly dissected in 1x PBS and transferred to 250 μl 1x PBS on ice (either single retina or pooled samples depending on application, or an equivalent amount of tissue from other organs). Tissue was homogenised using a glass dounce homogeniser (Duran Wheaton Kimble LifeSciences) after which 750 μl Trizol LS (Ambion) was added, mixed, and either immediately processed or frozen on dry ice and stored at -80˚C. To isolate RNA, 500 μl of the sample stored in Trizol LS was incubated for 5 min at room temp, after which 100 μl of chloroform was added, incubated for 7 min at room temp, and centrifuged for 15 min at 4˚C (12,000 x *g*). The colourless aqueous phase was transferred to a new tube with 10 μg RNase-free glycogen (Invitrogen). 250 μl isopropanol was then added and incubated for 10 min at room temp, then centrifuged (12,000 x *g*) 10 min at 4˚C. Supernatant was removed, and the RNA pellet was washed with 500 μl 75% ethanol, re-pelleted (7500 x *g* for 5 min at 4˚C), and air-dried after removing supernatant. The pellet was then resuspended in 20 μl RNase-free water, dissolved 15 min at 56˚C, and quantified by a

NanoDrop spectrophotometer (Thermo) and/or 2100 Bioanalyzer (Agilent) before storage at -80˚C.

2.2.7 Plasmid DNA isolation

A pipette tip was used to select a single bacterial colony from a plate (or an equivalent amount of frozen glycerol stock), then used to inoculate 3 ml of selective LB broth (containing 100 μg/ml ampicillin or 50 μg/ml kanamycin) in a 15 ml conical tube. This "starter culture" was then incubated overnight at 37˚C shaking at 250 rpm. For smaller preparations, 2 ml of this starter culture was used for plasmid miniprep following the NucleoSpin Plasmid Miniprep Kit manufacturer's instructions (Macherey Nagel). For larger preparations, 300 μl of this starter culture was used to inoculate 300 ml of selective LB broth which was then incubated overnight at 37˚C at 250 rpm and used for plasmid maxiprep following the NucleoBond Xtra Kit manufacturer's instructions (Machery Nagel). Glycerol stocks were prepared from starter cultures by mixing equal amounts of starter culture with 50% glycerol and storing at -80˚C.

2.2.8 DNA precipitation

Plasmid maxiprep DNA was precipitated by adding 0.1 volumes 3M sodium acetate (pH 5.2) and 2.5 volumes 100% ethanol and freezing for at least 15 min at -80˚C. The DNA was then pelleted by centrifugation for 30 min at 15,700 x *g* at 4˚C. Supernatant was removed and the pellet was washed with 200 μl of 70% ethanol then re-centrifuged at same speed/temp for 5 min. DNA pellets were air-dried and resuspended in molecular grade water to give a final concentration of ~5 μg/μl for use in transfections and *in vivo* electroporation.

2.2.9 In vivo electroporation

DNA solutions were prepared from concentrated plasmid DNA stocks (Section 2.2.7-8) and 0.3 μg/μl fast green tracking dye diluted to desired end concentrations (1-5 μg total DNA) in molecular grade water. Neonatal (P1) CD1 mouse pups were anesthetised by placing on ice for several minutes, after which the right eyelid was sterilised with 70% ethanol. A cut was carefully made along the future eyelid furrow using a sterile 30-gauge needle to expose the eye, and a small puncture was made using another sterile 30-gauge needle at the nasal side of the corneal-scleral junction. A custom blunt-ended syringe (Hamilton Company) was then carefully passed through the puncture and behind the lens to the subretinal space (between retina and RPE/sclera), where 0.2-0.4 μl of DNA solution was slowly and uniformly injected. Tweezer electrodes (Tweezertrodes, BTX Harvard Bioscience) were then dipped in 1x PBS and gently applied to either side of the pup's head with as much surface area contact as possible (with positive electrode contacting the right eyelid). Electrical pulses (5 pulses at 80 V, 50 ms pulse with 950 ms interval) were applied across the head using a BTX ECM 830 apparatus (BTX Harvard Bioscience) and the pups were placed on a heating pad until recovered.

2.2.10 Retina cryosectioning

Eyes were enucleated and fixed for 30 min in 4% paraformaldehyde (PFA) in 1x phosphate buffered saline (PBS), then hemisected to remove cornea and lens and placed back in 4% PFA for remainder of total fixation time (either 1 hr room temp or overnight at 4˚C depending on downstream application). Fixed eyecups were then cryoprotected overnight at 4˚C in 30% sucrose in 1x PBS, then snap frozen in plastic

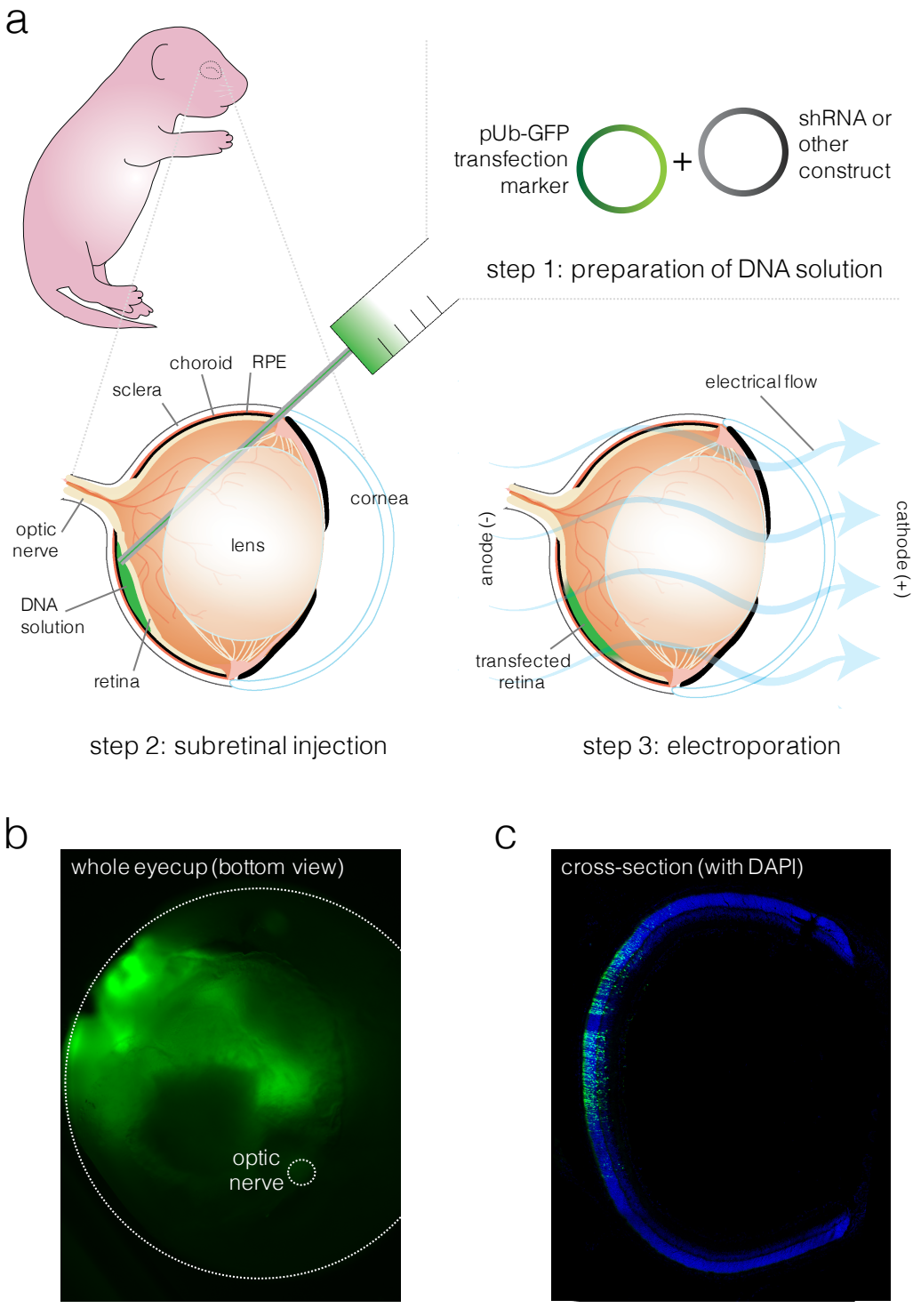

Figure 2.0.2: *In vivo* electroporation of neonatal mouse retina. (A) Injection procedure. Neonatal (P1) CD1 mouse pups received a subretinal injection of 0.2-0.4 μl of DNA solution containing 1-4 $\mu g/\mu l$ of shRNA or tagged protein construct(s) with 1 $\mu g/\mu l$ of a GFP reporter construct (pUb-GFP) to label transfected cells. Electrical pulses were applied across the head to transfect retinal cells, and eyes were harvested at various ages (P10, P15, P21) for downstream analysis. (B) Typical transfection efficiency. A retina was harvested at P21 (20 days post- *in vivo* electroporation). A bottom view of the eyecup before sectioning shows a large area of transfected retina, and cross-section (C) shows the typical coverage and morphology of a transfected retina.

molds filled with optimal cutting temperature (OCT, Sakura) compound by placing molds in a slurry of acetone and dry ice. Samples were cryosectioned at -20˚C at a thickness of 12 μm (routine IHC) or 18 μm (electroporated retinae) onto Superfrost Plus (Thermo Fisher) slides and stored at -80˚C until needed.

2.2.11 In situ hybridisation (ISH)

In situ hybridisation was performed on 1 hr PFA fixed cryosections (Section 2.2.10) from P21 mouse retina using RNAscope technology and HybEZ Hybridization Oven (Advanced Cell Diagnostics) according to manufacturer's instructions with minor modifications. Slides were washed in 1X PBS and incubated in Pretreat 2 solution (Advanced Cell Diagnostics) at 100°C for 3 min, followed by incubation in Pretreat 4 solution (Advanced Cell Diagnostics) at 40°C for 30 min. RNAscope probes were then hybridised at 40°C for 2 hr, followed by amplification steps according to the manufacturer's instructions. The signal was visualised and captured using a Zeiss 700 confocal microscope. Experiments were performed in biological triplicate. Custom probes were designed to target either all *Frmpd1* transcripts (Exons 3-12) or Exon 1a specifically:

Probe name	Catalog #	Target region (bp)	ZZ pairs
Mm-Frmpd1	440451	188-1197 of NM_001081172.2	20
Mm-Frmpd1-Exon 1a	440461	2-478 of ENSMUSE00000674488	10
Mm-Galnt7	440471	319-1417 of NM_144731.4	20
Mm-Glb1l2	440481	1029-2038 of NM_153803.1	20

2.3 Results

2.3.1 Differential expression analysis of purified rod photoreceptors

Using the mapping and filtering criteria described in Section 2.2.2, a total of 11,686 genes were detectably expressed in the flow-sorted rod photoreceptors from P2 to P28 with FPKM values ranging from 0 to 36,805. To select for differentially expressed genes within this dataset, fold changes in expression between all pairwise combinations of time points were calculated in Cuffdiff (Trapnell et al., 2013), filtering for fold change ≥ 2 and p-value ≤ 0.05. This analysis identified 5400 genes that were differentially expressed during rod photoreceptor development (Figure 2.3). Interestingly, a dramatic shift in gene expression patterns was observed between the P6 and P10 time points in flow-sorted rod photoreceptors, which is consistent with the onset of expression of Nr2e3 (nuclear receptor subfamily 2, group E, member 3) and concomitant reinforcement of a rod-specific cell fate discussed previously (Section 1.2, Figures 1.3,1.4). cone-specific genes are acutely downregulated in the rods during this time frame as well through repression by Nrl-Nr2e3 complexes (Chen et al., 2005).

To further select for genes likely to be involved in rod photoreceptor development, these 5400 differentially expressed genes (DEGs) were filtered further based on Nrl and Crx (2 key regulators of rod cell fate specification) occupancy of the gene *in vivo* as evidenced by chromatin immunoprecipitation (ChIP) followed by high-throughput sequencing (Hao et al., 2012, Corbo et al., 2010). Of these DEGs, 161 contained both Nrl and Crx ChIP-Seq peaks, providing further evidence for their potential enrichment in rods. To identify patterns of RNA expression in these 161 genes, hierarchical clustering based on $\log_2$FPKM values (to normalize for extremely

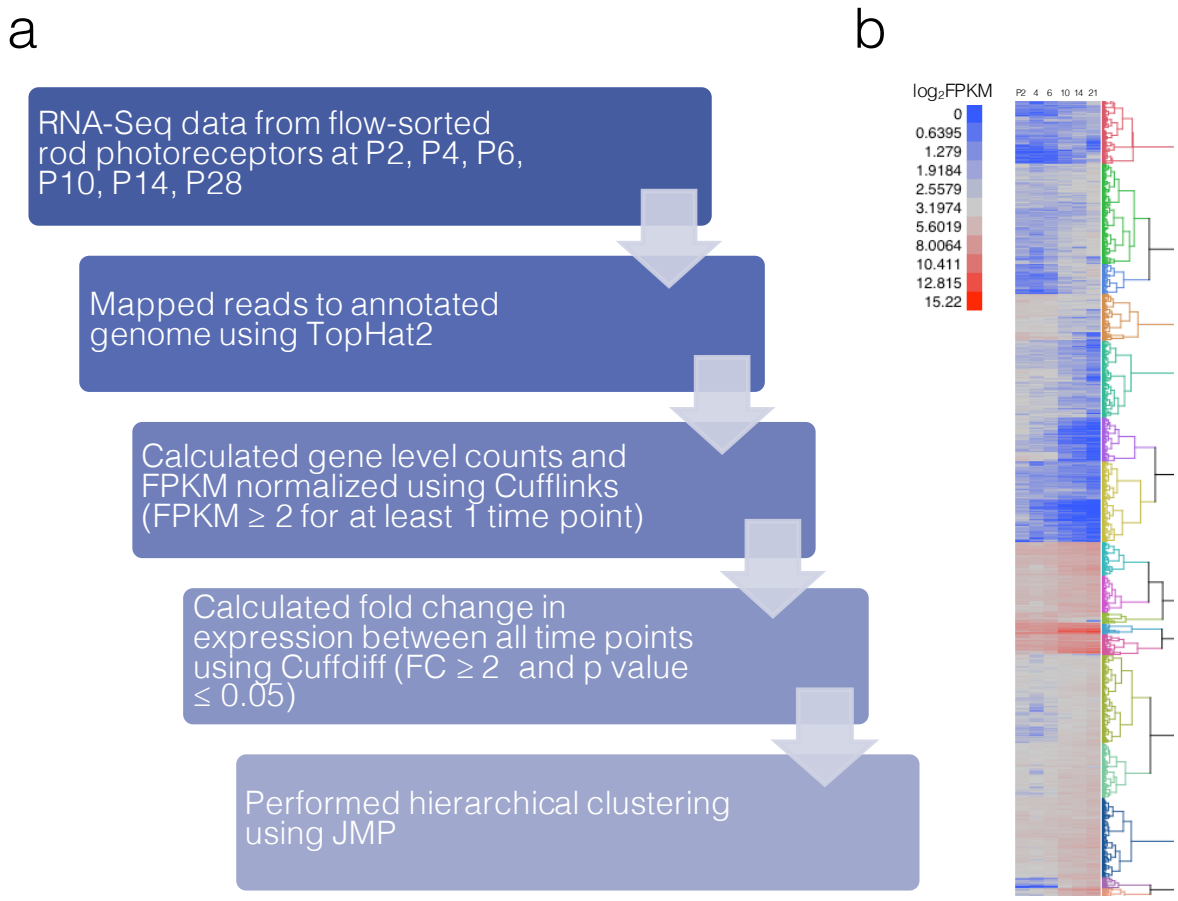

Figure 2.0.3: Hierarchical clustering of differentially expressed genes. (A) RNA was isolated from flow-sorted murine photoreceptors expressing GFP under control of the *Nrl* promoter and used for RNA-Seq (Figure 2.1). Reads were mapped to an annotated genome using TopHat2, after which gene levels were quantified and FPKM normalized using Cufflinks (filtering for FPKM ≥ 2 for at least 1 time point). Fold changes in expression between all time points were calculated in Cuffdiff (filtering for fold change ≥ 2 and p-value ≤ 0.05). FPKM values were normalized (log_2FPKM) and hierarchical clustering was then performed in JMP. (B) Heat map of log-normalized FPKM gene expression values. Columns represent timepoints P2, P4, P6, P10, P14, and P28. Each row represents an individual gene identified by differential expression analysis, with expression level (log_2FPKM) indicated by colour.

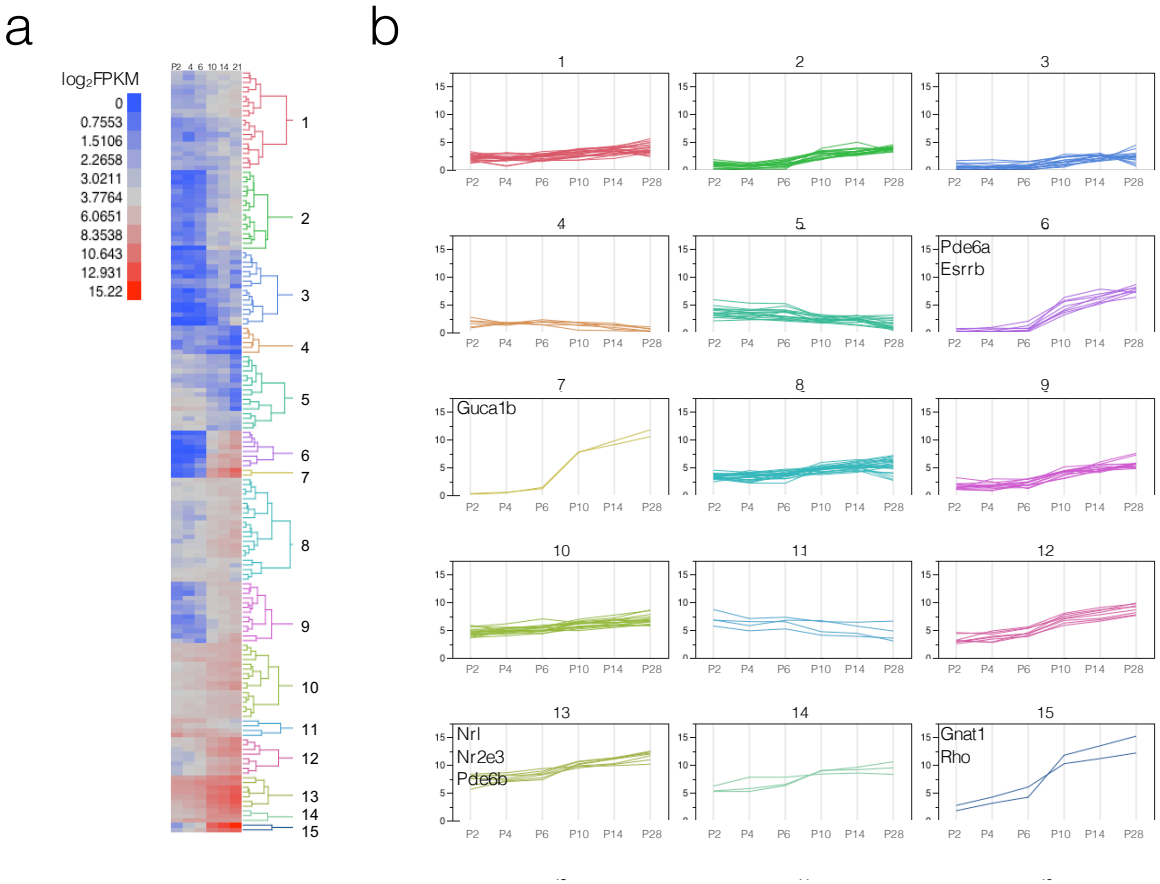

Figure 2.0.4: Hierarchical clustering of Nrl-Crx filtered differentially expressed genes. (A) Heat map of log-normalized FPKM gene expression values. Differentially expressed genes from Figure 2.3 were filtered for those containing both Nrl and Crx ChIP-Seq peaks for 161 genes total. Columns represent timepoints P2, P4, P6, P10, P14, and P28. Each row represents an individual gene, with expression level (log_2FPKM) indicated by colour. (B) Graphical representation of expression values for all genes within each cluster. Patterns of expression are depicted in graphical format (x-axis: age; y-axis: log_2FPKM).

highly expressed genes such as rhodopsin) was performed in JMP (Figure 2.4). A full list of these 161 genes and their clusters can be found in Appendix E.

Since we were most interested in selecting novel candidate genes that were likely to be critical for rod morphogenesis and/or homeostasis, we were most interested in selecting genes from clusters with dramatic upregulation of expression between P6-P10. As outlined in Section 1.2, this is a pivotal time frame for rod morphogenesis and the induction of cell-specific gene expression signatures through Nrl-Nr2e3 complexes (Oh et al., 2008). Genes undergoing dramatic upregulation during this time frame include those necessary for key processes in rod maturation and homeostasis such as outer segment formation, phototransduction, and synaptogenesis (Section 1.2, Figures 1.3,1.4). Indeed, many well-studied genes belonging to these categories were among the filtered DEGs when a Gene Ontology Enrichment Analysis (pantherdb.org) was performed, with highest enrichment in the phototransduction category (Table 2.1). Of greater interest, however, were the multitudes of uncharacterised genes also identified through this screen.

2.3.2 Selection of candidate genes for further analysis

Several of the 161 DEGs identified in Section 2.3.1 have already been extensively characterised in the retina and established as necessary for rod function and homeostasis (for example: rhodopsin, transducin, phosphodiesterase, Nrl, and Nr2e3). To make the screening process more manageable, we further selected 3 novel candidates of the remaining uncharacterised DEGs for additional analysis and to test for knockdown phenotypes before settling on a single gene of interest. Additional selection criteria used to select these 3 genes included the presence of a human

Table 2.1: Overrepresented gene ontology categories of differentially expressed genes containing Nrl and Crx ChIP-seq peaks.

Gene ontology biological process	# genes in reference	161 DEGs containing Nrl and Crx ChIP-seq peaks			
		# DEGs predicted	# DEGs actual	Fold enrich.	p-value
phototransduction	26	0.17	5	29.68	7.82E-03
photoreceptor cell maintenance	41	0.27	6	22.58	3.00E-03
eye photoreceptor cell development	35	0.23	5	22.04	3.30E-02
retina homeostasis	51	0.33	7	21.18	4.75E-04
detection of light stimulus	47	0.3	6	19.7	6.59E-03
eye photoreceptor cell differentiation	49	0.32	6	18.9	8.38E-03
photoreceptor cell differentiation	62	0.4	6	14.93	3.21E-02
sensory perception of light stimulus	142	0.92	13	14.13	1.21E-07
visual perception	138	0.89	12	13.42	1.36E-06
retina development in camera-type eye	138	0.89	8	8.95	3.34E-02
eye development	346	2.24	14	6.24	6.19E-04
camera-type eye development	303	1.96	11	5.6	4.56E-02
sensory organ development	544	3.53	18	5.11	1.63E-04
establishment of localisation in cell	1354	8.77	26	2.96	5.28E-03
anatomical structure	2031	13.16	34	2.58	1.81E-03

morphogenesis

Gene ontology biological process	# genes in reference	161 DEGs containing Nrl and Crx ChIP-seq peaks			
		# DEGs predicted	# DEGs actual	Fold enrich.	p-value
regulation of biological quality	3281	21.26	44	2.07	9.83E-03
establishment of localisation	3586	23.24	47	2.02	6.93E-03
system development	3943	25.55	49	1.92	1.75E-02
multicellular organism development	4506	29.2	54	1.85	1.22E-02
anatomical structure development	4795	31.07	57	1.83	6.64E-03
developmental process	5122	33.19	60	1.81	4.57E-03
localisation	4577	29.66	53	1.79	4.69E-02
positive regulation of biological process	5342	34.62	60	1.73	1.99E-02
cellular process	13735	89.01	116	1.3	8.35E-03
unclassified	1678	10.87	4	0.37	0.00E+00

a

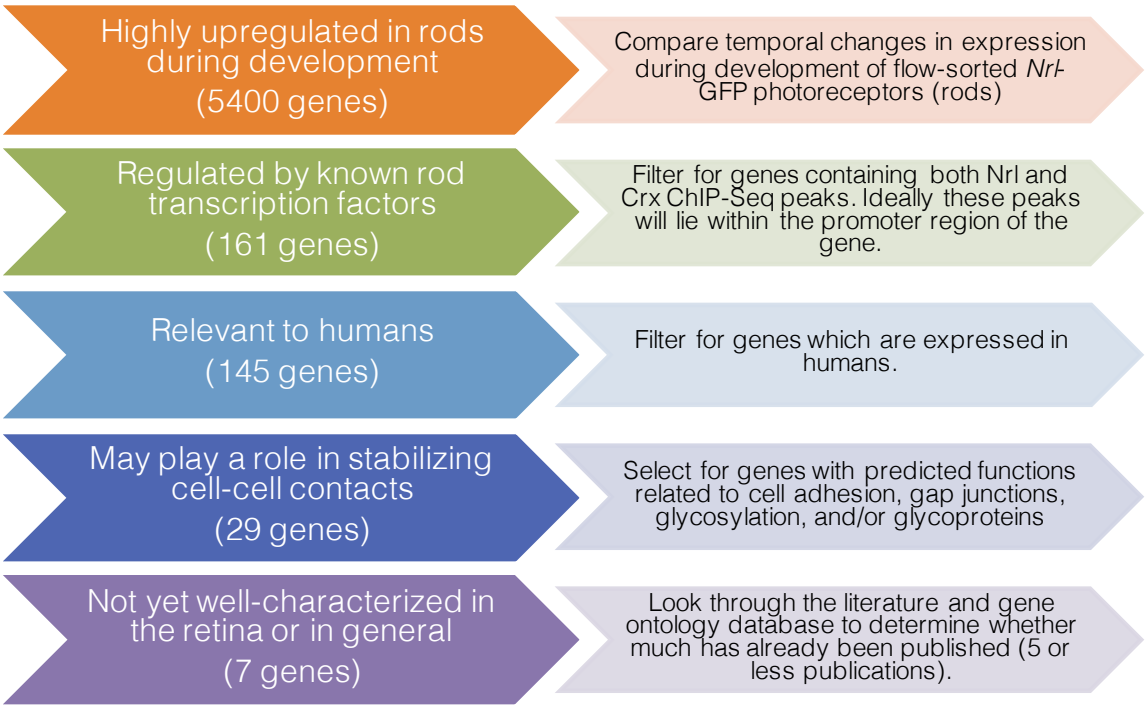

b

Gene Symbol	Gene Name	Gene Ontology Functions, Location
Galnt7	UDP-N-Acetyl-Alpha-D-Galactosamine:Polypeptide N-Acetylgalactosaminyl transferase 7	Polypeptide N-acetylgalactosaminyltransferase activity; O-glycan processing; carb metabolism; post-translational protein modification; golgi membrane
Glb1l2	Galactosidase, Beta 1-Like 2	Beta-galactosidase activity; carbohydrate metabolism; extracellular region
Frmpd1	FERM And PDZ Domain Containing 1	Cytoplasm, cytoskeleton, cytosol, plasma membrane localization

Figure 2.0.5: Candidate gene selection overview. (A) Three candidate genes for further molecular and functional analysis were selected based on their high expression in purified rod photoreceptors, binding by transcription factors Nrl and Crx, relevance to humans, novelty, and predicted gene ontology functions pertaining to cell adhesion and cell-cell interactions. Based on these criteria, the genes in (B) were selected. (B) Summary of gene ontology functions obtained from a search on PubMed using gene symbols (http://www.ncbi.nlm. nih.gov/pubmed).

homologue (to select for those relevant to human development and disease), novelty based on a literature search on Pubmed (to select for genes with unknown function especially in the retina), and gene ontology annotations related to membrane glycoproteins and/or cellular adhesion (to select for genes that may play a role in mediating cell-cell contacts) (Figure 2.5). Based on these criteria, the following candidates were selected for further screening:

1. *Galnt7* (UDP-N-Acetyl-Alpha-D-Galactosamine:Polypeptide N-Acetyl galactosaminyl transferase 7)

   Galnt7 is an enzyme that catalyses the transfer of N-acetylgalactosamine to serine and threonine residues and has been suggested to function in O-glycosylation (Bennett et al., 1999). Glycosylation of cell surface and matrix proteins can mediate cell-cell interactions (Kleene and Schachner, 2004).

2. *Glb1l2* (Galactosidase, Beta 1-Like 2)

   Glb1l2 is putative secreted or membrane protein and is a member of the β-galactosidase-1-like family (Otsuki et al., 2005). β-galactosidase activity has been associated with cell adhesion (Tang et al., 2014).

3. *Frmpd1* (FERM And PDZ Domain Containing 1)

   Frmpd1 is a membrane-associated protein (An et al., 2008) containing FERM and PDZ domains which have both been implicated in cell-cell junctions (Arpin et al., 2011, Ebnet et al., 2000).

2.3.3 Validation of RNA expression profiles of candidate genes

We next wanted to confirm the rod-enriched RNA expression of *Galnt7*, *Glb1l2*, and *Frmpd1*. To visualise RNA localisation of each of these genes in adult mouse retina, *in situ* hybridisation was performed on P21 retina cryosections using RNA probes specific for each of the 3 genes (Figure 2.6). These were performed both on rod-dominated $Nrl^{+/+}$ retina, to assess expression in a wildtype mouse, as well as in $Nrl^{-/-}$ retina to assess expression in a rodless mouse. The $Nrl^{-/-}$ retina also provided a means to assess whether each gene is regulated by *Nrl* as predicted by prior ChIP-seq filtering.

While *Galnt7* was observed in all cell body layers as well as in the $Nrl^{-/-}$ retina, implicating that this gene is not restricted to rods, *Glb1l2* and *Frmpd1* did appear to have rod-enriched localisation (Figure 2.6). Both genes are clearly expressed in the ONL (where only rod and cone nuclei are found) in the wildtype retina. Furthermore, this ONL expression is drastically reduced in the $Nrl^{-/-}$, cone-dominated retina. *Glb1l2* and *Frmpd1* maintain some expression in the INL, implying that their expression is rod-enriched rather than rod-specific. The expression of *Glb1l2* within the centre of the INL implies that it may be localised within the Müller glia, whereas *Frmpd1* expression in the upper portion of the INL would be more consistent with horizontal or bipolar cell expression. With respect to the photoreceptors, however, both *Glb1l2* and *Frmpd1* are selectively expressed in rods rather than cones based on their differential expression in $Nrl^{+/+}$ and $Nrl^{-/-}$ ONL; this loss of expression in $Nrl^{-/-}$ also provides further evidence that these genes are indeed regulated by Nrl, which is consistent with the RNA-seq and ChIP-seq filtering used to select for these candidates.

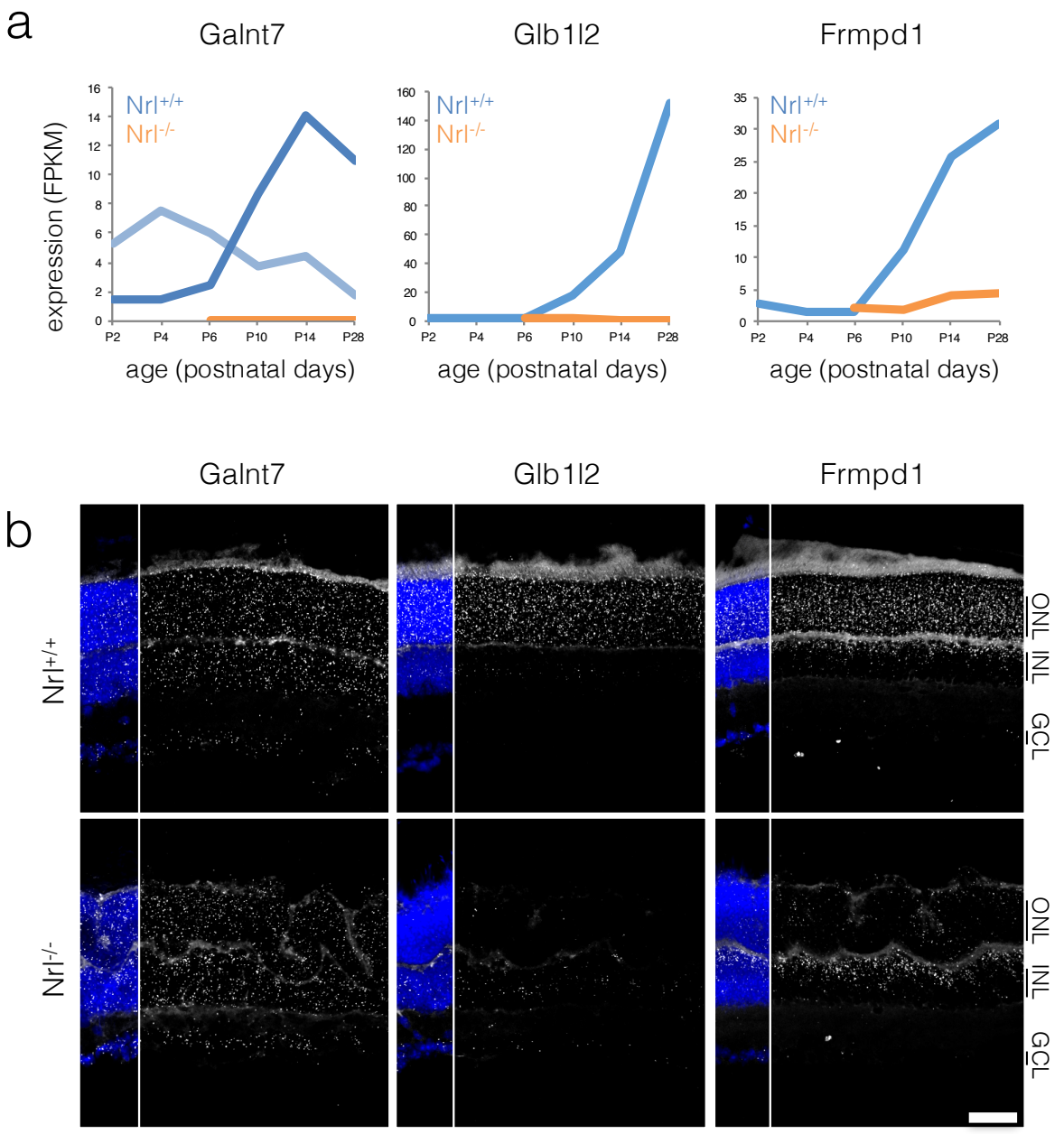

Figure 2.0.6: RNA expression of candidate genes in *Nrl*$^{+/+}$ and *Nrl*$^{-/-}$ retina. (A) RNA expression in flow-sorted photoreceptors. RNA-seq expression profiles (in FPKM) are given for each gene during the course of development. *Nrl*$^{+/+}$ refers to flow-sorted GFP+ cells (rod photoreceptors) of *Nrl*$^{+/+}$retina. *Nrl*$^{-/-}$ refers to flow-sorted GFP+ cells (cone-like photoreceptors) of *Nrl*$^{-/-}$ retina. In the case of *Galnt7*, the blue lines represent 2 separate isoforms of the gene. (B) RNA localisation by *in situ* hybridisation. *In situ* hybridisation using probes specific to each gene was performed on P21 *Nrl*$^{+/+}$ and *Nrl*$^{-/-}$retina cryosections. Background autoflourescence can be seen in the outer plexiform and outer segment regions; bright punctate staining represents RNA. Scale bar: 50 µm.

2.3.4 ShRNA-mediated Frmpd1 knockdown disrupts retinal organisation

Although *Galnt7, Glb1l2,* and *Frmpd1* appear to be highly expressed in rods, which make up >95% of the mouse photoreceptors (Carter-Dawson and LaVail, 1979a), the function of these genes in the retina has not yet been studied. To determine the gross effect on retina morphology upon knockdown of these candidate genes, a variety of commercially available shRNA constructs (Appendix B, Section 6.5.3, 6.5.4) targeting different regions of each were used to transfect retinal cells at P1 by *in vivo* electroporation (Section 2.2.9). As these shRNA constructs had not been tested for knockdown efficacy by the manufacturer, as a first screen they were injected as mixtures of 1 or more constructs to later be injected individually based on which produced the most obvious phenotypes at ages P10 and P21. Each shRNA construct was coinjected with a ubiquitin promoter-driven GFP construct to fluorescently tag transfected cells, in which shRNA had also been taken up, with a molar ratio of 2:3 GFP:shRNA to reduce false positive GFP-labelled cells that did not also receive shRNA.

An shRNA-mediated knockdown of *Galnt7* did not result in any overt retinal phenotype. Lamination of the retina and individual photoreceptor morphologies appear largely unaffected, with the possible phenotype of transfected cell bodies lying closer to the OPL at P10 (Figure 2.7a, arrowhead). An shRNA-mediated knockdown of *Glb1l2*, however, did appear to affect the photoreceptors in the majority of cases. Not only do the transfected cells exhibit a rounded morphology at P21, but very few GFP-positive photoreceptors were found at all (Figure 2.7b, arrowhead).

Most interestingly, shRNA-mediated knockdown of *Frmpd1* resulted in severe disruption of retina organisation and photoreceptor morphology (Figure 2.7c, 2.8).

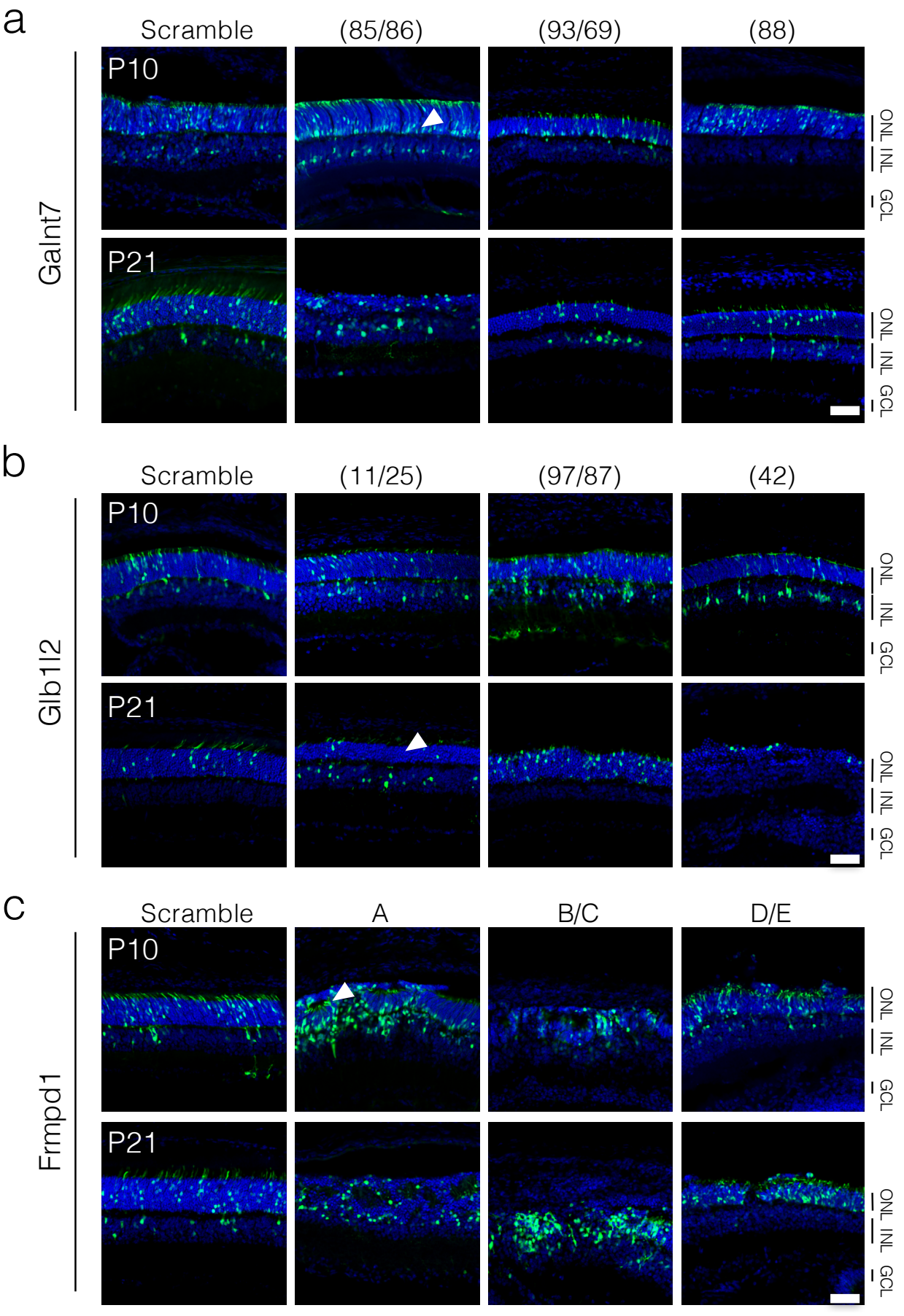
a
Scramble
(85/86)
(93/69)
(88)
P10
P21
Galnt7
ONL
INL
GCL
b
Scramble
(11/25)
(97/87)
(42)
P10
P21
Glb1l2
ONL
INL
GCL
c
Scramble
A
B/C
D/E
P10
P21
Frmpd1
ONL
INL
GCL

Figure 2.0.7: Retina morphology after shRNA knockdown screen (previous page). Neonatal (P1) mouse pups were transfected with 0.2 μl of DNA solution containing 2 μg/μl of shRNA construct(s) targeting different regions of *Galnt7* (A), *Glb1l2* (B), or *Frmpd1* (C) with 1 μg/μl of GFP reporter construct (pUb-GFP) by *in vivo* electroporation. Scrambled non-targeting shRNA was used as control. Eyes were harvested at P10 and P21 to assess morphological consequences of shRNA-mediated gene knockdown in transfected cells (GFP, green) and the surrounding retina (DAPI, blue). OS= outer segments, ONL= outer nuclear layer, INL= inner nuclear layer. Scale bar: 50 μm.

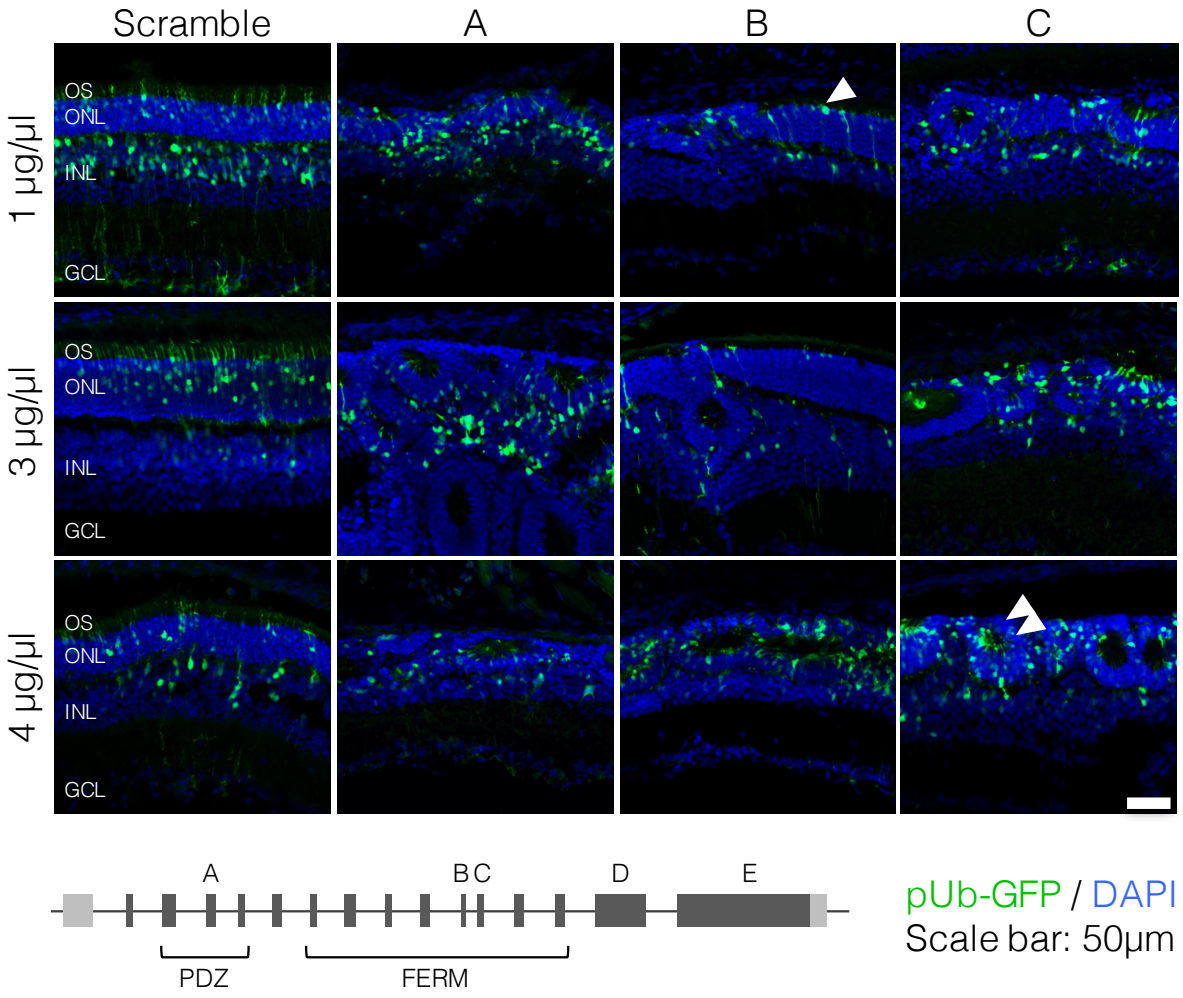

Figure 2.0.8: Retinal architecture is disrupted with *Frmpd1* knockdown. Neonatal (P1) mouse pups were transfected with 0.2 μl of DNA solution containing 1-4 μg/μl of shRNA construct(s) targeting different regions of *Frmpd1* with 1μg/μl of GFP reporter construct (pUb-GFP) by *in* vivo electroporation. Scrambled non-targeting shRNA was used as control. Eyes were harvested at P15 to assess morphological consequences of shRNA-mediated gene knockdown in transfected cells (GFP,

green) and the surrounding retina (DAPI, blue). OS= outer segments, ONL= outer nuclear layer, INL= inner nuclear layer. Scale bar: 50 μm.

Many of the *Frmpd1* knockdown cells were abnormally distributed within the inner and outer nuclear layers and in some cases appeared to have shortened outer segments (Figure 2.8 arrowhead); in other cases, the outer segments clustered together to form "puckered" regions and rosettes in the ONL (Figure 2.7c arrowhead, 2.8 double arrowhead). Since shRNA clone A and the mixture of B+C exhibited the most notable differences from retinae injected with the scrambled control shRNA, varying concentrations of each of these constructs were then used to test dose dependence on knockdown phenotype at age P15 (Figure 2.8). In all cases, transfection with *Frmpd1*-targeting shRNA resulted in abnormal retinal architecture with many of the same rosette and "puckered" formations as seen in the previous shRNA screen. This effect was visible regardless of shRNA construct or concentration tested, and was confirmed by injections performed independently by 2 other students as a technical control.

2.4 Discussion

We predicted that genes dramatically increasing in expression during rod photoreceptor development would play a substantial role in the functional maturation and homeostasis of these cells, which led to the selection of *Galnt7*, *Glb1l2*, and *Frmpd1* as potential candidates for further study. The presence of Nrl and Crx ChIP-Seq peaks within *Galnt7*, *Glb1l2*, and *Frmpd1*, combined with their very low RNA expression in flow-sorted $Nrl^{-/-}$ cone-like photoreceptors compared to flow-sorted rods, indicated that these genes are enriched in rod photoreceptors. The upregulation of these genes during rod development and maturation provided further evidence for their potential requirement in the establishment and maintenance of these highly

specialised neurons. Although all 3 genes were confirmed as expressed in the rod photoreceptors by *in situ* hybridisation, only 2 (*Glb1l2* and *Frmpd1*) seemed to produce a visible phenotype when knocked down by shRNA *in vivo*.

Potential explanations for the lack of detectable phenotype in *Galnt7* knockdowns could be that there is a subtler change induced by knockdown that is not readily visible by histological analysis, or that knockdown of the gene was not optimal either because of inefficient shRNA design, too low concentration, or compensatory mechanisms by cells. There may also have been compensation by other enzymes that could catalyse N-acetylgalactosamine transfer in the absence of Galnt7 such as Galnt10 which was also upregulated in rod photoreceptors (Cluster 3, Appendix E). Since RNA expression of *Galnt7* did not show a rod-enriched localisation by *in situ* hybridisation, this gene was eliminated from further analyses.

The paucity of GFP-positive photoreceptors in *Glb1l2* knockdown did not seem to be an issue of transfection coverage, as many GFP-positive cells could still be found in the INL, suggesting that the electroporation was successful and would have also transfected ONL cells in these regions. It is unclear if the transfected photoreceptors died, and if so as a result of *Glb1l2* knockdown or other reasons. It would be interesting to assess cell death after knockdown by TUNEL assay (terminal deoxynucleotidyl transferase dUTP nick-end labelling, to detect apoptotic cells) or other methods and to determine how early it occurs; by P10 the effect is already seen, but it may be apparent even earlier. The expression pattern and knockdown phenotype of *Glb1l2* suggest that it may play an important role in rod photoreceptors; interestingly, its family member Glb1l3 showed altered expression in a mouse model of Leber's congenital amaurosis (Le Carre et al., 2011).

While *Glb1l2* is indeed an interesting candidate, due to time limitations only one gene could be further characterised in detail. We ultimately selected *Frmpd1* for a more in-depth molecular and functional characterisation (Chapters 3-5) due to the striking phenotype observed upon *Frmpd1* shRNA knockdown. Regardless of the sequence region targeted by shRNA, concentration of shRNA used, or age at which a phenotype was assessed, there was a clear disruption of retinal architecture when *Frmpd1* was knocked down by *in vivo* electroporation. Rosettes similar to those observed with *Frmpd1* knockdown have been seen in mouse models with inhibited Sonic Hedgehog (Shh) signalling (Wang et al., 2002) and humans with NR2E3 mutations (Wang et al., 2009). They have also been described for mice deficient in Crumbs1 and Crumbs2 (Alves et al., 2014), proteins involved in establishing adherens junctions between photoreceptors and Müller glia at the outer limiting membrane (OLM). Rosettes in the $Nrl^{-/-}$ retina have similarly been attributed to defects in the OLM (Stuck et al., 2012). It is therefore possible that the rosettes formed after Frmpd1 knockdown are also a result of a disruption of the OLM, suggesting a potential role for Frmpd1 in forming photoreceptor cell-cell contacts. A more thorough review of the predicted functions of Frmpd1 and its family members is provided in Section 3.1.

While *in vivo* electroporation is a useful tool for high-throughput screening applications such as this which allowed us to quickly assess phenotypes, the technique does have a few weaknesses. One is the inherent variability based on injection site and electroporation efficiency; this necessitates the use of many replicates to verify results. Care was also taken to ensure that the rosettes seen in *Frmpd1* knockouts were not an artefact of injection- images were taken away from the injection site, which often has

a disruption in structure even with control shRNAs, and multiple people injected the same constructs with similar results. However, this would not account for potential off-target effects of the shRNA. While the target sequences used in each shRNA were selected to be highly dissimilar to any other genes, it is still possible that they could non-specifically knock down unintended targets. It is important to note that the most dramatic *Frmpd1* shRNA phenotypes were seen with constructs targeting sequences within the FERM and PDZ domains, which are more likely to contain higher sequence similarity with other genes. Knockdown efficacy and specificity could be assessed by flow-sorting GFP-positive transfected cells and performing qPCR or RNA-seq on them. Another point to note is that albino CD1 mice are typically used for *in vivo* electroporation because of the ease of injection visibility, large litter sizes, and lower risk of cannibalisation of pups by mothers after surgery. However, albino mice are known to have visual difficulties which could result in inconsistencies in phenotypes when compared to other backgrounds (Sanyal and Hawkins, 1986, Balkema, 1988, Balkema and Drager, 1991). Finally, knockdown of genes does not always phenocopy a full knockout. In the case of retina transcription factor Pias3, for example, shRNA knockdown exhibited a much more dramatic phenotype than that observed in transgenic knockout mice (Campla et al., 2017).

Nevertheless, knockdown of genes by *in vivo* electroporation of shRNA was used to narrow down the list of candidate genes to a single target for characterisation as it provided a means to quickly screen the genes of interest for any obvious phenotypes. Admittedly this method could generate false-positives and false-negatives, but still proved useful for our purposes: further characterisation of *Frmpd1* revealed an interesting tissue-specific regulatory mechanism, protein-protein interactome, and role

in the maintenance of rod homeostasis and phototransduction which are described in detail in the following chapters.

3

Alternative promoter of *Frmpd1* is regulated by Nrl and Crx

3.1 Introduction

3.1.1 The Frmpd family of proteins

The Frmpd (FERM and PDZ domain containing) proteins are a relatively recently identified family consisting of 4 members (Frmpd1, Frmpd2, Frmpd3, and Frmpd4) whose functions are widely unknown but generally considered to act as scaffolding proteins (Moleirinho et al., 2013). As the name implies, the Frmpd proteins all contain FERM (4.1/ezrin/radixin/moesin) and PDZ (PSD-95/Dlg1/ZO-1) domains which are described in more detail in the following sections (Figure 3.1). Frmpd1 and Frmpd4 are most closely related in protein sequence, followed by Frmpd3 (Figure 3.1a); these 3 proteins all share a common domain organisation consisting of an N-terminal PDZ domain followed by a FERM domain (Figure 3.1b). Although the remaining portions of Frmpd proteins are thought to have an intrinsically disordered

structure (Uversky, 2014), this is also where binding sites for other proteins are located (Pan et al., 2013, An et al., 2008), at least one of which is particularly well-conserved between Frmpd1 and Frmpd4 (Takayanagi et al., 2015). Frmpd2 differs considerably from the other Frmpd family members (Figure 3.1a), instead consisting of a KIND (kinase non-catalytic C-lobe domain), FERM, and 3 PDZ domains (Figure 3.1b). The FERM and PDZ domains common to all 4 Frmpd family members, and the family members themselves, are described in detail below:

3.1.2 FERM domain

FERM (4.1/ezrin/radixin/moesin) is a cysteine-rich hydrophobic domain consisting of ~300 amino acids most commonly found at the N-terminus of proteins. It is composed of 3 subdomains (F1, F2, and F3), which interact with one another to form a globular structure. These subdomains have a ubiquitin-like structure with a Ras-binding domain (F1), an acyl-CoA-binding-protein-like domain (F2), and a phosphotyrosine-binding, plekstrin homology, Ena/vasodilator-stimulated phosphoprotein homology 1 domain (F3)(Moleirinho et al., 2013).

Most proteins with FERM domains interact with both the plasma membrane and cytoskeleton and are considered to act as scaffolding proteins, although they display tissue- and context-dependent functions (Moleirinho et al., 2013). The two main protein families associated with this domain are Frmd (FERM domain)- and Frmpd (FERM and PDZ domain)- containing proteins that fall into three general groups (Moleirinho et al., 2013):

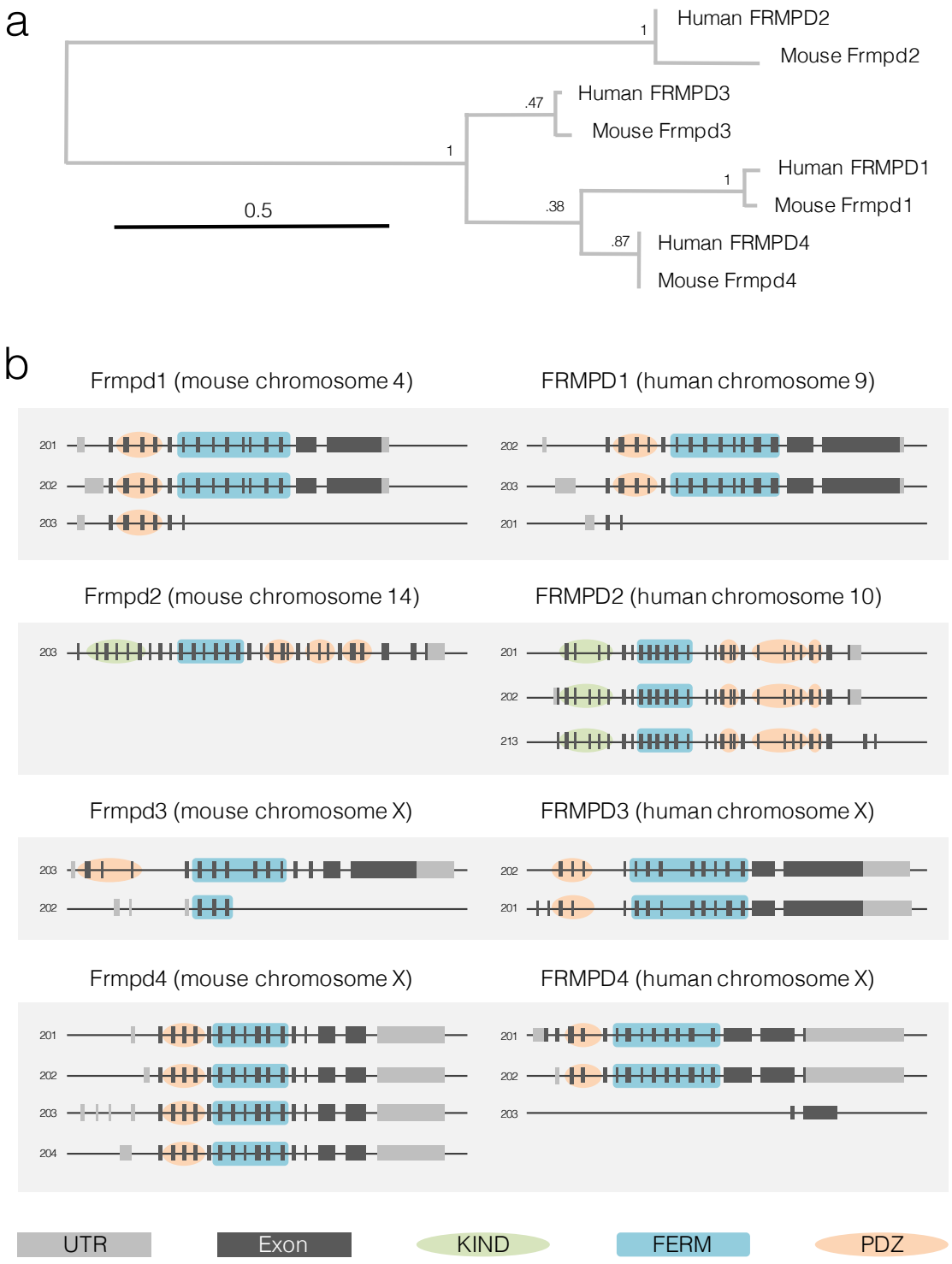

Figure 3.1: The Frmpd family of proteins. (A) Phylogenetic analysis. Relatedness of the Frmpd family members was calculated based on protein sequences obtained from CCDS. Protein sequences were entered into (http://www.phylogeny.fr/simple_phylogeny.cgi). Lengths of branches indicate degree of similarity (out of 1), and branch support values are given at each node. (B) Protein domain structures. All annotated transcripts from Ensembl.org are provided for each gene, with untranslated exons (UTR) in light grey and protein-coding exons (Exon) in dark grey.

1) Talins and kindlins: these proteins bind to and activate integrins, also playing a role in cell adhesion, spreading, and signalling (Calderwood et al., 2013).

2) ERMs (ezrin/radixin/moesin), GEFs (guanine-nucleotide-exchange factors), kinases and phosphatases: ERMs are involved in organizing membrane domains through interactions between transmembrane proteins and the cytoskeleton (Fehon et al., 2010), GEFs are guanine nucleotide exchange factors that facilitate the exchange of guanosine diphosphate (GDP) for guanosine triphosphate (GTP) thus activating GTPases (Cherfils and Zeghouf, 2013), while kinases and phosphatases catalyse the addition or removal of phosphate groups, respectively.

3) Myosins and KRITS (Krev interaction trapped proteins): Myosins are a large group of ATP-dependent actin-based motor proteins which act to transport various cargo including vesicles, biomolecules, and organelles (Syamaladevi et al., 2012, Hartman and Spudich, 2012). KRIT proteins have been implicated in controlling endothelial permeability and stabilizing endothelial cell-cell junctions (Liu et al., 2011, Corr et al., 2012).

3.1.3 PDZ domain

PDZ domains are 80-100 amino acid domains commonly found in signalling proteins (Ponting, 1997), named for the initials of the first proteins in which they were discovered: PSD-95 (95 kDa protein involved in signalling at the post-synaptic

density), DLG (Drosophila melanogaster discs large protein) and ZO-1 (zonula occludens 1 protein involved in maintenance of epithelial polarity) (Harris and Lim, 2001). The domain structure is not highly conserved, but usually consists of 2-3 α-helices and 5-6 β-strands (Lee and Zheng, 2010). PDZ domains are highly abundant in the mammalian genome and typically function in establishing and maintaining cell polarity and/or in anchoring membrane receptors to the cytoskeleton, forming signal transduction complexes and keeping them in place (Harris and Lim, 2001); this is generally accomplished through binding interactions with the extreme C-terminus of target proteins (Lee and Zheng, 2010). Even within the same protein, different PDZ domains can serve distinct functions and form unique protein-protein interactions, contributing further to their functional diversity. These protein-protein interactions can then be further modulated through mechanisms such as allosteric interactions and post-translational modifications; for example, phosphorylation at the C-terminus of PDZ-binding proteins or of the PDZ domain itself can either promote or inhibit PDZ interactions (Lee and Zheng, 2010).

3.1.4 Frmpd family members 2-4

3.1.4.1 Frmpd2

Frmpd2 is located on human chromosome 10 and mouse chromosome 14; it was initially cloned as part of The National Institutes of Health Mammalian Gene Collection (MGC) Program in 2002 (Strausberg et al., 2002) and has only recently been annotated in the mouse genome within the past year (which is why it was not included in the original candidate gene screen in Chapter 2, since RNA-seq reads were mapped against an older annotated genome).

Frmpd2 differs from the other Frmpd family members in its domain organisation; rather than 1 FERM and PDZ, Frmpd2 contains 1 FERM, 1 KIND (kinase non-catalytic C-lobe domain), and 3 PDZ domains. It appears that Frmpd2 plays a role in tight junction formation, where it may also possibly act as a scaffold for other molecules (Stenzel et al., 2009). Moreover, Frmpd2 can bind to catenin family proteins (Stenzel et al., 2009), including δ-catenin, a component of synaptic junctions (Kosik et al., 2005).

3.1.4.2 Frmpd3

Frmpd3 is located on the X chromosome in both mice and humans and was first identified from a sequencing project of human brain cDNA clones encoding large proteins (Nomura et al., 1994). According to the Human Protein Atlas (proteinatlas.org), Frmpd3 is most highly expressed in the cerebral cortex, thyroid gland, and ovaries. Frmpd3 is the least studied of the Frmpd family proteins, with no published literature concerning its function whatsoever. Its predicted function based on Ensembl (ensembl.org) gene ontology is neutrophil degranulation, where it may play a role in immunity, although there is currently no experimental evidence for this.

3.1.4.3 Frmpd4

Frmpd4 is located on the X chromosome in both mice and humans and was initially cloned as part of The National Institutes of Health Mammalian Gene Collection (MGC) Program (the same project that identified Frmpd2) (Strausberg et al., 2002). It received little attention until a yeast two hybrid screen revealed its interaction with Psd95, a postsynaptic density protein

involved in synapse formation and regulation (Lee et al., 2008). Frmpd4, also known as Preso or Preso1, is localised at the tips of growing dendrites in immature neurons and increases dendritic spine density (Lee et al., 2008). It is also asymmetrically distributed in the cytosol of neural stem/progenitor cells where it may contribute to asymmetric cell division (Lee et al., 2014). Furthermore, Frmpd4 has been shown to interact with and regulate glutamate receptors (Hu et al., 2017, Hu et al., 2012) and has been implicated in schizophrenia, perhaps contributing to altered glutamatergic signalling in this disorder (Matosin et al., 2016a, Matosin et al., 2016b, Matosin et al., 2015).

3.1.5 Frmpd1

Frmpd1 is located on human chromosome 9 and mouse chromosome 4, and was initially cloned from a brain cDNA library (Nagase et al., 1999). It remained unstudied until nearly 10 years later when it was identified by yeast two-hybrid screen as a binding partner of Gpsm1 (G Protein Signaling Modulator 1, also known as Ags3) (An et al., 2008). Expressed endogenously in brain, lung, testis, CAD, NG108-15, PC-12, and F9 cell lines, *Frmpd1* is most similar to *Frmpd3* and *Frmpd4* in its domain structure compared to *Frmpd2* (An et al., 2008). While both the FERM and PDZ domains of Frmpd1 are required for its membrane localisation, it is the central portion of Frmpd1 that interacts with Gpsm1, suggesting that it functions as a scaffolding molecule to position Gpsm1 near the membrane (An et al., 2008). Frmpd1 may act to bring Gpsm1 and Gα subunits together, since Gpsm1 switches its binding partner from Frmpd1 to Gα as the concentration of Gα increases (An et al., 2008). Similarly, Frmpd1 has also been shown to interact with Gpsm2 (G Protein Signaling Modulator

2, also known as LGN) through Gpsm2's TPR (tetratricopeptide) motif; the TPR motifs between Gpsm1/2 share 77% sequence identity (Pan et al., 2013). The portion of Frmpd1 that interacts with Gpsm1/2 is highly conserved amongst species and also with its family member Frmpd4 (Pan et al., 2013), although Frmpd4 makes multiple contacts with the TPR motif of Gpsm2 whereas Frmpd1 only interacts with the core domain (Takayanagi et al., 2015). Beyond the characterisation of its interactions with Gpsm1/2 as a potential scaffolding molecule, Frmpd1 and its function have remained largely unstudied.

The candidate gene screen described in Chapter 2 led to the identification of *Frmpd1* as a novel gene likely to play a role in rod photoreceptor development and homeostasis. Since the retina frequently expresses tissue-specific isoforms of genes (Popova et al., 2017, Farkas et al., 2013, Hao et al., 2011, Hao et al., 2014), we wanted to determine if this was also the case for *Frmpd1*. We first validated its rod-enhanced RNA-seq expression profile during development by *in situ* hybridisation. To more closely examine the regulatory mechanisms contributing to high *Frmpd1* levels in rods, we then determined its transcription start site (TSS) in brain and retina by 5' rapid amplification of cDNA ends (5'-RACE). Interestingly, 5'-RACE revealed that Frmpd1 uses a retina-specific alternative promoter, which we then characterised in further detail using a variety of *in silico*, *in vitro*, and *in vivo* approaches as described in the following chapter.

3.2 Materials and methods

3.2.1 Materials

For reagent details, buffer compositions, and plasmid maps refer to Appendices A-D.

3.2.2 Methods described in other sections

2.2.2 RNA-seq differential expression analysis 31
2.2.3 Hierarchical clustering and heat maps 34
2.2.5 Mouse lines & husbandry 35
2.2.6 RNA isolation 35
2.2.7 Plasmid DNA isolation 36
2.2.8 DNA precipitation 36
2.2.9 In vivo electroporation 37
2.2.10 Retina cryosectioning 37
2.2.11 *In situ* hybridisation (ISH) 39

3.2.3 Immunohistochemistry

Frozen cryosections were covered with 1x PBS to dissolve OCT and equilibrated to room temperature, then blocked for 1 hr at room temp in blocking solution (5% normal donkey serum, 0.3% Triton X-100 dissolved in 1x PBS then passed through a 0.22 μm filter). Depending on fixation time and primary antibody used, sections were then incubated either overnight or multiple nights in a humidified chamber at 4˚C with primary antibody diluted in blocking solution. The next day, sections were washed 4x with 0.1% Triton X-100 in 1x PBS for 10 min each at room temp, then incubated at room temp for 1 hr with appropriate secondary antibodies diluted in blocking solution. Sections were again washed 4x with 0.1% Triton X-100 in 1x PBS for 10 min each at room temp, stained for 5 min with DAPI in 1x PBS, washed again, then mounted with Fluoromount-G (Southern Biotech) and stored at 4˚C. Samples were imaged on a Zeiss 700 confocal microscope and processed with ImageJ software. Experiments were performed in technical triplicate and at least biological duplicate. A complete list of antibodies and concentrations used can be found in Appendix D.

3.2.4 In situ hybridisation and immunohistochemistry

In situ hybridisation was performed as described (see 2.2.11), but with Pretreat 3 instead of Pretreat 4 (Advanced Cell Diagnostics) for less protease digestion. Following the ISH protocol, slides were immediately washed with 1x PBS, then 2x with blocking buffer (5% normal donkey serum and 0.3% Triton X-100 in 1X PBS) before being blocked for 1 hr at room temp with blocking buffer. Slides were then incubated in a humidified chamber for 2 nights at 4˚C with primary antibody diluted in blocking solution. Subsequent washes, secondary staining, mounting, and imaging were performed as described in Section 3.2.3.

3.2.5 General PCR protocol and primer design

The PCR reaction is composed of several steps involving denaturation to separate double-stranded DNA into single strands, annealing for primers to hybridise with single-stranded DNA, and extension for *Taq* polymerase to synthesise complementary DNA in the 5’ to 3’ direction. Optimal annealing and extension temperatures/times vary depending on sequence composition and length of DNA target region to be amplified. Refer to Appendix C for specific primer sequences.

3.2.5.1 Primer design

Primers for use in polymerase chain reaction (PCR) were designed using Primer3 (http://primer3.ut.ee/) and tested for intended target specificity by Primer-BLAST (http://www.ncbi.nlm.nih.gov/tools/primerblast/). Primers were designed using the following parameters and ordered from Integrated DNA Technologies:

Product size: 100-150 bp

Primer size: 18-22 bp

T_m: 55-65, optimal 60˚C

% GC: 50-60

3.2.5.2 PCR reaction

In general, the following reaction was set up on ice and placed in a thermocycler at the given conditions:

1 μl	DNA Template
2 μl	NEB 10x Standard Taq (Mg-free) Reaction Buffer
1.2 μl	25nM $MgCl_2$
0.16 μl	25nM dNTPs
0.1 μl	NEB Standard Taq DNA Polymerase
0.2 μl	Forward primer (100 μM)
0.2 μl	Reverse primer (100 μM)
15.14 μl	H_2O
20 μl	Total

1 cycle		
94 ˚C	Denaturation	5 min
35 cycles		
94 ˚C	Denaturation	30 sec
56 ˚C (variable)	Annealing	30 sec (variable)
72 ˚C (variable)	Extension	1 min / kb (variable)
1 cycle		
72 ˚C	Extension	5 min

3.2.5.3 Agarose gel electrophoresis

To visualize PCR products, 10 μl of product + 2 μl 6x loading dye (NEB) was electrophoresed at 150 V on a 1-2% agarose (SeaKem, Lonza) gel in containing 0.1 μg/ml ethidium bromide (Invitrogen) and imaged on an Azure C200 Gel Doc Station (Azure Biosystems).

3.2.6 Recombinant DNA plasmid cloning

3.2.6.1 Insert amplification

DNA fragments of interest were PCR amplified from C57BL/6J mouse genomic DNA using a high-fidelity Taq polymerase (SeqAmp DNA polymerase, Clontech), appropriate primers including desired restriction sites and overhangs, and the following PCR conditions (details of primers are provided in Appendix C):

0.4 μl	Mouse genomic DNA template (40ng) or plasmid template (1ng)
12.5 μl	2X SeqAmp buffer (Clontech)
0.5 μl	Forward Primer (10 μM)
0.5 μl	Reverse Primer (10 μM)
0.5 μl	SeqAmp DNA polymerase (Clontech)
10.1 μl	H_2O

1 cycle	
94 ˚C	5 min
35 cycles	
94 ˚C	30 sec
60 ˚C (variable)	30 sec (variable)
72 ˚C (variable)	1 min / kb (variable)
1 cycle	
72 ˚C	5 min

3.2.6.2 Restriction enzyme digestion

PCR products were either purified directly, or gel extracted after being run on a 1.2% agarose gel at 60 V according to NucleoSpin Gel and PCR Cleanup manufacturer instructions (Machery Nagel). Insert and plasmid backbones were digested for 1 hr at 37˚C with appropriate restriction enzymes in CutSmart Buffer (New England Biolabs) and “PCR” purified again before ligation.

3.2.6.3 Ligation

Digested inserts and backbones were ligated overnight at 4˚C by T4 DNA Ligase according to manufacturer protocol (New England Bioscience). A 3:1 insert:vector molar ratio with 25 ng vector was used in a total volume of 10 μl. Ligation reactions were inactivated the next day for 10 mins at 65˚C and 2 μl was used to transform bacteria.

3.2.6.4 Bacterial transformation

Chemically competent Subcloning Efficiency DH5α bacterial cells were transformed with plasmid DNA according to manufacturer's protocol (Invitrogen). Briefly, cells were thawed on ice and 50 μl was aliquoted into a 1.5 ml microcentrifuge tube to which 0.5-5 μl of plasmid DNA was added and gently mixed. After a 30 min incubation on ice, cells were heat shocked for 20 sec in a 42˚C water bath then placed back on ice for 2 min. Pre-warmed SOC (Super Optimal broth with Catabolite repression, Quality Biological) media was added to the cells to bring the total volume to 1 ml, followed by incubation for 1 hr at 37˚C at 225 rpm. 100 μl of the transformation reaction was spread onto pre-warmed selective agar plates (100 μg/ml ampicillin or 50 μg/ml kanamycin) and incubated overnight at 37˚C.

3.2.6.5 Colony PCR

To quickly screen colonies for presence of correctly oriented inserts, a PCR reaction was set up with H_2O in place of cDNA template. A single colony from the original agar plate was picked up with a pipette tip and streaked onto a fresh plate, then used to inoculate the PCR mix before placing into the thermocycler.

3.2.7 Cell lines

HEK293 cells were cultured at 37˚C in 5% CO_2 in Dulbecco's Modified Eagle Medium (Thermo) supplemented with 10% fetal bovine serum, 1% penicillin/streptomycin, and 1% L-glutamine. Cells were passaged at 75-80% confluence and maintained for no more than 15 passages total for use in experiments.

3.2.8 Cell passaging and seeding

Media was removed from each flask, and cells were washed briefly with 1x PBS followed by addition of 4 ml 0.25% trypsin. After cells had detached (by 2-3 min incubation at 37˚C and gently tapping flask), 10 ml of complete media was added to quench the reaction. The cell suspension was transferred to a 15 ml aliquot tube and pelleted by centrifugation for 5 minutes at 1200 x *g*. Supernatant was removed and the cell pellet was resuspended in 5 ml of complete media and quantified by a Cellometer T4 Cell Counter (Nexcelcom). The cell suspension was then pipetted into new flasks (500 μl resuspension + 14.5 ml fresh complete media) or seeded at the desired density for transfections.

3.2.9 Cell transfection

HEK293 cells were seeded in 450 μl complete media at a density of 50,000 cells/well into 24-well plates. After 2 days, cells were transfected using Lipofectamine 2000 (Invitrogen) by adding 50 μl of concentrated DNA:lipid complex directly to each well containing cells and media for desired end concentrations of each plasmid construct per well. The DNA:lipid complexes were prepared by first combining all plasmids in OptiMEM (Life Technologies) media, then adding DNA solution to

Lipofectamine preincubated for 5 min at room temp in an equal volume of OptiMEM for a final DNA:Lipofectamine ratio of 1μg:3μl. Lipofectamine-DNA complexes were formed by incubating for 20 min at room temp before transfection.

3.2.10 Dual luciferase assay

HEK293 cells were cotransfected (Section 3.2.9) in biological triplicates with 50 ng of promoter-luciferase construct, 1 ng of pRL-CMV, 150 ng of NRL and/or CRX expression construct, and 0-300 ng of empty pcDNA4/HisMax C to bring total amount of DNA to 351 ng per well. The NRL and CRX expression constructs were previously cloned in the lab by insertion of the human coding region of each gene into pcDNA4/HisMax C (Cheng et al., 2004). Plasmid maps are provided in Appendix B. Forty-eight hours post-transfection, cells were harvested and luminescence of firefly and renilla luciferases measured according to the Dual Luciferase Reporter Assay System manufacturer's protocol (Promega). Briefly, each well of cells was washed with 1x PBS then lysed in 100 μl of Passive Lysis Buffer for 30 min while rocking at room temp. Lysates were collected and frozen at -20˚C until the assay was performed. 100 μl of Luciferase Assay Reagent II + 20 μl of cell lysate was mixed in each well of an opaque white 96-well flat-bottomed plate (Greiner) and firefly luciferase activity recorded, then 100 μl of Stop & Glo reagent (Promega) was added and renilla luciferase activity recorded as an internal control to normalize for transfection efficiency. Luminescence measurements were recorded with the Modulus Microplate Luminometer (Turner BioSystems)

3.2.11 Site-directed mutagenesis

Mutations were introduced into the Frmpd1 minimal promoter luciferase construct (Appendix B) according to Q5 Site-Directed Mutagenesis Kit manufacturer's instructions (New England Biolabs). Briefly, mutagenesis primers were designed with the NEBaseChanger online tool (http://nebasechanger.neb.com) and the following PCR reaction was performed (primer sequences can be found in Appendix C):

1.0 μl	Plasmid template (10 ng)
12.5 μl	Q5 Hot Start High-Fidelity 2X Master Mix
1.25 μl	Forward Primer (10 μM)
1.25 μl	Reverse Primer (10 μM)
9.0 μl	H_2O

1 cycle	
98 ˚C	30 sec
25 cycles	
98 ˚C	10 sec
62 ˚C (Nrl), 72 ˚C (Crx)	20 sec
72 ˚C	3 min
1 cycle	
72 ˚C	2 min

Methylated plasmid template was digested with *DpnI*, and PCR products were phosphorylated and circularised by kinase and ligase, respectively, in the following KLD (kinase, ligase, *DpnI*) reaction incubated at 5 min at room temp: 1 μl PCR product, 5 μl 2X KLD Reaction Buffer, 1 μl 10X KLD Enzyme Mix, 3 μl H_2O. Five μl of the KLD reaction was then used to transform 50 μl DH5α competent cells (Section 3.2.6.4) and correctly targeted clones were identified by Sanger sequencing (Genewiz) of plasmid minipreps (Section 2.2.7).

3.2.12 5'-Rapid Amplification of cDNA Ends (RACE)

5'-Rapid Amplification of cDNA Ends (RACE) is a technique used to amplify the 5'-end of an mRNA transcript using only a single primer specific to the target, and is therefore frequently used to determine transcription start sites (TSSs) of full-length mRNAs when only part of the target sequence is known (Scotto-Lavino et al., 2006). Here, we have used a commercially available kit (SMARTer RACE 5'/3' kit, Clontech). Briefly, mRNA is used to prepare 5'-RACE-ready cDNA, using a reverse transcriptase that adds several additional residues when it reaches the end of the mRNA template that are annealed to an oligonucleotide of known sequence during the cDNA synthesis reaction (Zhu et al., 2001) (Figure 3.2). This provides a universal "forward" primer at the end of every transcript that can then be used with a gene-specific "reverse" primer for PCR amplification of transcripts of interest from total cDNA preparations. Gene-specific primer sequences are given in Appendix C. Each of these primers also contains a 15-bp overlap for rapid In-Fusion HD cloning into the pRACE sequencing vector (Clontech) so that the amplified 5'-RACE product's sequence can then be determined by Sanger sequencing (Genewiz).

Mouse 5'-RACE

Mouse 5'-RACE cDNA was prepared from 138 ng (retina), 246 ng (brain), or 366 ng (lung) total RNA according to manufacturer's protocol (Clontech SMARTer RACE 5'/3' kit) and diluted in 10, 90, or 30 μl of Tricine EDTA (Clontech), respectively. The following touchdown PCR reaction was performed:

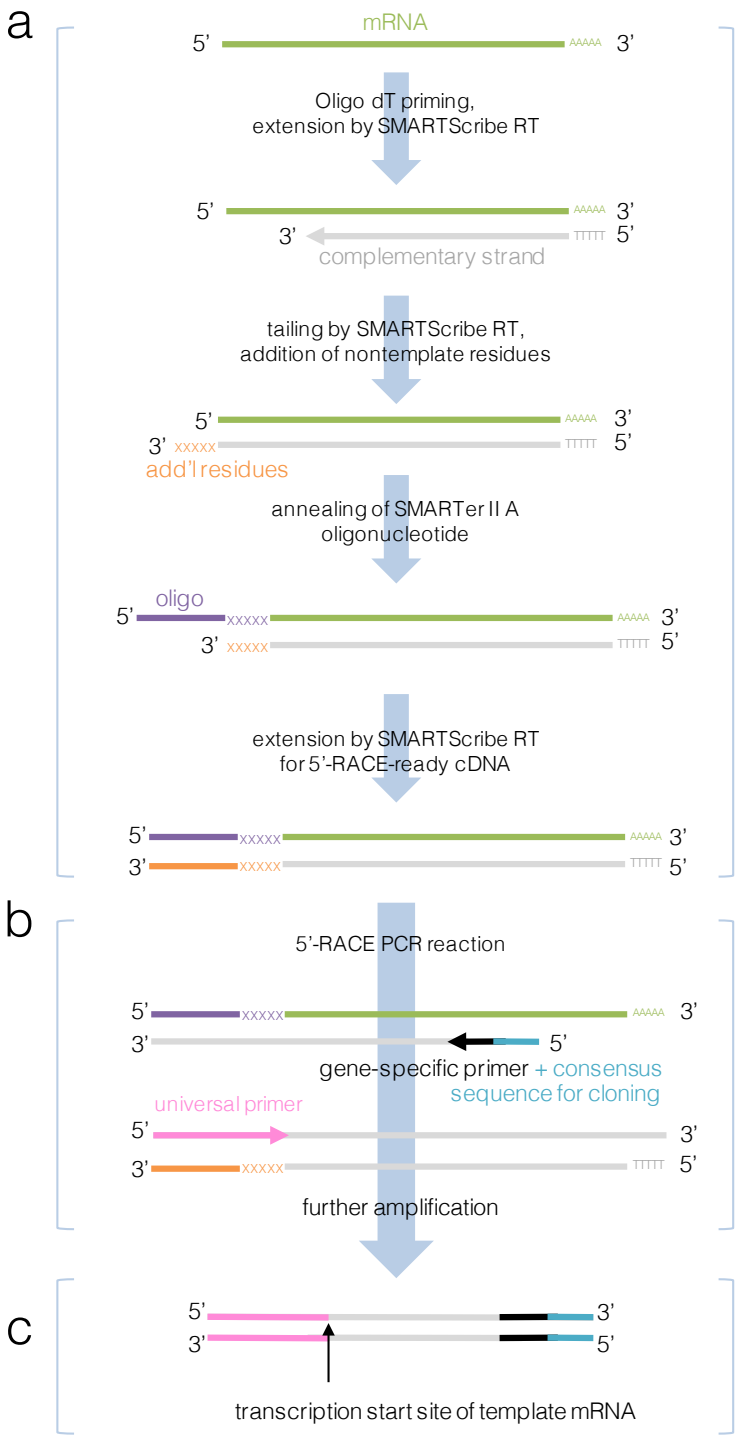

Figure 3.2: 5'-Rapid amplification of cDNA ends (5'-RACE). (A) RACE-ready cDNA synthesis. Oligo dT primers are used to prime polyadenylated mRNA template, which is reverse transcribed by SMARTScribe reverse transcriptase (RT). The RT enzyme adds additional residues when it reaches the end of the template, allowing for annealing of the SMARTerII A oligonucleotide. The new overhang produced is filled in by RT as well. (B) 5' amplification of cDNA ends. Every cDNA transcript generated in (A) now contains a known sequence at its 5' end, allowing for priming by a complementary universal primer in the "forward" direction. Gene-specific primers allow for "reverse" priming. (C) RACE PCR product. The final 5'-RACE PCR product contains consensus sequences on both ends, one originally derived from the SMARTer II A oligonucleotide, and one inserted by appending a consensus sequence to the gene-specific primer. These consensus sequences allow for directional cloning into the pRACE sequencing vector for downstream sequence analysis.

2.5 μl	RACE cDNA template (11.5 ng retina, 5.6 ng brain, 18.3 ng lung)
5 μl	10X Universal primer mix (UPM)
1 μl	10 μM Mouse Exon 8 Primer
41.5 μl	Master mix (15.5 μl H_2O + 25 μl 2X SeqAmp Buffer + 1 μl SeqAmp DNA Polymerase)

5 cycles	
94 ˚C	30 sec
72 ˚C	3 min
5 cycles	
94 ˚C	30 sec
70 ˚C	30 sec
72 ˚C	3 min
25 cycles	
94 ˚C	30 sec
65 ˚C	30 sec
72 ˚C	3 min

The following nested PCR reaction was then performed:

5 μl	Touchdown RACE PCR product (brain) or 2.5 μl PCR product + 2.5 μl H_2O (retina)
1 μl	UPM Short
1 μl	10 μM Mouse Exon 6 Primer
43 μl	Master mix (17μl H_2O + 25 μl 2X SeqAmp Buffer + 1 μl SeqAmp DNA Polymerase)

20 cycles	
94 ˚C	30 sec
65 ˚C	30 sec
72 ˚C	1 min

Reactions were also performed using retina cDNA with and nested primers within Exon 1a to confirm retina transcription start site (TSS), and with a touchdown primer

within Exon 16 to compare transcripts between wild type and *Nrl*$^{-/-}$ retina cDNA. Primer sequences are provided in Appendix C.

3.2.12.1 Human 5'-RACE

Human 5'-RACE cDNA was prepared from 1 μg retina (Clontech #636579) or brain (Clontech #636530) total RNA then diluted in 90 μl Tricine EDTA. The touchdown PCR was performed as described for mouse but using a primer specific to Human Exon 8. The following nested PCR reaction was then performed:

2.5 μl	Touchdown RACE PCR product
1 μl	UPM Short
1 μl	10 μM Human Exon 6 Primer
45.5 μl	Master mix (19.5 μl H_2O + 25 μl 2X SeqAmp Buffer + 1 μl SeqAmp DNA Polymerase)

20 cycles	
94 ˚C	30 sec
65 ˚C	30 sec
72 ˚C	3 min

3.2.12.2 5'-RACE product cloning and sequence alignments

10 μl of each final nested PCR product was run at 60 V on a 1.2% agarose gel (Section 3.2.5.3), after which bands were excised under UV light and gel purified according to manufacturer protocol (Macherey Nagel NucleoSpin Gel and PCR Clean-Up Kit). Products were eluted in 25 μl NE; 7 μl of this was used for In-Fusion cloning into the pRACE vector and transformed into Stellar Competent Cells as described in the SMARTer RACE 5'/3' protocol (Clontech).

At least 10 independent clones were sequenced using M13R primer. All sequence before and including vector overlap region (5'-gcagtggtatcaacgcagagtacatgggg-3') was

removed before submitting to Cap3 (http://doua.prabi.fr/software/cap3) to generate RACE consensus sequences.

3.2.13 5'-untranslated region (UTR) analysis

3.2.13.1 DNAse hypersensitivity, Nrl ChIP-seq, and Crx ChIP-seq alignments

FASTQ alignments described here were performed by Vijender Chaitankar and were made available as BAM files to view in IGV (Integrated Genomics Viewer, Broad Institute). FASTQ files from Crx transcription factor ChIP-seq were downloaded from Gene Expression Omnibus (GEO) with accession IDs GSE20012 and GSE54084 (Corbo et al., 2010). Nrl ChIP-seq data (Hao et al., 2012) was downloaded from https://datashare.nei.nih.gov/nnrlMain.jsp. DNase-seq data was downloaded from the mouse ENCODE project (Wilken et al., 2015). The low-quality bases of FASTQ reads were trimmed using Trimmomatic (Bolger et al., 2014) with parameters SLIDINGWINDOW:4:15 and MINLEN:24. The cleaned FASTQ reads were then aligned to the mouse reference genome (mm10) using BWA backtrack algorithm (Li and Durbin, 2009). Alignments that were unmapped, having a mapping score < 20, and secondary alignments were filtered using Samtools (Li et al., 2009) with the following parameters: '-q 20 -F 1796'.

3.2.13.2 Mammalian conservation and putative binding site prediction

Mammalian conservation (Placental Mammal Basewise Conservation by PhyloP) track on UCSC Genome Browser (https://genome.ucsc.edu/) was visualised using the December 2011 (GRCm38/mm10) assembly. Mammalian sequence alignments (17 Eutherian Mammals EPO) of the *Frmpd1* gene were exported as a ClustalW file from

Ensembl.org. MatInspector (Genomatix) was used to identify predicted transcription factor binding sites.

3.2.14 cDNA synthesis

Complementary DNA (cDNA) was synthesised from 2 μg total RNA (Section 2.2.6) using either Superscript II Reverse Transcriptase (Invitrogen) or QuantiTect Reverse Transcription Kit (Qiagen) with Oligo(dT)$_{12\text{-}18}$ according to manufacturer's instructions. Briefly, 2 μg total RNA, 1 μl of 5 μg/ml Oligo(dT)$_{12\text{-}18}$, and 1 μl 10 mM dNTP mix and water to bring total volume to 12 μl was added to a microcentrifuge tube and incubated 5 min at 65˚C. The reaction was chilled on ice, then 4 μl 5X First-Strand Buffer, 2 μl 0.1 M DTT, and 1 μl of RNaseOUT were added and incubated for 2 min at 42˚C. 1 µL (200 units) of SuperScript II reverse transcriptase and water to bring total volume to 20 μl was added, then incubated for 50 min at 42˚C. The reaction was then terminated by heating for 15 min at 70˚C.

3.2.15 Nuclear protein extraction

Snap-frozen P21 mouse retinae (8-10) were thawed in ice-cold hypotonic buffer (20 mM Tris HCl, pH 7.4, 10 mM NaCl, 3 mM $MgCl_2$) on ice, homogenised using a handheld plastic pestle homogenizer, and incubated on ice for 15 min. 25 μl of 10% 4-Nonylphenyl-polyethylene glycol (Sigma) was added and vortexed at highest setting for 10 sec, then centrifuged for 10 min at 3,600 x *g* 4˚C. The supernatant (cytoplasmic fraction) was aspirated and the nuclear pellet was resuspended in 50 μl complete cell extraction buffer (10 mM Tris, pH 7.4, 100 mM NaCl, 1% Triton X100, 1 mM EDTA, 10% glycerol, 1 mM EGTA, 0.1% SDS, 0.5% sodium deoxycholate, 1x

protease inhibitor, 1x phosphatase inhibitor) with plastic pestle handheld homogenizer. After a 10 min incubation on ice, the nuclear suspension was sonicated twice for 5 sec, amp 1 then incubated for 20 min on ice with vortexing at 10 min intervals. The lysate was then centrifuged for 30 min at 14,000 x *g* at 4˚C and supernatant (nuclear fraction) was quantified by BCA assay (Section 3.2.16) and stored at -20˚C.

3.2.16 Bicinchoninic acid (BCA) assay

Twenty-five µl each of Bovine Serum Albumin (BSA) standards (0, 25, 50, 100, 250, 500, 750, 1000, 2000 µg/ml) and protein lysates were pipetted into a clear flat-bottomed 96-well plate in duplicate. BCA reagent was prepared according to manufacturer's protocol (BCA Protein Assay Kit, Thermo Scientific) and 200 µl of the reagent was added to each well. The plate was then incubated for 30 mins at 37°C, after which absorbance at 570 nm was read in a SpectraMax M5 plate reader (Molecular Devices). A standard curve was then generated and analysed to determine protein concentration of each sample.

3.2.17 Electrophoretic mobility shift assay (EMSA)

Total nuclear extract was isolated (Section 3.2.15) from P21 mouse retina and quantified by BCA assay (Section 3.2.16). EMSA was performed using a LightShift Chemiluminescent EMSA Kit (Thermo) with minor modifications. Briefly, 5 μg nuclear extract was incubated at room temp for 45 min with 1x Binding Buffer, 50 ng/μl Poly dI dC, 5 mM $MgCl_2$, and 0 or 1 pmol unlabeled competitor DNA in H_2O up to 19 μl. Following this incubation, 5 fmol of biotin-labeled DNA was added and allowed to

incubate at room temp 1 hr longer. Reactions were terminated by addition of loading buffer, separated on 6% DNA retardation gel (Invitrogen), and transferred to a nylon membrane before being developed according to Chemiluminescent Nucleic Acid Detection Module Kit manufacturer instructions (Thermo).

3.3 Results

3.3.1 Frmpd1 RNA expression is upregulated primarily in rod photoreceptors during development

As Frmpd1 was identified through the candidate screen as upregulated in flow-sorted rod photoreceptors from postnatal day (P)2-28, we wanted to assess if its expression was restricted to this cell type. A 25-cycle PCR amplification of *Frmpd1* from a cDNA panel of tissues from adult wildtype mice (P21) shows that Frmpd1 expression is highest in the retina, with trace amounts also found in the lung and brain (Figure 3.3a). The absence of rhodopsin in the lung and brain samples indicate that these samples were not contaminated with retina tissue and that *Frmpd1* is indeed expressed in these tissues, albeit at low levels. Endpoint PCR to detect *Frmpd1* was used to ascertain which tissues had the most obvious enrichment of expression, although more sensitive methods such as quantitative PCR may be more effective at detecting lower expression levels such as those in brain and lung (Gal et al., 2006).

A comparison of temporal RNA expression profiles from whole retina, flow-sorted rods, and flow-sorted "cone-like" photoreceptors suggests that the rod expression accounts for most of the expression of *Frmpd1* in the retina (Figure 3.3b). A student's t-test indicated no statistically significant differences between rod and whole-retina expression during development except at P10 ($p=0.011$). Rods comprise ~70% of the

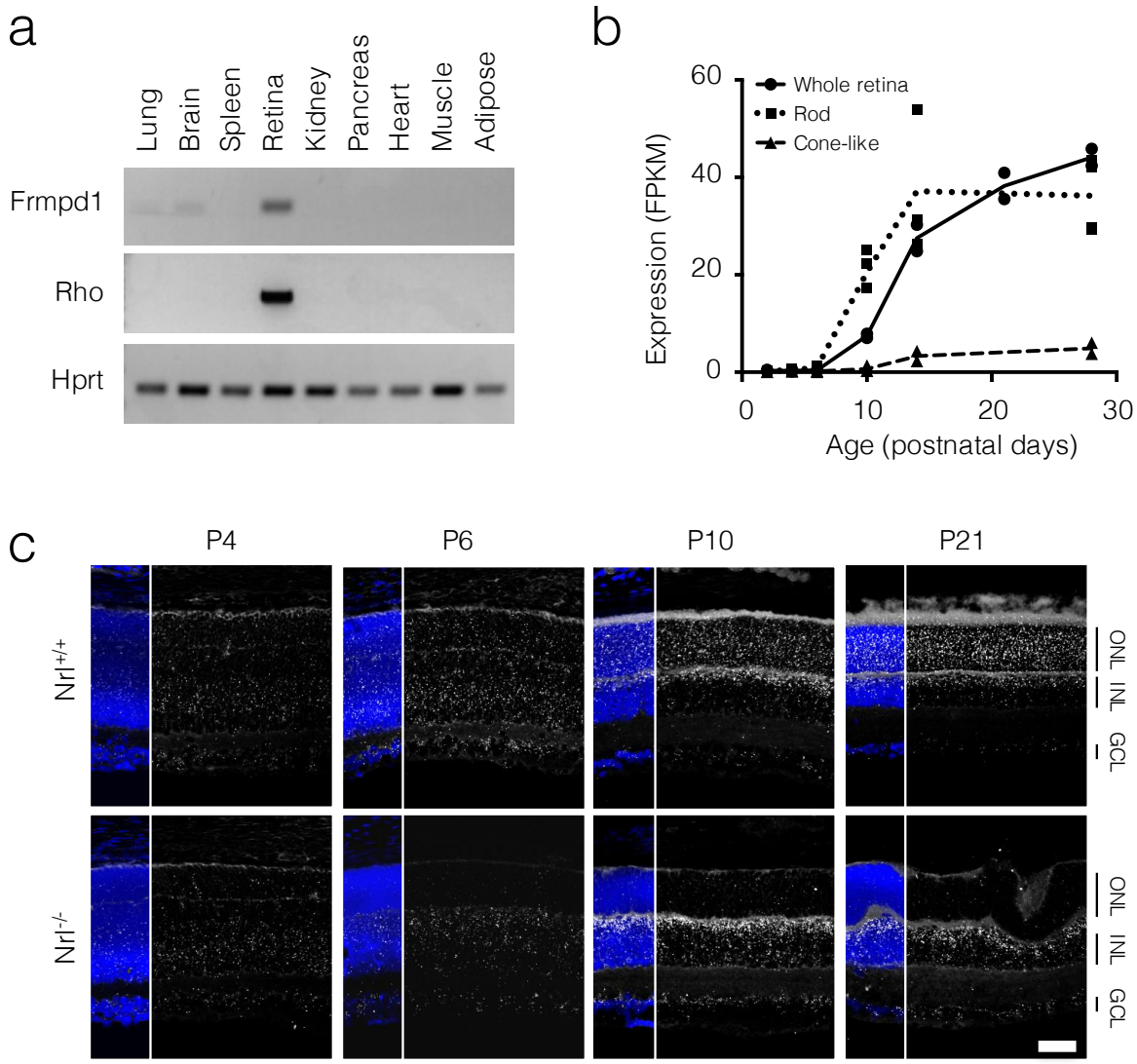

Figure 3.3: *Frmpd1* expression is enriched in rod photoreceptors during development. (A) *Frmpd1* expression in various tissues. Presence of *Frmpd1* mRNA was assessed in various tissues via PCR using P21 mouse cDNA as template. *Rhodopsin* (Rho) primers were used to detect for retina contamination in other samples, and *Hprt* was used as a loading control. (B) *Frmpd1* expression in flow-sorted photoreceptors. Relative expression (fragments per kilobase of exon per million reads mapped; FPKM) of *Frmpd1* transcripts were assessed by RNA-seq transcriptome profiling of whole wild-type retina, flow-sorted rod (*Nrl*-GFP), and flow-sorted cone-like (*Nrl*-GFP:*Nrl*$^{-/-}$) photoreceptors. Data points represent each of 2-4 biological replicates as described in Section 2.2.2. (C) RNA expression of *Frmpd1* during development. Localisation of *Frmpd1* RNA was assessed by *in situ* hybridisation during development of rod-dominated (*Nrl*$^{+/+}$) and cone-dominated (*Nrl*$^{-/-}$) mouse retina. Background autoflourescence can be seen in the outer plexiform and outer segment regions; bright punctate staining represents RNA. Scale bar, 50 μm. ONL, outer nuclear layer; INL, inner nuclear layer; GCL, ganglion cell layer.

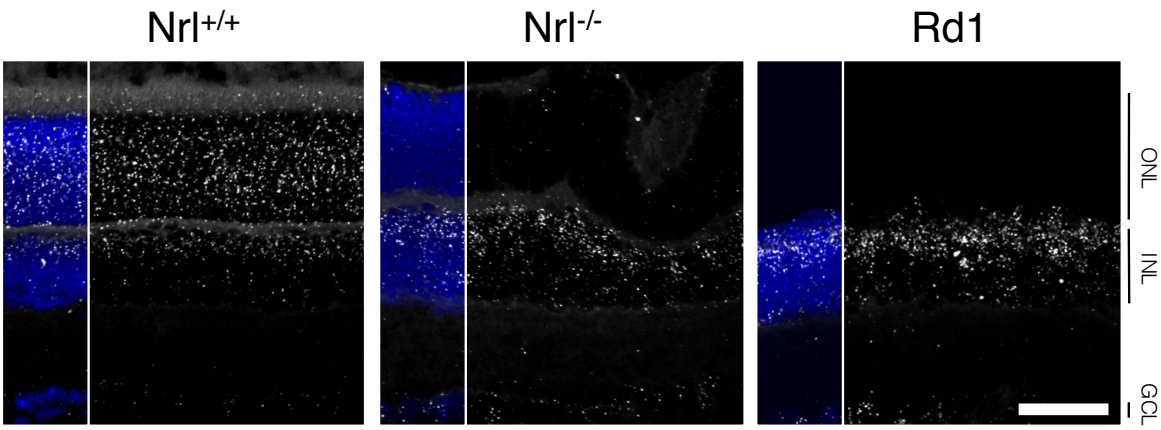

Figure 3.4: *Frmpd1* expression can be detected in the inner nuclear layer. Localisation of *Frmpd1* RNA in retina. Localisation of *Frmpd1* RNA was assessed by *in situ* hybridisation of P21 mouse retina from wild-type ($Nrl^{+/+}$), rodless ($Nrl^{-/-}$), and rodless/coneless degeneration model (*Rd1*) mice. Background autoflourescence can be seen in the outer plexiform and outer segment regions; bright punctate staining represents RNA. Scale bar, 50 μm. ONL, outer nuclear layer; INL, inner nuclear layer; GCL, ganglion cell layer.

cells in the murine retina (Swaroop et al., 2010), so this does not necessarily indicate rod specificity, but does imply enrichment in this cell type. Differences in expression between flow-sorted rods and cone-like photoreceptors were apparent, and became more pronounced in the second half of development (P10, $p=0.0003$; P14, $p=0.054$; P28, $p=0.006$) (Figure 3.3b). To validate RNA-seq expression profiling, *in situ* hybridisation (ISH) was used to visualise *Frmpd1* RNA within the retina during development (Figure 3.3c). Consistent with the pattern of expression from RNA-seq, ISH revealed that the level of *Frmpd1* RNA increased from P4-21 with an enrichment in the ONL where rod nuclei are present. Moreover, by P21, the top row of nuclei in the ONL (where cone nuclei are found) appears to contain much less *Frmpd1*, providing further evidence for rod vs. cone cell expression.

To further investigate the specificity of *Frmpd1* expression, ISH was performed on a cone-dominated $Nrl^{-/-}$ retina where all rods have been converted into S-cone-like photoreceptors. In this model, all ONL expression was lost, suggesting that *Frmpd1* expression in the ONL is restricted to the rods and also regulated by rod-specific transcription factor *Nrl*. Interestingly, in both $Nrl^{+/+}$ and $Nrl^{-/-}$ models, expression was also observed in the INL and to a lesser extent in the GCL (Figure 3.3, 3.4). This expression persisted when tested in the retinal degeneration model *Rd1*, whose rods and cones have degenerated by P21 to leave only an INL and GCL (Figure 3.4). The localisation of RNA towards the upper portion of the INL suggests horizontal or bipolar cell expression, since this is where the nuclei of these cell types are typically positioned.

3.3.2 Frmpd1 uses an alternative tissue-specific 5'-UTR in the retina

It is well-documented that the retina often uniquely expresses tissue-specific isoforms of genes (Popova et al., 2017, Farkas et al., 2013). As the expression of *Frmpd1* seemed restricted almost entirely to the retina in adult mice, with very minimal expression elsewhere, we were curious as to whether the transcripts varied according to tissue type. There are 2 annotated murine *Frmpd1* transcripts with human homologs (Ensembl ID 201 and 202, ensembl.org) (Figure 3.1). These 2 transcripts vary only in their 5' transcription start site, initiated with untranslated Exon 1 or 1a (Figure 3.5). The remainder of both genes after splicing to Exon 2, which contains the ATG translation start site, is identical in both transcripts. The protein product encoded by each isoform is therefore identical and the transcripts differ only in their 5' untranslated regions (UTRs).

3.3.2.1 Transcription of Frmpd1 is initiated from different sites in retina and brain

To identify the transcription start sites used in brain and retina (amplification from lung samples was unsuccessful), 5'-Rapid Amplification of cDNA Ends (Section 3.2.12) was performed with an initial amplification from a gene-specific primer in Exon 8 followed by a nested amplification from Exon 6 (Figure 3.5). In the retina, a larger product of 1000 bp was amplified in comparison to a smaller, 650 bp product in the brain; this was true for 5'-RACE reactions performed on both mouse and human-derived samples (Figure 3.5). These products were cloned into a pRACE vector and at least 10 independent clones from each RACE product were analysed. Sequencing of each product revealed that the retina transcript corresponded with 202,

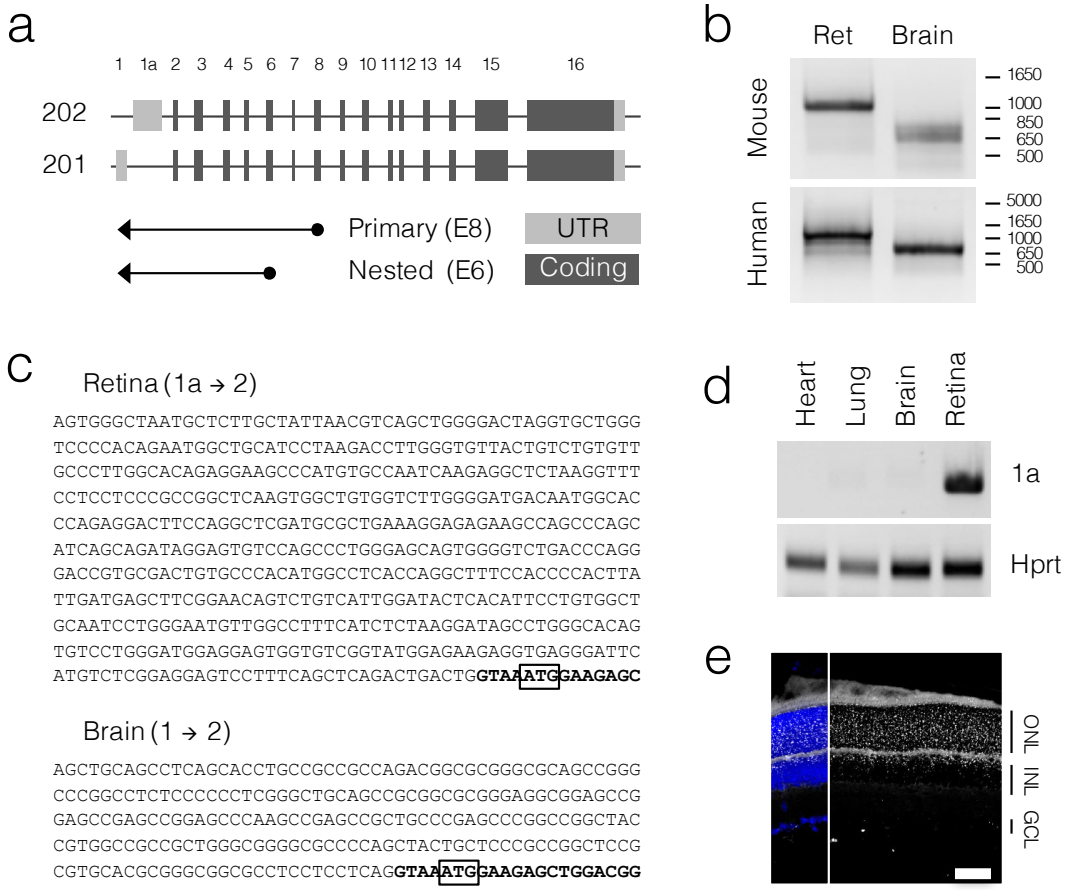

Figure 3.5: *Frmpd1* uses a retina-specific 5'UTR in mice and humans. (A) Schematic of primers used for 5'-RACE. To determine transcriptional start sites used in brain and retina, a primary RACE reaction was performed using a gene-specific primer in Exon 8 followed by a nested RACE reaction using a gene-specific primer in Exon 6 to target both *Frmpd1-202* and *Frmpd1-201* transcript isoforms. (B) Tissue-specific RACE products in mouse and human. 5'-RACE PCR products were visualised on an agarose gel, purified, and cloned for sequencing. (C) *Frmpd1* 5'-UTR sequences in murine retina and brain. Sequencing of 5'-RACE products revealed the use of alternative 5'-UTR sequences in each tissue. The retina transcript begins with Exon 1a, while brain begins with Exon 1. Both are spliced to Exon 2 (bold) where the translation start site is located (ATG; boxed). (D) Exon 1a expression is limited to the retina. PCR using primers specific for Exon 1a using cDNA from various P21 mouse tissues reveal that it is only expressed in the retina. (E) Localisation of Exon 1a RNA in retina. Localisation of Exon 1a RNA was assessed by *in situ* hybridisation of P21 mouse retina. Background autoflourescence can be seen in the outer plexiform and outer segment regions; bright punctate staining represents RNA. Scale bar, 50 μm. ONL, outer nuclear layer; INL, inner nuclear layer; GCL, ganglion cell layer.

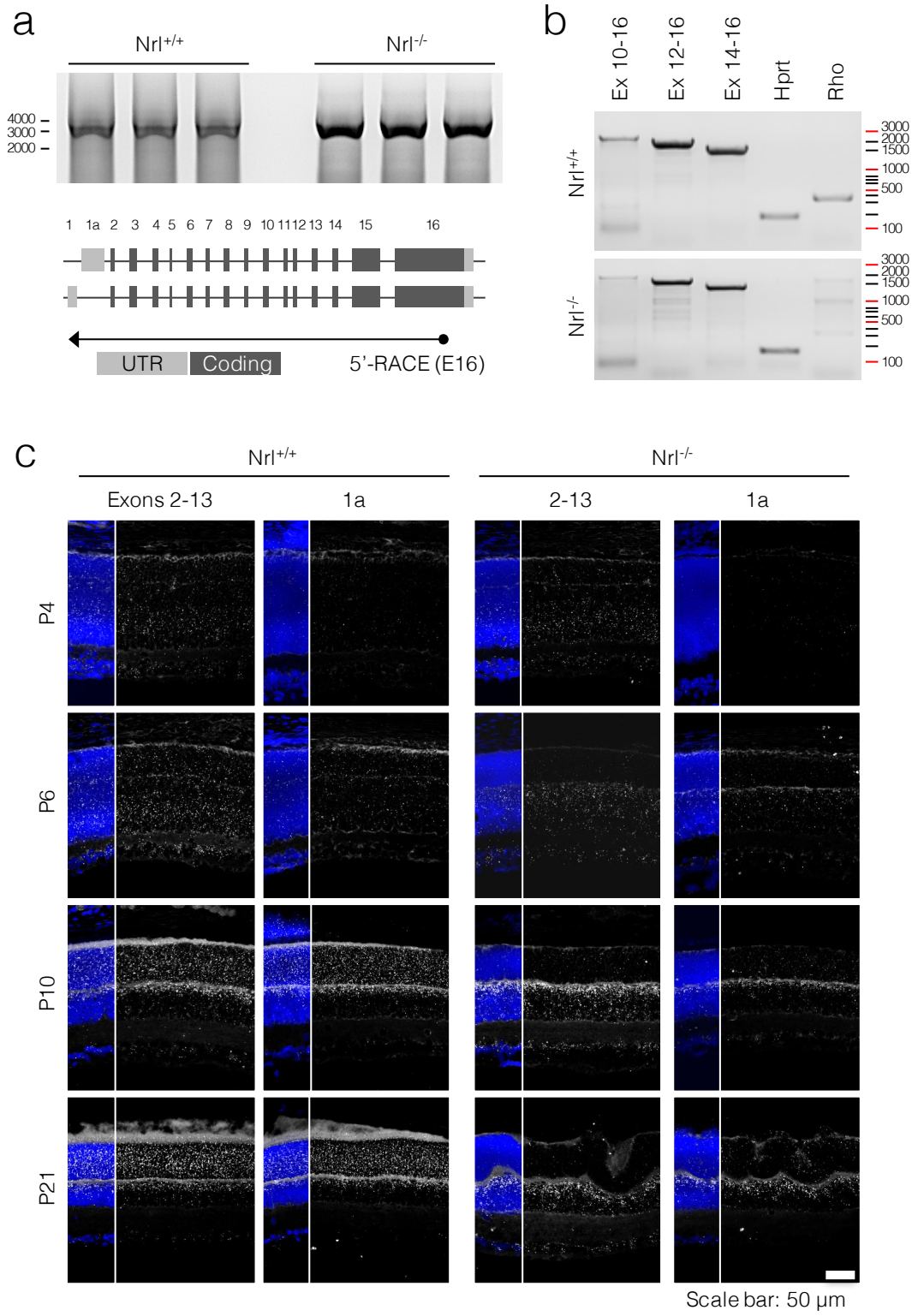

Figure 3.6: Exon 1a is expressed by all *Frmpd1*-expressing retinal cell types. (A) Full transcript 5'-RACE. To determine alternative exon usage in *Nrl*$^{+/+}$ and *Nrl*$^{-/-}$ retina, a 5'-RACE reaction was performed using a gene-specific primer in Exon 16 to target both Frmpd1-202 and Frmpd1-201 transcript isoforms. 5'-RACE PCR products were visualised on an agarose gel. (B) Exon-junction PCR. Exon usage in both *Nrl*$^{+/+}$ and *Nrl*$^{-/-}$ retina was assessed by PCR using primers flanking various ranges of exons. *Hprt* was used as an internal control, and *rhodopsin* as a control for genotypes. (C) Transcript-specific *in situ* hybridisation. Total *Frmpd1* (Exons 2-13, to target both transcripts) and Exon 1a were assessed by *in situ* hybridisation using probes specific to each. Expression was tested at various ages during development (P4-P21). Background autoflourescence can be seen in the outer plexiform and outer segment regions; bright punctate staining represents RNA. Scale bar, 50 µm.

beginning transcription from Exon 1a, while the brain transcript corresponded with 201, beginning transcription from Exon 1 (Figure 3.5).

3.3.2.2 The rod-enriched isoform of Frmpd1 is tissue-specific and used by all cells of the retina

To assess whether the 5'-UTR used in retina could be found in any other tissues, a PCR reaction (Section 3.2.5) using primers specific to Exon 1a was performed on all tissues found expressing *Frmpd1* previously (retina, brain, lung) along with a negative control (heart) (Figure 3.5). Indeed, Exon 1a was retina-specific, indicating that the retina expresses a unique isoform of *Frmpd1* not found in any other tissues examined previously (Figure 3.5). To visualise Exon 1a RNA localisation, ISH was performed on P21 retina cryosections using probes designed for specific detection of this exon which was found to be expressed predominantly in the ONL and to a lesser degree in the INL, recapitulating earlier ISH experiment results using probes that did not distinguish between the 2 unique transcripts (Figure 3.5).

As rods comprise ~70% of cells in the retina, it is possible that the rod signal in both RNA-seq and 5'-RACE (a PCR-dependent technique that would preferentially amplify the most abundant transcript in a sample) could bias results to represent rod photoreceptors over other cell types in whole retina samples. Since the RNA expression of *Frmpd1* was only reduced in the ONL but not the INL of $Nrl^{-/-}$ retina (Figure 3.3), we investigated whether Exon 1a was unique to rod photoreceptors and/or if any other differences in isoforms between different *Frmpd1*-expressing cells may be related to their differential expression. To determine the primary isoforms expressed in the ONL and INL, a 5'-RACE reaction was performed on rod-dominated $Nrl^{+/+}$ retina where Frmpd1 is primarily expressed in the ONL, and a cone-dominated

Nrl$^{-/-}$ retina where *Frmpd1* was only expressed in the INL (Figure 3.6). In both models, the primary transcript identified corresponded to transcript 202 which begins transcription from Exon 1a and includes all exons from 2-16; this was further confirmed by PCR using primers flanking various exon boundaries within this transcript in both *Nrl*$^{+/+}$ and *Nrl*$^{-/-}$ retina (Figure 3.6). To confirm these findings, ISH was performed on *Nrl*$^{+/+}$ and *Nrl*$^{-/-}$ retina cryosections throughout development using probes specific to Exons 2-13 (targeting both 202 and 201 transcripts) or specific to Exon 1a (targeting only 202 transcript). The high similarity of the expression patterns seen with each probe set indicate that the 202 transcript is indeed expressed by all *Frmpd1*-positive cells in the retina, although INL expression appears to be less compared to rod photoreceptor ONL expression.

3.3.3 The minimal promoter of Frmpd1 is upregulated by Nrl and Crx in the retina

3.3.3.1 Identification of the minimal promoter of Frmpd1in the retina

The 5'-UTR regions of genes often aid in mRNA stability and/or regulation (Mignone et al., 2002). Since the regulation of *Frmpd1* appears to be stringently controlled based on its high enrichment in retina and tissue-specific transcript usage, we next wanted to identify the cis-regulatory elements necessary for upregulation of this gene in the retina. Regulatory elements (promoters, enhancers, etc.) are often highly conserved amongst species, so to identify potential promoter regions we examined the degree of conservation of the genomic sequence upstream of both the brain and retina transcriptional start sites (TSSs) of *Frmpd1* identified by 5'-RACE

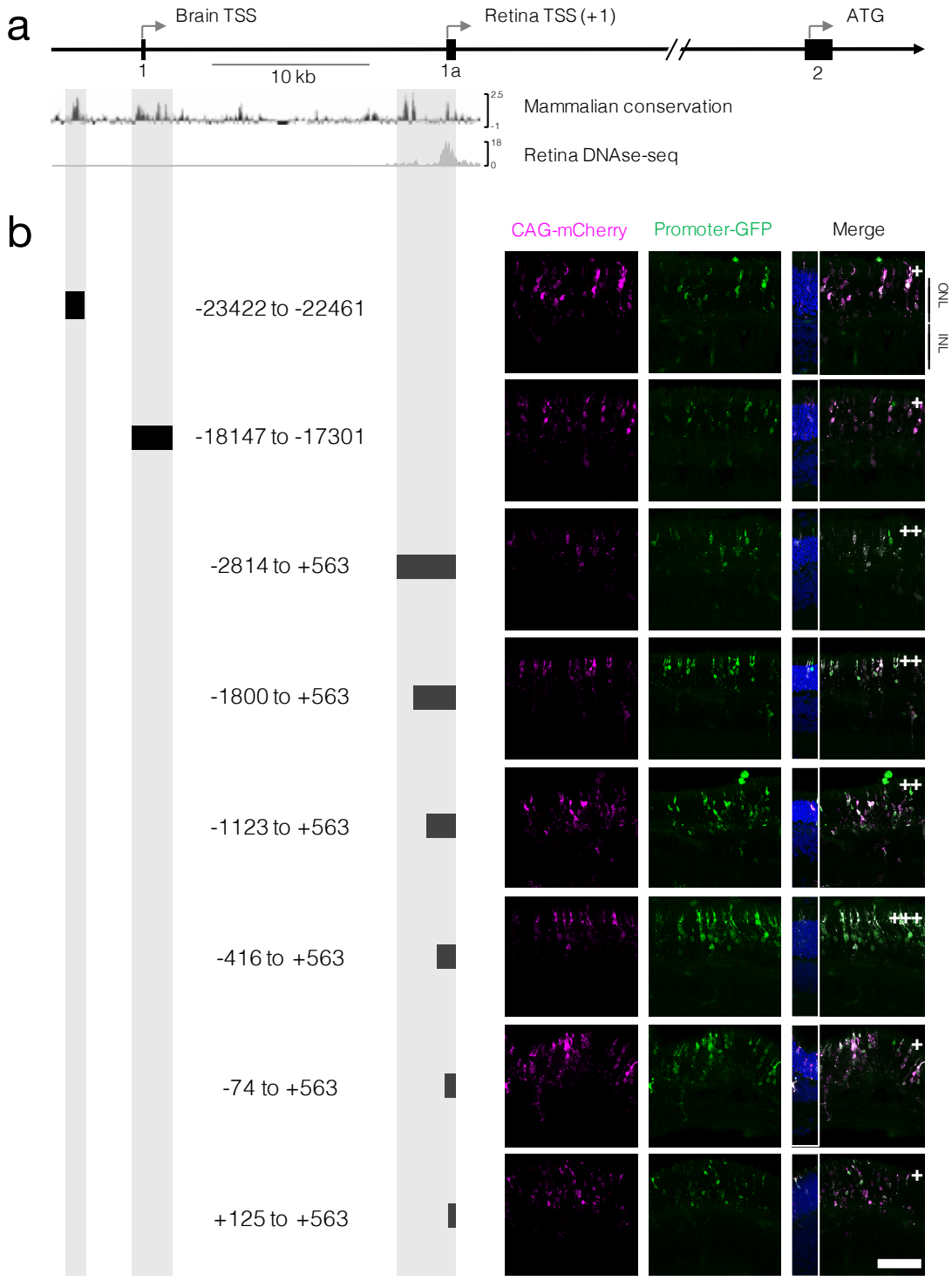

Figure 3.7: Identification of sequence elements upstream of *Frmpd1* required for ONL expression *in vivo*. (A) *Frmpd1* upstream genomic sequence showing major conserved and accessible regions. Conservation diagram displays sequence homology among several mammals, whereas DNase-seq diagrams display DNase hypersensitive regions in retina, brain, heart, and lung. (B) *In vivo* promoter activity of conserved and accessible DNA clusters. Multiple DNA fragments were cloned upstream of a GFP reporter and transfected into neonatal mouse retina with CAG-mCherry transfection marker. Retinas were harvested at P21 to examine expression of the reporter indicated as follows: +, low/basal expression; ++, moderate expression; +++, high expression. Scale bar, 50 μm. ONL, outer nuclear layer; INL, inner nuclear layer; GCL, ganglion cell layer.

(Figure 3.7). To complement the conservation analysis and to identify regions of genomic DNA that are more likely to be readily accessible by transcription factors, we also compared the mammalian conservation to open regions of chromatin as evidenced by DNase-seq (Figure 3.7).

Conservation and DNase hotspot alignments revealed several regions both immediately upstream of brain and retina TSS as well as some further away that could potentially contain important regulatory elements (Figure 3.7). To identify the minimal sequence needed to drive *Frmpd1* expression in the retina, several of the conserved sequence clusters were cloned upstream of a GFP reporter to drive its expression (by replacing the CMV reporter of EGFP-N1 with the promoter fragment of interest) and were transfected into neonatal mouse retina by *in vivo* electroporation (Section 2.2.9, Figure 3.7). Equimolar amounts of each expression construct were injected to assess which fragments were sufficient to activate GFP expression in the retina. While all constructs activated GFP expression to some extent (Figure 3.7), the construct containing a fragment from -416 to +563 maintained the highest level of GFP expression at P21, suggesting that it contains all of the necessary elements to activate high levels of transcription in the retina.

3.3.3.2 Prediction of transcription factor binding sites within Frmpd1 minimal promoter

To identify transcription factors that may play a role in the upregulation of *Frmpd1*, an *in silico* analysis of the -416 to +563 region driving high GFP expression in the retina was performed. Putative binding sites within this region were identified by MatInspector analysis (Genomatix.de), yielding predicted binding sites for 290 transcription factor families corresponding to 647 different transcription factors. Many

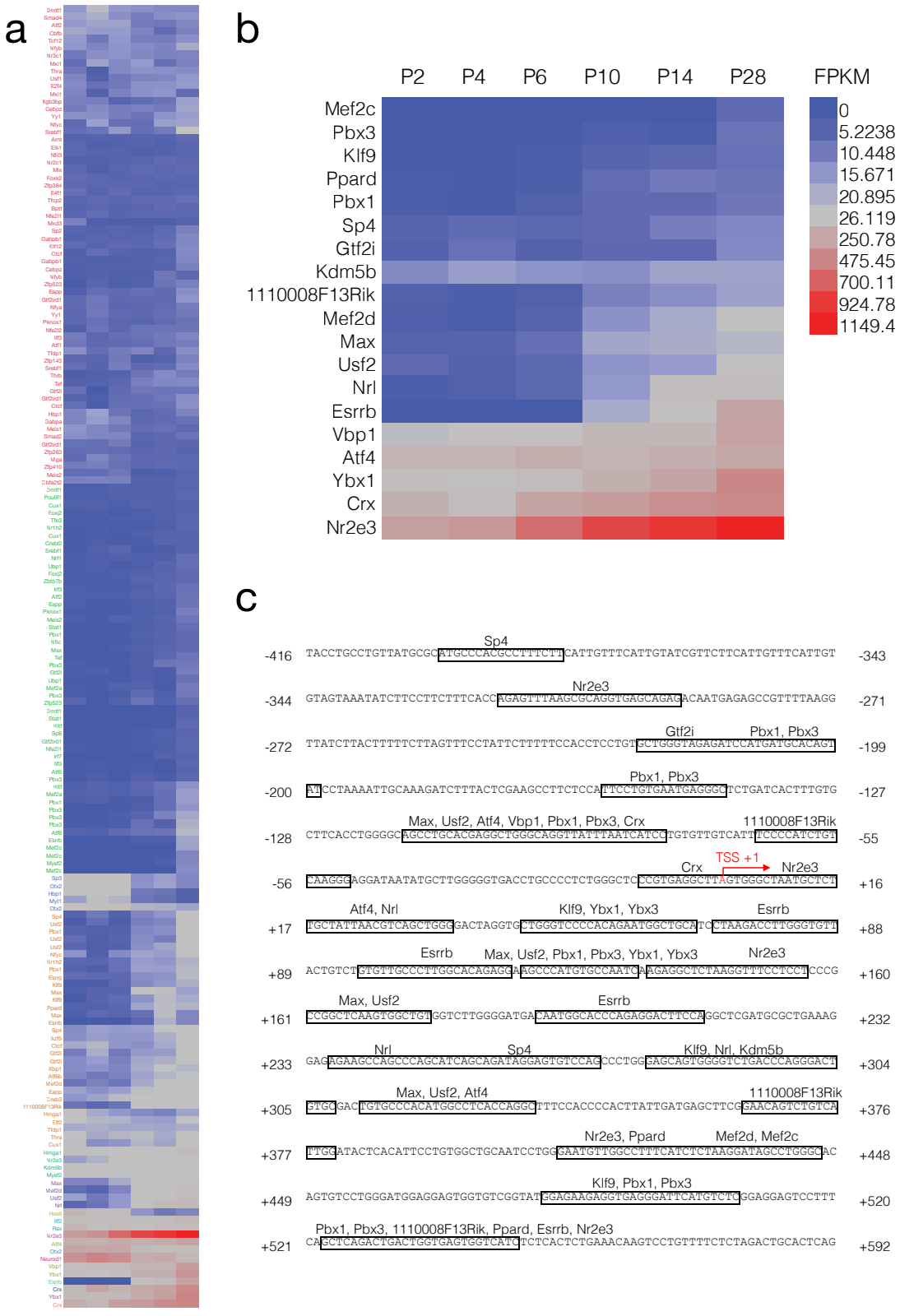

Figure 3.8: Putative transcription factor binding sites in *Frmpd1* minimal promoter. (A) Heat map of expression values (in FPKM). A heat map was generated from the 171 transcription factors containing putative binding sites within the *Frmpd1* minimal promoter region (-416 to +563) which also had an FPKM value of at least 5 in flow-sorted rod photoreceptors at P28. Heat map and row/column keys are the same as for (B); each column represents a different age (P2-P28) and each row a different gene transcript. (B) Close-up heat map of 19 transcripts of interest. (C) Annotated *Frmpd1* promoter, indicating several overlapping predicted binding sites for the transcription factors in (B). The red arrow indicates the transcription start site (TSS) identified by 5'-RACE.

of these transcription factors are not expressed in the retina; to filter for those more likely to play a role in the regulation of *Frmpd1*, whose expression is highest in adult rods, only those transcription factors with a FPKM of at least 5 in flow-sorted rod photoreceptors at P28 were considered for further study (171 genes total, Figure 3.8). Of these, 19 transcription factors were selected for a more in-depth analysis based on their high and/or increasing expression from P2-28 (Figure 3.8). The binding sites of many of these transcription factors overlapped with one another, and many of them contained multiple potential binding motifs within the -416 to +563 region (Figure 3.8).

3.3.3.3 Nrl and Crx directly bind to the minimal promoter of Frmpd1

Interestingly, multiple Nrl and Crx predicted binding sites were contained within this minimal promoter region (Figure 3.8, 3.9). Moreover, upon further analysis, the -166 to +33 region also contained Nrl and Crx ChIP-seq peaks which perfectly overlapped with a region of high mammalian conservation and open chromatin structure in the retina as evidenced by DNase-seq (Figure 3.9). To determine the precise DNA binding sites of Nrl and Crx within this region, an EMSA (electrophoretic mobility shift assay) was performed using oligonucleotides containing the predicted core binding motifs within this -166 to +33 proximal promoter region (Figure 3.8, 3.9). When biotinylated dsDNA probes containing core binding motifs of Nrl or Crx were incubated with P21 retina nuclear extract, multiple band shifts were observed. These shifts indicate DNA-protein interactions, which were reduced when incubated with an excess of unlabeled dsDNA (Figure 3.10a).

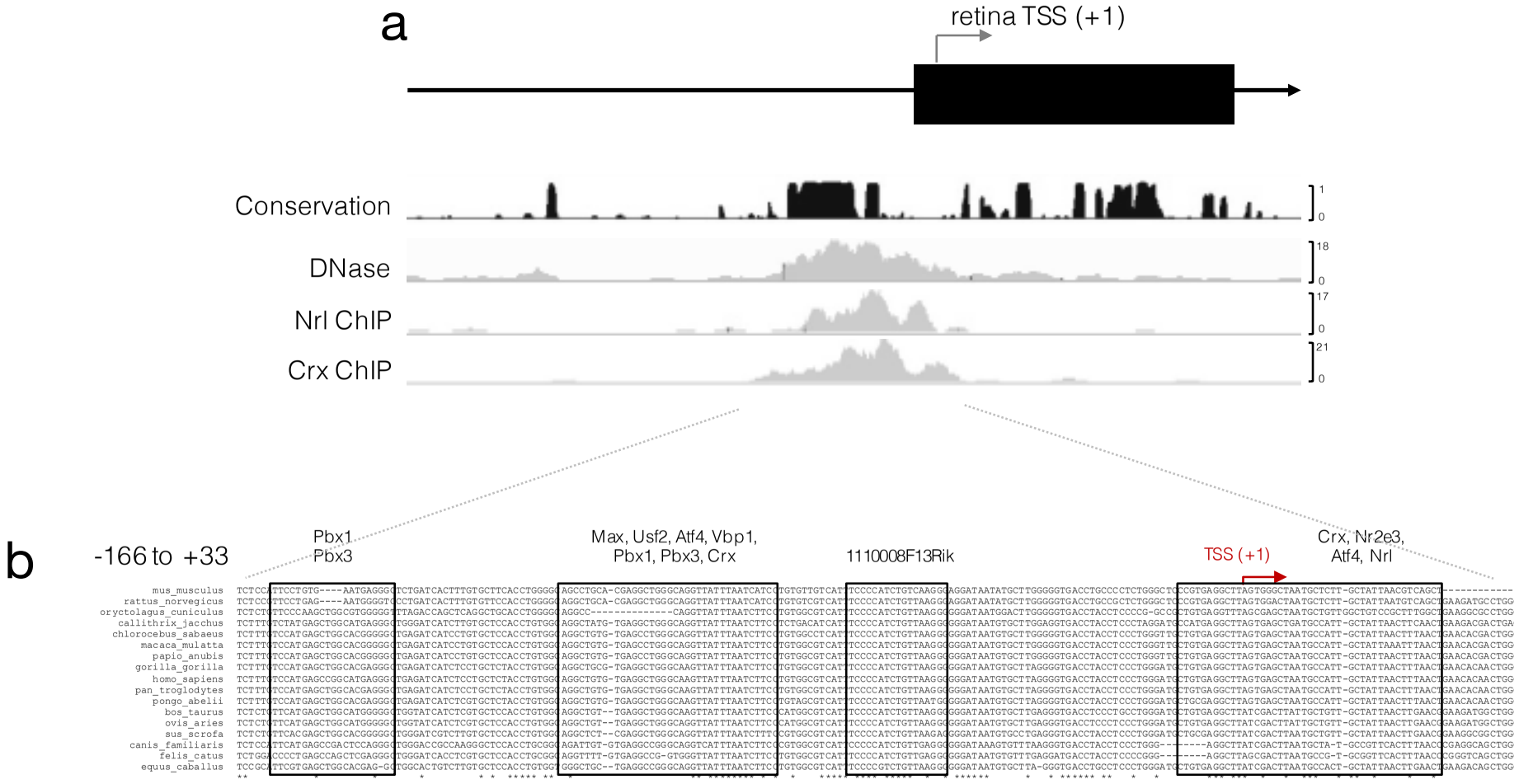
a
retina TSS (+1)
Conservation
DNase
Nrl ChIP
Crx ChIP
b
-166 to +33
Pbx1
Pbx3
Max, Usf2, Atf4, Vbp1,
Pbx1, Pbx3, Crx
1110008F13Rik
TSS (+1)
Crx, Nr2e3,
Atf4, Nrl
mus_musculus
rattus_norvegicus
oryctolagus_cuniculus
callithrix_jacchus
chlorocebus_sabaeus
macaca_mulatta
papio_anubis
gorilla_gorilla
homo_sapiens
pan_troglodytes
pongo_abelii
bos_taurus
ovis_aries
sus_scrofa
canis_familiaris
felis_catus
equus_caballus

Figure 3.9: Mammalian conservation of Nrl and Crx binding sites within Frmpd1 promoter (previous page). (A) Mammalian conservation (from Ensembl) is shown as percent identity (0-100%) amongst representative mammalian species. DNase hypersensitivity, Nrl ChIP-seq, and Crx ChIP-seq reads are shown as histograms. (B) Aligned genomes from 17 representative mammals were downloaded from Ensembl. Putative binding sites from Figure 3.8 are boxed. Asterisks represent 100% identity. The retina transcription start site (TSS) identified by 5'-RACE is indicated in red.

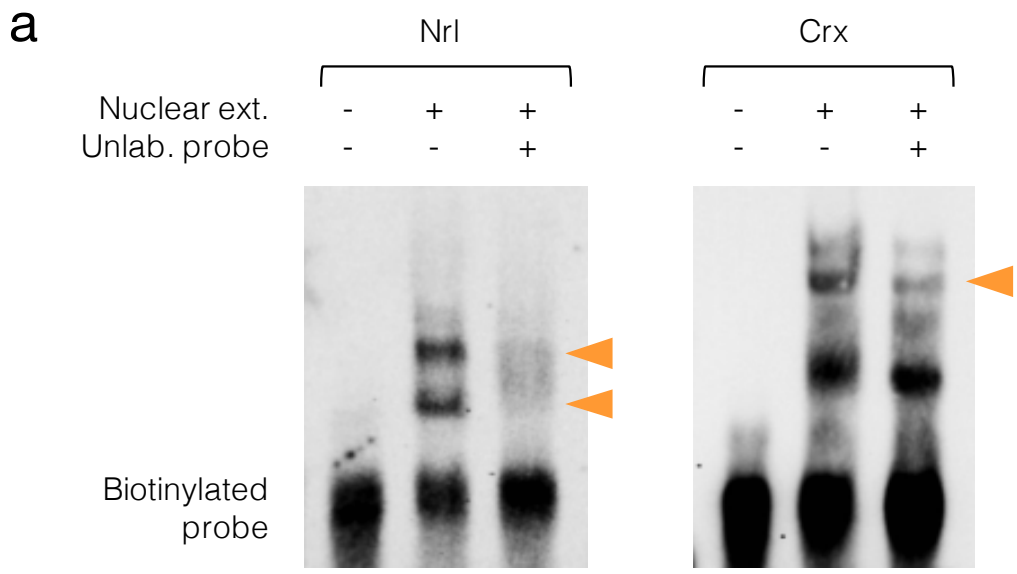

b

Crx-wild type	GCAGGTTATTTAATCATCCTGTGTTGTCATTTCCCC
Crx-mutant	GCAGGTTATTGCCGCATCCTGTGTTGTCATTTCCCC
Nrl-wild type	AGTGGGCTAATGCTCTTGCTATTAACGTCAGCTGGGG
Nrl-mutant	AGTGGGCTAACTATCTTGCTATTAACGTCAGCTGGGG

Figure 3.10: Nrl and Crx directly bind to and upregulate *Frmpd1* minimal promoter. (A) Nrl and Crx directly bind to *Frmpd1* proximal promoter *in vitro*. Biotinylated probes containing putative Nrl or Crx binding sites (B) were incubated with nuclear extract of P21 mouse retina. The shift created by protein-DNA binding was reduced by the addition of unlabeled probe in 200x molar excess.

3.4 Discussion

While it is estimated that the human genome contains ~19,000 protein-coding genes (Ezkurdia et al., 2014), the actual number of unique mRNA and protein variants arising from these genes is far greater. Alternative splicing of pre-mRNAs can generate vast proteomic diversity from a single gene by inserting or removing stretches of amino acids, and can even result in the addition or removal of regulatory elements to control gene expression. It is estimated that more than 95% of human multi-exon genes express multiple splice variants (Pan et al., 2008, Wang et al., 2008), many of which are regulated in specific manners related to cell type, developmental stage, gender, or in response to stimuli (Faustino and Cooper, 2003). The generation of cell-type specific isoforms allowing the same gene to be expressed in multiple ways is particularly prevalent in the vertebrate central nervous system (CNS), and is believed to contribute to the generation of functional diversity amongst neurons related to protein-protein interactions, transcription networks, and development (Raj and Blencowe, 2015). Alternative splicing is particularly common in the retina and recent reports have shown that alternative promoter usage and novel transcripts are abundant in this tissue (Popova et al., 2017, Farkas et al., 2013). Thus, it is not entirely surprising that *Frmpd1*, which is highly enriched in the retina and likely plays a unique role in this tissue, is regulated through a highly tissue-specific mechanism as well.

We have focused primarily on the regulation of *Frmpd1* by transcription factors Nrl and Crx, as these are considered to be 2 key regulators of rod photoreceptor differentiation. Crx is required to make both rods and cones, while Nrl is necessary to

establish a rod cell fate (Swaroop et al., 2010). In the absence of Nrl, cells initially fated to become rods instead develop as cone-like photoreceptors (Mears et al., 2001, Oh et al., 2007). Conversely, ectopic overexpression of Nrl drives cone photoreceptors to develop as rods (Oh et al., 2007). Indeed, key phototransduction genes which are expressed abundantly in rods (rhodopsin, transducin, phosphodiesterase, etc.) contain binding sites for both Nrl and Crx and are synergistically upregulated by the combination of these proteins (Hao et al., 2012, Cheng et al., 2004, Mitton et al., 2000). Transcription factors downstream of Nrl and Crx (like Nr2e3, Nr1d1, etc.) also modulate these genes, but tend to reinforce patterns already established by Nrl and Crx to further augment or repress expression (Haider et al., 2009, Swaroop et al., 2010, Cheng et al., 2004). Activation by Nr2e3 would be consistent with the dramatic upregulation of *Frmpd1* expression from P6-10 as this is when the transcription factor also increases in expression and activity (Oh et al., 2008, Haider et al., 2009). Nr1d1 binding would have interesting implications in the circadian regulation of *Frmpd1* (described in more detail in Chapter 5), as this transcription factor is implicated in this process and is known to form complexes with Nr2e3 (Cheng et al., 2004, Crumbley and Burris, 2011). There also likely exist other regulatory elements for *Frmpd1* outside of the minimal promoter, such as enhancer regions (particularly in the retina) and/or silencers (particularly in tissues other than the retina) that could further fine-tune its expression.

The unique Exon 1a utilised in the retina likely plays a role in this sensitive fine-tuning of *Frmpd1* expression. Indeed, 5'-UTR regions are often implicated in mRNA stability and can provide alternative pathways for translational regulation (Mignone et al., 2002). The retina 5'-UTR of *Frmpd1* is much more AT rich (55% GC) and unstable

than the UTR used by brain (81% GC) and may be more prone to degradation and/or regulation. It is interesting to note that the minimal promoter region is DNase sensitive in the retina, which implicates a selective chromatin reorganisation of this region that could potentially be mediated by histone modifications such as acetylation. It is unclear whether these changes are induced by Nrl binding, or if upstream mechanisms establish the open chromatin state of this region; for example, Crx can recruit histone acetyltransferases to open up the chromatin and facilitate Nrl, Nr2e3, and RNA polymerase II binding (Peng and Chen, 2007). Some known upstream transcription factors like Otx2, Pax6, etc. also have predicted binding sites in this region and may play a role in this process; reverse ChIP coupled with mass spectrometry during several different time points throughout development could help to provide insights into the upstream regulatory processes occurring before the onset of *Frmpd1* upregulation.

Undoubtedly, the minimal promoter of *Frmpd1* is regulated by more than just Nrl/Crx. Exon 1a is expressed both in the ONL and INL, yet Nrl and Crx are expressed almost exclusively in photoreceptors of the ONL, and INL expression of *Frmpd1* persists in $Nrl^{-/-}$ animals. *In silico* analyses suggest that there exist many other highly conserved binding sites for transcription factors expressed in the retina, which could also be tested by EMSA and luciferase assays to confirm. To further identify regulatory elements within the *Frmpd1* minimal promoter not predicted by *in silico* tools, techniques like reverse ChIP could be performed with labelled double-stranded DNA corresponding to this region of the genome followed by mass spectrometry to identify protein complexes bound to this region of DNA both directly and indirectly. It is entirely possible that there exist additional transcription factors which are critical for

the rod-specific upregulation of *Frmpd1* and that these transcription factors are also necessary for the regulation of other rod genes. Interestingly, a role in the retina for some of the transcription factors identified by *in silico* analysis of *Frmpd1* promoter has not yet been described, making them interesting candidates for further validation and study.

4

Localisation and interacting partners of Frmpd1 in the retina

4.1 Introduction

The high enrichment of *Frmpd1* expression in rod photoreceptors and tissue-specific regulation from an alternative promoter in these cells imply that *Frmpd1* may play an important role in rod development and/or function. To help elucidate the function of Frmpd1, a combination of three general approaches was employed: (1) localisation of the protein product to determine the subcellular compartments in which it can act, (2) identification of protein-protein interactions to garner insights into the molecular pathways it may be involved in, and (3) loss of function studies to assess phenotypic consequences of an absence of the protein. In this Chapter, the localisation and protein-protein interactions of Frmpd1 will first be addressed. Loss of function studies are described in Chapter 5. Together, these three approaches have provided some useful clues as to the role that Frmpd1 may play in modulating rod photoreceptor function.

Frmpd1 has been identified as a binding partner of Gpsm1 (G-protein signalling modulator 1; also known as Ags3) and Gpsm2 (G-protein signalling modulator 2; also known as Lgn) in yeast-two-hybrid assays and *in vitro* cell culture, but has received little attention beyond these studies and has not yet been studied in an *in vivo* system such as the retina (Yuzawa et al., 2011, An et al., 2008). Gpsm1 and Gpsm2 are two closely related proteins (59% shared sequence identity), each containing 7 tetratricopeptide (TPR) motifs at their N-terminus and 4 GoLoco/GPR (G-protein regulatory) motifs at their C-terminus (Blumer et al., 2002). TPR motifs consist of 3-16 tandem repeats of 34 amino acids and can act to scaffold multiprotein complexes involved in processes such as protein folding and degradation, cell-cycle regulation, mitosis, neurogenesis, transcription, splicing, pathogen defence, and protein transport (Blatch and Lassle, 1999, Allan and Ratajczak, 2011, Goebl and Yanagida, 1991). This interaction is mediated via binding between Gpsm2's TPR (tetratricopeptide repeat) motif and a conserved domain of Frmpd1 that is highly similar to the TPR binding motif of Frmpd4 (Takayanagi et al., 2015). Frmpd1 has been shown to regulate the subcellular location of Gpsm1 in a membrane fraction via this interaction; a similar membrane-scaffolding function of Frmpd1 may also exist for Gpsm2, which is almost exclusively detected in the membrane fraction of retinal lysates (Yuzawa et al., 2011, An et al., 2008).

GPR motifs, consisting of 19 amino acids, function as guanine dissociation inhibitors (GDIs) preventing dissociation of GDP from G-protein receptor coupled alpha subunits (T_{α}) through direct interaction with GDP phosphates (Kimple et al., 2002). This stabilises an inactive form of T_{α} by inhibiting GTP uptake, preventing its re-association with $T_{\beta\gamma}$ and allowing for continued signalling by these subunits

independent of T_α activation (Kimple et al., 2002). Interestingly, Gpsm1 can bind several T_α subunits simultaneously through its GPR motifs, acting as a guanine dissociation inhibitor to stabilise T_α in an inactive GDP-bound form (T_α^{GDP}) (De Vries et al., 2000); more specifically, Gpsm1 has been shown to inhibit rhodopsin-dependent activation of T_α *in vitro* (Natochin et al., 2000). While previous studies indicated that Gpsm1 is not expressed in the postnatal retina (Nair et al., 2005b), Gpsm2 is expressed in ON bipolar (Dhingra et al., 2008) and rod photoreceptor (Nair et al., 2005b) cells. Furthermore, Gpsm2 has been shown to interact preferentially with T_α^{GDP} and to slow its rate of GTP exchange (Nair et al., 2005b, Kerov et al., 2005b).

As mentioned in Section 1.4, T_α is a key component of the phototransduction cascade that transduces the photon signal detected by G-protein-coupled receptor rhodopsin. In an inactive dark-adapted state, holotransducin (consisting of a GDP-bound alpha subunit, T_α^{GDP}, complexed with $T_{\beta\gamma}$) is localised on disc membranes in the rod outer segment. A photoactivated rhodopsin molecule contacts T_α^{GDP} to prompt its release of GDP in exchange for cytosolic GTP (Shichida and Morizumi, 2007). This activated T_α^{GTP} can then dissociate from $T_{\beta\gamma}$ and interact with Pde6 to further propagate the phototransduction cascade (Wensel and Stryer, 1990). T_α possesses intrinsic GTPase activity and eventually hydrolyses its bound GTP molecule to GDP with the help of a GTPase accelerating protein (GAP) complex of Rgs9, R9ap1, Gβ5, and Pde6 gamma subunit (Hu and Wensel, 2002, Lishko et al., 2002, Burns and Arshavsky, 2005, Tsang et al., 2006). T_α^{GDP} then re-associates with $T_{\beta\gamma}$ on the disc

membrane to form holotransducin ready to be activated again by rhodopsin (Makino et al., 1999, He et al., 1998).

The exchange of GDP for GTP on T_α also promotes its dissociation from the disc membrane so that it can localise in the cytosol (Rosenzweig et al., 2007). In canonical rod phototransduction signalling with dim light stimuli, T_α tends to remain in the outer segments and associate with its effectors and GAP complexes on proximal disc membranes, rapidly hydrolysing GTP to GDP and reassembling with $T_{\beta\gamma}$ (Lobanova et al., 2007). Upon extended illumination and/or higher light thresholds, however, GTPase activity of T_α is not rapid enough to compensate for the overabundance of activated subunits that have now dissociated from the membrane, leaving them free to translocate to the inner segments and synapses (Lobanova et al., 2007, Rosenzweig et al., 2007, Kerov et al., 2005a). Without T_α reinforcing membrane localisation, $T_{\beta\gamma}$ also becomes more soluble and translocates to the inner segments and synapses with the help of phosducin (Sokolov et al., 2004, Sokolov et al., 2002). The translocation of phototransduction machinery is thought to confer a neuroprotective role through suppression of overactive rod photoresponse in bright light situations where cone vision takes over (Burns and Arshavsky, 2005, Artemyev, 2008, Majumder et al., 2013); indeed, some human retinal diseases are associated with constitutively active phototransduction in rod photoreceptors (Szabo et al., 2007, Park, 2014).

The exact mechanism behind transducin translocation is not yet fully understood, although one prevailing theory is that it occurs through diffusion with directional and light-dependent properties mediated by binding site “sinks” within the different compartments of the cell (Slepak and Hurley, 2008). Recent work has also suggested

that translocated transducin subunits and other phototransduction mediators such as phosducin also play additional signalling roles downstream of phototransduction to mediate synaptic transmission to bipolar cells (Majumder et al., 2013, Herrmann et al., 2010). Thus, transducin subunits may play distinct roles dependent on and specific to altered GTP/GDP binding and localisation in response to light stimuli, conferring selective binding to distinct pools of protein interacting partners within different cellular compartments. While much is known about the canonical role of transducin in phototransduction within rod outer segments, its interacting partners in the inner segments and synapses and potential role of these protein complexes within these subcellular compartments is still under investigation. Since Gpms2 binds preferentially to T_{α}^{GDP} and localises to inner segments and synapses, we were interested to see if the Frmpd1-Gpsm2 interaction observed *in vitro* also occurs *in vivo* in the retina, as Frmpd1 may then play a role as a scaffolding and/or signalling complex contributing to rod photoreceptor function and/or homeostasis. We therefore examined the localisation of both proteins in the retina by *in vivo* electroporation and immunohistochemistry to determine if they exist in the same subcellular compartments where they could potentially interact *in vivo*.

4.2 Materials and methods

4.2.1 Materials

For reagent details, buffer compositions, and plasmid maps refer to Appendices A-D.

4.2.2 Methods described in other sections

2.2.5 Mouse lines & husbandry 35
2.2.7 Plasmid DNA isolation..... 36
2.2.8 DNA precipitation 36

2.2.9 *In vivo* electroporation..... 37
2.2.10 Retina cryosectioning..... 37
3.2.3 Immunohistochemistry..... 67
3.2.5 General PCR protocol and primer design..... 68
3.2.6 Recombinant DNA plasmid cloning..... 70
3.2.7 Cell lines..... 72
3.2.8 Cell passaging and seeding..... 72
3.2.9 Cell transfection..... 72
3.2.16 Bicinchoninic acid (BCA) assay..... 81

4.2.3 Preabsorption assay with blocking peptide for commercial Frmpd1 antibody

Antigen oligopeptide (Atlas PrEST Antigen APrEST75173, sequence: RRGGVKKYAKTLRKRRSFLQTDYTSQVSFPLVPSASLESVDDVCYYDREPYLALGAPSPTVS SLQDMQGEPGLLETKALGLLAPLRETKSTNPASRVMEMEPET) and polyclonal antibody (Rabbit anti-Frmpd1, Atlas HPA042934) were diluted in 500 μl blocking buffer (5% normal donkey serum, 0.3% Triton-X 100 in 1x PBS) with the normal titre of antibody used for IHC (1:200) and either 0x, 10x, or 100x molar excess of blocking peptide. Antibodies were preabsorbed with blocking peptide by incubating at room temp for 30 min shaking at 70 rpm, then used in place of regular primary antibody following the protocol described in Section 3.2.3.

4.2.4 Antigen prediction

Full-length mouse Frmpd1 amino acid sequence was submitted to several online antigen prediction tools to predict small peptide sequences likely to elicit an immune response. The Predicted Antigenic Peptides tool (http://imed.med.ucm.es/Tools/antigenic.pl) was used to identify peptides by the Kolaskar and Tongaonkar method (Kolaskar and Tongaonkar, 1990) and cross-referenced with peptides identified based on tripeptide similarity and propensity scores by SVMTriP (Yao et al., 2012) (http://sysbio.unl.edu/SVMTriP). Peptides identified by both methods,

dissimilar to other mouse proteins when analyzed by BLAST (https://blast.ncbi.nlm.nih.gov/Blast.cgi), and with a score >2.4 given by Thermo Scientific Antigen Profiler (https://www.thermofisher.com/us/en/home/lifescience/antibodies/customantibodies/customantibodyproduction/antigenprofilerantigenpreparation.html) were considered for downstream immunisations. The following 2 peptides were ultimately selected after consultation with CoCalico Biologicals:

Name	Sequence	Amino acids
A	LSSDHPNPDNPGPHH-C	1016-1030
B	VAGNLRDVVYTYHQFVEAAKLT-C	1491-1512

4.2.5 Custom polyclonal antibody production

Custom anti-Frmpd1 antibodies were produced in 2 guinea pigs and 2 chickens by CoCalico Biologicals. Briefly, target peptides (Section 4.2.3) were synthesised with a C-terminal cysteine residue for conjugation to Keyhole limpet haemocyanin (KLH). KLH-conjugated antigens (a mixture of Peptides A and B) were prepared in Complete Freund's Adjuvant for initial subcutaneous and/or intramuscular injection, and with Incomplete Freund's Adjuvant for subsequent booster injections. The immunisation schedule and serum collection proceeded as follows:

Day 0: Pre-bleed/Initial Inoculation

Day 14: Boost

Day 21: Boost

Day 35: Test Bleed

Day 49: Boost

Day 56: Test Bleed

To test each bleed for immunoreactivity against Frmpd1, a 1:2000 dilution of serum in 1% milk in TBST was used as primary antibody for detection of denatured protein (Section 4.2.8) Purified IgY from egg yolks of immunised chickens was also provided by CoCalico Biologicals.

4.2.6 Quantitative PCR (qPCR)

The fluorescent SYBR-Green dye (N',N'-dimethyl-N-[4-[(E)-(3-methyl-1,3-benzothiazol-2-ylidene) methyl]-1-phenylquinolin-1-ium-2-yl]-N-propylpropane-1,3-diamine) preferentially binds to double-stranded DNA, allowing for the real-time quantification of the amplification of DNA during PCR reactions by increases in fluorescence by SYBR with each cycle (Ponchel et al., 2003). Hence by measuring the cycle threshold (Ct), or number of PCR cycles needed to reach a specific level of SYBR fluorescence, relative levels of target genes in template cDNA can be quantified (Ponchel et al., 2003).

The following reactions were set up on ice and placed in a StepOnePlus Real-Time PCR System (Applied Biosystems) at the given conditions to measure Ct values:

1 μl	cDNA template (1:10 dilution from reverse transcription)
12.5 μl	2x Quantifast SYBR Green master mix (Qiagen)
2.5 μl	Forward primer (10 μM)
2.5 μl	Reverse primer (10 μM)
6.5 μl	H_2O

1 cycle

95 ˚C	5 min
40 cycles	
95 ˚C	10 sec
60 ˚C	20 sec
72 ˚C	20 sec (read SYBR)
1 cycle (melt curve)	
95 ˚C	15 sec
60 ˚C	1 min

When possible, samples were run in both biological and technical triplicate. Hypoxanthineguanine phosphoribosyltransferase (Hprt) was used as an internal control to normalize for cDNA concentration variation between samples. Primer sequences are included in Appendix C.

4.2.7 Immunoprecipitation

Mice were dark adapted overnight, and retinae were dissected under red light in DMEM (Dulbecco's Modified Eagle Medium, Gibco) followed by permeabilisation with α-haemolysin (50 μg/ml) and 100 μM nucleotides (Guanosine 5'-O-3-thiotriphosphate-boron-dipyrromethene (GTPγS-BODIPY) or Guanosine 5′-[β-thio]diphosphate (GDPβS), Sigma-Aldrich) in DMEM for 45 min at room temp. Permeabilised retinae were illuminated (10 min ~1000 lux) and snap frozen on dry ice after removal of media. Frozen retinae were resuspended in ice-cold immunoprecipitation (IP) buffer (150 mM NaCl, 3 mM EDTA, 40 mM Tris, 10% glycerol, 1% w/v n-dodecyl-β-D-maltoside, 1x Roche protease inhibitors, and 100 μM GTPγS-BODIPY or GDPβS, prepared fresh) on ice, homogenised with a handheld plastic pestle homogenizer, and sonicated. Lysates were centrifuged at 4˚C 2 min 12,000 x *g* to pellet unbroken cells, and supernatant was quantified by BCA assay.

Lysates (1600 μg) were diluted in immunoprecipitation buffer for a total volume of 300 μl and a 50 μl aliquot was saved as “input” fraction. 3 μg of polyclonal antibody or normal rabbit/goat IgG (refer to Appendix D for antibody details) was added to each tube of retina lysate and mixed on a rotating wheel overnight 4˚C. The next day, 50 μl (1.5 mg) of Dynabeads protein A (for rabbit antibodies) or protein G (for goat antibodies) were washed briefly 2x then blocked in 1% BSA in 1X PBS for 1 hr mixing on a rotating wheel at 4˚C. Supernatant was removed from the beads and protein lysates were added and mixed on a rotating wheel at 4˚C for 2 hr to capture protein complexes. The beads were sedimented by placing tubes in a magnetic rack, and the supernatant was removed and saved as “unbound” fraction. Beads were washed 3x 10 min on a rotating wheel at 4˚C in IP buffer, and protein complexes were released from beads by a denaturing elution in 45 μl IP buffer + 25 μl 4x Laemmli buffer (BioRad) + 355 mM β-mercaptoethanol for 10 min at 105℃. 45 μl of “input” and “unbound” fractions were denatured in the same way, and 25 μl of each sample (42% total bound, 5% total unbound, and 5% total input fraction) were separated by SDS-PAGE for immunoblotting using Easyblock reagents as described below in Section 4.2.8.

4.2.8 Immunoblotting

Snap-frozen tissues were lysed by sonication in ice-cold radioimmunoprecipitation buffer (RIPA) supplemented with protease inhibitors (Roche Applied Science) and 1% n-dodecyl-β-D-maltoside (Sigma). For 1 retina or an equivalent amount of tissue, 100 μl of RIPA was used; for adherent cells in 24-well plates, media was first removed and wells were washed with 1X PBS before addition of 100 μl RIPA followed by transfer of

cells + RIPA to a microcentrifuge tube. Supernatants were quantified by BCA assay (Section 3.2.16) and solubilised in 4x Laemmli buffer (BioRad) + β-mercaptoethanol (355 mM final concentration) for 10 min at 105˚C. After denaturation, 50-200 µg of the total protein extract was separated by SDS-PAGE using Mini-PROTEAN TGX Precast Gels (BioRad) and transferred to polyvinylidene (PVDF) membrane using the preprogrammed high molecular weight protocol of TransBlot Turbo Transfer System (BioRad). Membranes were blocked for 1 hr room temp in either 5% milk in TBST or Easyblock (Genetex), then incubated with primary antibody diluted in 1% milk or Easyblock overnight at 4˚C. The next day, membranes were washed 4x for 10 min each with TBST at room temp, then incubated for 1 hr room temp with HRP-conjugated secondary antibody diluted in 1% milk or Easyblock. After 4 more TBST washes, membranes were developed with SuperSignal West Pico Chemiluminescent Substrate (Thermo) or SuperSignal West Femto Maximum Sensitivity Substrate (Thermo) depending on signal strength, then imaged on ChemiDoc Touch Gel Imaging System (BioRad). For subsequent probing, membranes were stripped with a mild 0.2 M glycine solution (pH 2.2) for 4 min 50˚C before being re-blocked and re-probed. A complete list of antibodies and concentrations used can be found in Appendix D.

4.3 Results

4.3.1 Frmpd1 protein localises to photoreceptor inner segments and synapses

To determine the localisation of Frmpd1 protein within the retina, we obtained a commercially available antibody (Atlas Antibodies, Sweden; see Appendix D). Optimal fixation, antigen retrieval, and staining conditions for immunohistochemistry are

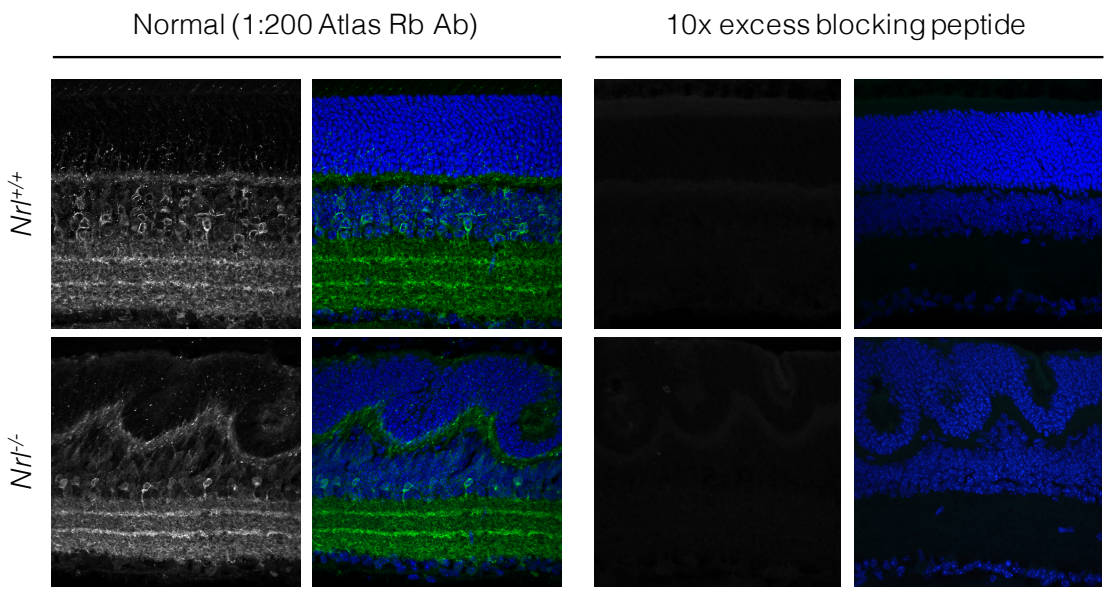

Figure 4.1: Preabsorption assay for commercial Frmpd1 antibody. Commercial rabbit antibody was tested for IHC on P21 cryosections of both *Nrl*$^{+/+}$ and *Nrl*$^{-/-}$ retina. Immunoreactivity of commercial Frmpd1 antibody was abolished by preabsorption with 10x molar excess of the corresponding immunising peptide.

highly variable as well as tissue and antibody-specific. We therefore tested a variety of fixation conditions (fresh frozen, 5 min, 15 min, 30 min, 1 hr, or overnight 4% PFA fixation) and primary antibody concentrations (1:50, 1:100, 1:200, 1:500, 1:1000, 1:2000) for those which gave the most distinct staining patterns on retina cryosections. Optimal staining was produced on retinae fixed for 1 hr in 4% PFA incubated with antibody diluted 1:200 in blocking buffer (Figure 4.1). This staining was specific to the antigen/epitope used to produce the antibody, since blocking with a molar excess of the immunising peptide used to generate the antibody was sufficient to prevent binding of primary antibody elsewhere in the tissue (Figure 4.1). To determine if this epitope is specific to Frmpd1, cryosections were produced from *Nrl*$^{-/-}$ retina which does not express Frmpd1 in the ONL. Unfortunately, the primary antibody produced the same staining pattern even in the OPL (Figure 4.1), suggesting that while the antibody staining is specific to the intended antigen, this antigen may not be specific to Frmpd1 protein.

As an alternative to IHC using anti-Frmpd1 antibody, *in vivo* electroporation was used to localise Frmpd1 protein (Figure 4.2). The full-length protein coding region of Frmpd1 was cloned in-frame with FLAG epitope on either the N- or C-terminus under control of human ubiquitin promoter and electroporated into neonatal mouse retina along with a transfection marker (GFP also under control of ubiquitin promoter). At P21, eyes were harvested and processed for staining with anti-FLAG antibody that would detect FLAG-tagged Frmpd1 protein. The C-term tagged Frmpd1 localised to electroporated photoreceptor inner segments and synapses, whereas the N-term tagged Frmpd1 localised throughout the electroporated cell bodies (Figure 4.2). To assess the possibility of localising Frmpd1 without the use of antibodies, we next

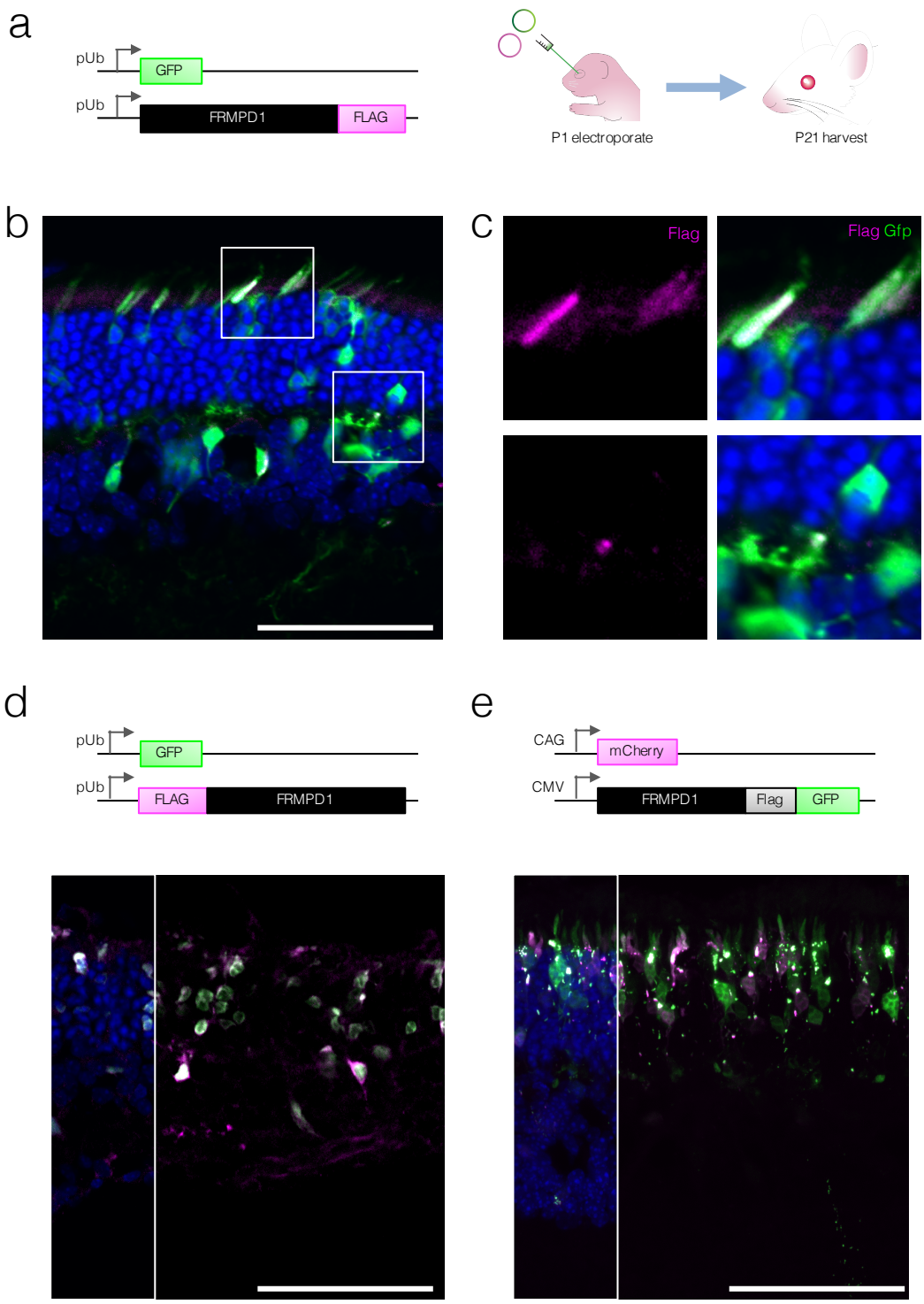

Figure 4.2: Tagged Frmpd1 protein localisation in electroporated retina. (A) C-terminus FLAG-tagged construct. FLAG tag was cloned in-frame with the C-terminus of full-length Frmpd1 protein under control of human ubiquitin promoter (pUb). Tagged construct was cotransfected with pUb driving GFP expression to mark transfected cells. *In vivo* electroporation was performed at P1, and eyes were harvested at P21. (B) Localisation of C-term FLAG-tagged Frmpd1. Immunoreactivity for the FLAG tag could be detected in photoreceptor inner segments and synapses (C). (D) FLAG tag cloned in-frame with the N-terminus of Frmpd1 resulted in diffuse localisation of the protein throughout the cell bodies. (E) A combination of FLAG and GFP cloned in-frame with the C-terminus of Frmpd1 resulted in diffuse GFP fluorescence in the transfected cell bodies. mCherry under control of CAG promoter was used as a transfection marker for these cells. Scale bar, 50 μm.

added a C-term GFP flag to the full-length protein for use in electroporation (along with an mCherry transfection marker). While a small FLAG tag within the C-terminus of the protein did not appear to negatively interfere with its localisation, adding a larger GFP tag to this same region resulted in mislocalisation of Frmpd1 to the entire cell body as with an N-term FLAG tag (Figure 4.2).

4.3.2 *Generation of custom polyclonal antibodies against Frmpd1*

Since expression of a large amount of Frmpd1 protein for use as an antigen was problematic (the large ~170 kDa protein did not express well in bacteria), the full-length coding sequence of Frmpd1 was used for analysis by several prediction software to determine the most antigenic regions for generating antibodies (Figure 4.3). Small peptide sequences that were identified by more than one program were then checked for specificity by BLAST nucleotide search to ensure that they were not similar to other proteins expressed in the retina to minimise the potential for non-specific staining. As anticipated, the FERM and PDZ domain regions were poor targets because they had too high of sequence similarity with many other proteins; however, Exon 16 contained several stretches of amino acids that were both predicted to be antigenic and specific to Frmpd1 (Figure 4.3). Each peptide was synthesised by CoCalico Biologicals (Stevens, PA) with a C-terminal cysteine residue to couple the peptide to KLH (keyhole limpet haemocyanin).

A combination of KLH-conjugated Peptides A & B was used to immunise 2 guinea pigs and 2 chickens over the course of several months to elicit an immune response to the antigens (Figure 4.3). A series of 4 booster immunisations was given and serum drawn after each injection. To determine which animals had the best immune

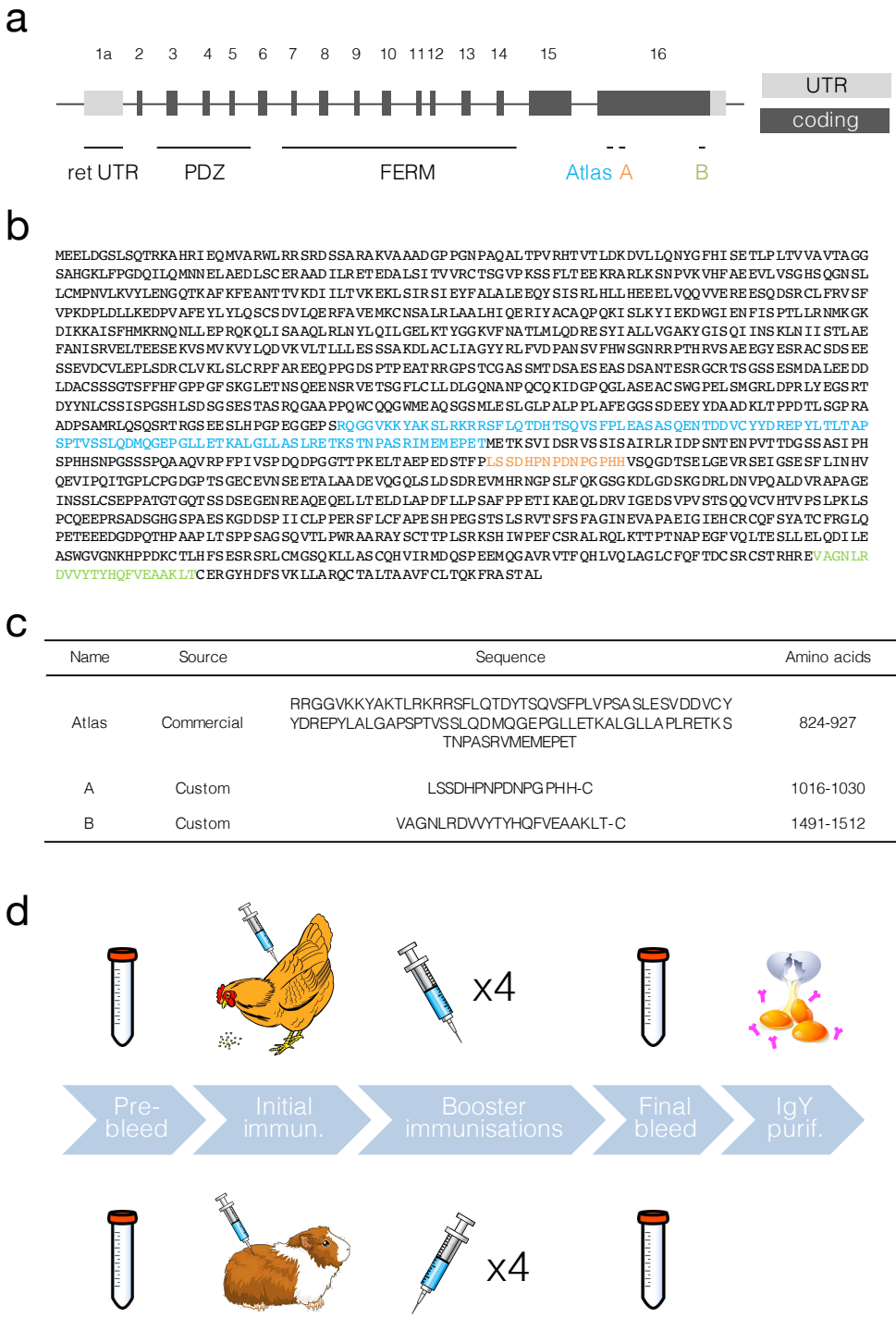

Figure 4.3: Custom Frmpd1 immunising peptide design. (A) Schematic of Frmpd1 exon structure with key elements and location of each peptide sequence indicated. The commercial antibody (Atlas) and Peptide A sequences are within Exon 16, towards the centre of the protein. Peptide B sequence is also in Exon 16, toward the C-terminus of the protein. (B) Full amino acid sequence of Frmpd1 is shown, with commercial (Atlas) and Peptide A and B sequences coloured. Amino acid numbers are provided in (C). (D) Immunisation and serum collection schedule. After conjugation to KLH, a mixture of both Peptides A & B was used to immunise 2 chickens and 2 guinea pigs. Serum was collected before immunisation and after each booster immunisation. Eggs were also collected from chickens after all booster immunisations for purification of IgY antibodies from yolks.

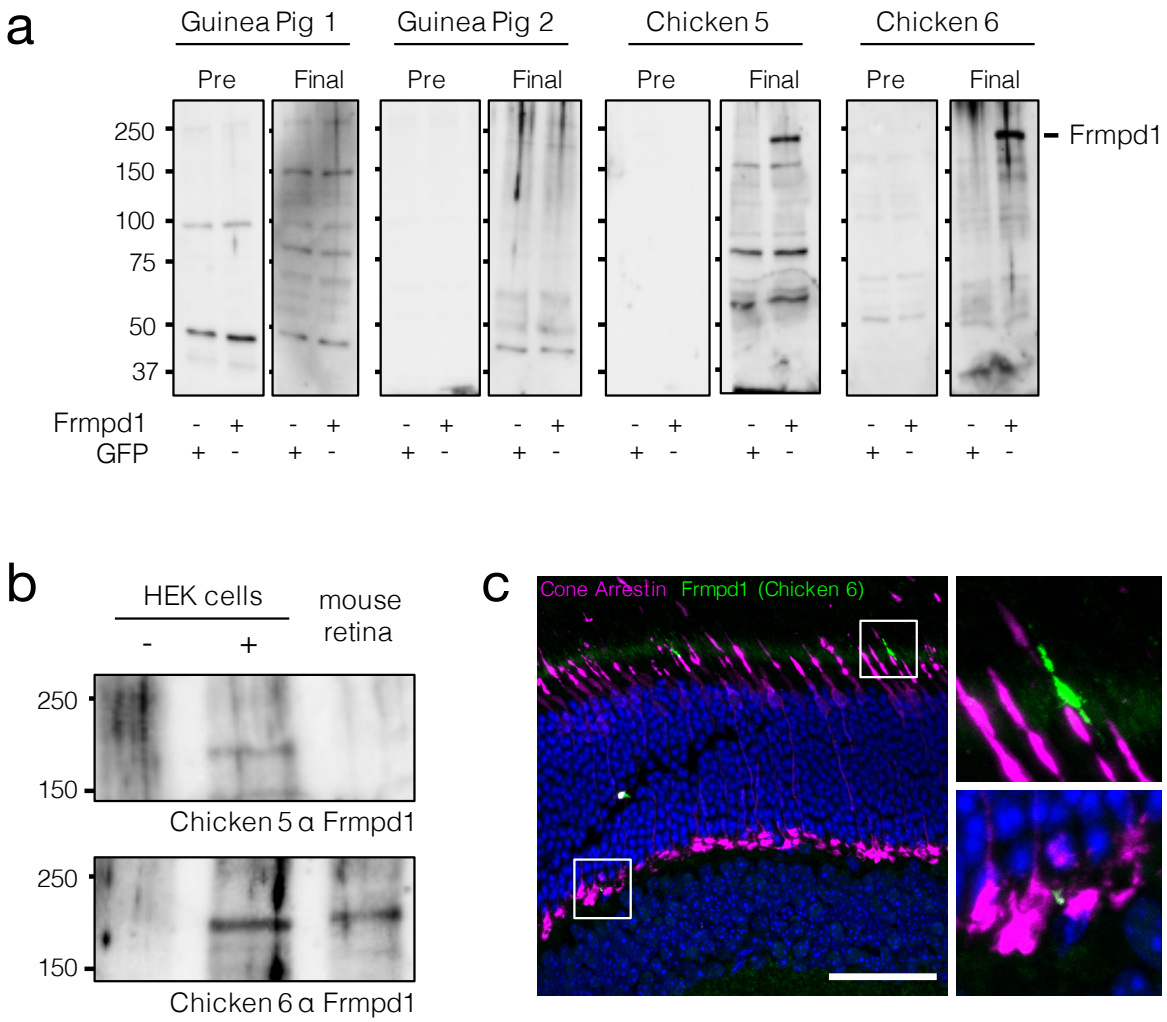

Figure 4.4: Immunoreactivity of guinea pig and chicken custom antibody sera. (A) HEK293 cells were transfected with either pUb-GFP (GFP) or C-terminus FLAG-tagged Frmpd1 construct (Frmpd1) and 30 μg of each lysate was used for immunoblot analysis. Pre-immunised serum (Pre) and serum from animals that had completed 4 rounds of booster immunisations (Final) were used at a 1:2000 dilution for probing HEK293 cell lysates. (B) Immunoblot analysis was performed for both chicken sera on 30 μg of HEK lysates transfected as in (A) and 60 μg of protein lysate from P21 mouse retina. (C) Serum from Chicken 6 was used at a 1:200 dilution for immunohistochemistry on P21 mouse retina cryosections and co-stained with cone arrestin to mark cone cell bodies. Scale bar, 50 µm.

response to the Frmpd1 peptides, both pre-immune serum and serum after all boosters were tested by immunoblot analysis using protein lysates obtained from HEK cells expressing the C-term FLAG-tagged Frmpd1 construct or a GFP transfection control (Figure 4.4). While guinea pig sera did not appear to have increased immunoreactivity to Frmpd1 after the course of immunisation, chicken sera did. This is likely because mouse sequence peptides were used in immunisation which are more closely related to the endogenous guinea pig proteins.

We obtained purified IgY from egg yolks from both immunised chickens, as this is a convenient, high yield, and non-invasive source of antibodies (Tini et al., 2002). The total IgY fraction from Chicken 6 worked particularly well on immunoblot analysis, and was better at detecting Frmpd1 from mouse retina lysate, whereas IgY from Chicken 5 eggs only recognised overexpressed Frmpd1 from HEK cell lysates (Figure 4.4). Despite binding Frmpd1 protein well, the IgY from Chicken 6 eggs produced multiple bands on immunoblots, suggesting some non-specific staining (Figure 4.4).

Since IgY from Chicken 6 was able to detect Frmpd1 in retina lysates on immunoblots (Figure 4.4), we next wanted to determine if it could detect Frmpd1 on retina cryosections. A variety of fixation conditions (including fresh-frozen, unfixed tissue) were tested, with no positive staining on adult retina cryosections at first. Because the protein in immunoblots was denatured by β-mercaptoethanol and could be detected that way, we next tested if the epitope is hidden in the native/fixed sections and could be exposed through antigen retrieval. Indeed, a 5 min treatment of 1% β-mercaptoethanol was sufficient to produce staining in PFA-fixed wildtype retina (Figure 4.4). As with electroporated FLAG-tagged Frmpd1, the protein localised to photoreceptor inner/outer segments and synapses. This staining appears to be rod-

specific and did not colocalise with cone cell marker cone arrestin, although intense staining was only observed in a small subset of the cells. Since Frmpd1 RNA was detected in many rods by ISH, further optimisation of antigen retrieval may be needed to expose the protein epitope in every cell.

4.3.3 Frmpd1 forms a complex with Gpsm2 and T_α

It has been previously reported from *in vitro* studies that Frmpd1 can interact with Gpsm1 and acts to hold this protein in a membrane-bound fraction (An et al., 2008). Another putative binding partner of Frmpd1 is Gpsm2 (Yuzawa et al., 2011). Since both of these studies were performed *in vitro*, we wanted to test whether these protein-protein interactions occur *in vivo* in the retina where Frmpd1 is most abundantly expressed. To determine if Gpsm1 and Gpsm2 are expressed in the retina, we performed immunoblotting on several tissues to assess protein expression levels (Figure 4.5). While Gpsm1 is not very highly expressed in the retina, Gpsm2 is quite abundant and could be the main interactor with Frmpd1 in this tissue. Moreover, the expression profile of Gpsm2 is similar to Frmpd1 in that its expression is enriched in rod photoreceptors and undergoes drastic upregulation from P6-P10 (Appendix E).

To determine if Gpsm2 colocalises with Frmpd1 lending support to the hypothesis that they may interact, we next performed immunostaining with anti-Gpsm2 antibody on adult retina cryosections. Interestingly, Gpsm2 localises to the inner segments and synapses much like Frmpd1 (Figure 4.5). We next wanted to assess whether Frmpd1 and Gpsm2 colocalise in the retina. Because the Gpsm2 antibody did not work under the same fixation/antigen retrieval conditions as the custom Frmpd1 antibody, colocalisation was assessed in retinae electroporated with FLAG-tagged Frmpd1

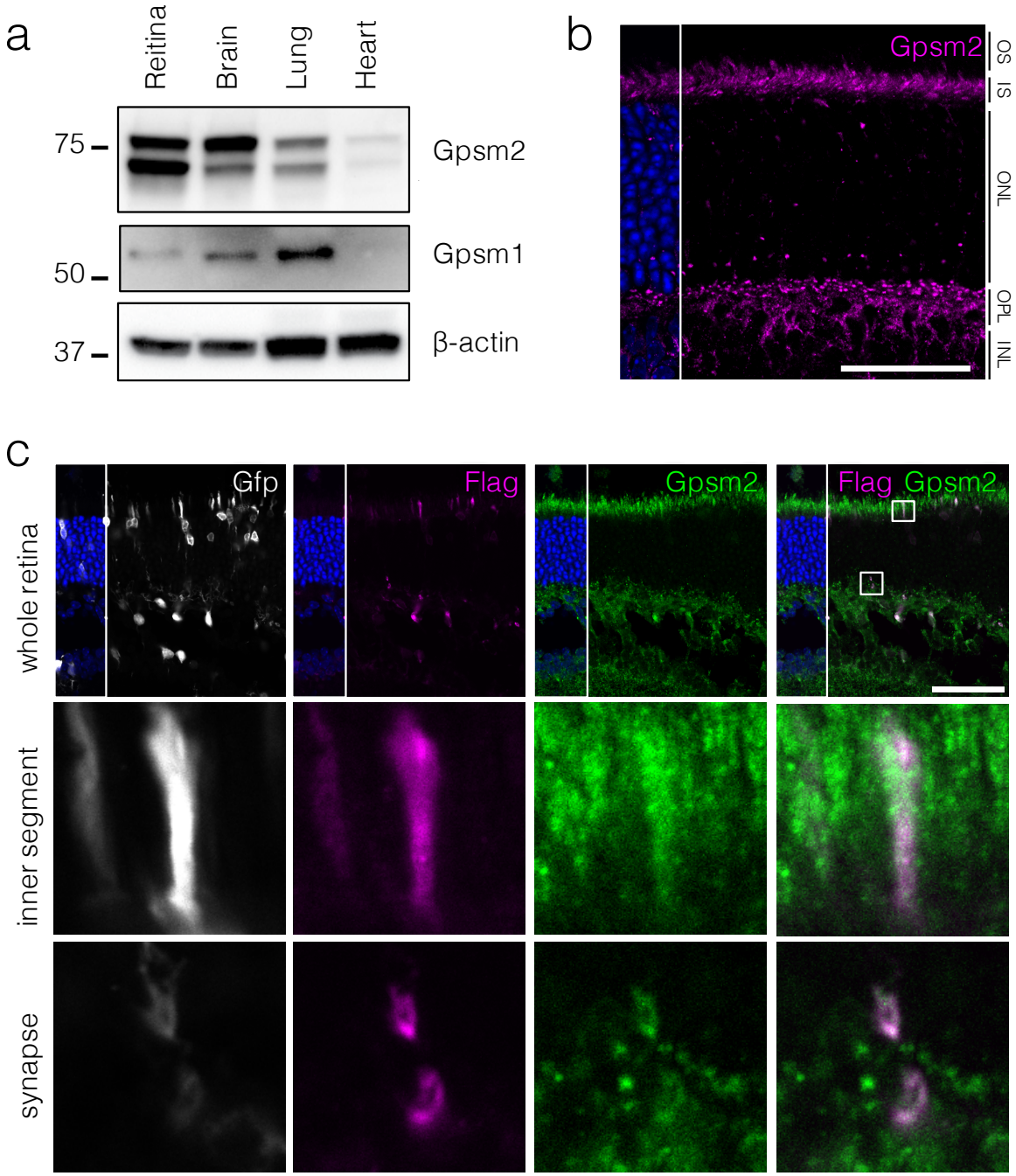

Figure 4.5: Frmpd1 and Gpsm2 colocalise in rod inner segments and synapses. (A) Immunoblot analysis of various tissues. Protein lysates from retina, brain, lung, and heart were probed with antibodies against Gpsm1 and Gpsm2. β-actin was used as a loading control. (B) Localisation of Gpsm2 in the retina. Anti-Gpsm2 antibody was used for immunohistochemistry on P21 mouse retina cryosections. (C) Colocalisation of Frmpd1 and Gpsm2 in the retina. Neonatal (P1) mouse retina was transfected with C-term FLAG-tagged full-length Frmpd1 expression construct with pUb-GFP to mark transfected cells. Immunohistochemistry was performed at P21 to stain Gpsm2 and FLAG epitope (Frmpd1 protein). Scale bar, 50 μm.

constructs. Gpsm2 and Frmpd1 were both colocalised to inner segments and synapses, and staining consistently overlapped (Figure 4.5). This suggests that Frmpd1 and Gpsm2 are localised within the same subcellular compartments.

We next wanted to test if Frmpd1 and Gpsm2 form protein complexes *in vivo* in the retina as they did in *in vitro* systems previously. Gpsm2 has previously been reported to interact preferentially with the GDP-bound form of transducin subunit alpha in crude inner/outer segment preparations (RIS-ROS). Therefore, we wanted to not only test whether Frmpd1 and Gpsm2 form complexes, but also if T_{α} in either GDP or GTP bound form was a part of these complexes. Because Frmpd1 and Gpsm2 are expressed in the synapse as well, we wanted to test whole cell lysate rather than RIS-ROS fractions only. To test this, T_{α} needed to be locked bound to either GDP or GTP before lysate preparation for immunoprecipitation. To accomplish this, the outer plasma membrane was permeabilised by α-haemolysin, a bacterial protein which forms a heptameric pore structure upon contact with lipids (Gouaux, 1998) (Figure 4.6). This allowed for the introduction of small molecules (such as GDP and a non-hydrolysable analogue of GTP, GTPγS) into the cell while preventing the loss of any small molecules/proteins over 2 kDa (Otto-Bruc et al., 1998, Nair et al., 2005a, Rosenzweig et al., 2007). Retinae were permeabilised after dark-adaptation while under red light in the presence of an excess of GDP or GTPγS to keep T_{α} bound to these molecules (Figure 4.6). In the dark-adapted state, T_{α} is tethered to the membrane and is bound to GDP. Upon light exposure, the GDP is released and GTP is taken up, releasing T_{α} into the cytoplasm. However, because T_{α} contains intrinsic GTPase activity, the GTP will be rapidly hydrolysed to GDP, necessitating the use of

non-hydrolysable GTPγS to maintain this interaction during lysate preparation and subsequent immunoprecipitation.

To test the feasibility of the haemolysin-GTPγS system, retina explants were permeabilised with haemolysin and incubated with GTPγS-BODIPY, a GTPγS molecule covalently linked to a fluorophore so that its introduction into the cell body could be visualised (Figure 4.6). When taken up by transducin, BODIPY-based dyes can exhibit enhanced fluorescence likely due to π–bond interactions with the protein (Dorh et al., 2015, Ramachandran and Cerione, 2004). Explants were prepared in the dark and incubated with GTPγS-BODIPY, then illuminated to induce transducin- GTPγS-BODIPY binding (Figure 4.6). Retinae were then fixed and processed for microscopy. While T_{α} did not translocate to the inner segments and synapses upon illumination, the increased fluorescence within the outer segments suggests that they did take up GTPγS-BODIPY and would therefore be locked in the GTP-bound form in lysates prepared for immunoprecipitation.

While the commercially available anti-Frmpd1 antibody did not work well for IHC, it was suitable for immunoprecipitation of Frmpd1 complexes from retina lysate. To capture protein complexes in both dark-adapted, GDP-bound T_{α} retinae and light-adapted, GTP-bound T_{α}, the haemolysin system was used before preparing equal amounts of total retina protein lysate from each condition (Figure 4.6). The detergent n-dodecyl-β-d-maltoside (DDM) was chosen for use in the lysis buffers to solubilise membrane protein complexes without breaking them apart based on results from several other groups (Lambeng et al., 2006, Whorton et al., 2008, Jastrzebska et al., 2013). Interestingly, Frmpd1 was found in complexes with Gpsm2 and T_{α} in both

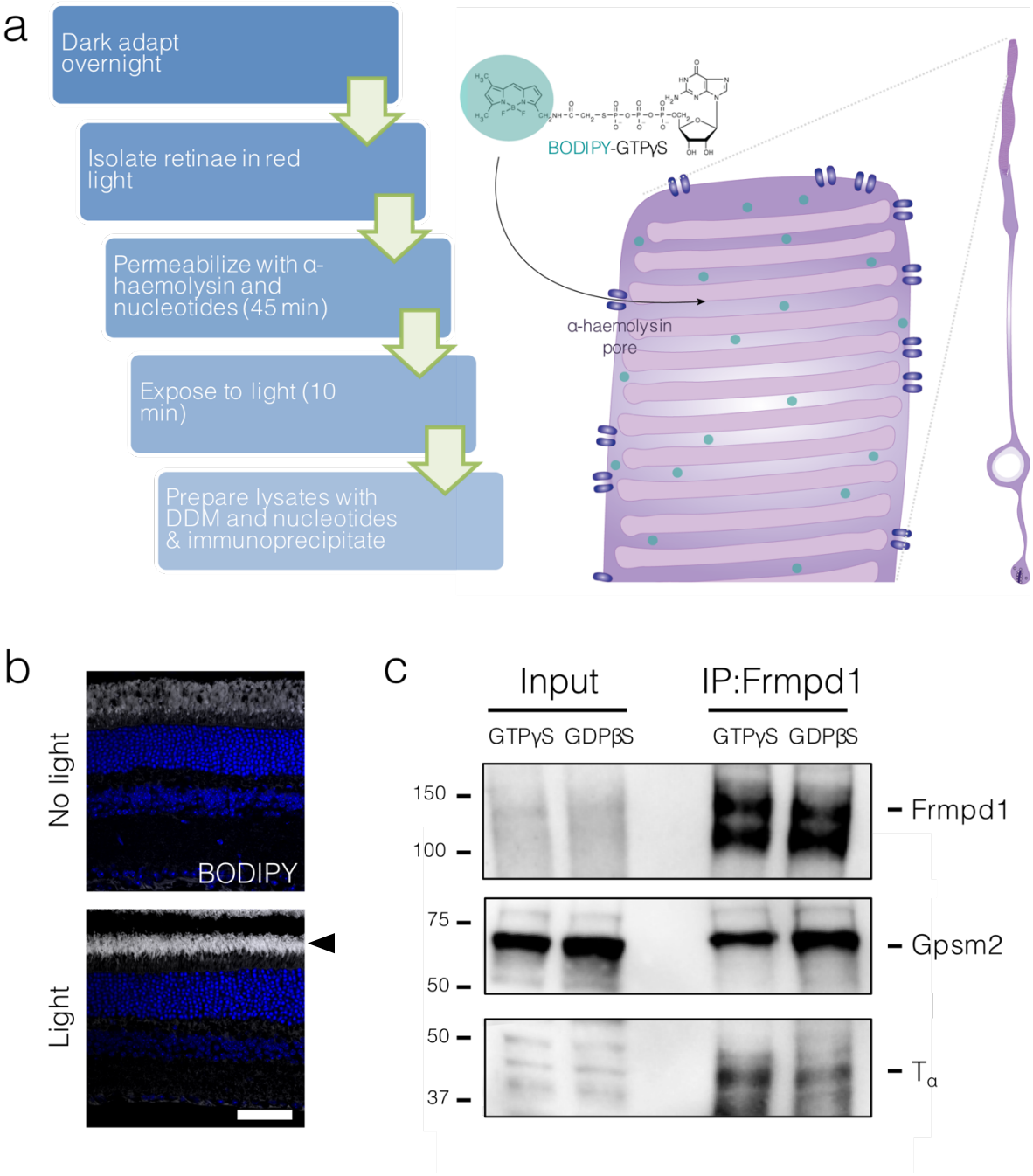

Figure 4.6: Immunoprecipitation of Frmpd1 complexes from dark- and light-adapted retinae. (A) Photoreceptor plasma membranes were permeabilised by incubation with α-haemolysin to allow for diffusion of GTPγS-BODIPY and GDPβS into the outer segments. Upon exposure to light, the excess of non-hydrolysable GTPγS-BODIPY will compete with endogenous GTP for T_α binding. (B) Retinae were permeabilised with α-haemolysin and incubated with GTPγS-BODIPY in red light. When exposed to white light, T_α binding to GTPγS-BODIPY enhances BODIPY fluorescence in the outer segments (arrowhead). (C) Immunoprecipitation with anti-Frmpd1 antibodies was performed on retina lysates prepared as in (A). 10% of input lysate and 50% of immunoprecipitated protein complexes were processed for immunoblotting with anti-Frmpd1, Gpsm2, and T_α antibodies. Results representative of 3 replicates.

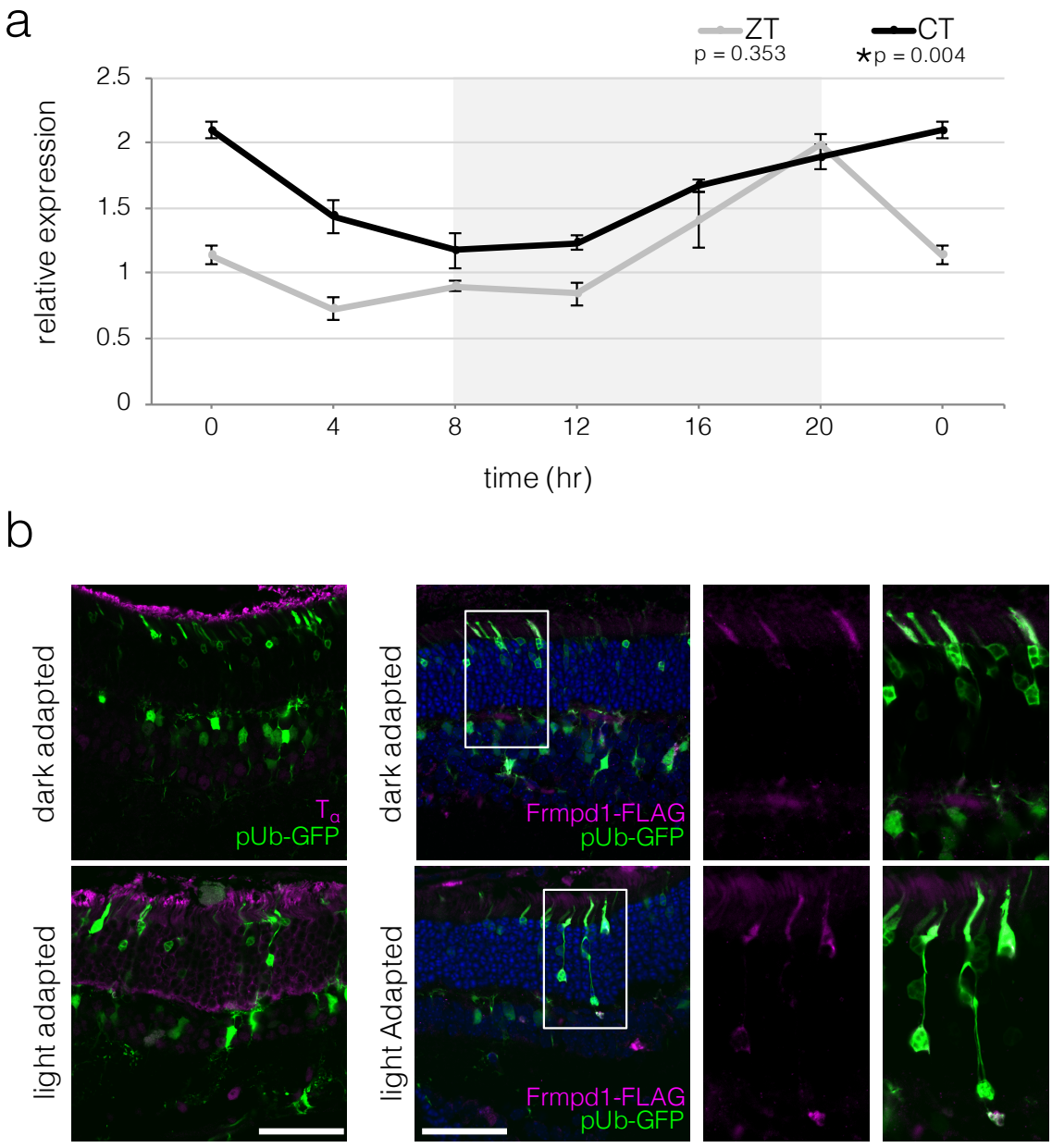

Figure 4.7: *Frmpd1* transcript expression and protein localisation in light and dark. (A) Diurnal (ZT, Zeitgeber time) and circadian (CT, circadian time) expression of Frmpd1 in the retina was assessed by quantitative PCR performed in biological and technical triplicate. *Frmpd1* expression was rhythmic, peaking in the late night phase when kept on a 12:12 light:dark cycle (ZT), and in the subjective night phase when kept in constant darkness (CT). Temporal changes in expression were analysed by one-way ANOVA. (B) Frmpd1 protein localisation in light- and dark-adapted conditions was tested in adult (P21) cryosections of retinas transfected with Frmpd1-FLAG construct by *in vivo* electroporation. T_α was used as a control to confirm light- and dark- adaptation of both samples.

conditions. It also appeared that more Gpsm2 was contained in these complexes in the GDP condition. Reverse-IP experiments using anti-Gpsm2 antibodies confirmed these results.

4.3.4 Frmpd1 expression, but not localisation, varies during light/dark cycles

Since *Frmpd1* appears to play a role in dark adaptation of rod photoreceptors and is very tightly transcriptionally regulated, we were curious as to whether its expression varies across the day according to light/dark cycles (Figure 4.7). To assess changes in RNA expression across a 24-hr period, C57BL6/FVB mice were kept in either a 12hr light/dark cycle (Zt) or constant darkness (Ct) and retinae were harvested at 4hr intervals for qPCR analysis (Katti et al., 2013). Under both circumstances, the expression of Frmpd1 RNA decreased upon light onset (subjective day) and then increased after dark onset (subjective night) (Figure 4.7a). Analysis with one-way ANOVA revealed a statistically significant effect of time on expression of *Frmpd1* when mice were kept in constant darkness ($p=0.004$). These results were independently validated on a circadian timecourse RNA-seq experiment from rat retinae performed by another lab as well (Marie-Paule Felder-Schmittbuhl, unpublished data).

We also investigated whether the localisation of Frmpd1 protein changes with different light/dark conditions along with its expression levels. To study this, Frmpd1-FLAG construct described previously (Section 4.3.1) was transfected into neonatal CD1 mouse retina by *in vivo* electroporation. At P21, mice were dark adapted overnight and then either placed in bright light for 1 hr or kept in darkness before eyes were harvested and processed for IHC. Staining with anti-FLAG antibody

revealed that the localisation of Frmpd1 to the inner segments remains constant between light- and dark-adapted animals (Figure 4.7b).

4.4 Discussion

Since a role for Frmpd1 in the retina had not previously been explored, we wanted to determine the localisation and protein-protein interactions of this molecule as a means of assessing its potential function. The inner segment and synaptic localisation of Frmpd1, as well as its interactions with Gpsm2 and T_α identified in this chapter, suggest that Frmpd1 may act as a scaffolding molecule that helps to modulate rod phototransduction.

To localise Frmpd1 in the retina, we relied on a combination of immunostaining and *in vivo* electroporation of tagged Frmpd1 protein. Tagging full-length Frmpd1 appeared to disrupt its localisation depending on size/location of the tag; mislocalisation with N-terminal tags has been previously reported for a variety of other proteins (Palmer and Freeman, 2004, Li et al., 2008), and is especially feasible for Frmpd1 since the N-terminus contains a PDZ domain which helps correctly position the protein. A C-terminal GFP tag also disrupted Frmpd1 localisation, likely due to its large size (27 kDa). Fortunately, a smaller C-terminal FLAG tag (1 kDa) produced a distinct localisation pattern in the rod inner segments and synapses that was reproducible with the custom chicken antibody. It is thus most likely that the true localisation of Frmpd1 is indeed within photoreceptor inner segments and synapses; this distribution is especially feasible considering that Frmpd1 binds to Gpsm2, which is also found in the same subcellular regions.

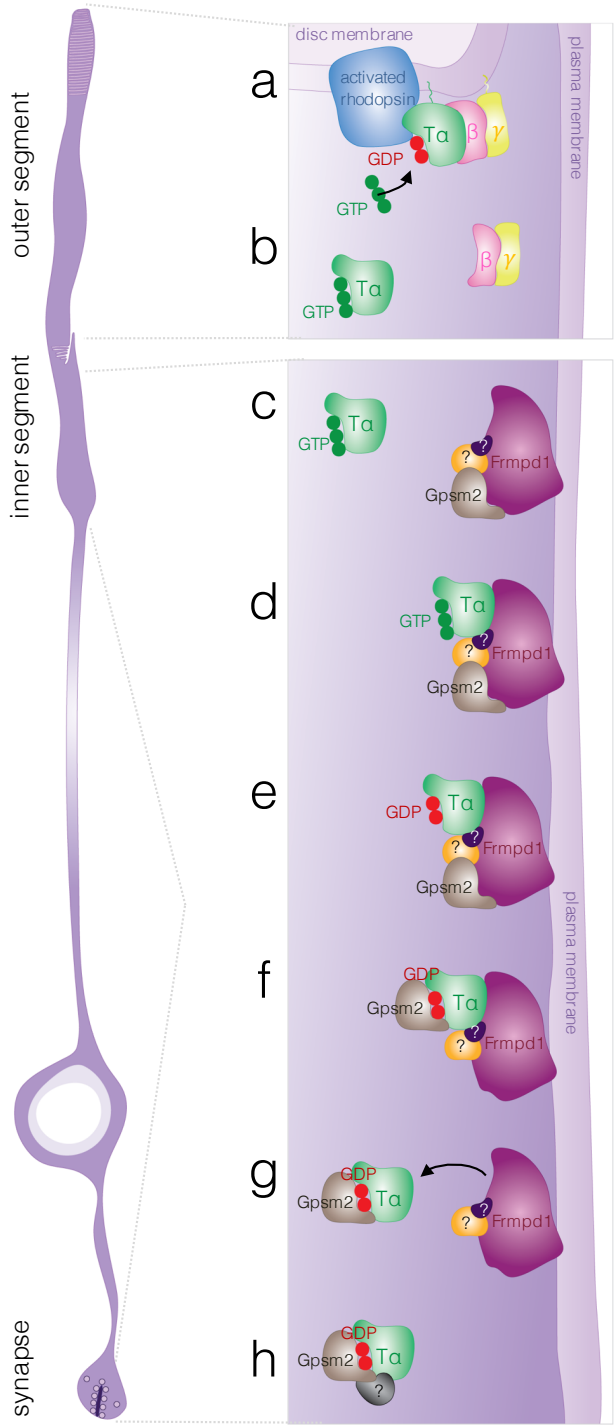

Figure 4.8: Proposed mechanism of Frmpd1-Gpsm2- T_α protein binding. (A) In outer segments, activated rhodopsin interacts with T_α^{GDP} (GDP-bound transducin α subunit), which releases GDP (guanosine diphosphate) for cytosolic GTP (guanosine triphosphate) and (B) dissociates from the disc membrane. (C) Soluble T_α^{GTP} translocates to inner segments and synapses, where the Frmpd1 scaffold complex is located. (D) On the plasma membranes of inner segments and synapses, T_α^{GTP} forms a transient protein complex with Frmpd1, Gpsm2, and additional unknown proteins. (E) While bound to the Frmpd1 complex, T_α^{GTP} hydrolyses its GTP to GDP. (F) Recognising the newly inactive T_α^{GDP}, Gpsm2 switches its binding partner from Frmpd1 to T_α^{GDP}. (G) The T_α^{GDP}-Gpsm2 complex then dissociates from the plasma membrane, (H) forming additional protein-protein interactions to facilitate the return of T_α^{GDP} to the outer segments.

In immunoprecipitation experiments, much of the Gpsm2 was not bound to Frmpd1, suggesting that there may be separate pools of the protein with some interacting in Frmpd1 complexes and some not. This is consistent with RNA-seq data, where Gpsm2 is expressed much more abundantly than Frmpd1 in adult rod photoreceptors (~187 vs. ~31 FPKM, Appendix E). Gpsm1 has been shown to switch binding partners from Frmpd1 to T_{α}^{GDP} (An et al., 2008), so perhaps the Frmpd1 interaction in inner segments or synapses only occurs as a small percentage of all Gpsm2 interactions.

Since Frmpd family proteins are often involved in scaffolding of multiprotein complexes to specific regions (Moleirinho et al., 2013), it is likely that Frmpd1 may act to bring several components together in the inner segments and synapses (Figure 4.8). Interestingly, Gpsm2 has been shown to react preferentially with T_{α}^{GDP} (Nair et al., 2005b), but Frmpd1 complexes containing Gpsm2 reported in this chapter appear to contain both T_{α}^{GTP} and T_{α}^{GDP}. One potential explanation for both T_{α}^{GTP} and T_{α}^{GDP} immunoprecipitating with Frmpd1 protein complexes is that Frmpd1 may bind activated T_{α}^{GTP} to bring it into close proximity to Gpsm2. Once T_{α}^{GTP} is hydrolysed to T_{α}^{GDP}, Gpsm2 may then bind and stabilise T_{α}^{GDP} (only then dissociating from the Frmpd1 scaffold) until it is trafficked back to the outer segment to be assembled as holotransducin. In this way, all detected proteins (Gpsm2, Frmpd1, T_{α}^{GTP}, and T_{α}^{GDP}) could theoretically exist in a complex together (Figure 4.8). Methods to further investigate this are described in (Section 6.3.2).

To test for direct interactions between Frmpd1 and T_{α}, co-immunoprecipitation experiments could be performed in HEK293 cells that do not endogenously express

these or other retina proteins. By introducing proteins exogenously through transfection of expression constructs in these cells, we could more reliably dissect whether direct binding occurs or if these interactions depend on the presence of additional factors (such as Gpsm2). The Frmpd1, Gpsm2, and T_α complex most likely contains additional proteins, and the composition of these complexes may even vary between the light- and dark-adapted states when various phototransduction proteins undergo light-induced translocation through the inner segments and synapses (Artemyev, 2008, Sommer et al., 2014, Strissel et al., 2005, Tian et al., 2013). There may also exist in the complexes proteins that accelerate the intrinsic hydrolase activity of T_α to facilitate the T_α^{GTP} to T_α^{GDP} transition. The role of Frmpd1 as a potential scaffold to bring these proteins together could be functionally relevant, as mutations in R9ap (which anchors several T_α GTPase enzymes to the membrane) exhibit the same functional defects as mutations in the enzymes themselves (Michaelides et al., 2010, Nishiguchi et al., 2004, Keresztes et al., 2004). Once immunoprecipitation experiments have been fully optimised, they could be coupled with mass spectrometry to help to identify additional proteins in the Frmpd1 complex. These interactions could then be confirmed by immunoblotting and colocalisation by immunohistochemistry and could form the basis for many interesting studies regarding the regulation of rod phototransduction and potential alternative roles that Frmpd1 may play (such as mediating cell-cell contacts as discussed in Sections 2.3.2 and 2.4).

5

Loss of *Frmpd1* modulates rod phototransduction

5.1 Introduction

The localisation and protein-protein interactions of Frmpd1 described in Chapter 4 suggest that Frmpd1 may mediate rod phototransduction, particularly as it pertains to the movement of T_α during light- and dark-adaptation. The *in vivo* knockdown screen performed in Chapter 1 showed formation of rosettes when *Frmpd1* was knocked down in CD1 mice. To further define the role of Frmpd1, we next wanted to examine the effects of its loss of function in the retina using a mouse model with a germline deletion of *Frmpd1*. Unlike *in vivo* electroporation, a transgenic mouse model would allow for ablation of gene expression across the entire retina, thereby permitting full-field visual function analysis by electroretinography (described in Section 5.2.5).

Traditionally, loss-of-function mouse lines are generated through the use of homologous recombination to introduce exogenous DNA into the genome of cultured murine embryonic stem cells (ESCs) (Figure 5.1) (Hall et al., 2009, Misra and Duncan, 2002, Bouabe and Okkenhaug, 2013). Correctly targeted ESCs are then injected into blastocysts and transferred to pseudopregnant foster mothers to generate chimeric founder mice (Longenecker and Kulkarni, 2009). In the Cre/loxP system, exogenous DNA that is incorporated into targeted ES cells is designed to contain loxP sites flanking a target region to be deleted (generating a "floxed" allele) (Van Duyne, 2015, Bouabe and Okkenhaug, 2013). Floxed mice can later be mated with mice expressing Cre recombinase, an enzyme that splices two loxP sites together to delete the intergenic DNA (Van Duyne, 2015). In this way, various tissue-specific, drug-inducible, or other conditional deletions can be generated through selective breeding of floxed mice with lines expressing Cre under specific promoters (Kos, 2004). While an incredibly useful method, generating homozygous conditional loss-of-function mice via the Cre/loxP system can take a considerable amount of time (often over a year) due to the reliance on host cell homologous recombination events to first introduce loxP sites into the genome paired with subsequent requirements of multiple rounds of breeding to express Cre (Liu et al., 2017).

More recently, Clustered Regularly Interspaced Short Palindromic Repeat / CRISPR associated protein 9 (CRISPR/Cas9) technologies have proven useful for more rapidly generating loss-of-function mouse models than the Cre/loxP system (Figure 5.1) (Singh et al., 2015). In one variation of this system, zygotes are directly edited through coinjection of Cas9 enzyme with targeting guide RNAs (gRNAs) specific to the intended target sequence before being implanted into foster mothers

(Liu et al., 2017, Singh et al., 2015). Cas9 is directed to the target region of genomic DNA by the gRNA and cuts one or both strands, which are then repaired by the host cell's machinery (Liu et al., 2017, Singh et al., 2015). Through error-prone non-homologous end joining (NHEJ), small insertions or deletions (indels) can be introduced at the break site during repair, thereby disrupting the reading frame of the gene and causing loss-of-function mutations (Liu et al., 2017, Singh et al., 2015). In another variation of CRISPR/Cas9 gene editing, stretches of DNA can be deleted through the use of 2 gRNAs flanking the target sequence (Ran et al., 2013). This induces strand breaks on either side of the sequence which are then joined through NHEJ (Ran et al., 2013).

CRISPR/Cas9 typically generates mosaic founder mice, although depending on efficacy some founder mice may be homozygous for mutations (Liu et al., 2017). In this way, using a CRISPR-based approach for generating loss-of-function mouse lines can be much more time effective than traditional Cre/loxP systems. However, this can pose problems in cases where widespread disruption of a gene results in prenatal death. One advantage that the Cre/loxP system offers over CRISPR/Cas9 is the flexibility of inducing deletions in a spatially and temporally regulated manner through selective Cre lines to bypass issues such as embryonic lethality (Ablain and Zon, 2016). Presently, the use of CRISPR/Cas9 to generate tissue-specific loss-of-function mouse models is limited and tends to rely on local delivery of gRNA and/or Cas9 at later stages of development rather than through germline genomic editing in zygotes (Carroll et al., 2016, Staahl et al., 2017, Stolfi et al., 2014).

Here, we present a novel method of generating a tissue-specific knockdown of *Frmpd1* through a CRISPR/Cas9-mediated deletion of its alternative promoter in

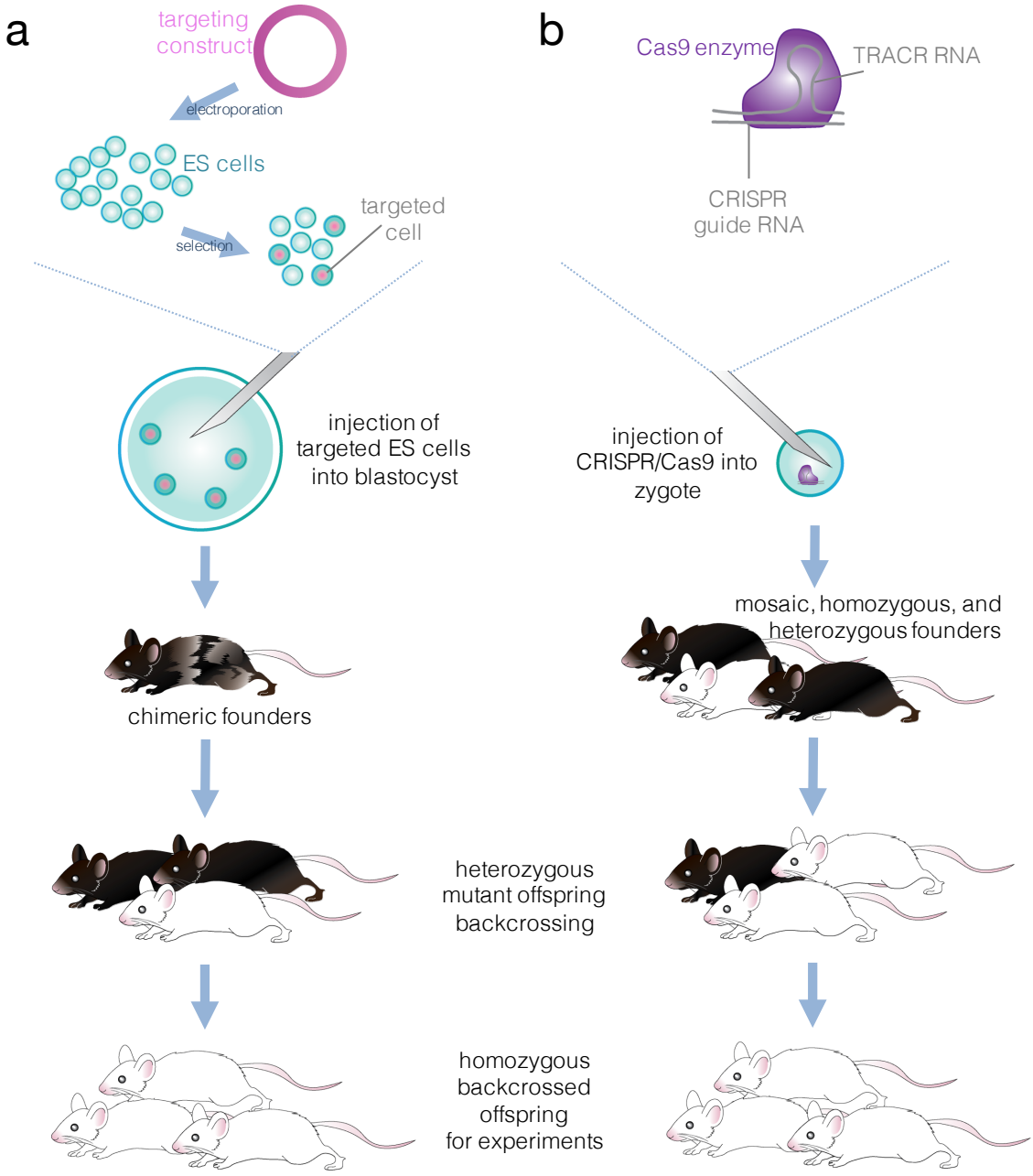

Figure 5.1: Comparison of traditional and CRISPR/Cas9 genetic engineering of mice. (A) In conventional gene targeting, a target construct is electroporated into embryonic stem (ES) cells. Through colony expansion and positive/negative selection, target ES cells with the intended mutations are selected and injected into blastocysts. Blastocysts are transferred to pseudopregnant foster mothers and give rise to chimeric founder offspring. These offspring are backcrossed several generations to reduce off-target events and then selectively bred to produce homozygous mutant mice. (B) In CRISPR/Cas9-mediated gene editing, zygotes are injected with the Cas9 enzyme along with CRISPR guide RNAs to target specific regions of DNA. These zygotes are transferred to pseudopregnant foster mothers and give rise to founder offspring, which are either mosaic, homozygous, or heterozygous for mutations. These offspring are backcrossed several generations to reduce off-target events and then selectively bred to produce homozygous mutant mice. Figure adapted from (Liu et al., 2017).

germline cells. Without altering the protein-coding portion of the gene, removal of *Frmpd1*'s retina-specific promoter element from the genome led to a deletion of RNA and protein in this tissue while permitting its expression in the brain. We have used this model to further investigate the morphological (using immunohistochemistry) and functional (using electroretinography) consequences of a loss of Frmpd1 in the retina as described in the following chapter.

5.2 Materials and methods

5.2.1 Materials

For reagent details, buffer compositions, and plasmid maps refer to Appendices A-D.

5.2.2 Methods described in other sections

2.2.5 Mouse lines & husbandry 35
.2.10 Retina cryosectioning 37
2.2.11 *In situ* hybridisation (ISH) 39
3.2.3 Immunohistochemistry 67
3.2.5 General PCR protocol and primer design 68
3.2.16 Bicinchoninic acid (BCA) assay 81
4.2.8 Immunoblotting 110

5.2.3 CRISPR/Cas9 genetic engineering

Introduction of multiple small insertions/deletions (indels) within the protein coding region of *Frmpd1* was achieved through the use of single CRISPR guide RNAs (gRNAs) to introduce double-stranded breaks near the target sequence, whereas deletion of the *Frmpd1* promoter was achieved with a double nickase method using two CRISPR guide RNAs flanking each side of the target sequence. Founder mice for both projects were produced by the Genetic Engineering Core Facility at the National

Eye Institute (Bethesda, MD). Briefly, guide RNAs were designed using an online CRISPR Design Tool (crispr.mit.edu). Oligonucleotide sequences for producing guide RNAs are provided below; they contain a T7 promoter sequence (taatacgactcactata) followed by at least one guanine for T7 RNA polymerase to begin transcription, a 20 nucleotide genomic target sequence (capitalised), which is followed in the genome by a PAM (protospacer adjacent motif, 5'-NGG-3') sequence, and a 14 nucleotide tracrRNA (transactivating CRISPR RNA) overlap sequence (gttttagagctagaa):

Target region	Strand	gRNA oligo sequence
Exon 5	-	taatacgactcactatagAGAGGTTTACCGATGTGCAGgttttagagctagaa
Exon 13	+	taatacgactcactataGTTCGCCAACATCAGCCGCGgttttagagctagaa
Promoter 5' nick	+	taatacgactcactataGGGGGTGACCTGCCCCTCTgttttagagctagaa
Promoter 3' nick	+	taatacgactcactataggATGGGGCGTGGATGCCATgttttagagctagaa

Oligonucleotides were annealed to an *S. pyogenes* Cas9 scaffold oligo through the overlap sequence, then filled in by DNA polymerase for dsDNA that would be transcribed into a final gRNA according to EnGen sgRNA Synthesis Kit manufacturer's instructions (New England Biolabs). gRNAs were tested for efficacy by co-injection with Cas9 mRNA into mouse ES cells followed by detection of indels by a Surveyor Mutation Detection Kit (IDT). Zygotes from C57BL/6J mice were microinjected with gRNA + Cas9 then transferred to a pseudopregnant C57BL/6J surrogate mother (25 embryos per mother; in embryonic lethality studies, B6SJLF1/J embryos were implanted into CD1 mothers). Targeted events in founder mice were screened via PCR genotyping as described (Section 5.2.4) and founders were backcrossed onto C57BL/6J background for a minimum of 3 generations to reduce off-target events.

5.2.4 PCR genotyping

Genomic DNA was extracted by incubating a 2 mm tail clip or whole dissected embryo in 200 μl Direct PCR Tail Lysis Buffer (Viagen) supplemented with 2 μl of 20 mg/ml Proteinase K (Sigma) overnight at 55˚C. The reaction was stopped the next day by incubating 1 hr at 85˚C. After a brief centrifugation (30 sec 12,000 x *g*), 1 μl of supernatant was used for PCR genotyping (see section 2.4). For 3-primer PCR genotyping, the same protocol was used replacing 0.2 μl of H_2O with 0.2 μl of additional primer (100 μM). Refer to Appendix B for primer sequences and optimal annealing/extension conditions.

5.2.5 Electroretinography

Mice were dark adapted overnight, then anesthetised with an intraperitoneal injection of normal saline solution containing ketamine (15 mg/g) and xylazine (7 mg/g body weight) and placed on a 37˚C heating pad to maintain body temperature. Pupils were dilated with 0.5% tropicamide (Akorn Pharmaceuticals) and 2.5% phenylephrine hydrochloride (Paragon Bioteck), and the cornea anesthetised with 0.5% proparacaine hydrochloride (Sandoz US). To ensure electrical contact and prevent corneal damage, 2.5% hypromellose gel (Gonak, Akorn Pharmaceuticals) was applied to the cornea. Gold loop electrodes were placed on the centre of the cornea of each eye, and a gold wire loop was placed in the mouth as a reference electrode. All stimuli were presented in a UV-equipped Ganzfeld dome connected to an Espion E2 system which measured electrical responses (Diagnosys LLC). Dark-adapted (scotopic) ERG was performed using white light flash intensities ranging from 0.0001 to 10 cd.s/m^2 (candela-seconds per metre squared). Light adapted (photopic) ERG was

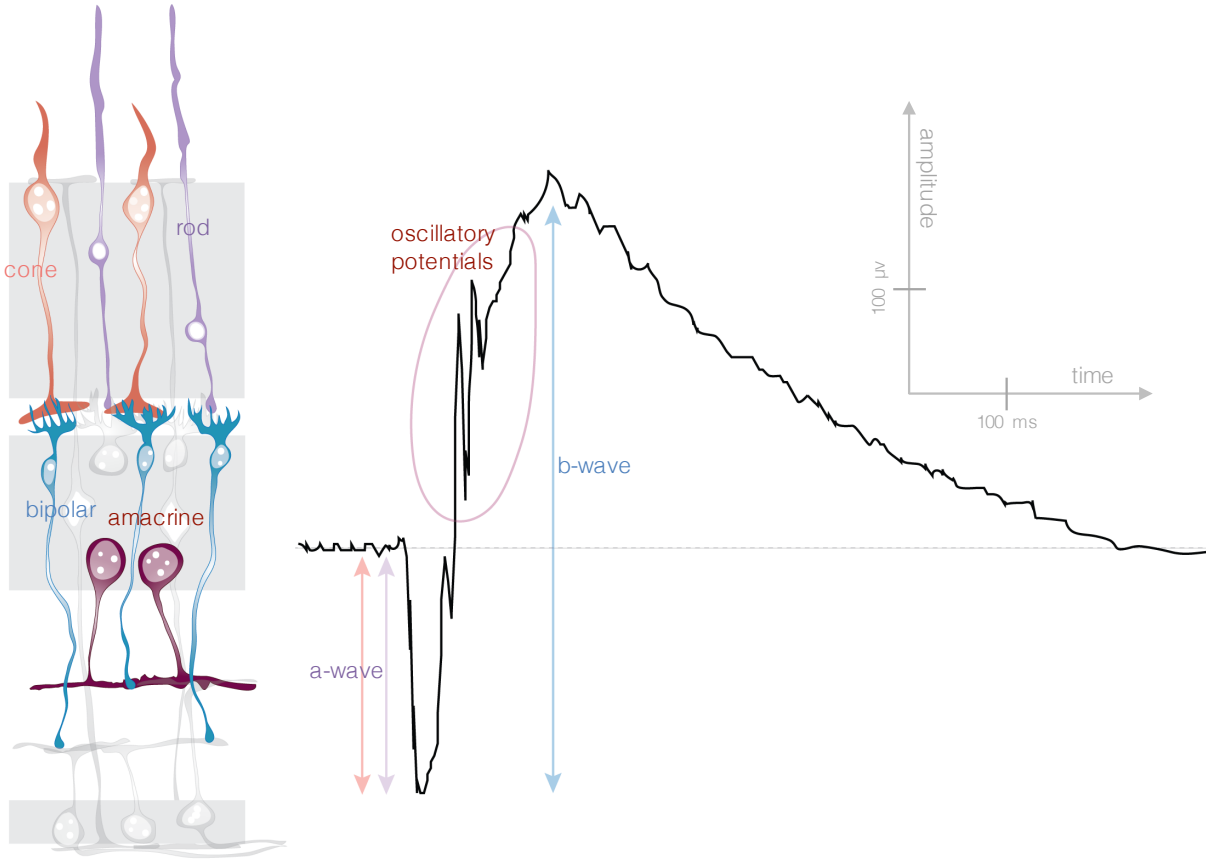

Figure 5.2: Electroretinography. The full-field electroretinogram is measured by an electrode contacting the corneal surface. Following a light stimulus, photoreceptors are hyperpolarised (a-wave) and signal to downstream inner retinal cells, which depolarise (bipolar cells, b-wave; amacrine cells, oscillatory potentials). Figure adapted from (Rossmiller et al., 2015).

performed by first bleaching rod photoreceptors with background white light at 20 cd.s/m^2 for 2 min, then the ERG response was recorded using alternating 530 nm (green, M-cone) and 365 nm (UV, S-cone) flashes with intensities ranging from 0.3 to 100 cd.s/m^2 with continuous background illumination. For dark recovery ERG, mice were dark adapted overnight and then subjected to a moderate (~10% of rhodopsin) visual pigment bleach with 1000 cd.s/m^2 of white light for 30s (Li et al., 2015). After the light was turned off, a single 10 cd.s/m^2 white light flash was then administered every 2 min for 60 min and ERG response recorded to monitor recovery of a-wave amplitude during dark adaptation. A minimum of six responses (2 eyes each from 3 animals of each age/genotype) to each light stimulus were recorded. Statistical analyses (two-tailed unpaired Student's *t*-test) were performed using GraphPad Prism 7 software.

5.3 Results

5.3.1 Disruption of Frmpd1 protein-coding region results in embryonic lethality before E10.75

To generate an Frmpd1 loss-of-function mouse line, we first attempted to use CRISPR/Cas9 technologies to introduce small insertions/deletions (indels) within the protein coding region of the gene to shift the reading frame and/or introduce premature stop codons to create non-functional protein or to result in mRNA degradation (Figure 5.3). Guide RNAs intended to induce double-stranded breaks were designed within protein-coding Exons 5 and 13 (Figure 5.3). Surprisingly, despite *Frmpd1* being expressed almost exclusively in the retina in postnatal mice, the only live births obtained were those with 3 base-pair (1 amino acid) deletions in Exon

13. No pups with Exon 5 mutations, or even with frameshift or early truncation mutations in Exon 13, were observed (Figure 5.3).

To determine the age at which embryos with CRISPR targeted Frmpd1 died, one of the most deleterious guide RNAs (targeting a region within Exon 5, which would induce disruptions the earliest in Frmpd1 protein) was used to target *Frmpd1* in ES cells, which were then implanted into foster mothers for timed pregnancies. The mothers were euthanised at varying stages of pregnancy (E6.75 n=3, E7.75 n=6, E8.75 n=6, E10.75 n=7, E14.75 n=6) and uteruses dissected to examine the number of implantation sites and to isolate remaining embryos for genotyping to determine the latest stage at which *Frmpd1* mutants could be identified (Figure 5.3). As predicted, many of the implantation sites contained resorbed embryos with dark, empty decidua indicative of aborted embryos. The only embryos surviving as far as E14.75 were wildtype, with all remaining (presumably mutated, correctly targeted embryos) implantation sites containing empty decidua (Figure 5.3). Live, mutant embryos could only be found in E7.75-8.75 pregnancies with none present by E10.75. The absence of any mutant embryos and replacement by aborted, resorbed empty implantation sites by E10.75 suggest an early embryonic lethality of *Frmpd1* mutant mice and potential role for this protein in embryogenesis.

5.3.2 Deletion of retina-specific Frmpd1 promoter and 5'-UTR results in tissue specific knockdown

Since manipulation of the protein-coding region of the *Frmpd1* gene resulted in an unexpected embryonic lethality (Figure 5.3), we next decided to create a tissue-specific disruption of *Frmpd1* that would allow us to examine its function in the retina

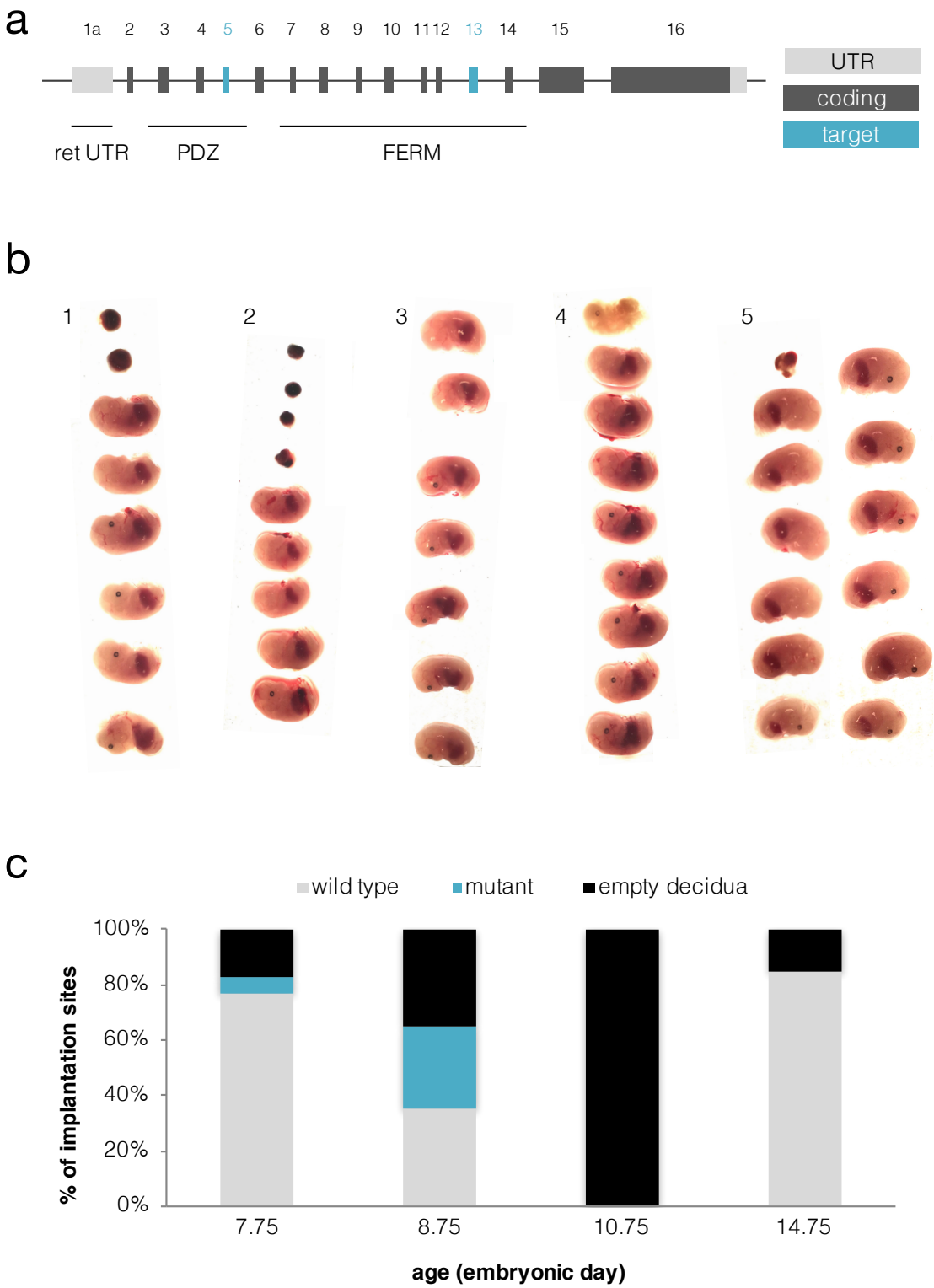

Figure 5.3: CRISPR targeting of protein-coding portion of *Frmpd1* results in early embryonic death. (A) CRISPR guide RNAs were designed to induce double-stranded breaks in either Exon 5 or 13. UTR, untranslated region; coding, protein-coding exon; target; CRISPR target. (B) Zygotes were targeted with CRISPR guide RNA targeting Exon 5, and implantation sites from foster mother were dissected at E14.75. Several empty deciduae can be seen from foster mothers 1 & 2. (C) Embryos were dissected at various ages and genomic DNA was extracted and genotyped. No embryonic material was found in the empty decidua.

while still permitting live birth. Since we previously identified the use of an alternative promoter of *Frmpd1* that appears to be used exclusively in the retina (Chapter 3), we wanted to explore the possibility of targeting this regulatory element to downregulate *Frmpd1* specifically in cells that use this promoter (i.e., rod photoreceptors and bipolar cells).

To accomplish this, a pair of guide RNAs was designed flanking either side of the Nrl binding site in the *Frmpd1* promoter to result in double-stranded breaks on either side of the genomic region (Figure 5.4). Through non-homologous end-joining (NHEJ) of the two disrupted sides, the region between both breaks would be eliminated from the genome resulting in a ~1000 bp of the genomic region containing many of the key regulatory elements driving *Frmpd1* expression in the retina but not in other tissues. Furthermore, the targeted region lies upstream of the translational start site, leaving the protein-coding portion of the gene completely unperturbed so that it can be produced in its native form in any cell where it is expressed.

Recombination events using this dual-guide RNA system in ES cells were extremely effective, with 6 out of 8 founder mice being either homo- or heterozygous for the deletion. Founder mice were generated on a C57BL/6J background and backcrossed for at least 3 generations to reduce off-target effects of CRISPR-Cas9 gene editing. To assess the efficacy of mRNA knockdown in *Frmpd1* mutant animals, ISH was performed on retina cryosections from mice homozygous for either the wildtype or promoter deletion allele (Figure 5.4). As expected, probes specific to Exon1a (within the region deleted by NHEJ) detected no RNA in the deletion retinae. To

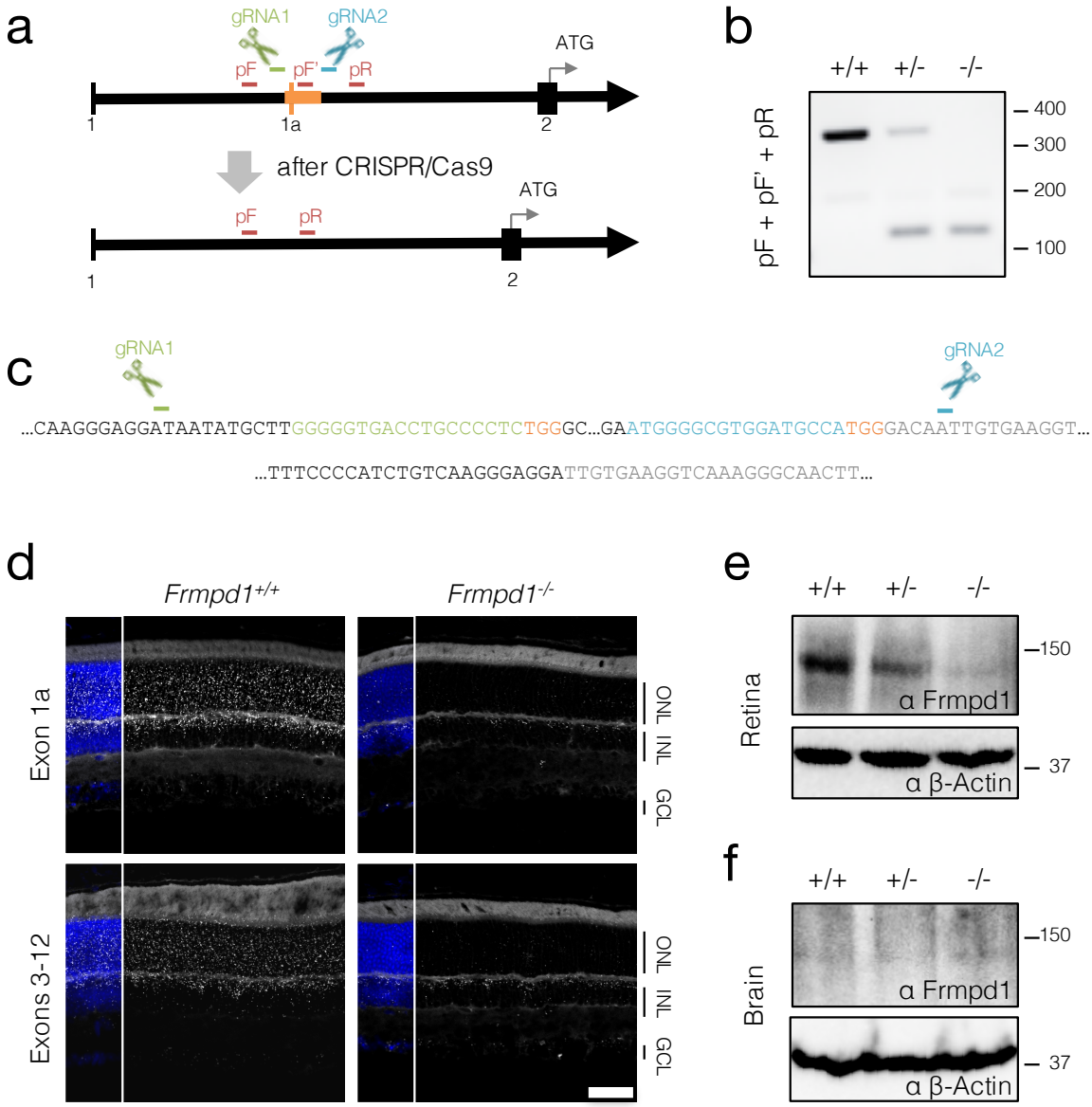

Figure 5.4: Deletion of *Frmpd1* retina 5'-UTR leads to tissue-specific protein knockout. (A) Schematic of guide RNAs and genotyping primers for CRISPR/Cas9 targeted genomic region. Guide RNAs (gRNA1, gRNA2) flanking either side of Exon1a were designed to delete a 1 kbp fragment upon non-homologous end joining (NHEJ). Primers pF,pF', and pR were designed to detect NHEJ events. (B) PCR genotyping of tail DNA. Genomic DNA was extracted from tail clippings and used for PCR amplification by 3 primers (pF, pF', pR). A 350 bp product corresponds to the wild-type allele, while a 150 bp product corresponds to a deletion allele. (C) Sequence of CRISPR/Cas9-mediated deletion. PAM sequences (orange) and CRISPR guide RNA target sequences (green and blue) are highlighted. Top line corresponds to wild type genomic sequence, while bottom line corresponds to genomic sequence after Exon 1a excision by NHEJ. (D) Exon 1a deletion abolishes full-length *Frmpd1* RNA expression in retina. *In situ* hybridization probes specific to Exon 1a or downstream Exons 3-12 were used to visualize *Frmpd1* RNA expression in wild type or CRISPR-targeted mouse retina. Background autoflourescence can be seen in the outer plexiform and outer segment regions; bright punctate staining represents RNA. (E) Frmpd1 protein expression in retina. Immunoblots of 50 μg of whole retina lysate from mice of each genotype were probed with anti-Frmpd1 antibody and anti-β-actin as a loading control. (F) Frmpd1 protein expression in brain. Immunoblots of 200 μg of total brain lysate from mice of each genotype were probed with anti-Frmpd1 antibody and anti-β-actin as a loading control.

determine whether the entire mRNA message is degraded or if it is simply transcribed without the deleted region, ISH probes targeting downstream Exons 3-12 within regions not targeted by CRISPR were also used to detect RNA (Figure 5.4). Strikingly, none of the probes detected RNA in the cryosections from mice in which the *Frmpd1* promoter region was deleted, indicating that the targeted deletion of this regulatory element was sufficient to ablate RNA expression either through never having it transcribed or through post-transcriptional degradation (Figure 5.4).

In either case, an absence of RNA would presumably make it impossible for the cells to produce protein. We next wanted to assess the extent of protein knockdown in mice heterozygous and homozygous for the promoter deletion. Whole retina protein lysate was prepared from wildtype, heterozygous, and homozygous *Frmpd1* promoter deletion littermates and probed with anti-Frmpd1 antibody to detect Frmpd1 protein expression (Figure 5.4). Just one deletion allele was sufficient to reduce protein expression, with virtually undetectable levels in the homozygous knockout mouse. To determine if this reduction in protein expression was specific to the retina, whole brain extract was also isolated from these animals and probed with anti-Frmpd1 antibody. The expression level in this tissue is extremely low even in wildtype animals; nevertheless, levels appear to remain stable between all 3 genotypes. Combined, these results show that deletion of the retina-specific *Frmpd1* regulatory region is sufficient to knock down RNA and protein expression within this tissue while leaving the expression in other tissues like brain and embryo (presumably, as live birth was permitted) unaltered.

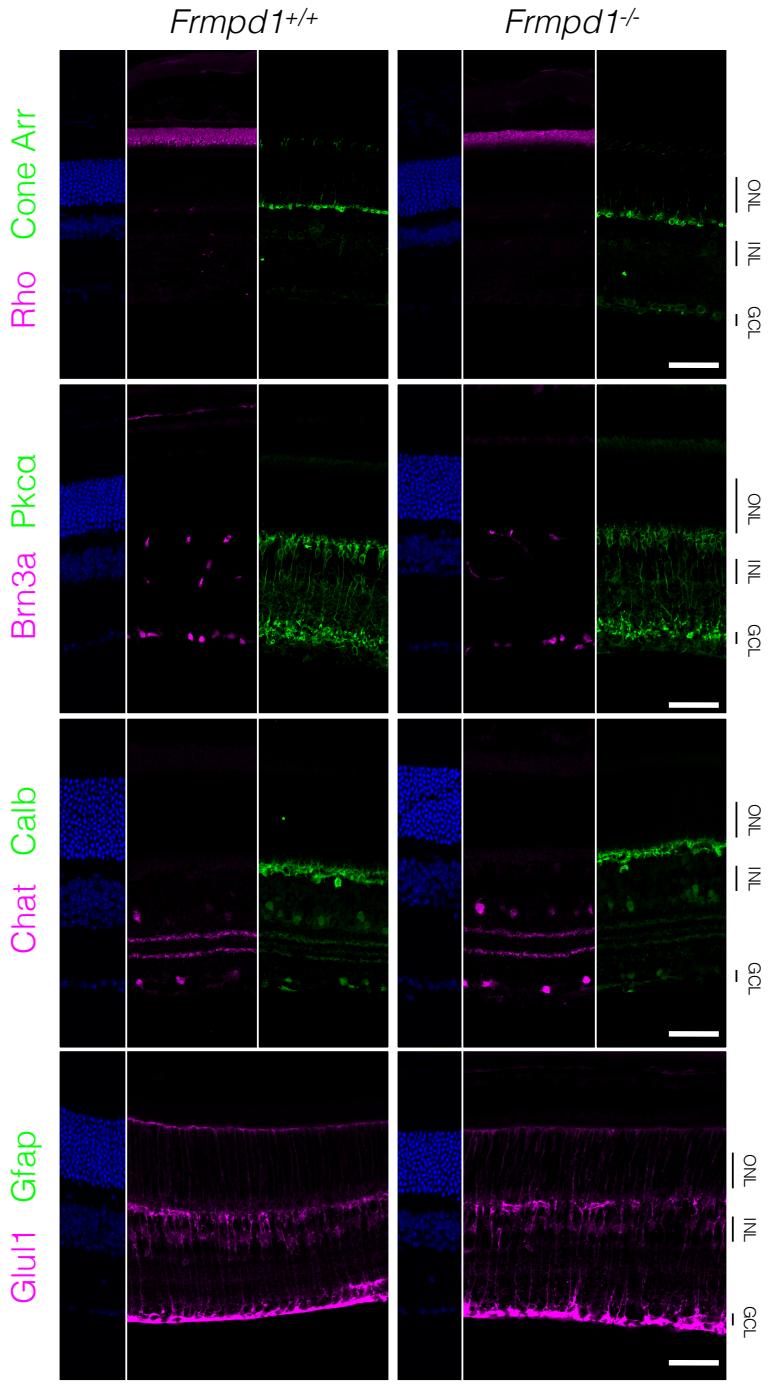

Figure 5.5: Retinal lamination and individual cell morphologies in *Frmpd1*$^{-/-}$ mice. Immunostaining of P21 mouse retina sections was performed to assess various cell types. Primary antibodies were used to detect rod outer segments (Rho), cones (Cone Arr.), ganglion cells (Brn3a), bipolar cells (Pkcα), Müller glia (Glull), and horizontal (Calb) and amacrine cells (Chat). Scale bar: 50 µm.

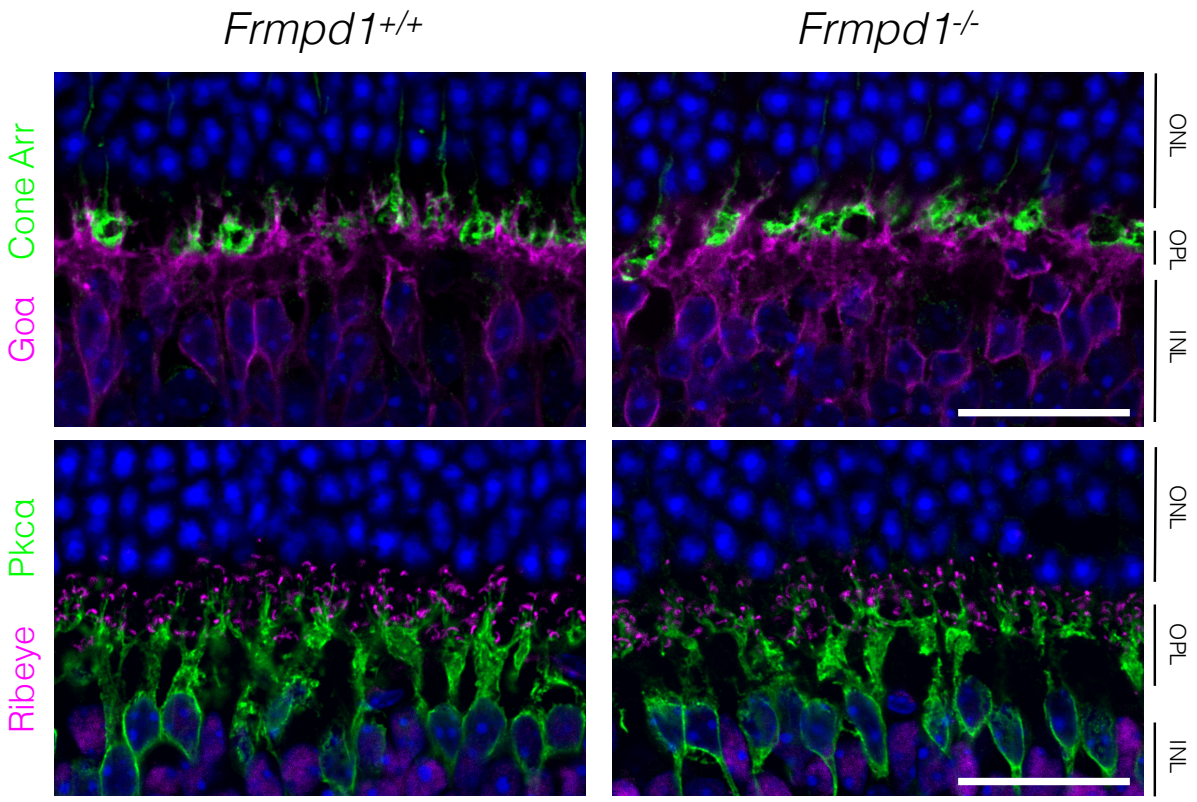

Figure 5.6: Immunostaining of *Frmpd1*$^{-/-}$ outer plexiform layer synapses. Morphologies of cone synapse (Cone Arr.), ON-bipolar synapse (Goα), ribbon synapse (Ribeye), and rod bipolar synapse (Pkcα) were examined by immunostaining using frozen retina sections from P21 mice. Scale bar: 25 μm.

5.3.3 *Retinal lamination and individual cell morphologies are unaltered in Frmpd1$^{-/-}$ mice*

ShRNA-mediated knockdown in CD1 mice resulted in rosette formation as early as P10 (Chapter 2). Interestingly, knockdown heterozygous and knockout homozygous *Frmpd1* mice generated by CRISPR targeting on C57BL6/J background did not exhibit this phenotype, with normal lamination even in the oldest mice tested (3 months). A series of IHC staining for markers of photoreceptors (rhodopsin and cone arrestin for rods and cones, respectively), ganglion (Brn3a), bipolar (Pkcα), horizontal and amacrine (Calbindin), starburst amacrine (Chat), and Müller glia (Glul1 and Gfap, respectively) cells did not reveal any overt defects with cell-type differentiation or morphology in *Frmpd1*$^{-/-}$ retina (Figure 5.5). Moreover, *Frmpd1*$^{-/-}$ photoreceptor and bipolar synapses in the OPL appeared normal when stained with markers for cone pedicles (cone arrestin) and bipolar cells (Goα) or ribbon synapses (ribeye) and bipolar cells (Pkcα) (Figure 5.6).

5.3.4 *Deletion of Frmpd1 delays T_α return to outer segments following light exposure*

Since Frmpd1 was immunoprecipitated in protein complexes with Gpsm2 and T_α (Section 4.3.3), we wanted to assess whether these proteins were mislocalised in *Frmpd1*$^{-/-}$ retina. *Frmpd1*$^{+/+}$ and *Frmpd1*$^{-/-}$ mice were dark adapted overnight (to move all transducin to outer segments), then exposed to bright light for 1 hr to induce transducin translocation to inner segments and synapses (Figure 5.7a). The mice were then placed back in the dark for 6 hrs to allow sufficient time for transducin to move back to the outer segments. In all 3 scenarios, transducin and Gpsm2 localised normally. For the next set of experiments, mice were light adapted the same way for 1 hr and then returned to the dark. Earlier time points of 30, 50, and 80 min were

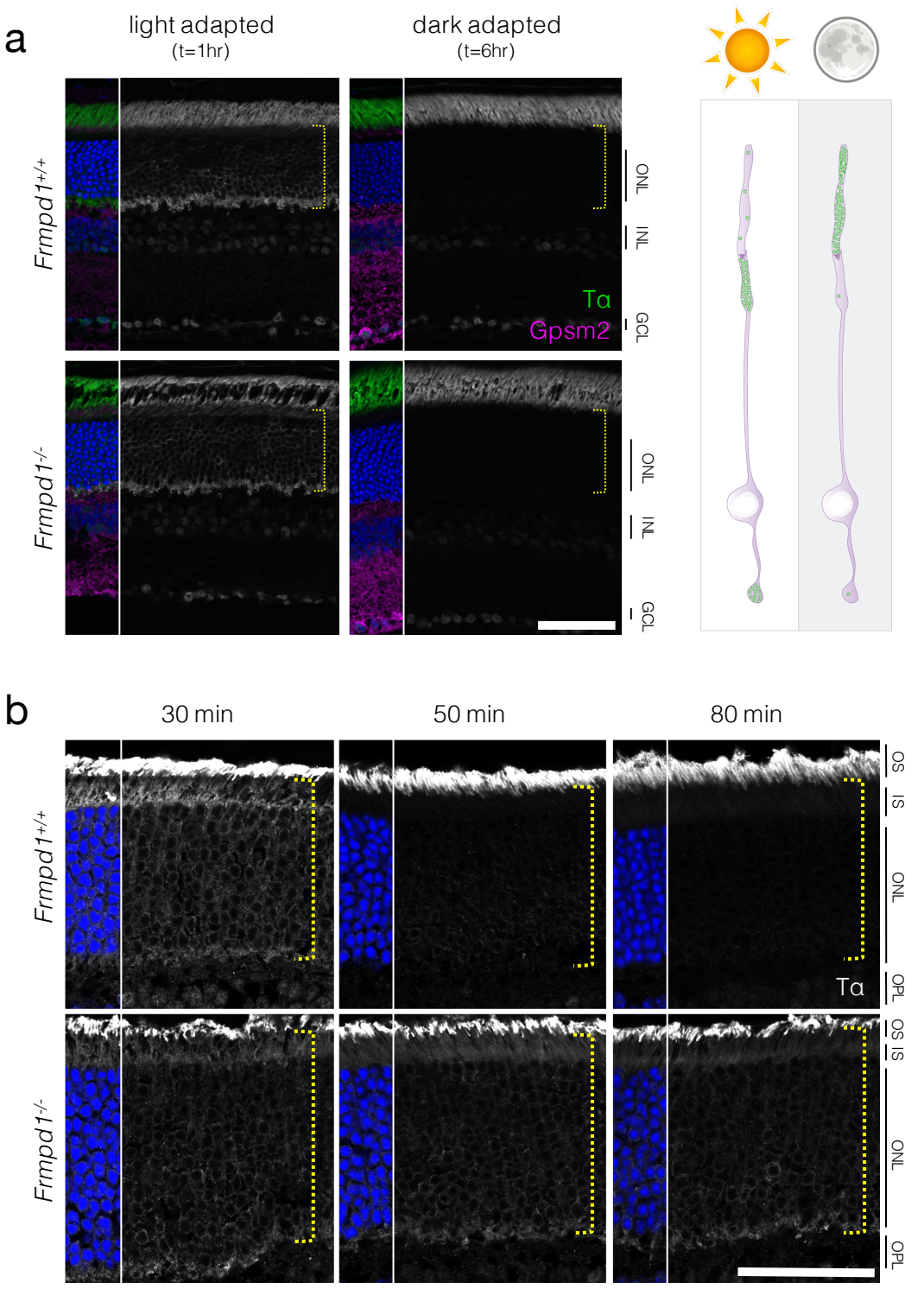

Figure 5.7: Transducin return to outer segments is delayed in *Frmpd1*$^{-/-}$ mice. (A) Fully light- and dark- adapted localisation of T_α and Gpsm2 in adult *Frmpd1*$^{-/-}$ mice. Mice were dark-adapted overnight, then light-adapted for 1 hr. Following light-adaptation, mice were dark-adapted for 6 hrs. Immunohistochemistry with anti-T_α and Gpsm2 antibodies was performed on retina cryosections. (B) Mice were light-adapted as in (A), then dark adapted for 30, 50, or 80 min. Immunohistochemistry with anti-T_α antibody was performed. Yellow brackets indicate inner segment and synapse regions of translocation. Scale bars: 50 µm.

collected to compare the degree of T_α return to the outer segments between *Frmpd1*$^{+/+}$ and *Frmpd1*$^{-/-}$ (Figure 5.7b) By 30 mins, some T_α had returned to the outer segments, while a large portion remained in the inner segments and synapses in both wildtype and *Frmpd1*$^{-/-}$. By 50 min, nearly all T_α returned to the outer segment in wildtype animals, whereas it remained in inner segments and synapses of the *Frmpd1*$^{-/-}$ retina (Figure 5.7b). This mislocalisation persisted even after 80 min. These results suggest that although *Frmpd1*$^{-/-}$ mice are capable of correctly redistributing T_α, the time course of this movement is delayed in the absence of Frmpd1.

5.3.5 Frmpd1 deletion delays a-wave recovery after moderate rhodopsin bleach

We next wanted to test whether the deletion of *Frmpd1* had any functional consequences on vision. To test visual response, a standard electroretinogram for both scotopic (dark-adapted, rod-mediated vision) and photopic (light-adapted, cone-mediated vision) was recorded on mice when exposed to different intensities and wavelengths of visual stimuli (Figure 5.8a). The responses to more intense stimuli for all conditions tested were slightly reduced in *Frmpd1*$^{-/-}$ animals for rod, M-, and S-cone mediated responses (Figure 5.8a). These defects were quite mild (an unpaired student's t-test determined statistical significance for only one scotopic stimulus); nevertheless, we were curious as to whether a more prominent phenotype could be observed in the rods following prolonged light exposure since this produced a defect in T_α translocation.

To measure the kinetics of the recovery of rod response following a moderate visual pigment bleach, mice were dark-adapted overnight then exposed to 30 sec of

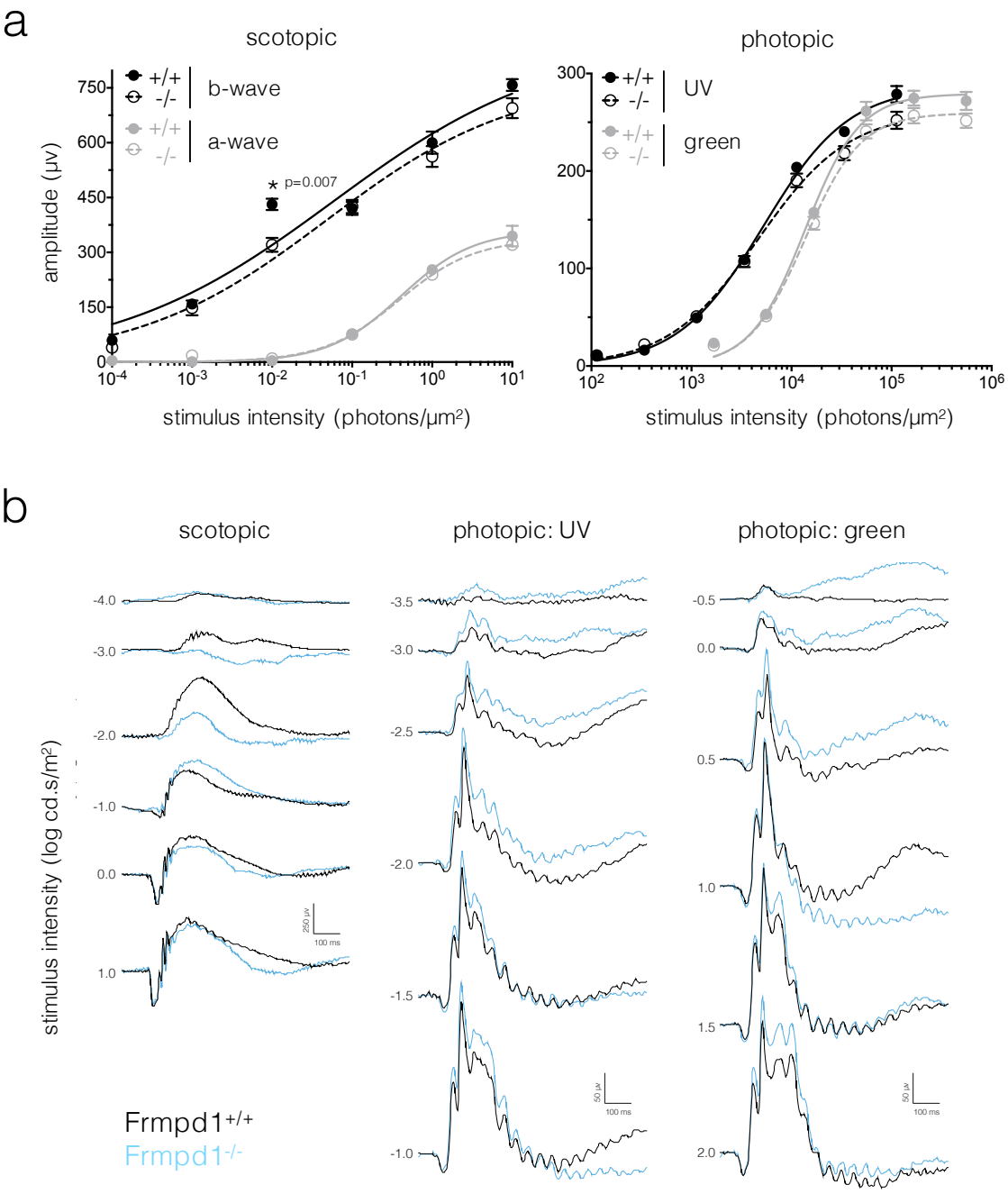

Figure 5.8: Photopic and scotopic ERG responses in *Frmpd1*$^{-/-}$ mice are largely unaffected. (A) Mice (2 months olds) were dark-adapted for 24 h before recording scotopic responses. Intensity response curves of the average a- and b-wave responses of 3 mice of each genotype (mean±s.e.m.) are shown. Mice were then light-adapted and responses to UV and green light flashes were recorded. Intensity response curves of the average photopic b-wave response (mean±s.e.m.) are shown. (B) Representative ERG traces for scotopic, UV, and green light responses from panel (A).

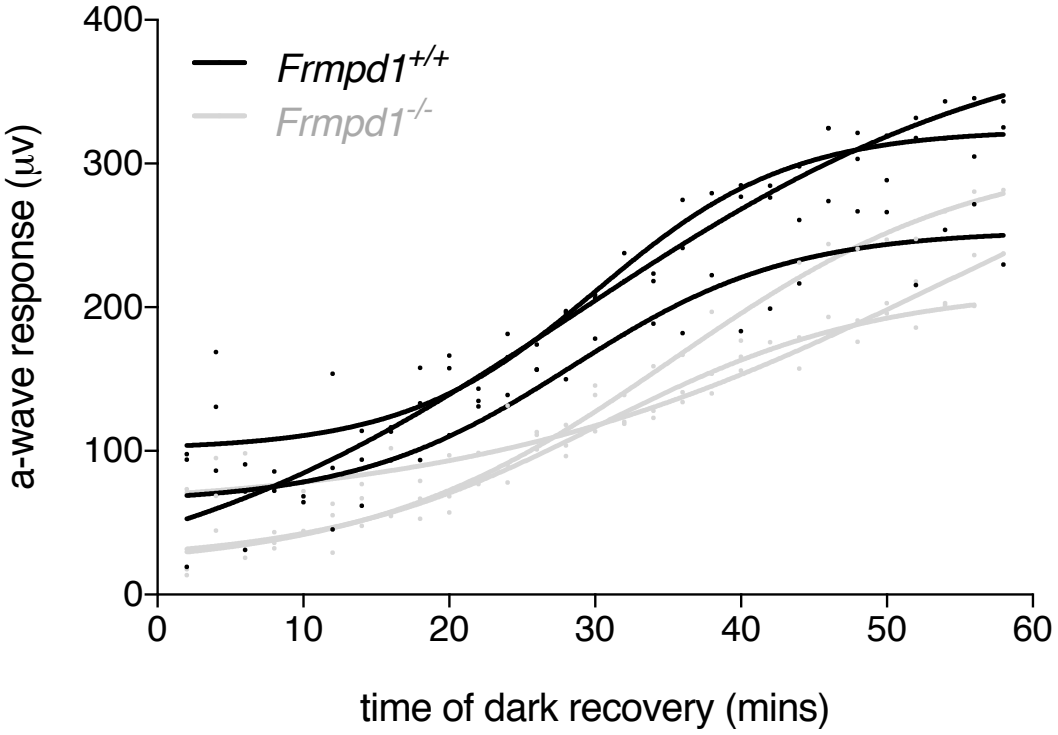

Figure 5.9: Recovery of rod photoresponse is delayed in *Frmpd1*$^{-/-}$ mice. Adult mice were dark-adapted overnight, then exposed to a moderate visual pigment bleach (~10% rhodopsin) with 1000 cd.s/m^2 of white light for 30 sec. Mice were then returned to the dark for 1 hr and rod visual response (maximum a-wave) to a dim light stimulus of 10 cd.s/m^2 was recorded every 2 min. Visual responses were recorded from 3 mice of each genotype, and sigmoid curves were fitted to the averaged response of both eyes from each mouse (plotted as data points).

1000 cds/m^2 background white light to bleach ~10% of rhodopsin (Li et al., 2015). Mice were then placed in the dark and a small (10 cds/m^2) stimulus intended to only stimulate rods was administered every 2 minutes over the course of an hour to monitor recovery of the a-wave (rod-mediated) response (Figure 5.9). Interestingly, not only did *Frmpd1*$^{-/-}$ animals have a lower initial recorded response to the light stimulus (29.29 vs. 66.16 μv after 2 mins of dark recovery), but the kinetics of a-wave recovery were also slowed down (37.82 vs. 29.5 mins to reach ½ of maximum response). However, the differences in time to reach ½ of maximum response did not reach statistical significance when an unpaired t-test was performed for 3 mice of each genotype ($p=0.374$) and may require larger sample sizes.

5.4 Discussion

This work has focused on the role of *Frmpd1* specifically in the retina; since *Frmpd1* expression was assessed postnatally and found to be primarily in the retina, we did not predict for its removal to be deleterious. Surprisingly, however, the only live births from embryos injected with gRNAs targeting the protein coding region of the gene were those which produced small in-frame indels which either added or removed a single amino acid and likely did not affect the protein drastically. In the case of frameshift or early truncation mutations, however, targeted embryos were aborted before E10.75. This could simply be a result of guide RNA toxicity or off-target effects. Alternatively, the embryonic lethality experienced with disruption of *Frmpd1* could be the result of an additional role of *Frmpd1* in embryogenesis separate from the role it plays in retinal development. Indeed, the primary binding partner of Frmpd1, Gpsm2, is involved mitotic spindle formation and asymmetric cell division

which could contribute to early embryogenesis (Yasumi et al., 2005, Saadaoui et al., 2014). Some potential areas for future investigation related to Frmpd1 in the developing embryo are addressed in Section 6.3.5.

Interestingly, we were able to bypass this embryonic lethality by instead removing the retina alternative promoter used by *Frmpd1* identified in Chapter 3 for a retina-specific knockdown of the gene. This was a novel use of the CRISPR/Cas9 system to generate a tissue-specific loss-of-function mouse line through gene editing of germline cells. Recent studies have indicated that a variety of genes use alternative transcription start sites in the retina compared to other tissues, even when those genes are widely expressed (Popova et al., 2017). Disruption of the retina promoter in these genes by CRISPR/Cas9 could therefore be a promising method to quickly generate mouse models to study their function in the retina while leaving other tissues and embryogenesis unperturbed.

Surprisingly, retinal lamination appeared completely normal in *Frmpd1*$^{-/-}$ mice while knockdown of *Frmpd1* by *in vivo* electroporation resulted in the formation of multiple rosettes and altered retinal morphology as early as P10 (Section 2.3.4). As discussed more thoroughly in Section 2.4, *in vivo* electroporation is a highly variable technique that is susceptible to off-target effects, and rosette formation could have been a result of this. Moreover, *in vivo* shRNA knockdowns do not always phenocopy germline deletions in the retina (Campla et al., 2017). Discrepancies between mutant/knockdown vs. knockout phenotypes has been documented in cell culture and zebrafish systems as well (Karakas et al., 2007, Rossi et al., 2015). Compensatory mechanisms are more likely to occur in a germline knockout mouse model where cells have had the entire course of development to overcome imbalances, which could

explain why retinal lamination in *Frmpd1*$^{-/-}$ mice appears normal whereas knockdown induced postnatally by *in vivo* electroporation disturbs ONL architecture.

An additional explanation for the phenotype variation is the mouse background strain difference: *in vivo* electroporation was performed on albino CD1 mice, while the CRISPR knockout was generated on a pigmented C57BL/6J background. The faulty recovery from light exposure resulting from a lack of Frmpd1 would be even further exacerbated on an albino background than it would on a pigmented background, since light more readily penetrates the retina of albino mice and they may be hypersensitive to light-induced damage (Wasowicz et al., 2002). A lowered threshold for light-induced transducin translocation to the inner segments and synapses in albino mice means that these molecules would enter these subcellular compartments earlier than they would in pigmented mice. Without *Frmpd1*, these proteins may remain mislocalised in these regions even longer in the albino mice as compared to pigmented mice, allowing them more time to exert adverse effects on the photoreceptors. Indeed, light-threshold-dependent phenotypes have been described for other mouse models with affected transducin translocation, namely *shaker1* and *whirlin*, where no overt phenotype is observed in normal animal housing conditions but at higher light intensities there is a clear retinal degeneration (Peng et al., 2011, Tian et al., 2014).

A difference in *Frmpd1* knockout effects on pigmented vs. unpigmented backgrounds would be relatively simple to test: *Frmpd1*$^{-/-}$ mice could be bred onto a mixed background (with an albino strain like CD1 or BALB/c) to produce both pigmented and non-pigmented littermates reared in the same light conditions to assess differences in phenotypes. Rearing C57BL/6J *Frmpd1*$^{-/-}$ mice in brighter light

conditions may induce the same cell death and rosette formation as observed in CD1 mice under milder conditions. Furthering this, retinal cell death resulting from rearing in constant light conditions and even after acute light damage could be assessed in *Frmpd1*$^{-/-}$ mice by histology and TUNEL assays (Organisciak and Vaughan, 2010).

Preliminary pilot studies in the *Frmpd1*$^{-/-}$ model generated in this chapter, combined with the localisation and protein-interaction studies in Chapter 4, provide evidence for a role of *Frmpd1* in modulating rod phototransduction that would be interesting to explore in further depth. The delayed T_α return to outer segments would likely prevent the timely re-formation of holotransducin on outer segment disc membranes following light exposure, which could make it more difficult for rhodopsin to interact with and activate it (Gao et al., 2017). Indeed, the amplification of phototransduction signals is reduced when concentration of T_α in the outer segments is decreased (Sokolov et al., 2002). This is probably a contributing factor to the a-wave recovery defect in *Frmpd1*$^{-/-}$ mice observed by electroretinography, but these two phenomena are not necessarily linked. The electroretinogram measures total response of the retina, and can be influenced by any combination of aberrant processes related to phototransduction (Pinto et al., 2007). Determining the precise mechanisms contributing to a-wave recovery delay in *Frmpd*$^{-/-}$ mice poses another interesting direction for future studies, particularly if any additional proteins involved in phototransduction are detected in Frmpd1 protein complexes by mass spectrometry (addressed in Section 6.3.1) or found to be altered in *Frmpd1*$^{-/-}$ retinas by methods such as RNA-seq.

6

Conclusions and future directions

6.1 Overview

This thesis presents studies on the rod photoreceptor specific expression and function of *Frmpd1* (FERM and PDZ domain containing 1), a previously uncharacterised gene that we now propose plays a role in modulating rod phototransduction (Figure 6.1). The key findings of this thesis are:

- *Frmpd1* is a rod-enriched gene whose expression is dramatically upregulated by Nrl and Crx during rod photoreceptor development (Chapter 2)

- Transcription of *Frmpd1* is initiated from a unique retina-specific alternative promoter (Chapter 3)

- Frmpd1 localises to the inner segments and synapses of rod photoreceptors, where it interacts with a key phototransduction component T_α (transducin alpha subunit) and its effector Gpsm2 (G-protein signalling modulator 2) (Chapter 4)

- Targeted deletion of the *Frmpd1* alternative promoter from the genome results in a retina-specific knockdown of the entire mRNA transcript and protein (Chapter 5)

- Retina-specific *Frmpd1*$^{-/-}$ mice exhibit delayed return of T_α to the outer segments after prolonged light exposure, and reduced recovery of the rod photoresponse (scotopic a-wave) following moderate light exposure (Chapter 5)

6.2 Significance and connection to original hypothesis

Our original hypothesis (Chapter 1) was that genes dramatically increasing in expression during rod photoreceptor development and regulated by key rod transcription factors Nrl and Crx would play a substantial role in the functional maturation and homeostasis of these cells. *Frmpd1*, which was identified by these initial filtering criteria, does indeed appear to play a role in the maintenance of rod phototransduction homeostasis through mediating the adaptive response of rods following prolonged light exposure.

A more in-depth characterisation of Frmpd1 and its mechanism of action (including the role of protein partners Gpsm2 and T_α in this context) could have important implications in elucidating how rod photoreceptors function and re-

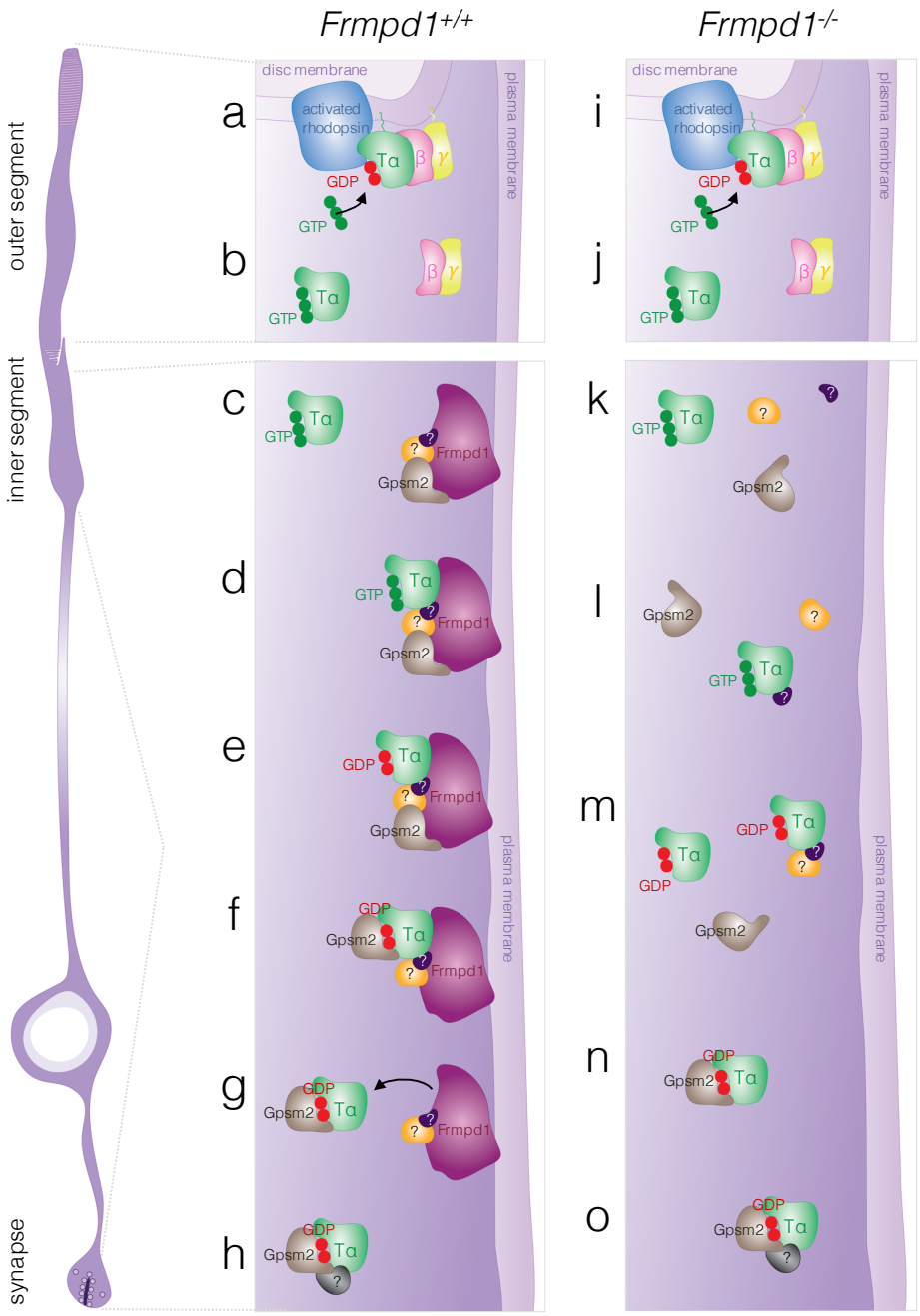

Figure 6.1: Proposed mechanisms of Frmpd1 function and resultant knockdown phenotype. Left panel: (A) In outer segments, activated rhodopsin interacts with T_a^{GDP} (GDP-bound transducin a subunit), which releases GDP (guanosine diphosphate) for cytosolic GTP (guanosine triphosphate) and (B) dissociates from the disc membrane. (C) Soluble T_a^{GTP} translocates to inner segments and synapses, where the Frmpd1 scaffold complex is located. (D) On the plasma membranes of inner segments and synapses, T_a^{GTP} forms a transient protein complex with Frmpd1, Gpsm2, and additional unknown proteins. (E) While bound to the Frmpd1 complex, T_a^{GTP} hydrolyses its GTP to GDP. (F) Recognising the newly inactive T_a^{GDP}, Gpsm2 switches its binding partner from Frmpd1 to T_a^{GDP}. (G) The T_a^{GDP}-Gpsm2 complex then dissociates from the plasma membrane, (H) forming additional protein-protein interactions to facilitate the return of T_a^{GDP} to the outer segments. **Right panel:** In the absence of Frmpd1, the activation and subsequent translocation of transducin to the inner segments and synapses proceeds as normal (I-J). (K) However, Frmpd1 no longer holds the interacting partners of T_a^{GTP} on the plasma membrane or in close proximity with one another in these subcellular compartments. (L) T_a^{GTP} may still encounter its binding partners, but at a reduced rate without the facilitation of these interactions by the Frmpd1 complex. (M) Eventually, T_a^{GTP} hydrolyses its GTP to GDP, potentially at a reduced rate without the aid of GTPase accelerating proteins. (N) After some time, Gpsm2 encounters and binds to T_a^{GDP}. (O) Finally, these proteins form additional interactions to facilitate the return of T_a^{GDP} to the outer segments. Thus, the inactivation and return of T_a to outer segments can still occur in *Frmpd1*$^{-/-}$ mice, but at a reduced rate since the necessary protein interactors are not readily assembled near each other by the Frmpd1 scaffolding complex.

establish homeostasis following bright light exposure, which is not yet completely understood but is a topic of active investigation (Miyagishima et al., 2009, Fain et al., 2001, Belcastro et al., 2012, Arshavsky and Burns, 2012). A thorough knowledge of the molecular mechanisms underlying these processes could aid in the diagnosis and improved design of therapeutic interventions for retinal diseases, since constitutive action of phototransduction is one known cause of photoreceptor degeneration (Szabo et al., 2007, Park, 2014) and could be targeted by gene therapies or manipulated in cell therapies for better function and survival of transplanted photoreceptors (Zhang et al., 2015).

Furthermore, these studies pioneered the use of targeting a tissue-specific promoter by the CRISPR-Cas9 system to generate a tissue-specific knockdown mouse line. This method could be more widely applied to tissues of the central nervous system which also often use tissue-specific isoforms of otherwise ubiquitously expressed genes (Popova et al., 2017, Farkas et al., 2013, Raj and Blencowe, 2015). This approach has also highlighted the critical role of genomic Nrl (and other) binding sites in rod photoreceptor gene expression; perhaps patient mutations in the untranslated regions of stringently regulated genes, such as *Frmpd1*, can substantially contribute to disease phenotypes and therefore warrant a closer look in patient screening.

6.3 Future directions

6.3.1 Identification of additional Frmpd1 protein interactors

The Frmpd family of proteins are generally described as scaffolding proteins (Moleirinho et al., 2013), so it is likely that Frmpd1 interacts with more than just

Gpsm2 and T_{α}. These interactions may be dependent on translocation of phototransduction components to the inner segments and synapses, and could also depend on the activation state of T_{α}. If so, those interactions would not be reflected in the immunoprecipitation experiments performed in Chapter 4 since most T_{α} (both GDP- and GTP- bound) remained in outer segments despite GTPγS-BODIPY being taken up when illuminated.

Further optimization of the haemolysin + immunoprecipitation experiments is required to ensure that (1) input lysates contain predominantly T_{α}^{GDP} or T_{α}^{GTP} as intended, and (2) T_{α} and other components translocate to the inner segments and synapses where they can form any compartment-specific complexes natively before lysates are prepared. Another way to differentiate the various protein complexes formed in their endogenous forms/cellular compartments would be to first induce translocation *in vivo* via light exposure, then isolate retinas and perform serial tangential sectioning followed by immunoprecipitation on specific fractions (Grossman et al., 2013, Sokolov et al., 2004).

Once immunoprecipitation experiments have been fully optimized, the protein complexes could be analysed by mass spectrometry to identify additional interactors which could then be confirmed by immunoblotting, colocalisation studies, and *in vitro* testing of direct interactions.

6.3.2 Effects of Frmpd1 on activation/inactivation of T_{α}

The immunoprecipitation experiments in Chapter 4 indicate that both T_{α}^{GDP} and T_{α}^{GTP} form complexes with Frmpd1. Two of the most direct ways to determine whether this is indeed the case and some obvious next steps for future studies are to

(1) probe the immunoprecipitation blots with anti-BODIPY antibodies, since detection of BODIPY in the GTPγS condition would indicate T_α^{GTP} in the complexes as intended, but no detection of BODIPY would instead indicate T_α^{GDP} in the complexes, and (2) perform tryptic digestion of the immunoprecipitated protein complexes in both conditions since T_α^{GDP} and T_α^{GTP} are uniquely sensitive to trypsin and produce different band patterns on immunoblots when digested (Nair et al., 2002). A combination of both experiments would help to discern whether T_α immunoprecipitated in the GTPγS and GDP conditions are indeed GTP and GDP-bound, respectively.

If both T_α^{GDP} and T_α^{GTP} are present in Frmpd1 complexes, then GTP hydrolysis assays in the presence and absence of Frmpd1 could be performed to determine if its presence does facilitate the T_α^{GTP} to T_α^{GDP} transition. Relative amounts of T_α^{GDP} and T_α^{GTP} could also be assessed on whole retina lysates by tryptic digestion during dark adaptation in both *Frmpd1*$^{+/+}$ and *Frmpd1*$^{-/-}$ mice to determine if the delayed rate of T_α return to outer segments in *Frmpd1*$^{-/-}$ rods correlates with a delay in T_α^{GTP} to T_α^{GDP}.

6.3.3 Function of Frmpd1 in bipolar cells

Although Frmpd1 is expressed predominantly in rod photoreceptors, expression was also detected by ISH in bipolar cells (Section 3.3.2). Interestingly, Gpsm2 is expressed in on-bipolar cells (Dhingra et al., 2008). It is unclear whether the function of Frmpd1 is the same in both cell types or if it has unique interacting partners in each. The *Nrl*$^{-/-}$ retina could serve as a useful model for dissecting the different binding partners of Frmpd1 in the two cell types, since Frmpd1 is still expressed in bipolar cells but not in rods in *Nrl*$^{-/-}$ animals and differential analyses could be performed. Additionally, single-

cell electroretinography recordings could be performed in *Frmpd1*$^{-/-}$ retina slices to isolate responses of rods vs. bipolar cells (Majumder et al., 2013).

6.3.4 Role of Frmpd1 in embryogenesis

Gpsm1 and Gpsm2 have both been implicated in asymmetric cell division, which is important for establishing cell polarity (Sanada and Tsai, 2005, Wolwer et al., 2017) and may be related to the early embryonic death observed during CRISPR targeting of the coding region of *Frmpd1*. While outside the scope of this thesis project, it would be interesting to examine this process further by determining the exact age of *Frmpd1* complete null death and to localise *Frmpd1* in the developing embryo by methods such as ISH and immunohistochemistry. Frmpd1 could also be immunoprecipitated from embryonic protein lysates and analysed by mass spectrometry to determine which complexes it is a part of and these results verified by immunoblotting and colocalisation by immunohistochemistry. If Frmpd1 is endogenously expressed in cultured embryonic stem cells, it would be interesting to knock the gene down (either by CRISPR or shRNA) and assess the effects on mitotic spindle formation and asymmetric cell division in this model system to determine if that is the root cause of potential embryonic lethality.

6.3.5 Patient screening

Since Frmpd1 may play a role in maintaining rod homeostasis, it would be interesting to screen patients with photoreceptor diseases whose genetic basis is unknown. We would predict that loss-of-function mutations in Frmpd1 may lead to diseases associated with rod degeneration or malfunction, and especially those related to adaptation following light exposure such as bradyopsia (where patients experience

difficulty adjusting to changes in light conditions) (Nishiguchi et al., 2004). Interestingly, delayed rod adaptation can also be an early indicator of age-related maculopathy, which eventually also exhibits cone cell death (Owsley et al., 2001, Owsley et al., 2007, Dimitrov et al., 2008).

If widespread loss-of-function of Frmpd1 is lethal in humans as it seems to be in mice, it is also possible that mutations in the protein-coding region of the gene result in more severe phenotypes or spontaneous abortion and that mutations in the noncoding retina-specific promoter of *Frmpd1* could lead to retinal phenotypes. This region of the genome would not typically be screened and may have been overlooked, but would be interesting to investigate further. If any such mutations are identified, their effects on Frmpd1 expression could easily be tested by luciferase assays and *in vivo* electroporation as in Chapter 3.

References

ABLAIN, J. & ZON, L. I. 2016. Tissue-specific gene targeting using CRISPR/Cas9. *Methods Cell Biol,* 135, 189-202.

AKIMOTO, M., CHENG, H., ZHU, D., BRZEZINSKI, J. A., KHANNA, R., FILIPPOVA, E., OH, E. C., JING, Y., LINARES, J. L., BROOKS, M., ZAREPARSI, S., MEARS, A. J., HERO, A., GLASER, T. & SWAROOP, A. 2006. Targeting of GFP to newborn rods by Nrl promoter and temporal expression profiling of flow-sorted photoreceptors. *Proc Natl Acad Sci U S A,* 103, 3890-5.

ALEXANDER, K. R. & FISHMAN, G. A. 1984. Prolonged rod dark adaptation in retinitis pigmentosa. *Br J Ophthalmol,* 68, 561-9.

ALLAN, R. K. & RATAJCZAK, T. 2011. Versatile TPR domains accommodate different modes of target protein recognition and function. *Cell Stress Chaperones,* 16, 353-67.

ALVES, C. H., PELLISSIER, L. P. & WIJNHOLDS, J. 2014. The CRB1 and adherens junction complex proteins in retinal development and maintenance. *Prog Retin Eye Res,* 40, 35-52.

AMES, J. B., LEVAY, K., WINGARD, J. N., LUSIN, J. D. & SLEPAK, V. Z. 2006. Structural basis for calcium-induced inhibition of rhodopsin kinase by recoverin. *J Biol Chem,* 281, 37237-45.

AN, N., BLUMER, J. B., BERNARD, M. L. & LANIER, S. M. 2008. The PDZ and band 4.1 containing protein Frmpd1 regulates the subcellular location of activator of G-protein signaling 3 and its interaction with G-proteins. *J Biol Chem,* 283, 24718-28.

APPLEBURY, M. L., ANTOCH, M. P., BAXTER, L. C., CHUN, L. L., FALK, J. D., FARHANGFAR, F., KAGE, K., KRZYSTOLIK, M. G., LYASS, L. A. & ROBBINS, J. T. 2000. The murine cone photoreceptor: a single cone type expresses both S and M opsins with retinal spatial patterning. *Neuron,* 27, 513-23.

ARPIN, M., CHIRIVINO, D., NABA, A. & ZWAENEPOEL, I. 2011. Emerging role for ERM proteins in cell adhesion and migration. *Cell Adh Migr,* 5, 199-206.

ARSHAVSKY, V. Y. & BURNS, M. E. 2012. Photoreceptor signaling: supporting vision across a wide range of light intensities. *J Biol Chem,* 287, 1620-6.

ARSHAVSKY, V. Y., LAMB, T. D. & PUGH, E. N., JR. 2002. G proteins and phototransduction. *Annu Rev Physiol,* 64, 153-87.

ARTEMYEV, N. O. 2008. Light-dependent compartmentalization of transducin in rod photoreceptors. *Mol Neurobiol,* 37, 44-51.

BAINBRIDGE, J. W., SMITH, A. J., BARKER, S. S., ROBBIE, S., HENDERSON, R., BALAGGAN, K., VISWANATHAN, A., HOLDER, G. E., STOCKMAN, A., TYLER, N., PETERSEN-JONES, S., BHATTACHARYA, S. S., THRASHER, A. J., FITZKE, F. W., CARTER, B. J., RUBIN, G. S., MOORE, A. T. & ALI, R. R. 2008. Effect of

gene therapy on visual function in Leber's congenital amaurosis. *N Engl J Med,* 358, 2231-9.

BALKEMA, G. W. 1988. Elevated dark-adapted thresholds in albino rodents. *Invest Ophthalmol Vis Sci,* 29, 544-9.

BALKEMA, G. W. & DRAGER, U. C. 1991. Impaired visual thresholds in hypopigmented animals. *Vis Neurosci,* 6, 577-85.

BELCASTRO, M., SONG, H., SINHA, S., SONG, C., MATHERS, P. H. & SOKOLOV, M. 2012. Phosphorylation of phosducin accelerates rod recovery from transducin translocation. *Invest Ophthalmol Vis Sci,* 53, 3084-91.

BELTRAN, W. A. 2009. The use of canine models of inherited retinal degeneration to test novel therapeutic approaches. *Vet Ophthalmol,* 12, 192-204.

BENNETT, E. P., HASSAN, H., HOLLINGSWORTH, M. A. & CLAUSEN, H. 1999. A novel human UDP-N-acetyl-D-galactosamine:polypeptide N-acetylgalactosaminyltransferase, GalNAc-T7, with specificity for partial GalNAc-glycosylated acceptor substrates. *FEBS Lett,* 460, 226-30.

BERGER, W., KLOECKENER-GRUISSEM, B. & NEIDHARDT, J. 2010. The molecular basis of human retinal and vitreoretinal diseases. *Prog Retin Eye Res,* 29, 335-75.

BESHARSE, J. C., DANA, R. & DARTT, D. A. 2010. *Encyclopedia of the eye,* Amsterdam, Elsevier/Academic Press.

BLANKS, J. C., ADINOLFI, A. M. & LOLLEY, R. N. 1974. Synaptogenesis in the photoreceptor terminal of the mouse retina. *J Comp Neurol,* 156, 81-93.

BLATCH, G. L. & LASSLE, M. 1999. The tetratricopeptide repeat: a structural motif mediating protein-protein interactions. *Bioessays,* 21, 932-9.

BLUMER, J. B., CHANDLER, L. J. & LANIER, S. M. 2002. Expression analysis and subcellular distribution of the two G-protein regulators AGS3 and LGN indicate distinct functionality. Localization of LGN to the midbody during cytokinesis. *J Biol Chem,* 277, 15897-903.

BOLGER, A. M., LOHSE, M. & USADEL, B. 2014. Trimmomatic: a flexible trimmer for Illumina sequence data. *Bioinformatics,* 30, 2114-20.

BOUABE, H. & OKKENHAUG, K. 2013. Gene targeting in mice: a review. *Methods Mol Biol,* 1064, 315-36.

BOYE, S. E., BOYE, S. L., LEWIN, A. S. & HAUSWIRTH, W. W. 2013. A comprehensive review of retinal gene therapy. *Mol Ther,* 21, 509-19.

BROOKS, M., RAJASIMHA, H. & SWAROOP, A. 2012. Retinal Transcriptome Profiling by Directional Next-Generation Sequencing Using 100 ng of Total RNA. *In:* WANG, S.-Z. (ed.) *Retinal Development.* Humana Press.

BURNS, M. E. 2010. Deactivation mechanisms of rod phototransduction: the Cogan lecture. *Invest Ophthalmol Vis Sci,* 51, 1282-8.

BURNS, M. E. & ARSHAVSKY, V. Y. 2005. Beyond counting photons: trials and trends in vertebrate visual transduction. *Neuron,* 48, 387-401.

BURNS, M. E., MENDEZ, A., CHEN, J. & BAYLOR, D. A. 2002. Dynamics of cyclic GMP synthesis in retinal rods. *Neuron,* 36, 81-91.

CALDERWOOD, D. A., CAMPBELL, I. D. & CRITCHLEY, D. R. 2013. Talins and kindlins: partners in integrin-mediated adhesion. *Nat Rev Mol Cell Biol,* 14, 503-17.

CAMPBELL, M., HUMPHRIES, M., KENNA, P., HUMPHRIES, P. & BRANKIN, B. 2007. Altered expression and interaction of adherens junction proteins in the developing OLM of the Rho(-/-) mouse. *Exp Eye Res,* 85, 714-20.

CAMPBELL, M., HUMPHRIES, M., KENNAN, A., KENNA, P., HUMPHRIES, P. & BRANKIN, B. 2006. Aberrant retinal tight junction and adherens junction protein expression in an animal model of autosomal dominant Retinitis pigmentosa: the Rho(-/-) mouse. *Exp Eye Res,* 83, 484-92.

CAMPLA, C. K., BREIT, H., DONG, L., GUMERSON, J. D., ROGER, J. E. & SWAROOP, A. 2017. Pias3 is necessary for dorso-ventral patterning and visual response of retinal cones but is not required for rod photoreceptor differentiation. *Biol Open,* 6, 881-890.

CARROLL, K. J., MAKAREWICH, C. A., MCANALLY, J., ANDERSON, D. M., ZENTILIN, L., LIU, N., GIACCA, M., BASSEL-DUBY, R. & OLSON, E. N. 2016. A mouse model for adult cardiac-specific gene deletion with CRISPR/Cas9. *Proc Natl Acad Sci U S A,* 113, 338-43.

CARTER-DAWSON, L. D. & LAVAIL, M. M. 1979a. Rods and cones in the mouse retina. I. Structural analysis using light and electron microscopy. *J Comp Neurol,* 188, 245-62.

CARTER-DAWSON, L. D. & LAVAIL, M. M. 1979b. Rods and cones in the mouse retina. II. Autoradiographic analysis of cell generation using tritiated thymidine. *J Comp Neurol,* 188, 263-72.

CHAN, I. S. & GINSBURG, G. S. 2011. Personalized medicine: progress and promise. *Annu Rev Genomics Hum Genet,* 12, 217-44.

CHANG, B. 2013. Mouse models for studies of retinal degeneration and diseases. *Methods Mol Biol,* 935, 27-39.

CHEN, J., RATTNER, A. & NATHANS, J. 2005. The rod photoreceptor-specific nuclear receptor Nr2e3 represses transcription of multiple cone-specific genes. *J Neurosci,* 25, 118-29.

CHENG, H., ALEMAN, T. S., CIDECIYAN, A. V., KHANNA, R., JACOBSON, S. G. & SWAROOP, A. 2006. In vivo function of the orphan nuclear receptor NR2E3 in establishing photoreceptor identity during mammalian retinal development. *Hum Mol Genet,* 15, 2588-602.

CHENG, H., KHANNA, H., OH, E. C., HICKS, D., MITTON, K. P. & SWAROOP, A. 2004. Photoreceptor-specific nuclear receptor NR2E3 functions as a transcriptional activator in rod photoreceptors. *Hum Mol Genet,* 13, 1563-75.

CHERFILS, J. & ZEGHOUF, M. 2013. Regulation of small GTPases by GEFs, GAPs, and GDIs. *Physiol Rev,* 93, 269-309.

CIDECIYAN, A. V. 2010. Leber congenital amaurosis due to RPE65 mutations and its treatment with gene therapy. *Prog Retin Eye Res,* 29, 398-427.

CIDECIYAN, A. V., ALEMAN, T. S., BOYE, S. L., SCHWARTZ, S. B., KAUSHAL, S., ROMAN, A. J., PANG, J. J., SUMAROKA, A., WINDSOR, E. A., WILSON, J. M., FLOTTE, T. R., FISHMAN, G. A., HEON, E., STONE, E. M., BYRNE, B. J., JACOBSON, S. G. & HAUSWIRTH, W. W. 2008. Human gene therapy for RPE65 isomerase deficiency activates the retinoid cycle of vision but with slow rod kinetics. *Proc Natl Acad Sci U S A,* 105, 15112-7.

CORBO, J. C., LAWRENCE, K. A., KARLSTETTER, M., MYERS, C. A., ABDELAZIZ, M., DIRKES, W., WEIGELT, K., SEIFERT, M., BENES, V., FRITSCHE, L. G., WEBER, B. H. & LANGMANN, T. 2010. CRX ChIP-seq reveals the cis-regulatory architecture of mouse photoreceptors. *Genome Res,* 20, 1512-25.

CORR, M., LERMAN, I., KEUBEL, J. M., RONACHER, L., MISRA, R., LUND, F., SARELIUS, I. H. & GLADING, A. J. 2012. Decreased Krev interaction-trapped 1 expression leads to increased vascular permeability and modifies inflammatory responses in vivo. *Arterioscler Thromb Vasc Biol,* 32, 2702-10.

CRUMBLEY, C. & BURRIS, T. P. 2011. Direct regulation of CLOCK expression by REV-ERB. *PLoS One,* 6, e17290.

CURCIO, C. A., OWSLEY, C. & JACKSON, G. R. 2000. Spare the rods, save the cones in aging and age-related maculopathy. *Invest Ophthalmol Vis Sci,* 41, 2015-8.

CURCIO, C. A., SLOAN, K. R., KALINA, R. E. & HENDRICKSON, A. E. 1990. Human photoreceptor topography. *J Comp Neurol,* 292, 497-523.

DANIELE, L. L., LILLO, C., LYUBARSKY, A. L., NIKONOV, S. S., PHILP, N., MEARS, A. J., SWAROOP, A., WILLIAMS, D. S. & PUGH, E. N., JR. 2005. Cone-like morphological, molecular, and electrophysiological features of the photoreceptors of the Nrl knockout mouse. *Invest Ophthalmol Vis Sci,* 46, 2156-67.

DE ROBERTIS, E. 1956. Morphogenesis of the retinal rods; an electron microscope study. *J Biophys Biochem Cytol,* 2, 209-18.

DE VRIES, L., FISCHER, T., TRONCHERE, H., BROTHERS, G. M., STROCKBINE, B., SIDEROVSKI, D. P. & FARQUHAR, M. G. 2000. Activator of G protein signaling 3 is a guanine dissociation inhibitor for Galpha i subunits. *Proc Natl Acad Sci U S A,* 97, 14364-9.

DELL'ORCO, D. 2013. A physiological role for the supramolecular organization of rhodopsin and transducin in rod photoreceptors. *FEBS Lett,* 587, 2060-6.

DHINGRA, A., SULAIMAN, P., XU, Y., FINA, M. E., VEH, R. W. & VARDI, N. 2008. Probing neurochemical structure and function of retinal ON bipolar cells with a transgenic mouse. *J Comp Neurol,* 510, 484-96.

DIMITROV, P. N., GUYMER, R. H., ZELE, A. J., ANDERSON, A. J. & VINGRYS, A. J. 2008. Measuring rod and cone dynamics in age-related maculopathy. *Invest Ophthalmol Vis Sci,* 49, 55-65.

DORH, N., ZHU, S., DHUNGANA, K. B., PATI, R., LUO, F. T., LIU, H. & TIWARI, A. 2015. BODIPY-Based Fluorescent Probes for Sensing Protein Surface-Hydrophobicity. *Sci Rep,* 5, 18337.

DOWLING, J. E. 1960. Chemistry of visual adaptation in the rat. *Nature,* 188, 114-8.

EBNET, K., SCHULZ, C. U., MEYER ZU BRICKWEDDE, M. K., PENDL, G. G. & VESTWEBER, D. 2000. Junctional adhesion molecule interacts with the PDZ domain-containing proteins AF-6 and ZO-1. *J Biol Chem,* 275, 27979-88.

ELIAS, R. V., SEZATE, S. S., CAO, W. & MCGINNIS, J. F. 2004. Temporal kinetics of the light/dark translocation and compartmentation of arrestin and alpha-transducin in mouse photoreceptor cells. *Mol Vis,* 10, 672-81.

EZKURDIA, I., JUAN, D., RODRIGUEZ, J. M., FRANKISH, A., DIEKHANS, M., HARROW, J., VAZQUEZ, J., VALENCIA, A. & TRESS, M. L. 2014. Multiple evidence strands suggest that there may be as few as 19,000 human protein-coding genes. *Hum Mol Genet,* 23, 5866-78.

FAIN, G. L., MATTHEWS, H. R., CORNWALL, M. C. & KOUTALOS, Y. 2001. Adaptation in vertebrate photoreceptors. *Physiol Rev,* 81, 117-151.

FARKAS, M. H., GRANT, G. R., WHITE, J. A., SOUSA, M. E., CONSUGAR, M. B. & PIERCE, E. A. 2013. Transcriptome analyses of the human retina identify unprecedented transcript diversity and 3.5 Mb of novel transcribed sequence via significant alternative splicing and novel genes. *BMC Genomics,* 14, 486.

FAUSTINO, N. A. & COOPER, T. A. 2003. Pre-mRNA splicing and human disease. *Genes Dev,* 17, 419-37.

FEHON, R. G., MCCLATCHEY, A. I. & BRETSCHER, A. 2010. Organizing the cell cortex: the role of ERM proteins. *Nat Rev Mol Cell Biol,* 11, 276-87.

FERRARI, S., DI IORIO, E., BARBARO, V., PONZIN, D., SORRENTINO, F. S. & PARMEGGIANI, F. 2011. Retinitis pigmentosa: genes and disease mechanisms. *Curr Genomics,* 12, 238-49.

FILIPEK, S., STENKAMP, R. E., TELLER, D. C. & PALCZEWSKI, K. 2003. G protein-coupled receptor rhodopsin: a prospectus. *Annu Rev Physiol,* 65, 851-79.

FISHER, L. J. 1979. Development of synaptic arrays in the inner plexiform layer of neonatal mouse retina. *J Comp Neurol,* 187, 359-72.

FRICK, K. D., ROEBUCK, M. C., FELDSTEIN, J. I., MCCARTY, C. A. & GROVER, L. L. 2012. Health services utilization and cost of retinitis pigmentosa. *Arch Ophthalmol,* 130, 629-34.

FU, Y., LIU, H., NG, L., KIM, J. W., HAO, H., SWAROOP, A. & FORREST, D. 2014. Feedback induction of a photoreceptor-specific isoform of retinoid-related orphan nuclear receptor beta by the rod transcription factor NRL. *J Biol Chem,* 289, 32469-80.

GAL, A. B., CARNWATH, J. W., DINNYES, A., HERRMANN, D., NIEMANN, H. & WRENZYCKI, C. 2006. Comparison of real-time polymerase chain reaction and end-point polymerase chain reaction for the analysis of gene expression in preimplantation embryos. *Reprod Fertil Dev,* 18, 365-71.

GAO, Y., WESTFIELD, G., ERICKSON, J. W., CERIONE, R. A., SKINIOTIS, G. & RAMACHANDRAN, S. 2017. Isolation and structure-function characterization of a signaling-active rhodopsin-G protein complex. *J Biol Chem,* 292, 14280-14289.

GOEBL, M. & YANAGIDA, M. 1991. The TPR snap helix: a novel protein repeat motif from mitosis to transcription. *Trends Biochem Sci,* 16, 173-7.

GONZALEZ-FERNANDEZ, F. 2002. Evolution of the visual cycle: the role of retinoid-binding proteins. *J Endocrinol,* 175, 75-88.

GOSENS, I., DEN HOLLANDER, A. I., CREMERS, F. P. & ROEPMAN, R. 2008. Composition and function of the Crumbs protein complex in the mammalian retina. *Exp Eye Res,* 86, 713-26.

GOUAUX, E. 1998. alpha-Hemolysin from Staphylococcus aureus: an archetype of beta-barrel, channel-forming toxins. *J Struct Biol,* 121, 110-22.

GOURAS, P. & MACKAY, C. J. 1989. Light adaptation of the electroretinogram. Diminished in retinitis pigmentosa. *Invest Ophthalmol Vis Sci,* 30, 619-24.

GREINER, J. V., WEIDMAN, T. A., BODLEY, H. D. & GREINER, C. A. 1981. Ciliogenesis in photoreceptor cells of the retina. *Exp Eye Res,* 33, 433-46.

GROSSMAN, G. H., EBKE, L. A., BEIGHT, C. D., JANG, G. F., CRABB, J. W. & HAGSTROM, S. A. 2013. Protein partners of dynamin-1 in the retina. *Vis Neurosci,* 30, 129-39.

HAIDER, N. B., MOLLEMA, N., GAULE, M., YUAN, Y., SACHS, A. J., NYSTUEN, A. M., NAGGERT, J. K. & NISHINA, P. M. 2009. Nr2e3-directed transcriptional regulation of genes involved in photoreceptor development and cell-type specific phototransduction. *Exp Eye Res,* 89, 365-72.

HALL, B., LIMAYE, A. & KULKARNI, A. B. 2009. Overview: generation of gene knockout mice. *Curr Protoc Cell Biol,* Chapter 19, Unit 19 12 19 12 1-17.

HAMEL, C. 2006. Retinitis pigmentosa. *Orphanet J Rare Dis,* 1, 40.

HAO, H., KIM, D. S., KLOCKE, B., JOHNSON, K. R., CUI, K., GOTOH, N., ZANG, C., GREGORSKI, J., GIESER, L., PENG, W., FANN, Y., SEIFERT, M., ZHAO, K. & SWAROOP, A. 2012. Transcriptional regulation of rod photoreceptor homeostasis revealed by in vivo NRL targetome analysis. *PLoS Genet,* 8, e1002649.

HAO, H., TUMMALA, P., GUZMAN, E., MALI, R. S., GREGORSKI, J., SWAROOP, A. & MITTON, K. P. 2011. The transcription factor neural retina leucine zipper (NRL) controls photoreceptor-specific expression of myocyte enhancer factor Mef2c from an alternative promoter. *J Biol Chem,* 286, 34893-902.

HAO, H., VELERI, S., SUN, B., KIM, D. S., KEELEY, P. W., KIM, J. W., YANG, H. J., YADAV, S. P., MANJUNATH, S. H., SOOD, R., LIU, P., REESE, B. E. & SWAROOP, A. 2014. Regulation of a novel isoform of Receptor Expression Enhancing Protein REEP6 in rod photoreceptors by bZIP transcription factor NRL. *Hum Mol Genet,* 23, 4260-71.

HARRIS, B. Z. & LIM, W. A. 2001. Mechanism and role of PDZ domains in signaling complex assembly. *J Cell Sci,* 114, 3219-31.

HARTMAN, M. A. & SPUDICH, J. A. 2012. The myosin superfamily at a glance. *J Cell Sci,* 125, 1627-32.

HARTONG, D. T., BERSON, E. L. & DRYJA, T. P. 2006. Retinitis pigmentosa. *Lancet,* 368, 1795-809.

HAUSWIRTH, W. W., ALEMAN, T. S., KAUSHAL, S., CIDECIYAN, A. V., SCHWARTZ, S. B., WANG, L., CONLON, T. J., BOYE, S. L., FLOTTE, T. R., BYRNE, B. J. & JACOBSON, S. G. 2008. Treatment of leber congenital amaurosis due to RPE65 mutations by ocular subretinal injection of adeno-associated virus gene vector: short-term results of a phase I trial. *Hum Gene Ther,* 19, 979-90.

HE, W., COWAN, C. W. & WENSEL, T. G. 1998. RGS9, a GTPase accelerator for phototransduction. *Neuron,* 20, 95-102.

HENDRICKSON, A., BUMSTED-O'BRIEN, K., NATOLI, R., RAMAMURTHY, V., POSSIN, D. & PROVIS, J. 2008. Rod photoreceptor differentiation in fetal and infant human retina. *Exp Eye Res,* 87, 415-26.

HERRMANN, R., LOBANOVA, E. S., HAMMOND, T., KESSLER, C., BURNS, M. E., FRISHMAN, L. J. & ARSHAVSKY, V. Y. 2010. Phosducin regulates transmission at the photoreceptor-to-ON-bipolar cell synapse. *J Neurosci,* 30, 3239-53.

HU, G. & WENSEL, T. G. 2002. R9AP, a membrane anchor for the photoreceptor GTPase accelerating protein, RGS9-1. *Proc Natl Acad Sci U S A,* 99, 9755-60.

HU, J. H., WORLEY, P. F. & KAMMERMEIER, P. J. 2017. Dynamic Regulation of Homer Binding to Group I Metabotropic Glutamate Receptors by Preso1 and Converging Kinase Cascades. *J Pharmacol Exp Ther,* 361, 122-129.

HU, J. H., YANG, L., KAMMERMEIER, P. J., MOORE, C. G., BRAKEMAN, P. R., TU, J., YU, S., PETRALIA, R. S., LI, Z., ZHANG, P. W., PARK, J. M., DONG, X., XIAO, B. & WORLEY, P. F. 2012. Preso1 dynamically regulates group I metabotropic glutamate receptors. *Nat Neurosci,* 15, 836-44.

HUBBARD, R. 1958. Bleaching of rhodopsin by light and by heat. *Nature,* 181, 1126.

INGRAM, N. T., SAMPATH, A. P. & FAIN, G. L. 2016. Why are rods more sensitive than cones? *J Physiol,* 594, 5415-26.

ISHII, T. 2017. The ethics of creating genetically modified children using genome editing. *Curr Opin Endocrinol Diabetes Obes*.

JACKSON, G. R., OWSLEY, C. & CURCIO, C. A. 2002. Photoreceptor degeneration and dysfunction in aging and age-related maculopathy. *Ageing Res Rev,* 1, 381-96.

JADHAV, A. P., MASON, H. A. & CEPKO, C. L. 2006. Notch 1 inhibits photoreceptor production in the developing mammalian retina. *Development,* 133, 913-23.

JASTRZEBSKA, B., RINGLER, P., PALCZEWSKI, K. & ENGEL, A. 2013. The rhodopsin-transducin complex houses two distinct rhodopsin molecules. *J Struct Biol,* 182, 164-72.

JIA, L., OH, E. C., NG, L., SRINIVAS, M., BROOKS, M., SWAROOP, A. & FORREST, D. 2009. Retinoid-related orphan nuclear receptor RORbeta is an early-acting factor in rod photoreceptor development. *Proc Natl Acad Sci U S A,* 106, 17534-9.

JOHNSON, P. T., RAVEN, M. A. & REESE, B. E. 2001. Disruption of transient photoreceptor targeting within the inner plexiform layer following early ablation of cholinergic amacrine cells in the ferret. *Vis Neurosci,* 18, 741-51.

JOHNSON, P. T., WILLIAMS, R. R., CUSATO, K. & REESE, B. E. 1999. Rods and cones project to the inner plexiform layer during development. *J Comp Neurol,* 414, 1-12.

KARAKAS, B., WEERARATNA, A. T., ABUKHDEIR, A. M., KONISHI, H., GUSTIN, J. P., VITOLO, M. I., BACHMAN, K. E. & PARK, B. H. 2007. P21 gene knock down does not identify genetic effectors seen with gene knock out. *Cancer Biol Ther,* 6, 1025-30.

KARPEN, J. W., ZIMMERMAN, A. L., STRYER, L. & BAYLOR, D. A. 1988. Gating kinetics of the cyclic-GMP-activated channel of retinal rods: flash photolysis and voltage-jump studies. *Proc Natl Acad Sci U S A,* 85, 1287-91.

KATTI, C., BUTLER, R. & SEKARAN, S. 2013. Diurnal and circadian regulation of connexin 36 transcript and protein in the mammalian retina. *Invest Ophthalmol Vis Sci,* 54, 821-9.

KAUTZMANN, M. A., KIM, D. S., FELDER-SCHMITTBUHL, M. P. & SWAROOP, A. 2011. Combinatorial regulation of photoreceptor differentiation factor, neural retina leucine zipper gene NRL, revealed by in vivo promoter analysis. *J Biol Chem,* 286, 28247-55.

KERESZTES, G., MARTEMYANOV, K. A., KRISPEL, C. M., MUTAI, H., YOO, P. J., MAISON, S. F., BURNS, M. E., ARSHAVSKY, V. Y. & HELLER, S. 2004. Absence of the RGS9.Gbeta5 GTPase-activating complex in photoreceptors of the R9AP knockout mouse. *J Biol Chem,* 279, 1581-4.

KEROV, V., CHEN, D., MOUSSAIF, M., CHEN, Y. J., CHEN, C. K. & ARTEMYEV, N. O. 2005a. Transducin activation state controls its light-dependent translocation in rod photoreceptors. *J Biol Chem,* 280, 41069-76.

KEROV, V. S., NATOCHIN, M. & ARTEMYEV, N. O. 2005b. Interaction of transducin-alpha with LGN, a G-protein modulator expressed in photoreceptor cells. *Mol Cell Neurosci,* 28, 485-95.

KIM, D., PERTEA, G., TRAPNELL, C., PIMENTEL, H., KELLEY, R. & SALZBERG, S. L. 2013. TopHat2: accurate alignment of transcriptomes in the presence of insertions, deletions and gene fusions. *Genome Biol,* 14, R36.

KIM, J. W., YANG, H. J., BROOKS, M. J., ZELINGER, L., KARAKULAH, G., GOTOH, N., BOLEDA, A., GIESER, L., GIUSTE, F., WHITAKER, D. T., WALTON, A., VILLASMIL, R., BARB, J. J., MUNSON, P. J., KAYA, K. D., CHAITANKAR, V., COGLIATI, T. & SWAROOP, A. 2016a. NRL-Regulated Transcriptome Dynamics of Developing Rod Photoreceptors. *Cell Rep,* 17, 2460-2473.

KIM, J. W., YANG, H. J., OEL, A. P., BROOKS, M. J., JIA, L., PLACHETZKI, D. C., LI, W., ALLISON, W. T. & SWAROOP, A. 2016b. Recruitment of Rod Photoreceptors from Short-Wavelength-Sensitive Cones during the Evolution of Nocturnal Vision in Mammals. *Dev Cell,* 37, 520-32.

KIMPLE, R. J., KIMPLE, M. E., BETTS, L., SONDEK, J. & SIDEROVSKI, D. P. 2002. Structural determinants for GoLoco-induced inhibition of nucleotide release by Galpha subunits. *Nature,* 416, 878-81.

KISER, P. D., GOLCZAK, M. & PALCZEWSKI, K. 2014. Chemistry of the retinoid (visual) cycle. *Chem Rev,* 114, 194-232.

KLEENE, R. & SCHACHNER, M. 2004. Glycans and neural cell interactions. *Nat Rev Neurosci,* 5, 195-208.

KOBERLEIN, J., BEIFUS, K., SCHAFFERT, C. & FINGER, R. P. 2013. The economic burden of visual impairment and blindness: a systematic review. *BMJ Open,* 3, e003471.

KOLASKAR, A. S. & TONGAONKAR, P. C. 1990. A semi-empirical method for prediction of antigenic determinants on protein antigens. *FEBS Lett,* 276, 172-4.

KOLB, H. 1995a. Photoreceptors. *In:* KOLB, H., FERNANDEZ, E. & NELSON, R. (eds.) *Webvision: The Organization of the Retina and Visual System.* Salt Lake City (UT).

KOLB, H. 1995b. Simple Anatomy of the Retina. *In:* KOLB, H., FERNANDEZ, E. & NELSON, R. (eds.) *Webvision: The Organization of the Retina and Visual System.* Salt Lake City (UT).

KOS, C. H. 2004. Cre/loxP system for generating tissue-specific knockout mouse models. *Nutr Rev,* 62, 243-6.

KOSIK, K. S., DONAHUE, C. P., ISRAELY, I., LIU, X. & OCHIISHI, T. 2005. Delta-catenin at the synaptic-adherens junction. *Trends Cell Biol,* 15, 172-8.

KRISHAN, K., KANCHAN, T. & SINGH, B. 2016. Human Genome Editing and Ethical Considerations. *Sci Eng Ethics,* 22, 597-9.

KRUPNICK, J. G., GUREVICH, V. V. & BENOVIC, J. L. 1997. Mechanism of quenching of phototransduction. Binding competition between arrestin and transducin for phosphorhodopsin. *J Biol Chem,* 272, 18125-31.

KUHN, H. & WILDEN, U. 1987. Deactivation of photoactivated rhodopsin by rhodopsin-kinase and arrestin. *J Recept Res,* 7, 283-98.

LAMBENG, N., GROSSMANN, M., CHATELAIN, P. & FUKS, B. 2006. Solubilization and immunopurification of rat brain synaptic vesicle protein 2A with maintained binding properties. *Neurosci Lett,* 398, 107-12.

LAVAIL, M. M. 1973. Kinetics of rod outer segment renewal in the developing mouse retina. *J Cell Biol,* 58, 650-61.

LAVAIL, M. M. 1976. Rod outer segment disc shedding in relation to cyclic lighting. *Exp Eye Res,* 23, 277-80.

LE CARRE, J., SCHORDERET, D. F. & COTTET, S. 2011. Altered expression of beta-galactosidase-1-like protein 3 (Glb1l3) in the retinal pigment epithelium (RPE)-specific 65-kDa protein knock-out mouse model of Leber's congenital amaurosis. *Mol Vis,* 17, 1287-97.

LEE, E. S., KIM, W. R., KIM, Y., LEE, H. W., KIM, H. & SUN, W. 2014. Polarized and Stage-Dependent Distribution of Immunoreactivity for Novel PDZ-Binding Protein Preso1 in Adult Neurogenic Regions. *Endocrinol Metab (Seoul),* 29, 349-55.

LEE, H. J. & ZHENG, J. J. 2010. PDZ domains and their binding partners: structure, specificity, and modification. *Cell Commun Signal,* 8, 8.

LEE, H. W., CHOI, J., SHIN, H., KIM, K., YANG, J., NA, M., CHOI, S. Y., KANG, G. B., EOM, S. H., KIM, H. & KIM, E. 2008. Preso, a novel PSD-95-interacting FERM and PDZ domain protein that regulates dendritic spine morphogenesis. *J Neurosci,* 28, 14546-56.

LI, H. & DURBIN, R. 2009. Fast and accurate short read alignment with Burrows-Wheeler transform. *Bioinformatics,* 25, 1754-60.

LI, H., HANDSAKER, B., WYSOKER, A., FENNELL, T., RUAN, J., HOMER, N., MARTH, G., ABECASIS, G., DURBIN, R. & GENOME PROJECT DATA PROCESSING, S. 2009. The Sequence Alignment/Map format and SAMtools. *Bioinformatics,* 25, 2078-9.

LI, W., BENGTSON, M. H., ULBRICH, A., MATSUDA, A., REDDY, V. A., ORTH, A., CHANDA, S. K., BATALOV, S. & JOAZEIRO, C. A. 2008. Genome-wide and functional annotation of human E3 ubiquitin ligases identifies MULAN, a mitochondrial E3 that regulates the organelle's dynamics and signaling. *PLoS One,* 3, e1487.

LI, Y., YU, S., DUNCAN, T., LI, Y., LIU, P., GENE, E., CORTES-PENA, Y., QIAN, H., DONG, L. & REDMOND, T. M. 2015. Mouse model of human RPE65 P25L hypomorph resembles wild type under normal light rearing but is fully resistant to acute light damage. *Hum Mol Genet,* 24, 4417-28.

LISHKO, P. V., MARTEMYANOV, K. A., HOPP, J. A. & ARSHAVSKY, V. Y. 2002. Specific binding of RGS9-Gbeta 5L to protein anchor in photoreceptor membranes greatly enhances its catalytic activity. *J Biol Chem,* 277, 24376-81.

LIU, E. T., BOLCUN-FILAS, E., GRASS, D. S., LUTZ, C., MURRAY, S., SHULTZ, L. & ROSENTHAL, N. 2017. Of mice and CRISPR: The post-CRISPR future of the mouse as a model system for the human condition. *EMBO Rep,* 18, 187-193.

LIU, J., ITAGAKI, Y., BEN-SHABAT, S., NAKANISHI, K. & SPARROW, J. R. 2000. The biosynthesis of A2E, a fluorophore of aging retina, involves the formation of the precursor, A2-PE, in the photoreceptor outer segment membrane. *J Biol Chem,* 275, 29354-60.

LIU, J. J., STOCKTON, R. A., GINGRAS, A. R., ABLOOGLU, A. J., HAN, J., BOBKOV, A. A. & GINSBERG, M. H. 2011. A mechanism of Rap1-induced stabilization of endothelial cell--cell junctions. *Mol Biol Cell,* 22, 2509-19.

LOBANOVA, E. S., FINKELSTEIN, S., SONG, H., TSANG, S. H., CHEN, C. K., SOKOLOV, M., SKIBA, N. P. & ARSHAVSKY, V. Y. 2007. Transducin translocation in rods is triggered by saturation of the GTPase-activating complex. *J Neurosci,* 27, 1151-60.

LONGENECKER, G. & KULKARNI, A. B. 2009. Generation of gene knockout mice by ES cell microinjection. *Curr Protoc Cell Biol,* Chapter 19, Unit 19 14 19 14 1-36.

MAGUIRE, A. M., SIMONELLI, F., PIERCE, E. A., PUGH, E. N., JR., MINGOZZI, F., BENNICELLI, J., BANFI, S., MARSHALL, K. A., TESTA, F., SURACE, E. M., ROSSI, S., LYUBARSKY, A., ARRUDA, V. R., KONKLE, B., STONE, E., SUN, J., JACOBS, J., DELL'OSSO, L., HERTLE, R., MA, J. X., REDMOND, T. M., ZHU, X., HAUCK, B., ZELENAIA, O., SHINDLER, K. S., MAGUIRE, M. G., WRIGHT, J. F., VOLPE, N. J., MCDONNELL, J. W., AURICCHIO, A., HIGH, K. A. & BENNETT, J. 2008. Safety and efficacy of gene transfer for Leber's congenital amaurosis. *N Engl J Med,* 358, 2240-8.

MAJUMDER, A., PAHLBERG, J., BOYD, K. K., KEROV, V., KOLANDAIVELU, S., RAMAMURTHY, V., SAMPATH, A. P. & ARTEMYEV, N. O. 2013. Transducin translocation contributes to rod survival and enhances synaptic transmission from rods to rod bipolar cells. *Proc Natl Acad Sci U S A,* 110, 12468-73.

MAKINO, E. R., HANDY, J. W., LI, T. & ARSHAVSKY, V. Y. 1999. The GTPase activating factor for transducin in rod photoreceptors is the complex between RGS9 and type 5 G protein beta subunit. *Proc Natl Acad Sci U S A,* 96, 1947-52.

MATOSIN, N., FERNANDEZ-ENRIGHT, F., FUNG, S. J., LUM, J. S., ENGEL, M., ANDREWS, J. L., HUANG, X. F., WEICKERT, C. S. & NEWELL, K. A. 2015. Alterations of mGluR5 and its endogenous regulators Norbin, Tamalin and Preso1 in schizophrenia: towards a model of mGluR5 dysregulation. *Acta Neuropathol,* 130, 119-29.

MATOSIN, N., FERNANDEZ-ENRIGHT, F., LUM, J. S., ENGEL, M., ANDREWS, J. L., GASSEN, N. C., WAGNER, K. V., SCHMIDT, M. V. & NEWELL, K. A. 2016a. Molecular evidence of synaptic pathology in the CA1 region in schizophrenia. *NPJ Schizophr,* 2, 16022.

MATOSIN, N., GREEN, M. J., ANDREWS, J. L., NEWELL, K. A. & FERNANDEZ-ENRIGHT, F. 2016b. Possibility of a sex-specific role for a genetic variant in FRMPD4 in schizophrenia, but not cognitive function. *Neuroreport,* 27, 33-8.

MEARS, A. J., KONDO, M., SWAIN, P. K., TAKADA, Y., BUSH, R. A., SAUNDERS, T. L., SIEVING, P. A. & SWAROOP, A. 2001. Nrl is required for rod photoreceptor development. *Nat Genet,* 29, 447-52.

MEHALOW, A. K., KAMEYA, S., SMITH, R. S., HAWES, N. L., DENEGRE, J. M., YOUNG, J. A., BECHTOLD, L., HAIDER, N. B., TEPASS, U., HECKENLIVELY, J. R., CHANG, B., NAGGERT, J. K. & NISHINA, P. M. 2003. CRB1 is essential for external limiting membrane integrity and photoreceptor morphogenesis in the mammalian retina. *Hum Mol Genet,* 12, 2179-89.

MERCER, A. J. & THORESON, W. B. 2011. The dynamic architecture of photoreceptor ribbon synapses: cytoskeletal, extracellular matrix, and intramembrane proteins. *Vis Neurosci,* 28**,** 453-71.

MEZER, E., BABUL-HIRJI, R., WISE, R., CHIPMAN, M., DASILVA, L., ROWELL, M., THACKRAY, R., SHUMAN, C. T. & LEVIN, A. V. 2007. Attitudes regarding predictive testing for retinitis pigmentosa. *Ophthalmic Genet,* 28**,** 9-15.

MICHAELIDES, M., LI, Z., RANA, N. A., RICHARDSON, E. C., HYKIN, P. G., MOORE, A. T., HOLDER, G. E. & WEBSTER, A. R. 2010. Novel mutations and electrophysiologic findings in RGS9- and R9AP-associated retinal dysfunction (Bradyopsia). *Ophthalmology,* 117**,** 120-127 e1.

MIGNONE, F., GISSI, C., LIUNI, S. & PESOLE, G. 2002. Untranslated regions of mRNAs. *Genome Biol,* 3**,** REVIEWS0004.

MISRA, R. P. & DUNCAN, S. A. 2002. Gene targeting in the mouse: advances in introduction of transgenes into the genome by homologous recombination. *Endocrine,* 19**,** 229-38.

MITTON, K. P., SWAIN, P. K., CHEN, S., XU, S., ZACK, D. J. & SWAROOP, A. 2000. The leucine zipper of NRL interacts with the CRX homeodomain. A possible mechanism of transcriptional synergy in rhodopsin regulation. *J Biol Chem,* 275**,** 29794-9.

MIYAGISHIMA, K. J., CORNWALL, M. C. & SAMPATH, A. P. 2009. Metabolic constraints on the recovery of sensitivity after visual pigment bleaching in retinal rods. *J Gen Physiol,* 134**,** 165-75.

MOLDAY, R. S. & MOLDAY, L. L. 1998. Molecular properties of the cGMP-gated channel of rod photoreceptors. *Vision Res,* 38**,** 1315-23.

MOLEIRINHO, S., TILSTON-LUNEL, A., ANGUS, L., GUNN-MOORE, F. & REYNOLDS, P. A. 2013. The expanding family of FERM proteins. *Biochem J,* 452**,** 183-93.

MORGAN, J. & WONG, R. 1995. Development of Cell Types and Synaptic Connections in the Retina. *In:* KOLB, H., FERNANDEZ, E. & NELSON, R. (eds.) *Webvision: The Organization of the Retina and Visual System.* Salt Lake City (UT).

MUSTAFI, D., ENGEL, A. H. & PALCZEWSKI, K. 2009. Structure of cone photoreceptors. *Prog Retin Eye Res,* 28**,** 289-302.

NAGASE, T., ISHIKAWA, K., SUYAMA, M., KIKUNO, R., HIROSAWA, M., MIYAJIMA, N., TANAKA, A., KOTANI, H., NOMURA, N. & OHARA, O. 1999. Prediction of the coding sequences of unidentified human genes. XIII. The complete sequences of 100 new cDNA clones from brain which code for large proteins in vitro. *DNA Res,* 6**,** 63-70.

NAIR, K. S., BALASUBRAMANIAN, N. & SLEPAK, V. Z. 2002. Signal-dependent translocation of transducin, RGS9-1-Gbeta5L complex, and arrestin to detergent-resistant membrane rafts in photoreceptors. *Curr Biol,* 12**,** 421-5.

NAIR, K. S., HANSON, S. M., MENDEZ, A., GUREVICH, E. V., KENNEDY, M. J., SHESTOPALOV, V. I., VISHNIVETSKIY, S. A., CHEN, J., HURLEY, J. B., GUREVICH, V. V. & SLEPAK, V. Z. 2005a. Light-dependent redistribution of

arrestin in vertebrate rods is an energy-independent process governed by protein-protein interactions. *Neuron,* 46, 555-67.

NAIR, K. S., MENDEZ, A., BLUMER, J. B., ROSENZWEIG, D. H. & SLEPAK, V. Z. 2005b. The presence of a Leu-Gly-Asn repeat-enriched protein (LGN), a putative binding partner of transducin, in ROD photoreceptors. *Invest Ophthalmol Vis Sci,* 46, 383-9.

NATOCHIN, M., LESTER, B., PETERSON, Y. K., BERNARD, M. L., LANIER, S. M. & ARTEMYEV, N. O. 2000. AGS3 inhibits GDP dissociation from galpha subunits of the Gi family and rhodopsin-dependent activation of transducin. *J Biol Chem,* 275, 40981-5.

NIKONOV, S. S., DANIELE, L. L., ZHU, X., CRAFT, C. M., SWAROOP, A. & PUGH, E. N., JR. 2005. Photoreceptors of Nrl -/- mice coexpress functional S- and M-cone opsins having distinct inactivation mechanisms. *J Gen Physiol,* 125, 287-304.

NISHIDA, A., FURUKAWA, A., KOIKE, C., TANO, Y., AIZAWA, S., MATSUO, I. & FURUKAWA, T. 2003. Otx2 homeobox gene controls retinal photoreceptor cell fate and pineal gland development. *Nat Neurosci,* 6, 1255-63.

NISHIGUCHI, K. M., SANDBERG, M. A., KOOIJMAN, A. C., MARTEMYANOV, K. A., POTT, J. W., HAGSTROM, S. A., ARSHAVSKY, V. Y., BERSON, E. L. & DRYJA, T. P. 2004. Defects in RGS9 or its anchor protein R9AP in patients with slow photoreceptor deactivation. *Nature,* 427, 75-8.

NOMURA, N., MIYAJIMA, N., SAZUKA, T., TANAKA, A., KAWARABAYASI, Y., SATO, S., NAGASE, T., SEKI, N., ISHIKAWA, K. & TABATA, S. 1994. Prediction of the coding sequences of unidentified human genes. I. The coding sequences of 40 new genes (KIAA0001-KIAA0040) deduced by analysis of randomly sampled cDNA clones from human immature myeloid cell line KG-1. *DNA Res,* 1, 27-35.

O'BRIEN, K. M., SCHULTE, D. & HENDRICKSON, A. E. 2003. Expression of photoreceptor-associated molecules during human fetal eye development. *Mol Vis,* 9, 401-9.

OH, E. C., CHENG, H., HAO, H., JIA, L., KHAN, N. W. & SWAROOP, A. 2008. Rod differentiation factor NRL activates the expression of nuclear receptor NR2E3 to suppress the development of cone photoreceptors. *Brain Res,* 1236, 16-29.

OH, E. C., KHAN, N., NOVELLI, E., KHANNA, H., STRETTOI, E. & SWAROOP, A. 2007. Transformation of cone precursors to functional rod photoreceptors by bZIP transcription factor NRL. *Proc Natl Acad Sci U S A,* 104, 1679-84.

OLNEY, J. W. 1968. An electron microscopic study of synapse formation, receptor outer segment development, and other aspects of developing mouse retina. *Invest Ophthalmol,* 7, 250-68.

ORGANISCIAK, D. T. & VAUGHAN, D. K. 2010. Retinal light damage: mechanisms and protection. *Prog Retin Eye Res,* 29, 113-34.

OTSUKI, T., OTA, T., NISHIKAWA, T., HAYASHI, K., SUZUKI, Y., YAMAMOTO, J., WAKAMATSU, A., KIMURA, K., SAKAMOTO, K., HATANO, N., KAWAI, Y.,

ISHII, S., SAITO, K., KOJIMA, S., SUGIYAMA, T., ONO, T., OKANO, K., YOSHIKAWA, Y., AOTSUKA, S., SASAKI, N., HATTORI, A., OKUMURA, K., NAGAI, K., SUGANO, S. & ISOGAI, T. 2005. Signal sequence and keyword trap in silico for selection of full-length human cDNAs encoding secretion or membrane proteins from oligo-capped cDNA libraries. *DNA Res,* 12, 117-26.

OTTO-BRUC, A. E., FARISS, R. N., VAN HOOSER, J. P. & PALCZEWSKI, K. 1998. Phosphorylation of photolyzed rhodopsin is calcium-insensitive in retina permeabilized by alpha-toxin. *Proc Natl Acad Sci U S A,* 95, 15014-9.

OWSLEY, C., JACKSON, G. R., WHITE, M., FEIST, R. & EDWARDS, D. 2001. Delays in rod-mediated dark adaptation in early age-related maculopathy. *Ophthalmology,* 108, 1196-202.

OWSLEY, C., MCGWIN, G., JR., JACKSON, G. R., KALLIES, K. & CLARK, M. 2007. Cone- and rod-mediated dark adaptation impairment in age-related maculopathy. *Ophthalmology,* 114, 1728-35.

PALCZEWSKI, K., RISPOLI, G. & DETWILER, P. B. 1992. The influence of arrestin (48K protein) and rhodopsin kinase on visual transduction. *Neuron,* 8, 117-26.

PALMER, E. & FREEMAN, T. 2004. Investigation into the use of C- and N-terminal GFP fusion proteins for subcellular localization studies using reverse transfection microarrays. *Comp Funct Genomics,* 5, 342-53.

PAN, Q., SHAI, O., LEE, L. J., FREY, B. J. & BLENCOWE, B. J. 2008. Deep surveying of alternative splicing complexity in the human transcriptome by high-throughput sequencing. *Nat Genet,* 40, 1413-5.

PAN, Z., SHANG, Y., JIA, M., ZHANG, L., XIA, C., ZHANG, M., WANG, W. & WEN, W. 2013. Structural and biochemical characterization of the interaction between LGN and Frmpd1. *J Mol Biol,* 425, 1039-49.

PARK, P. S. 2014. Constitutively active rhodopsin and retinal disease. *Adv Pharmacol,* 70, 1-36.

PARKER, R. O. & CROUCH, R. K. 2010. Retinol dehydrogenases (RDHs) in the visual cycle. *Exp Eye Res,* 91, 788-92.

PENG, G. H. & CHEN, S. 2007. Crx activates opsin transcription by recruiting HAT-containing co-activators and promoting histone acetylation. *Hum Mol Genet,* 16, 2433-52.

PENG, Y. W., ZALLOCCHI, M., WANG, W. M., DELIMONT, D. & COSGROVE, D. 2011. Moderate light-induced degeneration of rod photoreceptors with delayed transducin translocation in shaker1 mice. *Invest Ophthalmol Vis Sci,* 52, 6421-7.

PINTO, L. H., INVERGO, B., SHIMOMURA, K., TAKAHASHI, J. S. & TROY, J. B. 2007. Interpretation of the mouse electroretinogram. *Doc Ophthalmol,* 115, 127-36.

PONCHEL, F., TOOMES, C., BRANSFIELD, K., LEONG, F. T., DOUGLAS, S. H., FIELD, S. L., BELL, S. M., COMBARET, V., PUISIEUX, A., MIGHELL, A. J., ROBINSON, P. A., INGLEHEARN, C. F., ISAACS, J. D. & MARKHAM, A. F. 2003. Real-time PCR based on SYBR-Green I fluorescence: an alternative to the TaqMan assay

for a relative quantification of gene rearrangements, gene amplifications and micro gene deletions. *BMC Biotechnol,* 3, 18.

PONTING, C. P. 1997. Evidence for PDZ domains in bacteria, yeast, and plants. *Protein Sci,* 6, 464-8.

POPOVA, E. Y., SALZBERG, A. C., YANG, C., ZHANG, S. S. & BARNSTABLE, C. J. 2017. Identification and prediction of alternative transcription start sites that generate rod photoreceptor-specific transcripts from ubiquitously expressed genes. *PLoS One,* 12, e0179230.

PULIMENO, P., BAUER, C., STUTZ, J. & CITI, S. 2010. PLEKHA7 is an adherens junction protein with a tissue distribution and subcellular localization distinct from ZO-1 and E-cadherin. *PLoS One,* 5, e12207.

PURVES, D. 2001. *Neuroscience,* Sunderland, Mass., Sinauer Associates.

RAJ, B. & BLENCOWE, B. J. 2015. Alternative Splicing in the Mammalian Nervous System: Recent Insights into Mechanisms and Functional Roles. *Neuron,* 87, 14-27.

RAMACHANDRAN, S. & CERIONE, R. A. 2004. Stabilization of an intermediate activation state for transducin by a fluorescent GTP analogue. *Biochemistry,* 43, 8778-86.

RAN, F. A., HSU, P. D., LIN, C. Y., GOOTENBERG, J. S., KONERMANN, S., TREVINO, A. E., SCOTT, D. A., INOUE, A., MATOBA, S., ZHANG, Y. & ZHANG, F. 2013. Double nicking by RNA-guided CRISPR Cas9 for enhanced genome editing specificity. *Cell,* 154, 1380-9.

RATNAPRIYA, R. & SWAROOP, A. 2013. Genetic architecture of retinal and macular degenerative diseases: the promise and challenges of next-generation sequencing. *Genome Med,* 5, 84.

RAVIOLA, E. & GILULA, N. B. 1973. Gap junctions between photoreceptor cells in the vertebrate retina. *Proc Natl Acad Sci U S A,* 70, 1677-81.

REIN, D. B., ZHANG, P., WIRTH, K. E., LEE, P. P., HOERGER, T. J., MCCALL, N., KLEIN, R., TIELSCH, J. M., VIJAN, S. & SAADDINE, J. 2006. The economic burden of major adult visual disorders in the United States. *Arch Ophthalmol,* 124, 1754-60.

RICH, K. A., ZHAN, Y. & BLANKS, J. C. 1997. Migration and synaptogenesis of cone photoreceptors in the developing mouse retina. *J Comp Neurol,* 388, 47-63.

ROBERTS, A., PIMENTEL, H., TRAPNELL, C. & PACHTER, L. 2011. Identification of novel transcripts in annotated genomes using RNA-Seq. *Bioinformatics,* 27, 2325-9.

ROBERTS, M. R., SRINIVAS, M., FORREST, D., MORREALE DE ESCOBAR, G. & REH, T. A. 2006. Making the gradient: thyroid hormone regulates cone opsin expression in the developing mouse retina. *Proc Natl Acad Sci U S A,* 103, 6218-23.

RODIECK, R. W. & NIRENBERG, M. W. 1973. *The vertebrate retina : principles of structure and function,* San Francisco, W.H. Freeman and Company.

ROSENZWEIG, D. H., NAIR, K. S., WEI, J., WANG, Q., GARWIN, G., SAARI, J. C., CHEN, C. K., SMRCKA, A. V., SWAROOP, A., LEM, J., HURLEY, J. B. & SLEPAK, V. Z. 2007. Subunit dissociation and diffusion determine the subcellular localization of rod and cone transducins. *J Neurosci,* 27, 5484-94.

ROSSI, A., KONTARAKIS, Z., GERRI, C., NOLTE, H., HOLPER, S., KRUGER, M. & STAINIER, D. Y. 2015. Genetic compensation induced by deleterious mutations but not gene knockdowns. *Nature,* 524, 230-3.

ROSSMILLER, B. P., RYALS, R. C. & LEWIN, A. S. 2015. Gene therapy to rescue retinal degeneration caused by mutations in rhodopsin. *Methods Mol Biol,* 1271, 391-410.

SAADAOUI, M., MACHICOANE, M., DI PIETRO, F., ETOC, F., ECHARD, A. & MORIN, X. 2014. Dlg1 controls planar spindle orientation in the neuroepithelium through direct interaction with LGN. *J Cell Biol,* 206, 707-17.

SALINAS, R. Y., PEARRING, J. N., DING, J. D., SPENCER, W. J., HAO, Y. & ARSHAVSKY, V. Y. 2017. Photoreceptor discs form through peripherin-dependent suppression of ciliary ectosome release. *J Cell Biol,* 216, 1489-1499.

SANADA, K. & TSAI, L. H. 2005. G protein betagamma subunits and AGS3 control spindle orientation and asymmetric cell fate of cerebral cortical progenitors. *Cell,* 122, 119-31.

SANYAL, S. & HAWKINS, R. K. 1986. Development and degeneration of retina in rds mutant mice: effects of light on the rate of degeneration in albino and pigmented homozygous and heterozygous mutant and normal mice. *Vision Res,* 26, 1177-85.

SCHNAPF, J. L., KRAFT, T. W. & BAYLOR, D. A. 1987. Spectral sensitivity of human cone photoreceptors. *Nature,* 325, 439-41.

SCOTTO-LAVINO, E., DU, G. & FROHMAN, M. A. 2006. 5' end cDNA amplification using classic RACE. *Nat Protoc,* 1, 2555-62.

SEDMAK, T. & WOLFRUM, U. 2011. Intraflagellar transport proteins in ciliogenesis of photoreceptor cells. *Biol Cell,* 103, 449-66.

SHERRY, D. M., WANG, M. M., BATES, J. & FRISHMAN, L. J. 2003. Expression of vesicular glutamate transporter 1 in the mouse retina reveals temporal ordering in development of rod vs. cone and ON vs. OFF circuits. *J Comp Neurol,* 465, 480-98.

SHICHIDA, Y. & MORIZUMI, T. 2007. Mechanism of G-protein activation by rhodopsin. *Photochem Photobiol,* 83, 70-5.

SHINWARI, Z. K., TANVEER, F. & KHALIL, A. T. 2017. Ethical Issues Regarding CRISPR Mediated Genome Editing. *Curr Issues Mol Biol,* 26, 103-110.

SINGH, M. S. & MACLAREN, R. E. 2011. Stem cells as a therapeutic tool for the blind: biology and future prospects. *Proc Biol Sci,* 278, 3009-16.

SINGH, P., SCHIMENTI, J. C. & BOLCUN-FILAS, E. 2015. A mouse geneticist's practical guide to CRISPR applications. *Genetics,* 199, 1-15.

SLEPAK, V. Z. & HURLEY, J. B. 2008. Mechanism of light-induced translocation of arrestin and transducin in photoreceptors: interaction-restricted diffusion. *IUBMB Life,* 60, 2-9.

SMALLWOOD, P. M., WANG, Y. & NATHANS, J. 2002. Role of a locus control region in the mutually exclusive expression of human red and green cone pigment genes. *Proc Natl Acad Sci U S A,* 99, 1008-11.

SMITH, A. J., CARTER, S. P. & KENNEDY, B. N. 2017. Genome editing: the breakthrough technology for inherited retinal disease? *Expert Opin Biol Ther,* 17, 1245-1254.

SOKOLOV, M., LYUBARSKY, A. L., STRISSEL, K. J., SAVCHENKO, A. B., GOVARDOVSKII, V. I., PUGH, E. N., JR. & ARSHAVSKY, V. Y. 2002. Massive light-driven translocation of transducin between the two major compartments of rod cells: a novel mechanism of light adaptation. *Neuron,* 34, 95-106.

SOKOLOV, M., STRISSEL, K. J., LESKOV, I. B., MICHAUD, N. A., GOVARDOVSKII, V. I. & ARSHAVSKY, V. Y. 2004. Phosducin facilitates light-driven transducin translocation in rod photoreceptors. Evidence from the phosducin knockout mouse. *J Biol Chem,* 279, 19149-56.

SOLOMON, S. G. & LENNIE, P. 2007. The machinery of colour vision. *Nat Rev Neurosci,* 8, 276-86.

SOLOVEI, I., KREYSING, M., LANCTOT, C., KOSEM, S., PEICHL, L., CREMER, T., GUCK, J. & JOFFE, B. 2009. Nuclear architecture of rod photoreceptor cells adapts to vision in mammalian evolution. *Cell,* 137, 356-68.

SOMMER, M. E., HOFMANN, K. P. & HECK, M. 2014. Not just signal shutoff: the protective role of arrestin-1 in rod cells. *Handb Exp Pharmacol,* 219, 101-16.

SOROKIN, S. 1962. Centrioles and the formation of rudimentary cilia by fibroblasts and smooth muscle cells. *J Cell Biol,* 15, 363-77.

SOROKIN, S. P. 1968. Centriole formation and ciliogenesis. *Aspen Emphysema Conf,* 11, 213-6.

SRINIVAS, M., NG, L., LIU, H., JIA, L. & FORREST, D. 2006. Activation of the blue opsin gene in cone photoreceptor development by retinoid-related orphan receptor beta. *Mol Endocrinol,* 20, 1728-41.

STAAHL, B. T., BENEKAREDDY, M., COULON-BAINIER, C., BANFAL, A. A., FLOOR, S. N., SABO, J. K., URNES, C., MUNARES, G. A., GHOSH, A. & DOUDNA, J. A. 2017. Efficient genome editing in the mouse brain by local delivery of engineered Cas9 ribonucleoprotein complexes. *Nat Biotechnol,* 35, 431-434.

STENZEL, N., FETZER, C. P., HEUMANN, R. & ERDMANN, K. S. 2009. PDZ-domain-directed basolateral targeting of the peripheral membrane protein FRMPD2 in epithelial cells. *J Cell Sci,* 122, 3374-84.

STOLFI, A., GANDHI, S., SALEK, F. & CHRISTIAEN, L. 2014. Tissue-specific genome editing in Ciona embryos by CRISPR/Cas9. *Development,* 141, 4115-20.

STRAUSBERG, R. L., FEINGOLD, E. A., GROUSE, L. H., DERGE, J. G., KLAUSNER, R. D., COLLINS, F. S., WAGNER, L., SHENMEN, C. M., SCHULER, G. D.,

ALTSCHUL, S. F., ZEEBERG, B., BUETOW, K. H., SCHAEFER, C. F., BHAT, N. K., HOPKINS, R. F., JORDAN, H., MOORE, T., MAX, S. I., WANG, J., HSIEH, F., DIATCHENKO, L., MARUSINA, K., FARMER, A. A., RUBIN, G. M., HONG, L., STAPLETON, M., SOARES, M. B., BONALDO, M. F., CASAVANT, T. L., SCHEETZ, T. E., BROWNSTEIN, M. J., USDIN, T. B., TOSHIYUKI, S., CARNINCI, P., PRANGE, C., RAHA, S. S., LOQUELLANO, N. A., PETERS, G. J., ABRAMSON, R. D., MULLAHY, S. J., BOSAK, S. A., MCEWAN, P. J., MCKERNAN, K. J., MALEK, J. A., GUNARATNE, P. H., RICHARDS, S., WORLEY, K. C., HALE, S., GARCIA, A. M., GAY, L. J., HULYK, S. W., VILLALON, D. K., MUZNY, D. M., SODERGREN, E. J., LU, X., GIBBS, R. A., FAHEY, J., HELTON, E., KETTEMAN, M., MADAN, A., RODRIGUES, S., SANCHEZ, A., WHITING, M., MADAN, A., YOUNG, A. C., SHEVCHENKO, Y., BOUFFARD, G. G., BLAKESLEY, R. W., TOUCHMAN, J. W., GREEN, E. D., DICKSON, M. C., RODRIGUEZ, A. C., GRIMWOOD, J., SCHMUTZ, J., MYERS, R. M., BUTTERFIELD, Y. S., KRZYWINSKI, M. I., SKALSKA, U., SMAILUS, D. E., SCHNERCH, A., SCHEIN, J. E., JONES, S. J., MARRA, M. A. & MAMMALIAN GENE COLLECTION PROGRAM, T. 2002. Generation and initial analysis of more than 15,000 full-length human and mouse cDNA sequences. *Proc Natl Acad Sci U S A,* 99, 16899-903.

STRISSEL, K. J., LISHKO, P. V., TRIEU, L. H., KENNEDY, M. J., HURLEY, J. B. & ARSHAVSKY, V. Y. 2005. Recoverin undergoes light-dependent intracellular translocation in rod photoreceptors. *J Biol Chem,* 280, 29250-5.

STUCK, M. W., CONLEY, S. M. & NAASH, M. I. 2012. Defects in the outer limiting membrane are associated with rosette development in the Nrl-/- retina. *PLoS One,* 7, e32484.

SULLIVAN, L. S. & DAIGER, S. P. 1996. Inherited retinal degeneration: exceptional genetic and clinical heterogeneity. *Mol Med Today,* 2, 380-6.

SWAROOP, A., KIM, D. & FORREST, D. 2010. Transcriptional regulation of photoreceptor development and homeostasis in the mammalian retina. *Nat Rev Neurosci,* 11, 563-76.

SYAMALADEVI, D. P., SPUDICH, J. A. & SOWDHAMINI, R. 2012. Structural and functional insights on the Myosin superfamily. *Bioinform Biol Insights,* 6, 11-21.

SZABO, V., KREIENKAMP, H. J., ROSENBERG, T. & GAL, A. 2007. p.Gln200Glu, a putative constitutively active mutant of rod alpha-transducin (GNAT1) in autosomal dominant congenital stationary night blindness. *Hum Mutat,* 28, 741-2.

TAKAYANAGI, H., YUZAWA, S. & SUMIMOTO, H. 2015. Structural basis for the recognition of the scaffold protein Frmpd4/Preso1 by the TPR domain of the adaptor protein LGN. *Acta Crystallogr F Struct Biol Commun,* 71, 175-83.

TANG, Y., ZHANG, X., YIN, Y., HARDWIDGE, P. R. & FANG, W. 2014. Streptococcus suis type 2 SSU0587 protein is a beta-galactosidase that contributes to bacterial adhesion but not to virulence in mice. *J Vet Med Sci,* 76, 1055-9.

TIAN, M., WANG, W., DELIMONT, D., CHEUNG, L., ZALLOCCHI, M., COSGROVE, D. & PENG, Y. W. 2014. Photoreceptors in whirler mice show defective transducin

translocation and are susceptible to short-term light/dark changes-induced degeneration. *Exp Eye Res,* 118, 145-53.

TIAN, M., ZALLOCCHI, M., WANG, W., CHEN, C. K., PALCZEWSKI, K., DELIMONT, D., COSGROVE, D. & PENG, Y. W. 2013. Light-induced translocation of RGS9-1 and Gbeta5L in mouse rod photoreceptors. *PLoS One,* 8, e58832.

TINI, M., JEWELL, U. R., CAMENISCH, G., CHILOV, D. & GASSMANN, M. 2002. Generation and application of chicken egg-yolk antibodies. *Comp Biochem Physiol A Mol Integr Physiol,* 131, 569-74.

TOKUYASU, K. & YAMADA, E. 1959. The fine structure of the retina studied with the electron microscope. IV. Morphogenesis of outer segments of retinal rods. *J Biophys Biochem Cytol,* 6, 225-30.

TRAPNELL, C., HENDRICKSON, D. G., SAUVAGEAU, M., GOFF, L., RINN, J. L. & PACHTER, L. 2013. Differential analysis of gene regulation at transcript resolution with RNA-seq. *Nat Biotechnol,* 31, 46-53.

TRAPNELL, C., ROBERTS, A., GOFF, L., PERTEA, G., KIM, D., KELLEY, D. R., PIMENTEL, H., SALZBERG, S. L., RINN, J. L. & PACHTER, L. 2012. Differential gene and transcript expression analysis of RNA-seq experiments with TopHat and Cufflinks. *Nat Protoc,* 7, 562-78.

TSANG, S. H., WOODRUFF, M. L., CHEN, C. K., YAMASHITA, C. Y., CILLUFFO, M. C., RAO, A. L., FARBER, D. B. & FAIN, G. L. 2006. GAP-independent termination of photoreceptor light response by excess gamma subunit of the cGMP-phosphodiesterase. *J Neurosci,* 26, 4472-80.

TSYBOVSKY, Y., MOLDAY, R. S. & PALCZEWSKI, K. 2010. The ATP-binding cassette transporter ABCA4: structural and functional properties and role in retinal disease. *Adv Exp Med Biol,* 703, 105-25.

UVERSKY, V. N. 2014. Unreported intrinsic disorder in proteins: Building connections to the literature on IDPs. *Intrinsically Disord Proteins,* 2, e970499.

VAN DUYNE, G. D. 2015. Cre Recombinase. *Microbiol Spectr,* 3, MDNA3-0014-2014.

VELERI, S., LAZAR, C. H., CHANG, B., SIEVING, P. A., BANIN, E. & SWAROOP, A. 2015. Biology and therapy of inherited retinal degenerative disease: insights from mouse models. *Dis Model Mech,* 8, 109-29.

WALD, G. 1968. The molecular basis of visual excitation. *Nature,* 219, 800-7.

WALD, G. & BROWN, P. K. 1958. Human rhodopsin. *Science,* 127, 222-6.

WALD, G., DURELL, J. & ST GEORGE, C. C. 1950. The light reaction in the bleaching of rhodopsin. *Science,* 111, 179-81.

WALD, G. & HUBBARD, R. 1950. The Synthesis of Rhodopsin from Vitamin A(1). *Proc Natl Acad Sci U S A,* 36, 92-102.

WANG, E. T., SANDBERG, R., LUO, S., KHREBTUKOVA, I., ZHANG, L., MAYR, C., KINGSMORE, S. F., SCHROTH, G. P. & BURGE, C. B. 2008. Alternative isoform regulation in human tissue transcriptomes. *Nature,* 456, 470-6.

WANG, N. K., FINE, H. F., CHANG, S., CHOU, C. L., CELLA, W., TOSI, J., LIN, C. S., NAGASAKI, T. & TSANG, S. H. 2009. Cellular origin of fundus autofluorescence in patients and mice with a defective NR2E3 gene. *Br J Ophthalmol,* 93, 1234-40.

WANG, Y., SMALLWOOD, P. M., COWAN, M., BLESH, D., LAWLER, A. & NATHANS, J. 1999. Mutually exclusive expression of human red and green visual pigment-reporter transgenes occurs at high frequency in murine cone photoreceptors. *Proc Natl Acad Sci U S A,* 96, 5251-6.

WANG, Y. P., DAKUBO, G., HOWLEY, P., CAMPSALL, K. D., MAZAROLLE, C. J., SHIGA, S. A., LEWIS, P. M., MCMAHON, A. P. & WALLACE, V. A. 2002. Development of normal retinal organization depends on Sonic hedgehog signaling from ganglion cells. *Nat Neurosci,* 5, 831-2.

WASOWICZ, M., MORICE, C., FERRARI, P., CALLEBERT, J. & VERSAUX-BOTTERI, C. 2002. Long-term effects of light damage on the retina of albino and pigmented rats. *Invest Ophthalmol Vis Sci,* 43, 813-20.

WENSEL, T. G. & STRYER, L. 1990. Activation mechanism of retinal rod cyclic GMP phosphodiesterase probed by fluorescein-labeled inhibitory subunit. *Biochemistry,* 29, 2155-61.

WHEWAY, G., PARRY, D. A. & JOHNSON, C. A. 2014. The role of primary cilia in the development and disease of the retina. *Organogenesis,* 10, 69-85.

WHORTON, M. R., JASTRZEBSKA, B., PARK, P. S., FOTIADIS, D., ENGEL, A., PALCZEWSKI, K. & SUNAHARA, R. K. 2008. Efficient coupling of transducin to monomeric rhodopsin in a phospholipid bilayer. *J Biol Chem,* 283, 4387-94.

WILKEN, M. S., BRZEZINSKI, J. A., LA TORRE, A., SIEBENTHALL, K., THURMAN, R., SABO, P., SANDSTROM, R. S., VIERSTRA, J., CANFIELD, T. K., HANSEN, R. S., BENDER, M. A., STAMATOYANNOPOULOS, J. & REH, T. A. 2015. DNase I hypersensitivity analysis of the mouse brain and retina identifies region-specific regulatory elements. *Epigenetics Chromatin,* 8, 8.

WITKOVSKY, P., SCHMITZ, Y., AKOPIAN, A., KRIZAJ, D. & TRANCHINA, D. 1997. Gain of rod to horizontal cell synaptic transfer: relation to glutamate release and a dihydropyridine-sensitive calcium current. *J Neurosci,* 17, 7297-306.

WOLWER, C. B., GODDE, N., PASE, L. B., ELSUM, I. A., LIM, K. Y., SACIRBEGOVIC, F., WALKLEY, C. R., ELLIS, S., OHNO, S., MATSUZAKI, F., RUSSELL, S. M. & HUMBERT, P. O. 2017. The Asymmetric Cell Division Regulators Par3, Scribble and Pins/Gpsm2 Are Not Essential for Erythroid Development or Enucleation. *PLoS One,* 12, e0170295.

WRIGHT, A. F., CHAKAROVA, C. F., ABD EL-AZIZ, M. M. & BHATTACHARYA, S. S. 2010. Photoreceptor degeneration: genetic and mechanistic dissection of a complex trait. *Nat Rev Genet,* 11, 273-84.

YAO, B., ZHANG, L., LIANG, S. & ZHANG, C. 2012. SVMTriP: a method to predict antigenic epitopes using support vector machine to integrate tri-peptide similarity and propensity. *PLoS One,* 7, e45152.

YARON, O., FARHY, C., MARQUARDT, T., APPLEBURY, M. & ASHERY-PADAN, R. 2006. Notch1 functions to suppress cone-photoreceptor fate specification in the developing mouse retina. *Development,* 133**,** 1367-78.

YASUMI, M., SAKISAKA, T., HOSHINO, T., KIMURA, T., SAKAMOTO, Y., YAMANAKA, T., OHNO, S. & TAKAI, Y. 2005. Direct binding of Lgl2 to LGN during mitosis and its requirement for normal cell division. *J Biol Chem,* 280**,** 6761-5.

YOUNG, R. W. 1985. Cell differentiation in the retina of the mouse. *Anat Rec,* 212**,** 199-205.

YUZAWA, S., KAMAKURA, S., IWAKIRI, Y., HAYASE, J. & SUMIMOTO, H. 2011. Structural basis for interaction between the conserved cell polarity proteins Inscuteable and Leu-Gly-Asn repeat-enriched protein (LGN). *Proc Natl Acad Sci U S A,* 108**,** 19210-5.

ZHANG, J. X., WANG, N. L. & LU, Q. J. 2015. Development of gene and stem cell therapy for ocular neurodegeneration. *Int J Ophthalmol,* 8**,** 622-30.

ZHOU, R. & CASPI, R. R. 2010. Ocular immune privilege. *F1000 Biol Rep,* 2.

ZHU, Y. Y., MACHLEDER, E. M., CHENCHIK, A., LI, R. & SIEBERT, P. D. 2001. Reverse transcriptase template switching: a SMART approach for full-length cDNA library construction. *Biotechniques,* 30**,** 892-7.

Appendices

6.4 Appendix A: Reagents and buffer compositions

6.4.1 Reagents

All chemicals were ordered from Sigma, except where otherwise specified.

6.4.2 Enzymes

All enzymes and their respective buffers were ordered from New England Biolabs.

6.4.3 DNA sequencing

Sanger sequencing was performed by Genewiz (US) or Source BioScience (UK).

6.4.4 General buffers and solutions

10x Phosphate-Buffered Saline (PBS)

80 g NaCl

2 g KCl

14.4 g Na_2HPO_4

2.4 g KH_2PO_4

Dissolve in 800 ml of H_2O. Adjust pH to 7.4 with HCl, then add H_2O for a total volume of 1 L. Store at room temp ~ 6 months.

4% Paraformaldehyde (PFA)

10 ml 16% PFA (entire brown glass vial)

4 ml 10x PBS

26 ml H_2O

Prepare under fume hood and properly dispose of waste. Store at 4°C for short term, or make aliquots and store at -20°C.

Sucrose Solutions (for embedding)

5-15 g Sucrose (percentage divided in half)

50 ml 1x PBS (add up to 50 ml)

Put on rotator until completely dissolved. Store at 4°C.

Blocking Solution (for IHC)

15 ml 1x PBS

750 µl normal donkey (goat, etc) serum (final: 5%)

45 µl Triton 100x (final: 0.3%)

Pass through 0.22 µm filter. Should be prepared fresh. Otherwise aliquot and store at -20°C.

LB Broth

12.5 g LB Broth Powder

500 mL NANOpure H_2O

Autoclave before using

Antibiotic 1000x stocks

IPTG: 25 mg/ml in sterile H_2O, filter sterilize, aliquot and store at -20°C.

Ampicillin: 100 mg/ml in sterile H_2O, filter sterilize, aliquot and store at -20°C.

Kanamycin: 50 mg/ml in sterile H_2O, filter sterilize, aliquot and store at -20°C.

X-gal: 25 mg/ml in DMF, do NOT filter, aliquot and store in dark at -20°C.

Agar for Plates – 150 mL, 6 plates

150 ml dH_2O

1.875 g LB powder

3 g Agar powder (2%)

Mix well and autoclave. Before making plates, melt in microwave, allow to cool to RT, then add appropriate antibiotics.

Radioimmunoprecipitation Assay (RIPA) Buffer

0.606 g Tris base (final: 50 mM)

0.877 g NaCl (final: 150 mM)

1 ml Nonidet P-40 Substitute (final: 1%)

0.5 g Na-deoxycholate (Deoxycholic acid) (final: 0.5%)

1 ml 10% SDS (final: 0.1%)

Dissolve Tris and NaCl in ~75 ml of H_2O. Adjust pH to 8 with HCl, then add remaining ingredients until well dissolved. Add H_2O for a total volume of 100 ml. Keep at 4°C for 1-2 weeks, or aliquot and store at -20°C. Add protease inhibitors fresh for each experiment.

1X Running Buffer for SDS-PAGE

500ml NANOpure H_2O

1.515g Tris

7.213g Glycine

0.50g SDS

1X TBST

100 mL TBS

900 mL NANOpure H_2O

5 mL 20% Tween 20

1X TBST with 5% Milk

50 mL 1X TBST

2.5 g Powdered Milk (Carnation)

1X TAE Running Buffer

980 mL NANOpure H_2O

20 mL 50X TAE

1% Agarose Gel

1 g Agarose

100 mL of 1X TAE

Heat in microwave

Allow to cool to warm

10 μL Ethidium Bromide

6.5 Appendix B: Plasmid maps

6.5.1 *Empty vector backbones and transfection controls*

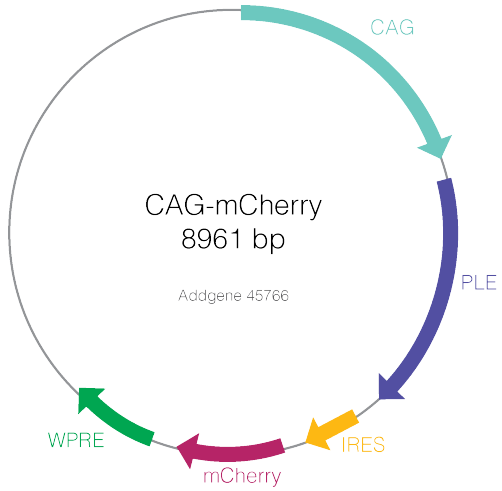

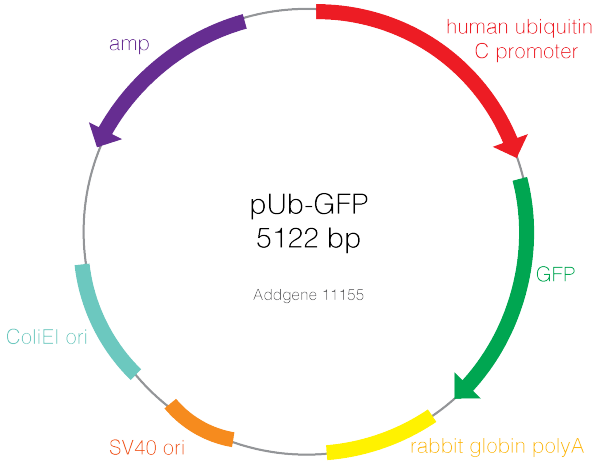

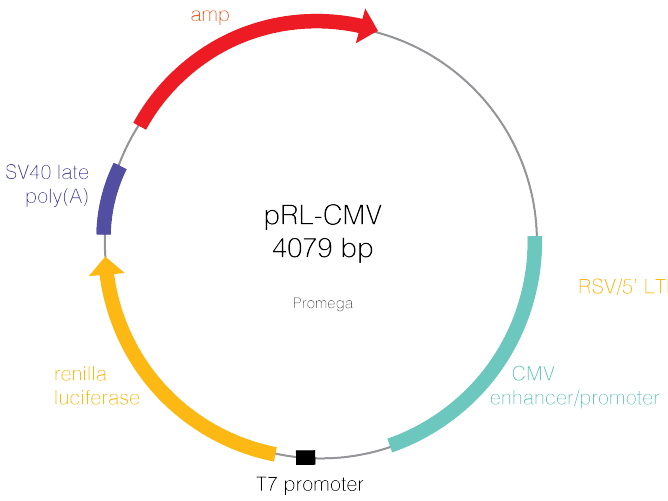

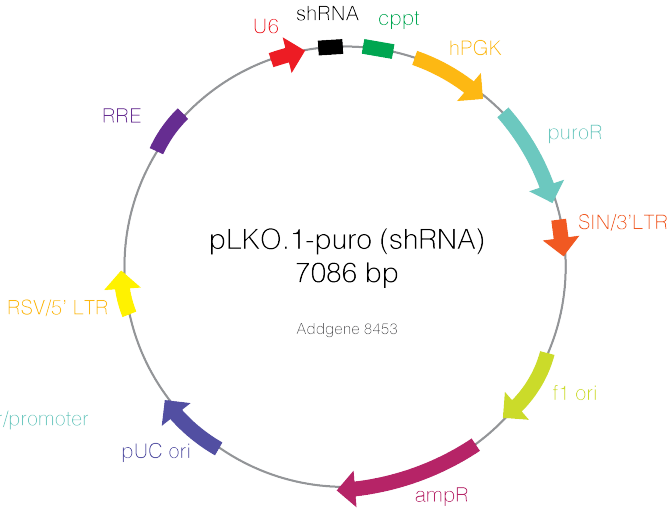

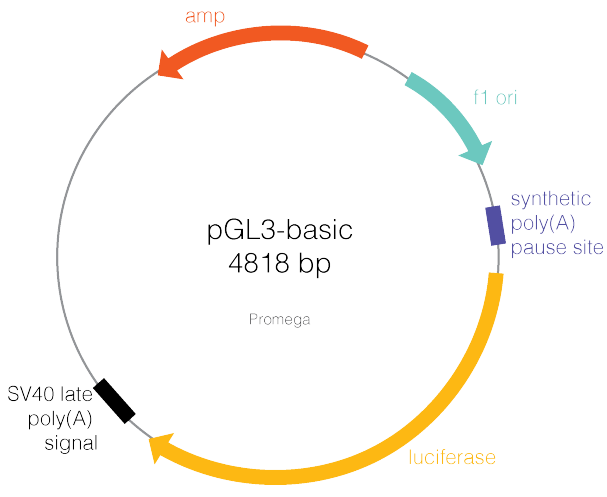

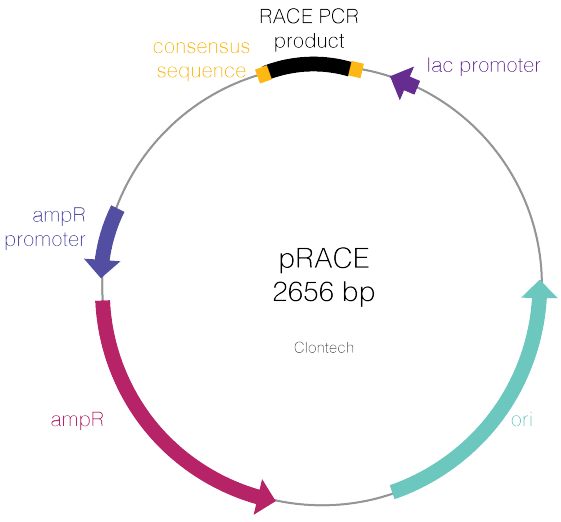

6.5.2 *Promoter constructs*

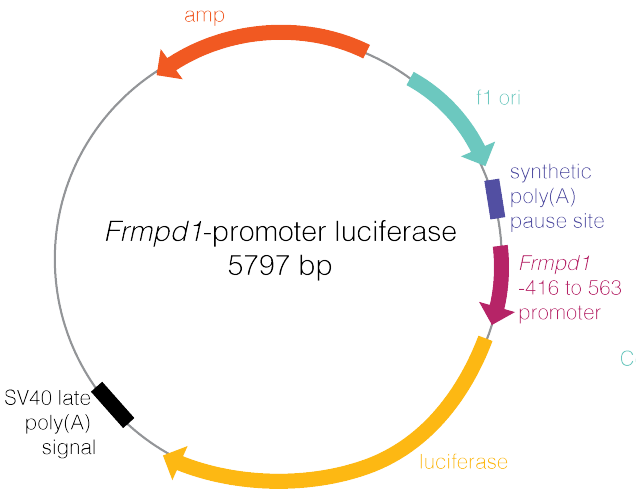

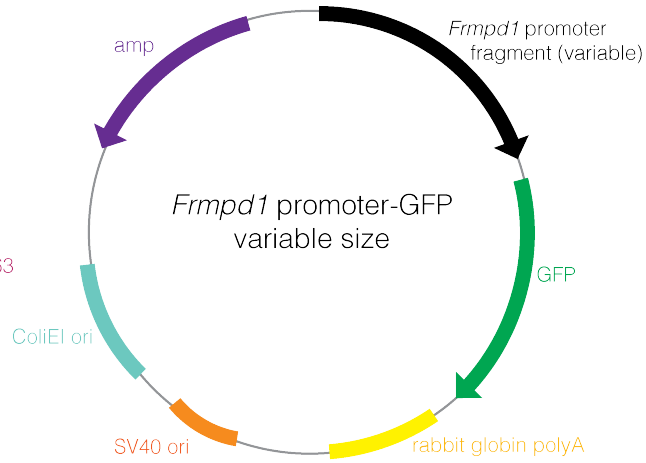

6.5.3 *Expression constructs*

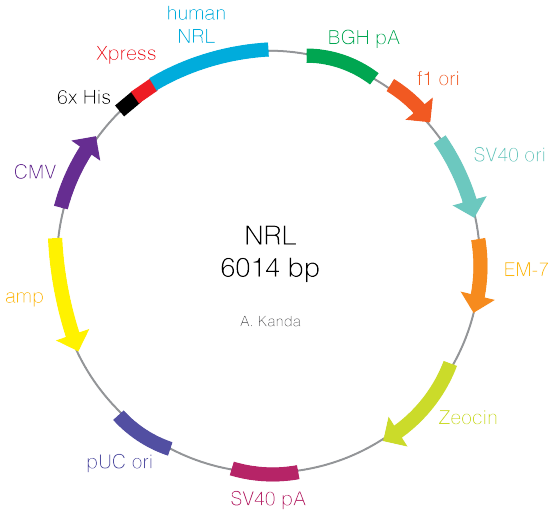

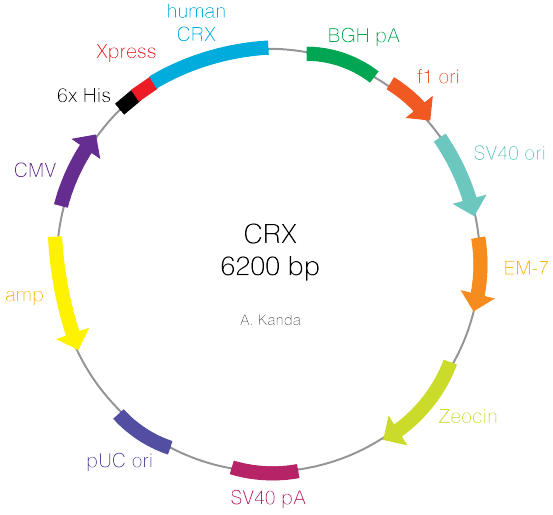

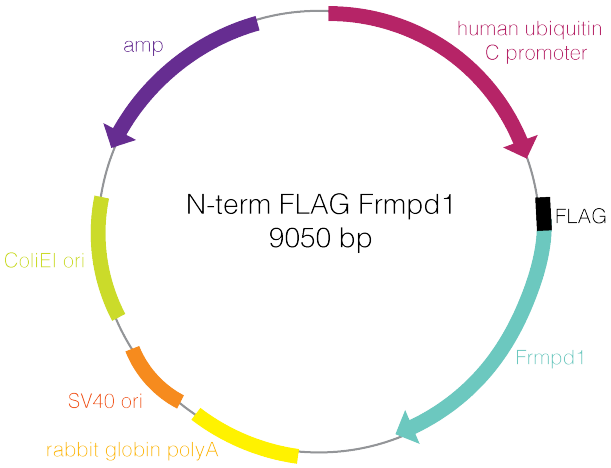

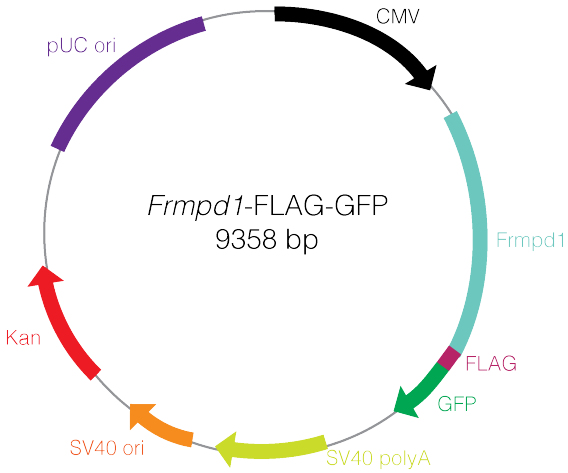

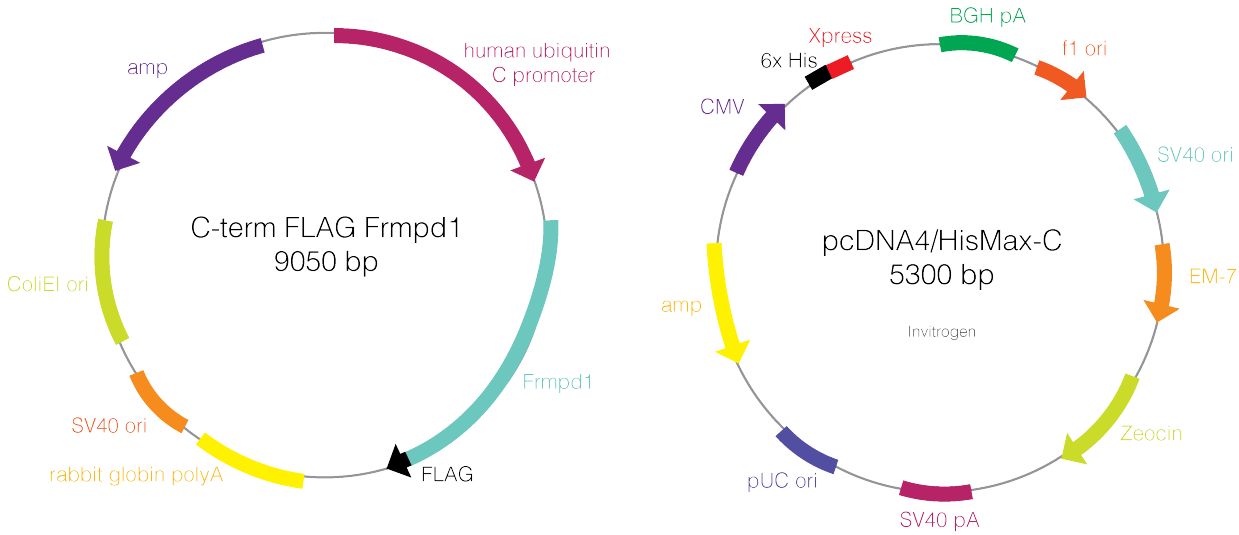

6.5.4 pLKO.1 shRNA target sequences and clone numbers

Gene	TRC number	AKA	Sequence (target underlined)
Galnt7	TRCN0000110285	85	CCGGGCCTCTTTCATTTCTCAGTATCTCGAGATACTGAGAAATGAAAGAGGCTTTTTG
	TRCN0000110286	86	CCGGGCCTCGAAACTGCATACTGTACTCGAGTACAGTATGCAGTTTCGAGGCTTTTTG
	TRCN0000110288	88	CCGGGCAAATTGTTATTTGTGCCTTCTCGAGAAGGCACAAATAACAATTTGCTTTTTG
	TRCN0000335093	93	CCGGGCCTCTTTCATTTCTCAGTATCTCGAGATACTGAGAAATGAAAGAGGCTTTTTG
	TRCN0000335169	69	CCGGGCCTCGAAACTGCATACTGTACTCGAGTACAGTATGCAGTTTCGAGGCTTTTTG
Glb1l2	TRCN0000174997	97	CCGGGCGCAAAGGTTTAATTGGAAACTCGAGTTTCCAATTAAACCTTTGCGCTTTTTTG
	TRCN0000175187	87	CCGGCAAAGGAATCAACAAGGTTATCTCGAGATAACCTTGTTGATTCCTTTGTTTTTTG
	TRCN0000175211	11	CCGGCCAGAACATATCATTGAGCTACTCGAGTAGCTCAATGATATGTTCTGGTTTTTTG
	TRCN0000193525	25	CCGGGCTGGTAGTTAAGAATAAGAACTCGAGTTCTTATTCTTAACTACCAGCTTTTTTG
	TRCN0000193842	42	CCGGCCATGTTAAGAGGTTGGCATTCTCGAGAATGCCAACCTCTTAACATGGTTTTTTG
Frmpd1	TRCN0000255536	A	CCGGGTGAACGAGCGGCTGATATTCCTCGAGGAATATCAGCCGCTCGTTCACTTTTTG
	TRCN0000255537	B	CCGGTCCAACTTTACTCCGAAATATCTCGAGATATTTCGGAGTAAAGTTGGATTTTTG
	TRCN0000255538	C	CCGGGCTGCTCAGCTACGCTTAAATCTCGAGATTTAAGCGTAGCTGAGCAGCTTTTTG
	TRCN0000255539	D	CCGGGTGACGACAGTCCTATCATTTCTCGAGAAATGATAGGACTGTCGTCACTTTTTG
	TRCN0000255540	E	CCGGAGCCGGACTGACTACTATAACCTCGAGGTTATAGTAGTCAGTCCGGCTTTTTTG
Control (Nontargeting)	Scramble	Scramble	CCGGTCCTAAGGTTAAGTCGCCCTCGCTCGAGCGAGGGCGACTTAACCTTAGGTTTTTG

6.6 Appendix C: Primers used for genotyping, cloning, RACE, and PCR assays.

6.6.1 PCR and genotyping primers

Product name	Use	Forward primer	Reverse primer
Frmpd1 promoter wildtype	Genotyping	gcaggttcgttctcaagcat	gttgccctttgaccttcaca
Frmpd1 promoter deletion	Genotyping	cctgtgaatgagggctctga	
Frmpd1 all	PCR	gccgctgtattctgtttgac	ggcaggtgaacaagaagagg
Exon 1a	PCR	cgctgaaaggagagaagcca	gccaacattcccaggattgc
Exon 6	PCR	tcttgactgaggagaagcgg	-
Exon 8	PCR	gagaagctgtccatccgaag	-
Exon 10	PCR	gctgtggagatgaagtgcaa	-
Exon 10	PCR	-	ttgcacttcatctccacagc
Exon 12	PCR	cagatccttggggaactcaa	-
Exon 14	PCR	caactccgtcttccactggt	-
Exon 16	PCR	-	gaggcgaatggcagagatag
Exon 12	PCR	-	acgtcttgagttccccaagg
Hprt	PCR	caaactttgctttccctggt	caagggcatatccaacaaca
Rho	PCR	tgttcctgctcatcgtgctgg	ggaagttgctcatcggcttgc

6.6.2 5'-RACE primers

Primer	Location	Sequence
Mouse primary PCR	Exon 8	gattacgccaagctttgcagaaggtgtaggcgggagatgctgt
Mouse nested PCR	Exon 6	gattacgccaagcttccgggcccgcttctcctcagtcaagaag
Mouse primary PCR	Exon 16	gattacgccaagcttctgcagggaggacacagttggggagggg
Human primary PCR	Exon 8	gattacgccaagcttgatgagttcctcttcgtgcagcaggtgc
Human nested PCR	Exon 6	gattacgccaagcttccgggcccgcttctcctcagtcaagaag

6.6.3 Cloning and mutagenesis primers

Product name	**Use**	**Forward primer**	**Reverse primer**
-23422 to -22461	Cloning	tcctttccacctatcctgct	ccctctgcacatctggtaca
-18147 to -17301	Cloning	gactgggagacaagggaagt	acgcttgtgtttgaatgcct
-2814 to +563	Cloning	caggtgcatcgaaagctagc	tgtttcagagtgagagatgacca
-1800 to +563	Cloning	gagccatctcagtagcccag	tgtttcagagtgagagatgacca
-1123 to +563	Cloning	cataccttttcgtctgcctgc	tgtttcagagtgagagatgacca
-416 to +563	Cloning	tacctgcctgttatgcgcat	tgtttcagagtgagagatgacca
-74 to +563	Cloning	tgtcatttccccatctgtca	tgtttcagagtgagagatgacca
+125 to +563	Cloning	tgccaatcaagaggctctaag	tgtttcagagtgagagatgacca
N-term FLAG	Cloning	cgcaggtaccatggactacaa agacgatgacgacaagatgg aagagctggacggcag	tgcagcggccgctcacagagcgg tggacgccc
C-term FLAG	Cloning	cgcaggtaccatggaagagct ggacggcag	tgcagcggccgctcacttgtcgtca tcgtctttgtagtccagagcggtgg acgcccgg
C-term GFP	Cloning	cgcagctagcatggaagagct ggacggcag	cgcaggtacctccttgtcgtcatcg tctttgtagtccagagcggtggac gcccgg
NRL site mutation	Mutagenesis	agtgggctaactatcttgctatt aacgtcagctgggg	aagcctcacgggagccca
CRX site mutation	Mutagenesis	gcaggttattgccgcatcctgt gttgtcatttcccc	ccagcctcgtgcaggctg

6.7 Appendix D: Antibodies used for immunofluorescence and immunoblot staining.

Antibody	Host	Source	Concentration	
			IHC	Immunoblot
βactin	Mouse	Sigma A5316	n/a	1:3000
Brn3a	Mouse	Santa Cruz sc8429	1:1000	n/a
Calbindin	Rabbit	Calbiochem PC253L	1:1000	n/a
Chat	Goat	Millipore AB144P	1:200	n/a
Cone arrestin	Rabbit	Millipore AB15282	1:1000	n/a
Cox IV	Rabbit	Abcam ab16056	1:500	1:1000
Crx	Rabbit	Santa Cruz sc30150 X	n/a	1:250
Flag	Rabbit	Cell Signaling 2368	1:600	1:1000
Frmpd1 (Chicken 6 IgY)	Chicken	Custom (CoCalico)	1:200	1:2000
Frmpd1 (Commercial)	Rabbit	Atlas HPA042934	n/a	1:1000
Gfap	Rabbit	Dako Z0334	1:1000	n/a
Glul1	Mouse	Millipore MAB302	1:1000	n/a
Goα	Mouse	Millipore MAB3073	1:1000	n/a
Gpsm1	Rabbit	Proteintech 114831AP	n/a	1:400
Gpsm2	Rabbit	Millipore ABT174	n/a	1:500
Gpsm2	Goat	AntibodiesOnline ABIN190875	1:500	n/a
M-opsin	Rabbit	Millipore AB5405	1:1000	n/a
Nr2e3	Rabbit	A. Swaroop	n/a	1:1000
Nrl	Rabbit	A. Swaroop	n/a	1:2000
Pkcα	Rabbit	Sigma P4334	1:1000	n/a
Pmca	Mouse	Abcam AB2825	1:200	n/a
R9ap	Goat	T. Wensel	1:500	n/a

Antibody	Host	Source	Concentration	
			IHC	Immunoblot
Recoverin	Rabbit	A. M. Dizhoor	1:500	n/a
Rgs9	Rabbit	T. Wensel	1:500	n/a
Rhodopsin	Mouse	R. Molday	1:1000	n/a
Rhodopsin kinase	Mouse	T. Li (ABR)	1:500	n/a
Ribeye	Mouse	BD Transduction 612044	1:500	n/a
Rod arrestin	Mouse	I. Gery	1:500	n/a
S-opsin	Chicken	C.M. Craft	1:1000	n/a
Snap25 (clone 71.2)	Mouse	Synaptic Systems 111 111	1:100	n/a
Snap25 (SP12)	Mouse	Abcam ab24732	1:200	n/a
Synaptophysin	Mouse	Chemicon MAB332	1:200	n/a
Transducin (alpha subunit)	Rabbit	Santa Cruz sc389	1:500	1:250
Unc119	Rabbit	G. Inana	1:500	n/a
AlexaFluor 488-conjugated anti-chicken IgG	Donkey	Jackson 703545155	1:1000	n/a
AlexaFluor 488-conjugated anti-mouse IgG	Donkey	Invitrogen A21202	1:1000	n/a
AlexaFluor 488-conjugated anti-rabbit IgG	Donkey	Invitrogen A21206	1:1000	n/a
AlexaFluor 555-conjugated anti-goat IgG	Donkey	Invitrogen A21432	1:1000	n/a
AlexaFluor 568-conjugated anti-mouse IgG	Donkey	Invitrogen A10037	1:1000	n/a
AlexaFluor 568-conjugated anti-rabbit IgG	Donkey	Invitrogen A10042	1:1000	n/a
AlexaFluor 568-conjugated PNA	n/a	Invitrogen L32548	1:2000	n/a

Antibody	Host	Source	Concentration	
			IHC	Immunoblot
HRP-conjugated anti-chicken IgY	Donkey	Jackson 703035155	n/a	1:3000
HRP-conjugated anti-guinea pig IgG	Goat	Millipore AP108P	n/a	1:1000
HRP-conjugated anti-mouse IgG	Donkey	Millipore AP192P	n/a	1:6000
HRP-conjugated anti-rabbit IgG	Donkey	Jackson 711035152	n/a	1:3000
HRP-conjugated Easyblot anti-mouse IgG	n/a	Genetex GTX22166701	n/a	1:3000
HRP-conjugated Easyblot anti-rabbit IgG	n/a	Genetex GTX22166601	n/a	1:3000

6.8 Appendix E: Differentially expressed genes also containing Nrl and Crx ChIP-seq peaks.

		FPKM in flow-sorted rod photoreceptors					
Cluster	Gene	P2	P4	P6	P10	P14	P28
1	1110020G09Rik	8.75	3.66	8.87	11.21	16.04	14.65
1	AI118078	1.54	2.09	3.08	4.75	6.91	9.11
1	B4galt1	4.13	4.14	4.02	6.76	10.68	4.14
1	C030046E11Rik	4.66	5.56	3.53	6.8	7.39	20.79
1	Camk2d	11.81	14.77	20.86	36.16	49.84	66.22
1	Ddx6	14.09	10.26	12.93	23.6	39.76	32.97
1	Dennd4a	2.19	0.69	2.22	2.37	3.13	7.89
1	Fam53b	6.27	5.59	6.41	8.26	12.37	9.73
1	Lifr	2.86	3.91	2.68	4.48	4.95	10.32
1	Mecr	3.9	3.64	3.78	13.1	16.47	19.94
1	Mpdz	6.45	7.01	6.42	12.82	15.65	47.82
1	Plekhf2	2.27	0.55	2.37	3.75	8.75	5.17
1	Rabgef1	1.02	0.75	3.84	21.06	43.36	51.28
1	Rnf150	3.84	3.12	4.23	7.42	9.01	16.61
1	Sntb2	2.19	2.36	1.81	4.21	9.09	5.38
1	Stk17b	4.99	3.21	2.23	2.33	5.17	8.6
1	Tjp2	4.94	2.43	4.39	8.47	11.31	6.96
1	Tmem201	5.26	4.22	4.15	4.67	6.19	12.32
1	Tmem35	2.72	2.1	5.52	6.08	12.9	22.13
1	Trim36	1.31	2.45	2.28	5.08	6.5	8.14
1	Wwox	4.09	3.43	5.85	11.67	15.01	28.4
2	Camk1d	0.21	0.2	0.29	6.23	8.5	15.79
2	Eepd1	0.91	0.82	1.06	5.53	8.89	22

		FPKM in flow-sorted rod photoreceptors					
Cluster	Gene	P2	P4	P6	P10	P14	P28
2	Ehd4	0.73	0.42	0.96	4.42	6.93	11.58
2	Galnt7	1.42	1.42	2.37	8.73	14.09	10.95
2	Guk1	36.69	36.99	78.26	525.96	578.44	721.6
2	Gzmm	0.58	0.7	1.43	10.3	5.79	15.08
2	Lrrc2	0.49	0.75	0.92	4.59	8.64	16.98
2	Opn1mw	0	0.1	0.1	13.57	30.79	8.86
2	Plekha8	1.71	0.57	0.76	3.25	6.49	9.78
2	Polg2	1.28	0.83	1.92	7.05	5.93	8.4
2	Prkca	2.61	1.3	3.2	7.73	5.11	13.08
2	St8sia1	0.49	0.14	0.62	2.83	5.91	17.09
2	Stat1	0.86	0.67	0.86	3.5	5.04	8.53
2	Stk35	1.09	0.65	1.46	2.47	9.89	18.08
2	Taok3	1.04	0.73	2.02	8.32	12.36	11.85
2	Tnfaip3	0.2	0.23	0.49	2.77	7.1	11.66
2	Whrn	1.83	1.04	2.62	9.77	14.02	13.13
3	Ahr	0.41	0.65	0.95	3.78	5.23	3.33
3	Dlg1	2.75	1.35	3.26	2.08	3.26	6.5
3	Fndc1	0.06	0	0.25	0.93	2.02	3.44
3	Galnt10	0.46	0.35	0.64	2.38	2.93	6.7
3	Gnaz	0.32	0	0.16	0.28	1.38	5.25
3	Grtp1	1.33	1.75	2.76	37.95	79.92	168.43
3	Pdia5	0.7	0.12	0.56	1.74	4.66	2.42
3	Pla2r1	1.04	2.51	3.2	19.57	42.24	59.29
3	Sh2d1a	0	0.04	0.09	0.4	3.65	13.42
3	Slc1a2	4.34	6.81	6.03	8.32	15.08	65.21

		FPKM in flow-sorted rod photoreceptors					
Cluster	Gene	P2	P4	P6	P10	P14	P28
3	Stk35	1.09	0.65	1.46	2.47	9.89	18.08
3	Syne1	0	0	0	0.61	2.31	21.16
3	Tmem108	0.29	0.43	0.75	4.28	5.45	4.45
3	Tnrc6b	2.18	2.5	1.79	3.92	5.32	2.44
3	Trim36	1.31	2.45	2.28	5.08	6.5	8.14
3	Whrn	1.83	1.04	2.62	9.77	14.02	13.13
4	Fam19a3	2.09	1.47	2.97	2.42	1.41	0.64
4	Kcnab1	3.35	2.43	2.71	2.64	2.17	0.49
4	Ppargc1b	0.31	0.12	0.66	9.46	18.04	6.24
4	Rgl3	5.72	2.18	1.63	0.33	0.28	0.07
4	Rhobtb1	0.98	2.45	1.65	1.61	1.63	1.03
4	Slc38a1	9.43	9.59	5.05	2.49	1.45	0.49
5	Bcat1	0	0.87	0	2.09	2.49	3.73
5	Ccdc136	18.85	10.21	11.88	2.97	1.68	0.69
5	**Galnt7**	1.42	1.42	2.37	8.73	14.09	10.95
5	Gulo	10.89	8.19	6.46	4.51	7.65	2.02
5	Jam3	27.97	17.24	15.87	4.56	3.56	0.62
5	Leprot	14.73	11.28	11.31	7.53	6.93	7.77
5	Nfkbia	19.11	15.25	26.51	6.47	5.4	4.43
5	Nufip2	10.94	4.67	13.11	6.2	6.8	5.33
5	Olfm1	16.44	15.27	15.24	8.4	4.31	1.18
5	Pcdh15	10.04	14.6	12.99	2.6	4.71	3.5
5	Prdm1	59.5	38.44	36.29	5.71	3.54	0.32
5	Pxn	0.81	0.46	1.49	1.4	0.87	1.95
5	Rspo2	7.64	4.66	3.2	2.28	2.63	2.54

		FPKM in flow-sorted rod photoreceptors					
Cluster	Gene	P2	P4	P6	P10	P14	P28
5	Scrn1	7.55	5.95	4.52	4.26	3.47	0.74
5	Slc38a1	9.43	9.59	5.05	2.49	1.45	0.49
5	Tnrc6b	2.18	2.5	1.79	3.92	5.32	2.44
6	2610034M16Rik	0.05	0.15	0.25	13.7	47.97	232.74
6	Aqp1	0.03	0.01	0.09	8.09	41.44	81.28
6	Drd4	0.13	0.13	0.36	78.65	224.81	148.19
6	Esrrb	0.09	0.17	1.36	47.6	90.6	285
6	Kcnj14	0.1	0.03	0.31	16	92.58	409.09
6	Optn	0.64	0.73	0.65	11.16	34.83	164.82
6	Pde6a	1.07	4.38	11.12	434.19	961	3057.02
6	Rtbdn	0.4	0.92	3.15	52.85	125.74	263.23
7	Guca1b	0.23	0.43	1.27	205.21	888.79	3511.12
7	Slc24a1	0.11	0.36	1.64	217.4	557.48	1510.54
8	Acadvl	12.99	14.1	21.58	39.45	37.87	26.73
8	Ankrd33b	49.33	45.2	48.34	74.77	101.91	110.46
8	Ap2a2	10.03	5.69	13.77	28.19	45.26	76.83
8	Arl13b	6.81	8.34	6.78	14.89	18.98	15.52
8	Atp11b	9.18	5.55	10.86	26.69	40.07	60.42
8	Atp2c1	8.62	20.56	14.08	28.47	27.61	34.96
8	Ddx6	14.09	10.26	12.93	23.6	39.76	32.97
8	Fam82a2	7.3	4.85	8.58	22.37	32.47	69.69
8	Fhod3	11.87	11.02	13.38	12.05	16.57	36.32
8	Fyco1	11.63	15.46	19.83	18.22	23.27	13.68
8	Hs3st3b1	7.69	9.21	11.16	13.85	21.48	5.35
8	Kif21b	13.48	14.34	20.85	29.47	33.81	9.16

		FPKM in flow-sorted rod photoreceptors					
Cluster	Gene	P2	P4	P6	P10	P14	P28
8	Nsf	8.79	3.81	10.48	26.63	66.61	124.13
8	Pip4k2c	6.15	4.31	9.84	16.38	27.32	41.31
8	Rdm1	6.93	3.55	3.47	29.34	31.7	28.32
8	Ric8b	4.28	9.61	10.95	58.51	84.45	66.31
8	Spry2	21.78	16.24	25.01	25.08	33.88	6.2
8	Syt1	8.14	8.06	17.24	30.02	38.23	121.96
8	Thoc5	10.19	11.03	11.75	42.79	72.2	143.17
8	Timm44	14.38	12.27	14.92	23.9	38.83	42.56
8	Usp33	9.77	13.46	14.3	34.73	59.92	93.02
8	Usp33	9.77	13.46	14.3	34.73	59.92	93.02
9	Adcy1	1.51	2.63	4.38	33.54	44.44	47.64
9	Asrgl1	1.08	0.83	2.66	13.87	16.35	49.24
9	Dhrs3	1.18	1.92	4.07	18.77	31.44	32.72
9	Epas1	2.05	1.93	2.31	7.64	20.52	26.87
9	**Frmpd1**	2.79	1.49	1.53	11.08	25.89	30.8
9	**Glb1l2**	1.5	2.53	2.58	18.34	47.7	151.43
9	Gpsm2	7.91	4.28	1.28	11.29	63.53	186.52
9	March1	1.29	6.7	6.39	18.65	24.33	54.58
9	Napb	6.02	8.25	10.26	30.31	34.19	87.08
9	Pex5l	6.21	12	19.73	107.03	136.94	287.37
9	Rabgef1	1.02	0.75	3.84	21.06	43.36	51.28
9	Slco4a1	1.17	1.22	2.54	7.07	21.77	40.57
9	Zfp365	1.96	2.65	4.15	18.18	18.7	48.13
10	Ankrd33b	49.33	45.2	48.34	74.77	101.91	110.46
10	Bbs7	13.67	26.38	27.67	90.79	117.69	226.77

		FPKM in flow-sorted rod photoreceptors					
Cluster	Gene	P2	P4	P6	P10	P14	P28
10	Cadm1	34.09	39.32	58.26	80.83	80.09	109.64
10	Camk2d	11.81	14.77	20.86	36.16	49.84	66.22
10	Ccdc126	20.88	35.94	46.38	123.27	209.89	371.64
10	Egflam	24.15	28.84	29.44	70.08	112.55	168.32
10	Elmod2	17.47	30.02	28.38	42.08	60.98	93.99
10	Fbxl5	24.78	42.06	40.26	99.76	147.66	397.8
10	Hist1h1c	57.81	29	40.73	45.92	73.4	124.48
10	Lrit1	11.38	27.38	30.55	71.74	125.35	92.09
10	Paqr4	17.32	18.86	26.13	43.05	58.17	58.97
10	Pitpnm3	15.67	21.89	19.27	52.44	61.01	53.86
10	Prkab1	27.48	24.78	49.56	68.39	79.55	140.55
10	Samd7	48.98	68.89	129.78	80.66	81.2	91.53
10	Tmed10	31.27	31.34	31.28	29.05	43.87	63.79
10	Tomm20	20.91	22.66	29.37	49.48	57.32	86.57
11	Btg2	110.4	91.77	90.71	25.44	20.4	7.38
11	Cxx1c	52.84	28.44	36.64	16.01	13.69	10.8
11	Gnb3	114.4	55.17	109.95	104.45	51.77	27.62
11	H2afz	421.21	136.14	160.02	91.11	85.08	97.9
12	Cpe	22.77	18.45	39.67	178.96	376.16	954.09
12	Fam3c	7.72	5.93	15.67	57.95	97.71	203.08
12	Gnb5	19.67	22.93	40.92	146.39	296.79	671.2
12	Herc3	4.82	9.48	13.38	76.74	118.71	218.75
12	Nxnl1	6.43	14.02	19.56	132.66	220.36	408.21
12	Pex5l	6.21	12	19.73	107.03	136.94	287.37
12	Rdh12	8.14	28.32	47.16	261.4	538.57	852.02

		FPKM in flow-sorted rod photoreceptors					
Cluster	Gene	P2	P4	P6	P10	P14	P28
12	Slc17a7	7.47	6.31	22.16	224.58	415.17	593.53
13	Cst3	201.3	151.77	305.72	724.64	1123.89	1995.14
13	Gnb1	85.42	129.18	164.21	1216.75	2267.88	5350.97
13	Nr2e3	330.02	396.06	661.07	866.17	954.58	1149.44
13	Nrl	263.41	295.84	483.37	1649.39	2558.22	4609.68
13	Pde6b	49.09	135.89	211.99	932.69	1236.53	3275.75
13	Rbp3	260.62	276.29	324.62	1095.74	2209.48	4028.39
13	Rom1	184.35	189.61	392.63	1537.81	2533.85	5884.94
14	Gnb1	85.42	129.18	164.21	1216.75	2267.88	5350.97
14	Guk1	36.69	36.99	78.26	525.96	578.44	721.6
14	Rp1	73.46	224.53	225	334.15	381.34	319.66
15	Gnat1	2.42	7.74	17.62	3543.25	11385.3	38043.8
15	Rho	23.73	84.63	255.71	5011.59	13407.7	45540.7